

The Pennsylvania State University

The Graduate School

Department of Chemistry

**STUDY OF SOLVATION EFFECTS IN POLAR-PROTIC SOLVENTS USING
COMPUTER SIMULATIONS**

A Thesis in

Chemistry

by

Scot Richard Mente

Submitted in Partial Fulfillment
of the Requirements
for the Degree of

Doctor of Philosophy

May 1999

UMI Number: 9938021

UMI Microform 9938021

Copyright 1999, by UMI Company. All rights reserved.


**This microform edition is protected against unauthorized
copying under Title 17, United States Code.**

UMI

**300 North Zeeb Road
Ann Arbor, MI 48103**

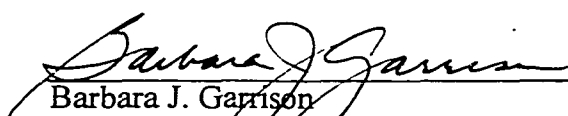
We approve the thesis of Scot Richard Mente.

Date of Signature



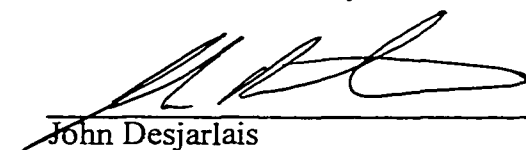
Mark Maroncelli
Professor of Chemistry
Thesis Advisor
Chair of Committee

3/4/99



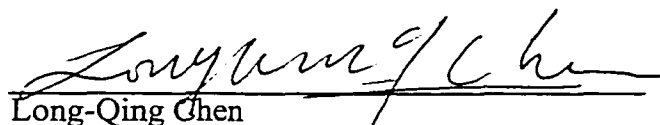
Barbara J. Garrison
Professor of Chemistry

3/4/99



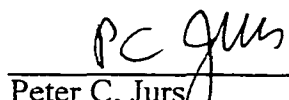
John Desjarlais
Assistant Professor of Chemistry

3/4/99



Long-Qing Chen
Associate Professor of Materials Science and
Engineering

3/4/99



Peter C. Jurs
Professor of Chemistry
Acting Head of the Department of Chemistry

3/4/99

ABSTRACT

Computational chemistry techniques are used to study various aspects of solvation and solvent effects in polar-protic systems. A variety of methods have been utilized, including Monte Carlo and molecular dynamics simulations, as well as semi-empirical and *ab initio* calculations.

The first part of this thesis examines the solvent catalyzed proton transfer reaction in 7-Azaindole and 1-Azacarbazole. In Chapter 2 classical Monte Carlo and molecular dynamics simulations are used to examine the structure and dynamics of solvation of aza-aromatic solutes in alcohol and water solvents in an effort to determine whether the existing interpretations of the solvent participation in these reactions are reasonable. Assuming that correct solvation involves formation of a cyclic 1:1 solute-solvent complex, reactive fractions are computed for a series of eight hydroxylic solvents: methanol, ethanol, 1-propanol, 2,2,2-trifluoroethanol, 2-propanol, *tert*-butyl alcohol, ethylene glycol, and water. In all cases the reactive fractions so calculated are small ($< 2\%$) and are of the correct magnitude to account for the relatively slow reaction observed in neat solvents. The underlying cause for these small reactive populations can be rationalized on the basis of the weak hydrogen bonds afforded by a cyclic arrangement. In nearly all cases these fractions correlate nicely with the observed reaction rates, thereby validating the picture of the solvent involvement in these reactions developed on the basis of experimental studies.

In addition to simulations in bulk polar-protic solvents, some simulations of hydrogen-bonded complexes in dilute solutions and in the gas phase have been performed and are reported in Chapter 3. The primary goal of these simulations was to examine the accuracy of the classical potentials used in Chapter 2. Simulated energies are compared to complexation energies generated via *ab initio* calculations as well as from experimental data in dilute solutions. For the cases examined, the classical potentials reproduced *ab initio* calculations and available experimental data on 1:1 complexes of 7-AI and 1-AC with various hydrogen-bonding partners to an accuracy of ± 3.8 kJ/mol or ± 13 % without adjustment of parameters.

The final two sections of the thesis use computational methods to examine solvatochromism. In Chapter 4 Monte Carlo methods are used to simulate the electronic spectral shifts of the betaine-30 molecule, which forms the basis of the ET(30) scale. These studies show that the classical potentials used throughout this thesis are capable of accurately reproducing the solvent polarity observed experimentally. In addition the simulations find that the overall contribution to the solvent-induced shift caused from solvents directly hydrogen-bonded to the betaine-30 spans a range from 20 to 50 %.

Chapter 5 of this thesis describes studies of the solvent-induced shifts in the vibrational spectra of trimethyl- and triethylphosphine oxide. Using Monte Carlo simulations and a calculation method based on computing the force and force derivatives related to the P-O bond stretching, the solvent-dependent band shifts have been determined and compared to experimental values. The methods employed qualitatively and semi-quantitatively reproduce experimental band shapes.

TABLE OF CONTENTS

LIST OF FIGURES	viii
LIST OF TABLES	xi
ACKNOWLEDGEMENTS	xiii
Chapter 1. INTRODUCTION	1
Chapter 2. SOLVATION AND THE EXCITED-STATE TAUTOMERIZATION OF 7-AZAINDOLE AND 1-AZACARBAZOLE: COMPUTER SIMULATIONS IN WATER AND ALCOHOL SOLVENTS	16
2.1. Introduction	16
2.2. Simulaton Methods	25
2.2.1. Methodology	25
2.2.2. Intermolecular Potential Functions	28
2.2.2.1. General Form	28
2.2.2.2. Solute Models	29
2.2.2.3. Solvent Models	32
2.3. Results and Discussion	34
2.3.1. General Behavior. Isolated Complexes versus Bulk Solvents	34
2.3.2. Possible Dynamical Solvent Effects on the Reaction Rate	42
2.3.3. Quantitative Estimation of Reactive Fractions and Reaction Rates	51
2.3.4. Solvation Structure and the Solvent Dependence of the Reactive Fractions	58

	vi
2.3.5. Temperature and Solute Dependence	75
2.4. Summary and Conclusions	77
2.5. Appendix	81
2.6. References and Notes	85
Chapter 3. EVALUATION OF CLASSICAL POTENTIAL FUNCTIONS FOR HYDROGEN BONDING IN 7-AZAINDOLE AND 1-AZACARBAZOLE COMPLEXES	93
3.1. Introduction	93
3.2. Computational Procedure	94
3.3. Results and Discussion	97
3.4. Summary and Conclusions	106
3.5. References	109
Chapter 4. MONTE CARLO SIMULATIONS OF SOLVATOCHROMISIM AND THE E _T (30) SOLVENT POLARITY SCALE	113
4.1. Introduction	113
4.2. Methods	121
4.2.1. Calculation of Electronic Shifts in Isolated Complexes and Bulk Solvents	121
4.2.2. Potential Functions and Simulation Methods	123
4.3. Results and Discussion	125
4.3.1. Quantum Chemical Calculations of the Betaine-30 Molecule	125
4.3.2. Betaine-30 Energetics in Isolated Complexes	132
4.3.3. Bulk Solvation of Betaine-30	133
4.3.3.1. Solvation Structure and Energetics	136

4.3.3.2. Reorganization Energies	138
4.3.3.3. Solvent Dependence of the Simulated Shifts	141
4.4. Summary and Conclusions	150
4.5. References and Notes	152
Chapter 5. MONTE CARLO SIMULATIONS OF SOLVENT EFFECTS OF THE P-O STRETCHING BAND OF TRIETHYLPHOSPHINE OXIDE IN ALCOHOLS AND WATER	154
5.1. Introduction	154
5.2. Experimental	152
5.3. Theoretical Background	163
5.3.1. Modeling Ω	163
5.3.2. Potential Functions and Simulation Methods	167
5.4. Results and Discussion	171
5.4.1. Vibrational Spectroscopy of the P-O Stretching Mode of TEPO and TMPO	171
5.4.2. Computer Simulations of TMPO: Solvation Structure and Energetics	183
5.4.2.1. Solvation Structure and Energetics	184
5.4.2.2. 0 th -Order Vibrational Shifts of TMPO in Bulk Solvent Systems	191
5.4.2.3. Model 2, 0 th -Order + Added Polarization	199
5.5. Summary and Conclusions	209
5.6. References and Notes	212
Chapter 6. SUMMARY	214

LIST OF FIGURES

Figure 2.1. Two views of the mechanism of the solvent-catalyzed tautomerization of 7-AI in alcohol solvents.	19
Figure 2.2. Charges used in modeling the solutes 7-AI and 1-AC.	31
Figure 2.3. Hydrogen-bonding distance distribution observed in simulations of 7-AI in cyclohexane containing either one or two molecules of methanol, one molecule of acetic acid, or bulk methanol solvent.	38
Figure 2.4. Pair energy distributions.	41
Figure 2.5. Structures of the energy-minimized (gas-phase) 7-AI-methanol and 7-AI-acetic acid complexes. These structures were derived with the classical potential energy functions used in the simulation.	43
Figure 2.6. Hydrogen-bonding distance and pair energy distribution simulated for the DPC solute in methanol.	44
Figure 2.7. Time-dependent survival probabilities of cyclic structures observed in methanol and water.	47
Figure 2.8. Structural time correlation functions (eq.2.3.4) in methanol and water.	50
Figure 2.9. Illustration of the effect of varying the solute charges on the hydrogen-bonding distance distributions of 7-AI in methanol solution.	57
Figure 2.10 A. Hydrogen-bonding distance distributions for 7-AI in four of the solvents studied: 2,2,2-trifluoroethanol, Methanol, Ethanol, and 1-Propanol.	62
Figure 2.10 B. Hydrogen-bonding distance distributions for 7-AI in four of the solvents studied: 2-Propanol, <i>tert</i> -Butanol, Ethylene Glycol and Water.	63
Figure 2.11. Comparison of simulated reactive fractions and observed reactions rates of 7-AI in bulk alcohol solvents.	70

Figure 2.12. Comparison of the approximate energy with the free energy required to form cyclic structures.	73
Figure 2.13. Arrhenius plots of the temperature dependence of the reactive fractions of 7-AI in methanol and water.	74
Figure 3.1. Structure of the energy-minimized (gas phase) 7-AI:methanol complex.	99
Figure 3.2. Comparison of simulated energies with observed free energies of association and ab initio determined interaction energies.	101
Figure 3.3. Comparison of simulated gas phase interaction energies with simulated free energies and simulated average complexation energies.	107
Figure 3.4. Comparison of energies for 7-AI complexes and 1-AC complexes.	108
Figure 4.1. Tautomerization times versus polarity.	114
Figure 4.2. Molecular structure of Betaine-30 and the ground and difference charge distributions.	115
Figure 4.3. Definition of nomenclature.	127
Figure 4.4. INDO/S calculated properties of Betaine-30	131
Figure 4.5. Space filling representations of two conformational structures of Betaine-30:water complexes.	135
Figure 4.6. Simulated versus Experimental values of the $E_T(30)$ parameter.	146
Figure 4.7. Experimental $E_T(30)$ versus Reaction Field factor.	147
Figure 4.8. Variation in atomic-site charges	148
Figure 5.1. Correlation between the $E_T(30)$ solvent polarity parameter and the ^{31}P -NMR shifts of TEPO.	159
Figure 5.2. Correlation between the $\nu(\text{P-O})$ frequency shift (from vapor) and the P-NMR shifts of TEPO.	160
Figure 5.3. Example of spectral subtraction: TEPO in bulk methanol.	162

Figure 5.4. Nuclear displacements corresponding to the normal mode associated with the $\nu(\text{P-O})$ spectral line computed at the HF/6-31G** level.	170
Figure 5.5. Infrared spectra of TEPO and TMPO in various bulk solvents.	176
Figure 5.6. Comparison of phosphine oxide vibrational shifts.	179
Figure 5.7. Correlation between $\nu(\text{P-O})$ frequency shift and $E_{\text{T}}(30)$.	180
Figure 5.8. Infrared spectra for TMPO in a range of $\text{H}_2\text{O} + \text{MeCN}$ solvents.	182
Figure 5.9. Energy pair distributions between TMPO and various ab initio and OPLS solvent molecules.	188
Figure 5.10. Solute-solvent OO radial distribution functions for TMPO-alcohol systems.	190
Figure 5.11. Comparison of “0 th -order” simulated shifts and observed experimental shifts.	197
Figure 5.12. TMPO vibrational frequency distribution decompositions.	198
Figure 5.13. Dipole moment variation along the P-O vibrational coordinate.	203
Figure 5.14. Experimental and simulated vibrational frequency distributions.	205

LIST OF TABLES

Table 2.1. Solute Properties and Potential Parameters.	30
Table 2.2. Parameters of the Solvent Models.	33
Table 2.3. 7-Azaindole-Methanol Results.	53
Table 2.4. Solvent-Solvent Hydrogen-Bonding Characteristics.	60
Table 2.5. Structural Characteristics of Solvation in Various Solvents.	61
Table 2.6. Summary of Reactive Fractions.	66
Table 2.7. Thermodynamic Properties of the Neat Solvents.	84
Table 3.1. Summary of Calculation Results.	100
Table 4.1. Solute Properties and Potential Parameters.	124
Table 4.2. Charge Difference Along the Backbone Structure of Betaine-30.	126
Table 4.3. INDO/S Calculations.	130
Table 4.4. Isolated Complex Energetics and Shifts.	134
Table 4.5. Summary of Energetic and Structural Features in Bulk Solvents.	137
Table 4.6. Estimated Betaine-30 Reorganization Energies.	140
Table 4.7. Betaine-30 Simulated Shifts in Bulk Solvents.	145
Table 5.1. Solute Potential Parameters.	169
Table 5.2. Comparison of Spectral Characteristics of TMPO and TEPO in Various Solvents.	175
Table 5.3. TMPO-Binary Solvent Spectra.	181

Table 5.4. Summary of Energetic and Structural Features: TMPO Simulations in Bulk Solvents.	187
Table 5.5. Simulated Shifts, Calculated Using Only Spatial Contributions to the Vibrational Shift.	196
Table 5.6. All Calculated and Observed Average TMPO Vibrational Frequency Shifts.	204

ACKNOWLEDGMENTS

A great many people have contributed to my life and education, and I would like to acknowledge their contributions here. My family has always been there for me (not that they have really had a choice), and so I will begin with them. My parents, Mom, Dad and Jude, and my brother, Joe, have always been influential in my life and deserve special thanks. They taught me the importance of an education, and always supported my career decisions. Without their love, support, and encouragement, I would not be where I am today. Thanks are also extended to my Aunt Sandra, my Uncle George and my cousin Jennifer for providing a “home-away-from-home” during some of the particularly lonely periods of graduate school.

Several people share the blame for sending me to Penn State in the first place. Certainly my undergraduate advisor, Dr. Scott Savage is a primary culprit. Indeed, I may have still been working towards my B.S. if it wasn't for his advisement and seemingly endless wisdom. Dr. Cynthia Hartzell provided me with my first real taste of science and patiently taught me how to do research. The work I did with her strengthened my self-confidence as well as my formal credentials, and made graduate school possible. Finally, Dr. Robert Zoellner instilled in me his infectious love for science that I hope I never lose.

Many wonderful people have contributed to my life in the past six years, and are responsible for making my stay at Penn State a truly rewarding experience. I honestly cannot say enough about my graduate advisor, Professor Mark Maroncelli. His

knowledge, support and advisement have been remarkably valuable. I will always be thankful for the opportunity to work in his group. I greatly appreciate all the helpful discussions that I have had with my research group. In particular, Sarah, Joe, Vijaya, Jennifer, Mark H., Nikhil and Kevin have all provided a wonderful environment as both fellow scientist and friends. Additionally, I would like to thank Dr. William Jorgensen of Yale University for generously providing the BOSS Monte Carlo program which made much of this research possible.

Countless other members of the Penn State community have made significant contributions to my graduate student experience. My best friend, Mark Panic, has always been there through times good, bad, and bizarre. I would like to thank both him and his wife, Leigh for their support and friendship. I will always remember and appreciate the support and discussion of my friends in the Horrock's lab. In particular, Ron Supkowski for his advise as a scientist, his camaraderie as a friend, and the spare bedroom which he, along with his wife, Laura, made available to me in my final year. Many other close friends deserve thanks: Dr. Scott Best, Dr. Brooke Best, Dr. Jeremy Lessmann, Dr. James Sands, Andrew Klauss, Eric Stover, Robert Campbell, and Kent Booker.

Most importantly, I would like to thank Jennifer McGuinn. While I always expected the academic environment provided at Penn State to enrich my mind, I never expected it to fill my heart. Jennifer's love, devotion, humor, and support have guided me to a new happiness. She has become my best friend, and I look forward to spending the remainder of my life in her company.

Chapter 1

INTRODUCTION

Understanding reactivity represents a fundamental goal of chemical research [1]. The general knowledge of how molecules break and form bonds is directly applicable to fields such as chemical synthesis, biochemistry, as well as materials research and design. Chemical reactivity in liquids represents a particularly important subset of general reactivity due to the reality that a great majority of chemical reactions occur in solution. Of course, the ability of solvents to dramatically alter chemical reaction rates and equilibria has been appreciated for decades [2]. Indeed, synthetic chemists have long used their knowledge of solvent effects to design and perfect synthetic procedures. Still, a detailed knowledge of the precise chemical events that take place during a reaction has only recently begun to emerge.

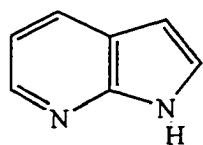
Progress towards a deeper understanding of solution phase processes has been fueled by two relatively recent developments: ultra-fast laser spectroscopy and computer simulation [3]. These techniques have been successfully applied to a variety of reactive systems such as intramolecular isomerization reaction [4], electron transfer [5], and proton transfer reactions [6-8]. Proton transfer reactions are representative of a specific class of reactions in which recent advances have been both numerous and insightful [8-15]. These reactions involve the simple translocation of a proton, and may occur via

either intramolecular or intermolecular mechanisms. Due in part to the partial positive charge of the proton, these reactions tend to be solvent dependent, regardless of the specific reaction mechanism involved.

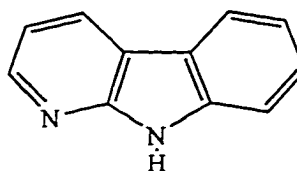
The excited-state solvent-assisted tautomerization of 7-azaindole (7-AI) and 1-azacarbazole (1-AC) is an example of such a solvent-dependent process, and is the primary of topic of this thesis. In dilute solutions, these molecules may form

Scheme 1

7-Azaindole (7-AI)



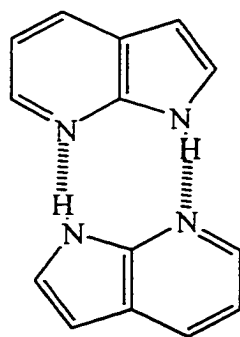
1-Azacarbazole (1-AC)



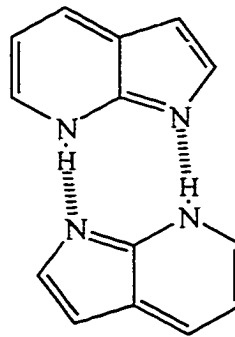
hydrogen-bonded aggregates with other protic molecules, or with each other, as in the case of hydrogen-bonded dimers. Once formed, these doubly hydrogen bonded structures facilitate the double proton transfer between molecules. Mother Nature has

Scheme 2

“Normal”



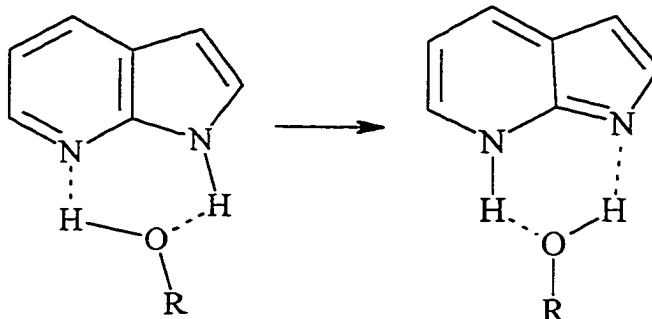
“Tautomer”



frequently utilized multiply hydrogen-bonded arrangements to lend vigor and directionality to molecular recognition processes and supermolecular structures, such as the two or three hydrogen bonds in Watson-Crick base pairs that bind the double-stranded DNA helix. In fact, due to the geometric similarity between DNA base pairs and 7-AI dimers, it has been hypothesized that an understanding of the potential energy surfaces along the reaction path for tautomerization of the 7-AI dimers will lead to a better understanding of photo-induced mutagenesis of DNA helices [16].

Tautomerization of 7-AI and 1-AC may also proceed via a solvent-catalyzed process in bulk polar-protic solvents. These reactions have also been explored by a variety of experimental [6, 7, 12, 17-28] and theoretical studies [8-11, 29].

Scheme 3

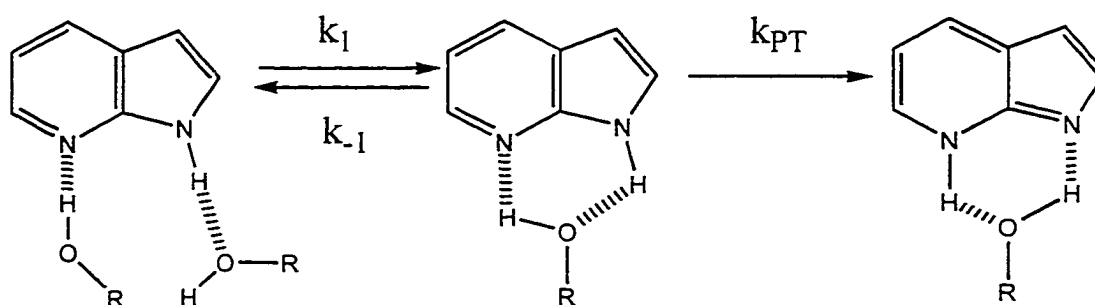


These solvent-catalyzed reactions differ markedly from the dimer reactions in being both hundreds of times slower and strongly activated. Similar examples of solvent induced retardation of reaction rates are common in the literature. For instance, the so-called “desolvation hypothesis” [30-33] in enzymatic catalysis, in which a non-polar active site may catalyze reactions by desolvating states which are strongly solvated in the

corresponding reaction in solution. In these cases, the solvent acts to slow the rate of the reaction in a similar manner as polar-protic solvents hinder the rate of tautomerization of 7-AI.

Due to the desire to better understand such solvent effects upon reaction rates, many researchers have been moved to study the solvent effects upon the proton transfer of 7-AI [6-10, 12, 17-19, 23-25, 29]. Although there is general agreement that a cyclic solute-solvent complex is a necessary precursor to the actual proton shuttling step, a variety of interpretations exist with respect to which precise structures and dynamics control the overall rate of tautomerization. A general reaction scheme may be employed to schematically outline the various kinetic possibilities that may be thought to be governing the overall rate:

Scheme 4:



Here, the overall rate may be thought to depend on either the solvation dynamics (k_1), the equilibrium between the differing types of solvation ($K_{eq} = k_1/k_{-1}$), or the implicit proton shuttling step (k_{pT}).

Chapter 2 of this thesis is concerned with determining how polar-protic solvents effect the overall reaction rate, and finding out what properties of these solvents correlate with the rates determined experimentally for a series of alcohols. The methods employed are purely classical Monte Carlo and molecular dynamics computer simulations of 7-AI and 1-AC in alcohol and water solvents. By adopting the perspective of scheme 4, the relative rates of reaction in different solvents should only reflect the equilibrium between reactive and non-reactive forms, and the proton-transfer step need not be considered in this investigation.

Comparison of simulations in bulk alcohols and those in dilute solutions clearly demonstrate that when multiple hydrogen-bonding partners are available, such as the case in bulk protic solvents, the cyclic complex is disfavored energetically. This is largely due to the steric strain introduced by the substantially non-linear hydrogen bonds. Non-cyclic/unreactive conformations are capable of forming strong, linear hydrogen bonds, and as a result are energetically favored. Thus, the percentage of “reactive” solvation states (f^*) is typically observed to be less than 1 %. The possible role of solvent dynamics is then examined using molecular dynamics simulations of 7-AI in bulk methanol and water systems. In both cases survival times of the reactive fractions are determined to be very short. In this limit, the relative probabilities of cyclic complex formation (K_{eq}) in these solvents determine the rates of reactions in different solvents (the solvent dependence). Indeed, for most of the solvents studied these reactive fractions correlate very well with the observed rates of tautomerization determined from experiment.

Although the agreement between the modeling and experiment is generally very good, the two non-primary alcohols examined are found to deviate considerably from the correlation established by the other solvents. These differences may be due to a variety of effects not accounted for in the simulations. Dynamical (k_1) effects may become important when the size of the alcohol becomes sufficiently large. The actual proton shuttling step, which is never modeled, may also vary substantially with solvent. It also seems reasonable to suspect that subtle differences between solvation in primary and secondary alcohols may not be properly represented using the simple potential functions employed here.

The last three chapters of this thesis consider the above aspects in more detail. In dealing with numerical modeling of any sort a certain level of skepticism is always advisable. Along these lines an attempt is made determine to what level the modeling of hydrogen-bonded systems using these simple potentials may be considered accurate. These types of potential energy functions have a long and rich history in the simulation of molecular systems, and recent commercialization of classical simulation programs have made simulations such as these common place [34-42].

The main issue in performing classical simulations is parameterization of the potential functions. There are a number of different philosophies, although all of them tend to share the common belief that the parameters should be chosen to reproduce some type of experimental data. For solids, one typically fits the packing density of the material. For gases one may chose to match the *ab initio* geometries, or perhaps geometries from gas-phase spectroscopic data. For pure liquids, the most common

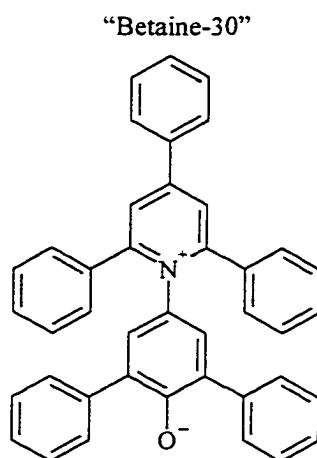
method of parameterization is to reproduce as closely as possible the experimentally derived heat of vaporization and density of the fluid.

What is known from experimental studies of the 7-azaindole and 1-azacarbazole systems? Perhaps the best experimental data is for the association of hydrogen-bonded species in dilute solution. In fact the complexation constants of 7-AI and 1-AC with different hydrogen bonding partners in dilute alkane solution have been measured for eight different systems by various research groups [43-46]. Results in Chapter 3 compare how well the classical potential functions employed in Chapter 2 are able to reproduce the known experimental complexation free energies. The classical complexation energies are also directly compared to the results from *ab initio* calculations. The general agreement is very good; the classical potentials are found to be able to reproduce *ab initio* and experimental data to an accuracy of ± 13 % without any adjustable parameters.

The classical potentials used for representing solvents have a 15-year history of condensed-phase simulations and parameterization from which rigorous tests for judging realism have been generated [47]. As stated above, the most common method of parameterizing solvent force fields is to reproduce the best available experimental data. Heats of vaporization and liquid densities are two excellent quantities to start with. Both have accurate, well-known, published values with which to compare simulation to. There is, however, a multitude of other solvent properties one could consider. The final two chapters of this thesis examine the potentiality of the current solvent models to reproduce reliable experimental data regarding quantities related to solvent “polarity” and hydrogen bond donating ability.

In Chapter 4, a method is presented in which the solvent polarity of classical models may be determined. This scheme involves the numerical simulation of the betaine-30 chromophore, which forms the basis of Reichardt's $E_T(30)$ solvent polarity scale [48], in various solvent environments.

Scheme 5

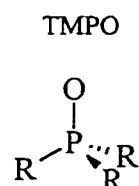


The wavelength maximum of the absorption band shifts drastically with solvent polarity due to the charge-shift character of the transition. Betaine-30 has a substantial ground-state dipole moment as well as a highly basic, hydrogen bond accepting group. As a result both specific and non-specific solute-solvent interactions are reflected in the position of the absorption band. In Chapter 4, the solvatochromic behavior of betaine-30 is modeled in various classical solvents simply by performing Monte Carlo sampling of the ground-state solute while recalculating the solute-solvent interaction energy for an excited-state solute at regular intervals. These simulations show that standard solvent models are indeed capable of reproducing the spectral shifts observed in experiment over an impressive range of polar-protic solvents. In all of the normal mono-alcohols

examined the simulated shifts match the experimental values in terms of a qualitative trend. The simulated results also suggest that about 20-50 % of the total shift can be directly related to the intermolecular interactions between the solute and the solvent molecules forming hydrogen bonds to the oxygen atom of betaine-30.

To focus even more on the hydrogen-bonding characteristics a second probe is considered in Chapter 5: the vibrational shifts of the P-O stretch of TMPO.

Scheme 6



Phosphine oxide compounds have been used in prior experimental studies to elucidate the so-called “acceptor” properties of solvents [49]. Both Mayer [50, 51] and Symons [52-54] have demonstrated the variation in the vibrational spectrum of triethylphosphine oxide (TEPO) in a variety of solvents. In alcohols, the spectrum is bimodal; a feature which has been attributed to the existence of multiple hydrogen-bonded species. In Chapter 5 a variation upon the methodology originally developed by Oxtoby [55] is presented for the calculation of solvent-induced vibrational frequency shifts. Although the polarization of the bond must be accounted for empirically, quantitatively accurate shifts and widths may be generated using physically sensible choices for the empirical adjustment parameter.

Taken together, Chapters 4 and 5 demonstrate that the classical potentials employed in the proton-transfer studies of Chapters 2 and 3 are surprisingly capable of

reproducing specific spectroscopic values. These results illustrate that potential functions parameterized on the basis of pure-solvent properties are also surprisingly robust in their ability to predict other aspects of the solvent's interactions with dissolved solutes.

Finally, some comment is necessary regarding the portions of this thesis which have been, or will be published elsewhere. Chapters 2 and 3 of this thesis are based on papers that have found their way into the scientific literature. I would like to thank the American Chemical Society and Elsevier Science for their generosity in this matter. Chapters 4 and 5 are currently manuscripts in preparation.

Chapter 2: Solvation and the Excited-State Tautomerization of 7-Azaindole and 1-Azacarbazole: Computer Simulations in Water and Alcohol Solvents, S. Mente and M. Maroncelli, *J. Phys. Chem. A*, **102** (1998) 3860-3876. Reprinted with permission from the *Journal of Physical Chemistry, A*. Copyright 1998 American Chemical Society.

Chapter 3: Reprinted from *Chemical Physics Letters*, **293**, S. Mente, S. J. V. Frankland, L. Reynolds and M. Maroncelli, Evaluation of Classical Potential Functions for Hydrogen Bonding in 7-Azaindole and 1-Azacarbazole Complexes, 515-522, Copyright 1998, with permission from Elsevier Science.

Chapter 4: Monte Carlo Simulations of Solvatochromism and the $E_T(30)$ Solvent Polarity Scale, S. Mente, M. Maroncelli, Manuscript in Preparation.

Chapter 5: Monte Carlo Simulations of Solvent Effects on the P-O Stretching Band of Triethylphosphine Oxide in Alcohols and Water, S. Mente, M. Maroncelli, Manuscript in Preparation.

Notes and References

1. Uppenbrink, J. *Science*. **1998**, 279, 1831.
2. Magat, M.Z. *Phys. Chem.* **1932**, A 162, 432-448.
3. Jimenez, R., *et al.* *Nature*. **1994**, 369, 471-473.
4. Waldeck, D.H. *Chem. Rev.* **1991**, 91, 415-436.
5. Walker, G.C., *et al.* *J. Phys. Chem.* **1992**, 96, 3728-3736.
6. Moog, R.S. and M. Maroncelli. *J. Phys. Chem.* **1991**, 95, 10359.
7. Chapman, C.F. and M. Maroncelli. *J. Phys. Chem.* **1992**, 96, 8430-8441.
8. Mente, S. and M. Maroncelli. *J. Phys. Chem. A*. **1998**, 102, 3860-3876.
9. Gordon, M.S. *J. Phys. Chem.* **1996**, 100, 3974-3979.
10. Chaban, G.M. and M.S. Gordon. *J. Phys. Chem. A*. **1999**, 103, 185-189.
11. Shukla, M.K. and P.C. Mishra. *Chemical Physics*. **1998**, 230, 187-200.
12. Smirnov, A.S., *et al.* *J. Phys. Chem. B*. **1997**, 101, 2758.
13. Chachisvilis, M., *et al.* *J. Phys. Chem. A*. **1998**, 102, 669.
14. Takeuchi, S. and T. Tahara. *J. Phys. Chem. A*. **1998**, 102, 7740-7753.
15. Herbich, J., *et al.* *J. Phys. Chem. A*. **1997**, 101, 5839-5845.
16. Ingham, K.C. and M.A. El-Bayoumi. *J. Am. Chem. Soc.* **1974**, 96, 1674.
17. Avouris, P., L.L. Yang, and M.A. El-Bayoumi. *Photochem. Photobiol.* **1976**, 24, 211.
18. Herbich, J., J. Sepiol, and J. Waluk. *J. Mol. Spectrosc.* **1984**, 114, 329-332.
19. McMorrow, D. and J. Aartsma. *Chem. Phys. Lett.* **1986**, 125, 581-585.

20. Konijnenberg, J., A.H. Huizer, and C.A.G.O. Varma. *J. Chem. Soc. Faraday Trans. 2*. **1988**, *84*, 1163-1175.
21. Chen, Y., *et al.* *J. Phys. Chem.* **1993**, *97*, 1770-1780.
22. Rich, R.L., *et al.* *J. Phys. Chem.* **1993**, *97*, 1781-1788.
23. Chen, Y., F. Gai, and J.W. Petrich. *J. Am. Chem. Soc.* **1993**, *115*, 10158-10166.
24. Chen, Y., F. Gai, and J. Petrich. *Chem. Phys. Lett.* **1994**, *222*, 329-334.
25. Chou, P.-T., *et al.* *J. Phys. Chem.* **1992**, *96*, 5203.
26. Waluk, J., S.J. Kamorowski, and J. Herbich. *J. Phys. Chem.* **1986**, *90*, 3868.
27. Boryshcuck, S.J., . 1993, Penn State University: University Park.
28. Reynolds, L.E., *et al.* **1999**, .
29. Mente, S., *et al.* *Chem. Phys. Lett.* **1998**, *293*, 515-522.
30. Wolfenden, R. *Science*. **1983**, *222*, 1087-1093.
31. Dewar, M.J.S. and D.M. Storch. *Proc. Natl. Acad. Sci. USA*. **1985**, *82*, 2225-2229.
32. Crosby, J., R. Stone, and G.E. Lienhard. *J. Am. Chem. Soc.* **1970**, *92*, 2891-2900.
33. Weiner, S.J., U.C. Singh, and P.A. Kollman. *J. Am. Chem. Soc.* **1985**, *107*, 2219-2229.
34. Weiner, S.J., *et al.* *J. Comp. Chem.* **1986**, *7*, 230-252.
35. Cornell, W.D., *et al.* *J. Am. Chem. Soc.* **1995**, *117*, 5179-5197.
36. Maple, J.R., *et al.* *J. Comput. Chem.* **1994**, *15*, 161-182.
37. Hwang, M.-J., T.P. Stockfisch, and A.T. Hagler. *J. Am. Chem. Soc.* **1994**, *116*, 2515-2525.

38. Nilsson, L. and M. Karplus. *J. Comput. Chem.* **1986**, 7, 591-616.
39. Halgren, T.A. *J. Comput. Chem.* **1996**, 7, 490-519.
40. Allinger, N.L., Y.H. Yuh, and J.-H. Lii. *J. Am. Chem. Soc.* **1989**, 111, 8551-8566.
41. Nevins, N., K. Chen, and N.L. Allinger. *J. Comput. Chem.* **1996**, 17, 669-694.
42. Jorgensen, W.L., . 1994, Yale University: New Haven, CT.
43. Chou, P.-T., *et al.* *J. Am. Chem. Soc.* **1995**, 117, 7259-7260.
44. Chang, C., N. Shabestary, and M.A. El-Bayoumi. *Chem. Phys.* **1980**, 75, 107.
45. Seipol, J. and U.P. Wild. *Chem. Phys. Lett.* **1982**, 93, 204.
46. Chang, C.-P., *et al.* *J. Phys. Chem.* **1994**, 98, 8801-8805.
47. vonRague, P., ed. *Encyclopedia of Computational Chemistry*. 1 ed. . Vol. 2. 1998, John Wiley and Sons, INC.: New York. 3429.
48. Reichardt, C. *Chemical Reviews*. **1994**, 94, 2319-2358.
49. Mayer, U., V. Gutmann, and W. Gerger. *Monatshefte fur Chemie*. **1975**, 106, 1235-1257.
50. Mayer, U., H. Hoffmann, and R. Kellner. *Monatshefte fur Chemie*. **1988**, 119, 1207-1221.
51. Mayer, U., H. Hoffmann, and R. Kellner. *Monatshefte fur Chemie*. **1988**, 119, 1223-1239.
52. Symons, M.C.R. and G. Eaton. *J. Chem. Soc., Faraday Trans. I.* **1982**, 78, 3033-3044.
53. Symons, M.C.R. *Chem. Soc. Rev.* **1983**, 12, 1-34.
54. Symons, M.C.R. *Pure and Appl. Chem.* **1986**, 58, 1121-1132.

55. Oxtoby, D.W. *J. Chem. Phys.* **1979**, *70*, 2605-2609.

Chapter 2

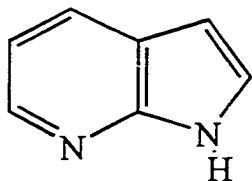
SOLVATION AND THE EXCITED-STATE TAUTOMERIZATION OF 7-AZAINDOLE AND 1-AZACARBAZOLE: COMPUTER SIMULATIONS IN WATER AND ALCOHOL SOLVENTS.

2.1. Introduction

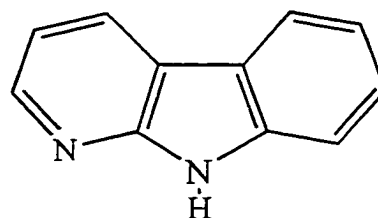
7-Azaindole ("7-AI") and 1-Azacarbazole ("1-AC"; Scheme 1) are representatives of a class of molecules that undergo rapid excited-state tautomerization in the presence of suitable hydrogen-bonding partners. These molecules have attracted considerable attention for a number of reasons. In the earliest work, excited-state tautomerization in 7-AI dimers was examined as a model for radiation-induced processes in DNA base pairs [1]. In dimers, tautomerization is believed to be effected by a double proton switch between the two components of the dimer (Scheme 1b), one of which is electronically excited and the other of which is in the ground state. Reaction in both 7-AI and 1-AC dimers occurs in a few picoseconds in room temperature solution [2-4] and nearly this quickly at the low temperatures achieved in supersonic expansion [5,6]. Studies of 1-AC and 7-AI complexed to single molecules of various carboxylic acids, amides, and lactams [4,7,8] have also shown very rapid reaction, especially in cases where the complexing partner acts as a catalyst (i.e. is chemically unchanged) in the process. In addition to

SCHEME 1

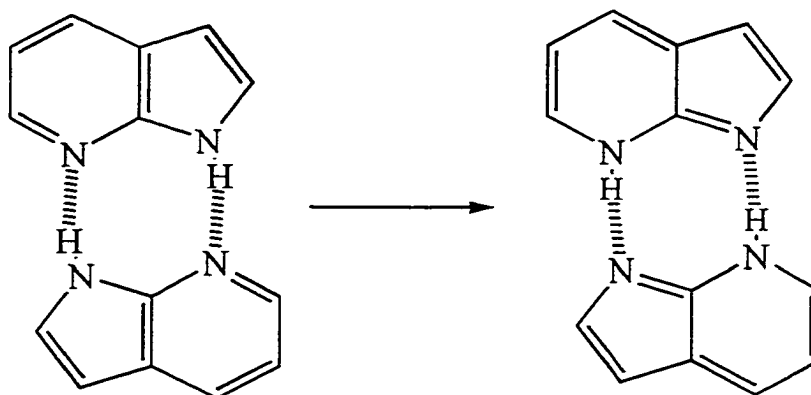
7-Azaindole (7-AI)



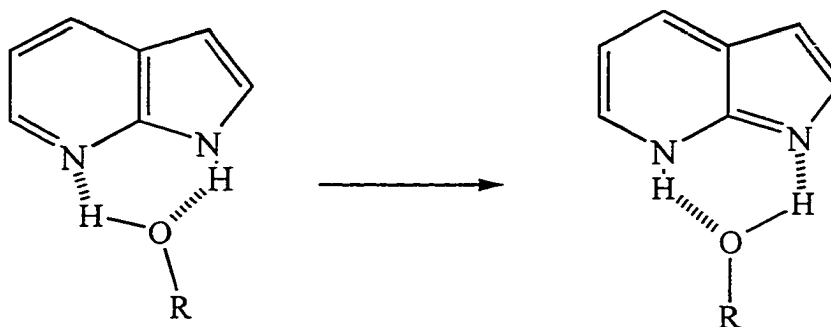
1-Azacarbazole (1-AC)



(b) Dimer Reaction



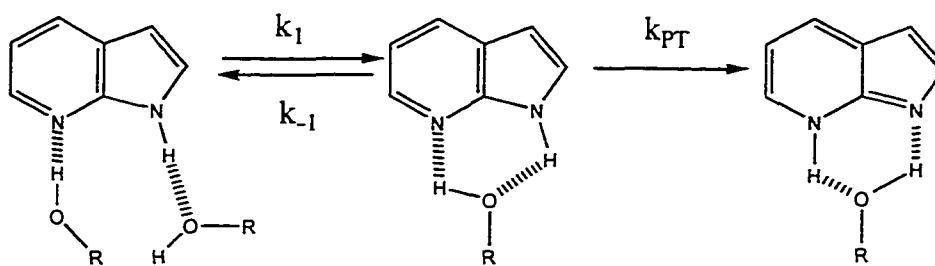
(c) Reaction in Solvent Complex



studies of isolated complexes, a number of workers have investigated the excited-state tautomerization of 7-AI [9-18] and 1-AC [19-21] in bulk alcohol and water solvents. These systems present a striking contrast to the former cases in that in bulk alcohols and water the reaction is found to occur hundreds to thousands of times more slowly at room temperature. In addition, in bulk solvents the reaction is strongly activated, such that decreasing the temperature to near 200 K results in unobservably slow reaction.

The mechanism of the solvent involvement in the tautomerization of 7-AI in bulk alcohols and especially in bulk water has been the subject of considerable discussion. Virtually all workers postulate that formation of a 1:1 cyclically bonded 7-AI:ROH complex of the sort shown in Scheme 1c is prerequisite to reaction. The difference between reaction rates in dilute solution and bulk protic solvents is generally attributed to difficulty of forming such reactive structures in bulk solution [22]. The kinetics is most simply described by the two-step mechanism shown in Fig. 2.1a. The second step of this mechanism, which involves the actual proton transfer, is assumed to be rapid ($k_{PT}^{-1} < 5$ ps) by analogy to reactions in isolated complexes. Prior to excitation, most 7-AI molecules are solvated in a manner not conducive to reaction. Little if any prompt reaction is observed, and the reaction rate is largely dictated by the initial, solvent-reorganization step. Two limits can be envisioned for how this solvent reorganization step affects reaction, and both limits have been used for interpretation of experimental data.

(a) 2-Step Model



(b) Continuous Solvation Model

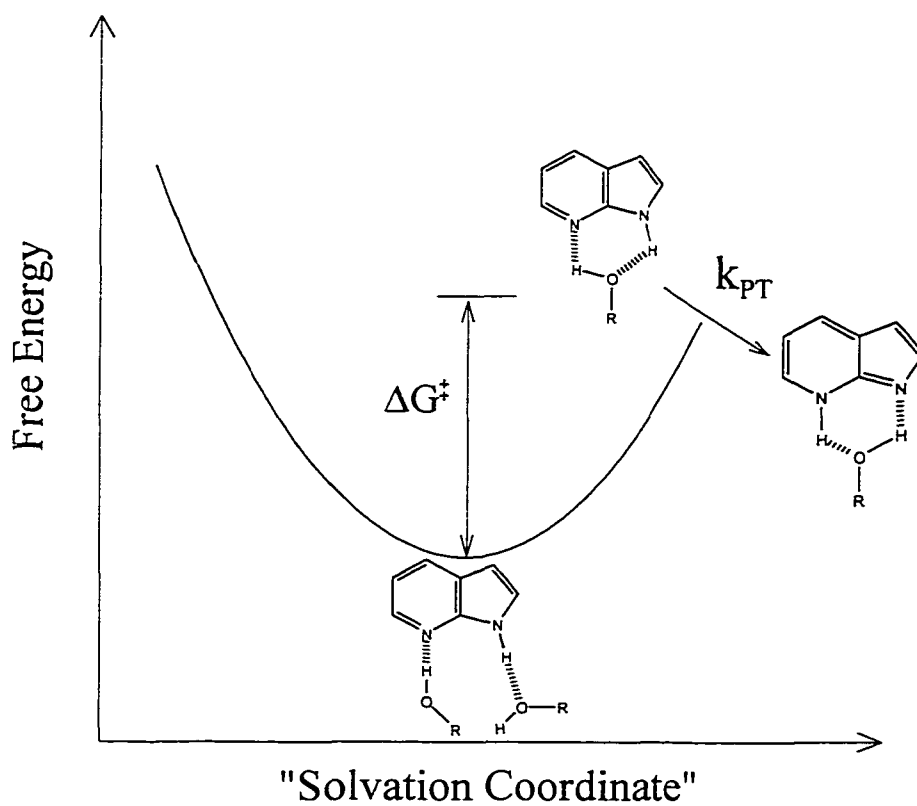


Figure 2.1. Two views of the mechanism of the solvent-catalyzed tautomerization of 7-AI in alcohol solvents.

In the first limit the solvent-reorganization step can be assumed to be rate-limiting such that the observed rate constant for reaction is roughly k_1 . Hebrich, Sepiol and Waluk were among the first to suggest such a mechanism [10]. They determined that the activation energies for the tautomerization and the viscosity activation energies measured in a number of alcohol solvents are nearly identical. They also argued that the observed rate must therefore reflect some sort of large amplitude molecular motions, which they assigned to a mutual twisting of 7AI and alcohol molecules required to form a planar-cyclic 1:1 complex. This was followed by the idea presented by McMorow and Aartsma [11] who distinguished between two ground-state species: 7-AI molecules that are cyclically hydrogen bonded and 7-AI molecules which are not. Upon excitation, the first group of molecules can tautomerize directly, while the second group can tautomerize only when a cyclical hydrogen bond is formed within the lifetime of the excited state via solvent reorientation (k_1). However, there is also an appreciable isotope effect on the rate [12,13], which means that k_1 cannot be completely rate limiting (since k_1 is not expected to be significantly sensitive to isotope). Moog and Maroncelli explained the temperature-dependent isotope effects by postulating that the reaction lies in an intermediate regime in which the rate of reaction in protic solvents primarily reflects solvent dynamics but the second (proton-transfer) step still impacts the overall rate [13]. Something that was not well explained in this model is the fact that the observed rates at room temperature are poorly correlated to solvent viscosity but are instead well correlated to measures of solvent hydrogen bond donating ability such as the $E_T(30)$ “polarity” scale [13,14] and various other acidity functions [16].

In the second limit the observed reaction rate has nothing to do with solvent dynamics, but is controlled by an equilibrium solvation property, the equilibrium constant $K_{solv}=k_1/k_{-1}$. Varma and coworkers were the first to propose a mechanism that does not require a viscosity related dynamic solvent motion to explain the observed rates [12]. Rather, they suggested thermal activation is required to form the specific solute-solvent complexes and only the rate of proton tunneling is sensitive to isotopic substitution. In this view, both solvent acidity and spatial structure are important factors which determine the geometry in the complex and ultimately the observed rate [12].

The view that the equilibrium solvation controls these reactions is illustrated in Fig. 2.1b. It is essentially the same as the equilibrium model discussed above except that the discrete solvation step is replaced by a more realistic continuous solvation potential. The observed rate of reaction is expressed in the manner of transition-state-theory (TST) as [23]:

$$k_{obs} = k_{PT} f^{\ddagger} = k_{PT} \exp(-\Delta G^{\ddagger} / k_B T) \quad (2.1)$$

In this expression f^{\ddagger} is the fraction of molecules correctly solvated for reaction and ΔG^{\ddagger} is their free energy relative to the more prevalent non-reactive forms. All of the features observed for 7-AI and 1-AC in bulk alcohol solvents can be rationalized by assuming that all isotope sensitivity comes from a rapid proton transfer process, $k_{PT} > (5 \text{ ps})^{-1}$, which is, to a reasonable first approximation both temperature- and solvent-independent and which is about 5-fold larger in 7-AI than in 1-AC. Variations in the reaction rates observed in

different alcohol solvents and the temperature dependence of these rates comes primarily from differences in the equilibrium fraction of correctly solvated species, f^* . The solvent-dependence of this fraction is approximately the same in 7-AI and 1-AC and at least in alkyl alcohols this dependence is well correlated to various measures of solvent hydrogen bonding ability [21].

The model portrayed in Figure 2.1b provides a consistent explanation of the behavior observed in all alcohol solvents and in water. However, Petrich and coworkers [15] argue that the situation in water is qualitatively different from that in alcohol solvents. They interpret their observations of the 7-AI reaction as indicating that only a small fraction (<20%) of the 7-AI species in a room-temperature aqueous solution are correctly solvated so as to tautomerize relatively rapidly (in 40-100 ps). The greater majority (>80%) of the solutes are envisioned to be in a state of solvation that “blocks” tautomerization for times longer than the ~1 ns lifetime of the excited state. Chou *et al.* [18] share the viewpoint that the emission characteristics of 7-AI in water reflect the inability of 7-AI to tautomerize as a result of the different solvation structure in water compared to alcohol solvents. Our interpretation of the emission spectra of 7-AI in water is that the observed lifetime of 800 ps in fact represents the reaction time of *all* of the 7-AI solutes [15]. Similar observations can be made with respect to 1-AC in water. While the reaction times are slower than in alcohols, we envision the mechanism and the solvation states involved to be much the same in water as in alcohol solvents [21].

The various interpretations of how solvent is involved in the tautomerization of 7-AI and 1-AC in water and alcohols reflect differing conceptions of the structures and dynamics of solvation in these systems. While schematic pictures and considerable discussion of solvation structure are available in the literature, no attempt to quantitatively model these systems has been made to date [24]. The present chapter represents such an attempt.

We have performed Monte Carlo (and to a much lesser extent molecular dynamics) simulations of 7-AI and 1-AC in alcohol and water solvents. Using what we believe to be realistic intermolecular potentials we explore the structure and dynamics of solvation in these systems in an effort to determine whether the existing interpretations of the solvent participation in these reactions are reasonable. The simulations undertaken here are purely classical. If one adopts the perspective of Figure 2.1(b), the relative rates of reaction in different solvents should only reflect the equilibrium reactive fractions f^\ddagger in these solvents. Thus, the proton transfer step, which would require consideration of quantal aspects of the reaction, need not be explicitly considered. The bulk of this chapter concerns Monte Carlo simulations used to test the extent to which variations in solvation structure (i.e. f^\ddagger) are sufficient to understand the variations observed in the experimental rates. We have simulated a total of eight different hydroxylic solvents with either 7-AI or 1-AC as the solute. The results show that, in spite of the uncertainties in intermolecular potentials, the solvation structures simulated in both aqueous and

alcoholic solutions are semi-quantitatively consistent with the mechanistic description discussed in connection with Figure 2.1(b).

The outline of the remainder of the chapter is as follows. Section 2 describes the details of the simulation methods and the intermolecular potential functions employed. The results are then presented in Sec. 3 which is divided into five parts. Part 1 contrasts the nature of the hydrogen bonding present in dilute solution (where reaction is assumed to be rapid) and bulk methanol in order to display the qualitative nature of the solvent effect on reaction. Part 2 concerns the possible role of solvent dynamics in controlling the reaction rates. Here we employ molecular dynamics simulations in methanol and water to show that the TST perspective of Eq. 2.1 is a valid approximation. These results are also used to discuss the improbability of long-lived or “blocked” solvation states in these solvents. In Part 3 we discuss quantitative measures for the reactive fractions f^\ddagger and how these fractions are influenced by uncertainties in the charges used to model the interactions between the solute and solvents. The main results of this study are contained in Section 3.4, where we describe the nature of the solvation of 7-AI in the eight solvents, methanol, ethanol, 1-propanol, 2,2,2-trifluoroethanol (TFE), 2-propanol, *t*-butanol, ethylene glycol, and water, and how differences in solvation lead to differences in the reactive fractions simulated. Finally, in Part 5 we consider two additional aspects of the simulations that can be compared to experiment, the temperature and solute dependence of the reactive fractions in methanol and water. A summary of the main results of this work along with ideas for future directions is provided in Section 4. There is also an

Appendix to this chapter, in which we examine some features of the new set of solvent potentials used in this work in comparison to more standard potentials and experimental data.

2.2. Simulation Methods

2.2.1. Methodology.

A majority of the simulations reported here were Monte Carlo calculations carried out using the “BOSS” molecular simulation program developed by Jorgensen [25]. Simulations were performed in the isothermal-isobaric (NPT) ensemble at a temperature of 25 °C and 1 atm pressure. Each simulation system consisted of 104 (or 252 in the case of water) solvent molecules and one solute in a cubic cell, with periodic boundary conditions. Tests with larger system sizes showed that these relatively small samples were adequate to display bulk-like behavior for the properties of interest here.

Solvent-solvent interactions were spherically truncated at cutoff distances r_c based on oxygen-oxygen atom distances. A solute-solvent cutoff r_{sc} was applied such that if any solute atom-solvent oxygen atom distance was less than r_{sc} , the interaction between the entire solute and solvent molecule was included. In both cases these cutoffs were taken to be approximately one half of the periodic cell length. New configurations were generated by randomly selecting a molecule, and performing random moves of

translational, (external) rotational, and internal rotational coordinates. The ranges of each type of move were chosen to yield acceptance ratios of approximately 0.4 for new configurations. These ranges were 0.2 Å for translations, 20° for external rotations, and 15° for internal rotations. Attempts to change the volume of the system (with a range of $\pm 150 \text{ Å}^3$) were made every 700 configurations, and all intermolecular distances were scaled accordingly.

All simulations were started from a random configuration which had been previously equilibrated from a liquid-like arrangement of solvent molecules for a period of at least 2×10^7 configurations. Energies and densities were monitored in order to ensure adequate convergence within the equilibration period. After equilibration, simulations for a given system were performed in five or more segments of 2×10^7 configurations each in order to compute statistical uncertainties. The uncertainty values reported here are ± 1 standard deviation of the mean of the averages obtained from individual runs.

Both Boltzmann and non-Boltzmann sampling methods were employed in this work [27]. Non-Boltzmann sampling was required in order to quantitatively determine equilibrium constants for cyclic complex formation due to the fact that in a Boltzmann-sampled Metropolis scheme the “cyclic” region of phase space is only infrequently visited. In the sampling method adopted here acceptance of moves which are uphill in energy is biased by a weighing factor dependent on two key solute-solvent hydrogen

bonding distance parameters, R_{NH} and R_{HO} discussed in more detail in Sec. III. (see Fig. 2.3).

$$P(R_{NH}, R_{HO}) = \frac{w(R_{NH}, R_{HO})_{new}}{w(R_{NH}, R_{HO})_{old}} \times \exp(-\beta \Delta U) \quad (2.2)$$

In this equation, $P(R_{NH}, R_{HO})$ is the probability of a move's acceptance, β is the inverse of the absolute temperature multiplied by Boltzmann's constant, ΔU is the difference in potential energy between old and new configurations, and $w(R_{NH}, R_{HO})$ refers to a biasing function whose value depends on the intermolecular distances of the solute-solvent pair. For the latter we chose a "Gaussian cliff" shape [28]:

$$w = \begin{cases} 1 + a_1 \left\{ \exp\left(-a_2 \left[(R_{NH} - R_{NH}^0)^2 + (R_{HO} - R_{HO}^0)^2 \right] \right) \right\} & R_{NH} \geq R_{NH}^0, R_{HO} \geq R_{HO}^0 \\ 1 + a_1 & R_{NH} < R_{NH}^0, R_{HO} < R_{HO}^0 \end{cases} \quad (2.3)$$

This weighing function is only applied for moves involving the particular solvent molecule closest to the solute (defined in terms of R_{NH}). The distances R_{NH}^0 and R_{HO}^0 were both set to 2.0 Å and the height ($20 < a_1 < 200$) and width parameters ($1 < a_2 < 3 \text{ Å}^{-1}$) of the "cliff" were chosen for each solvent so as to best sample both the "cyclic" region and the non-cyclic regions of phase space visited by a Boltzmann-weighted simulation. The latter condition is necessary in order to use a pair of simulations (one biased and one unbiased) in order to compute the desired equilibrium population densities, ρ_0 , from the density observed in the biased simulation ρ_w via the relation:

$$\rho_0(R_{NH}, R_{HO}) = \frac{\rho_w(R_{NH}, R_{HO})/w(R_{NH}, R_{HO})}{\langle 1/w(R_{NH}, R_{HO}) \rangle_w} \quad (2.4)$$

The results obtained for ρ_0 using this scheme were compared to those found using a regular Boltzmann sampled simulation in the region where both simulations sampled adequately to insure that the parameters were chosen reasonably.

In addition to the Monte Carlo calculations, which comprise the majority of this chapter's content, molecular dynamics simulations were also performed for two systems: 7-AI in methanol and water. These simulations were performed in the NVE ensemble with cubic periodic boundary conditions using programs described in Ref. 29. The number of molecules was the same as in the MC runs and the density and average kinetic energy were chosen to correspond as closely as possible to the (NVT) Monte Carlo simulations.

2.2.2. Intermolecular Potential Functions.

2.2.2.1. General Form. Molecules were represented as collections of interaction sites with intermolecular interactions modeled via site-site Lennard-Jones plus Coulomb terms,

$$v_{ij} = 4\epsilon_{ij} \left[\left(\frac{\sigma_{ij}}{r_{ij}} \right)^{12} - \left(\frac{\sigma_{ij}}{r_{ij}} \right)^6 \right] + \frac{q_i q_j}{r_{ij}} \quad (2.5)$$

The Lennard-Jones parameters between unlike atoms were determined from the like-atom parameters (provided below) using the mixing rules $\sigma_{ij} = \sqrt{\sigma_{ii}\sigma_{jj}}$ and $\varepsilon_{ij} = \sqrt{\varepsilon_{ii}\varepsilon_{jj}}$. In general, each atom within a molecule corresponded to an individual site, with the exception of the CH_n groups of the alcoholic solvents, which were taken as single units centered on carbon. (In the dilute solution studies the cyclohexane supporting solvent was also modeled as a single Lennard-Jones site.)

2.2.2.2. Solute Models. The solutes, 7-AI and 1-AC, were both represented by rigid all-atom models. The geometries were those optimized for the ground states calculated at the restricted Hartree-Fock level using the semi-empirical MNDO hamiltonian [30]. The Lennard-Jones parameters were taken from the OPLS potential functions for nucleotide bases [31], and are listed in Table 2.1.A. The charges used in the modeling were from electrostatic potential fits of the ground-state HF wave functions generated using a 6-31G* basis set [32]. These charges are shown in Fig. 2.2. A complete set of charges and coordinates for the solutes is available in the supplementary material.

Some comment should be made regarding the use of ground state charges to model solvation effects in these excited-state reactions. This choice is dictated by our inability to accurately calculate the excited state charge distributions of these molecules. Based on considerable prior work [33] as well as results with 7-AI and 1-AC [34] we

Table 2.1: Solute Properties and Potential Parameters

A. Lennard-Jones Parameters^a

atom type	σ (Å)	ϵ (kcal/mol)
C	3.5	0.08
N	3.25	0.17
H(-C)	2.5	0.05
H(-N)	0.0	0.0

B. Electrical Properties Calculated for the Ground and Low-Lying Excited States

state	calculation ^b	E^c (kJ/mol)	μ (D)	θ_μ^d (deg)	q_{N5}^e (au)	q_{N6}^e (au)	q_H^e (au)
7-Azaindole							
S_0	6-31G*	(0)	1.67	33	-0.57	-0.67	+0.41
S_0	AM1/CI	(0)	1.53	22	-0.44	-0.36	+0.40
S_1	AM1/CI	330 (412)	2.72	15	-0.44	-0.38	+0.41
S_2	AM1/CI	377	4.20	8	-0.38	-0.44	+0.39
1-Azacarbazole							
S_0	6-31G*	(0)	1.15	56	-0.81	-0.71	+0.46
S_0	AM1/CI	(0)	0.82	53	-0.71	-0.40	+0.45
S_1	AM1/CI	320 (361)	1.50	20	-0.61	-0.38	+0.45
S_2	AM1/CI	345	1.36	8	-0.69	-0.44	+0.46

^a Parameters optimized for nucleotide bases in ref 31. ^b See text and ref 35 for details.

^c Values in parentheses are experimental gas-phase values estimated from the data in ref 41. ^d Dipole orientation as defined in Figure 2. ^e ESP-fit charges of the nitrogen atoms of the five- and six-membered rings (“ q_{N5} ” and “ q_{N6} ”) and the transferring H atom (q_H).

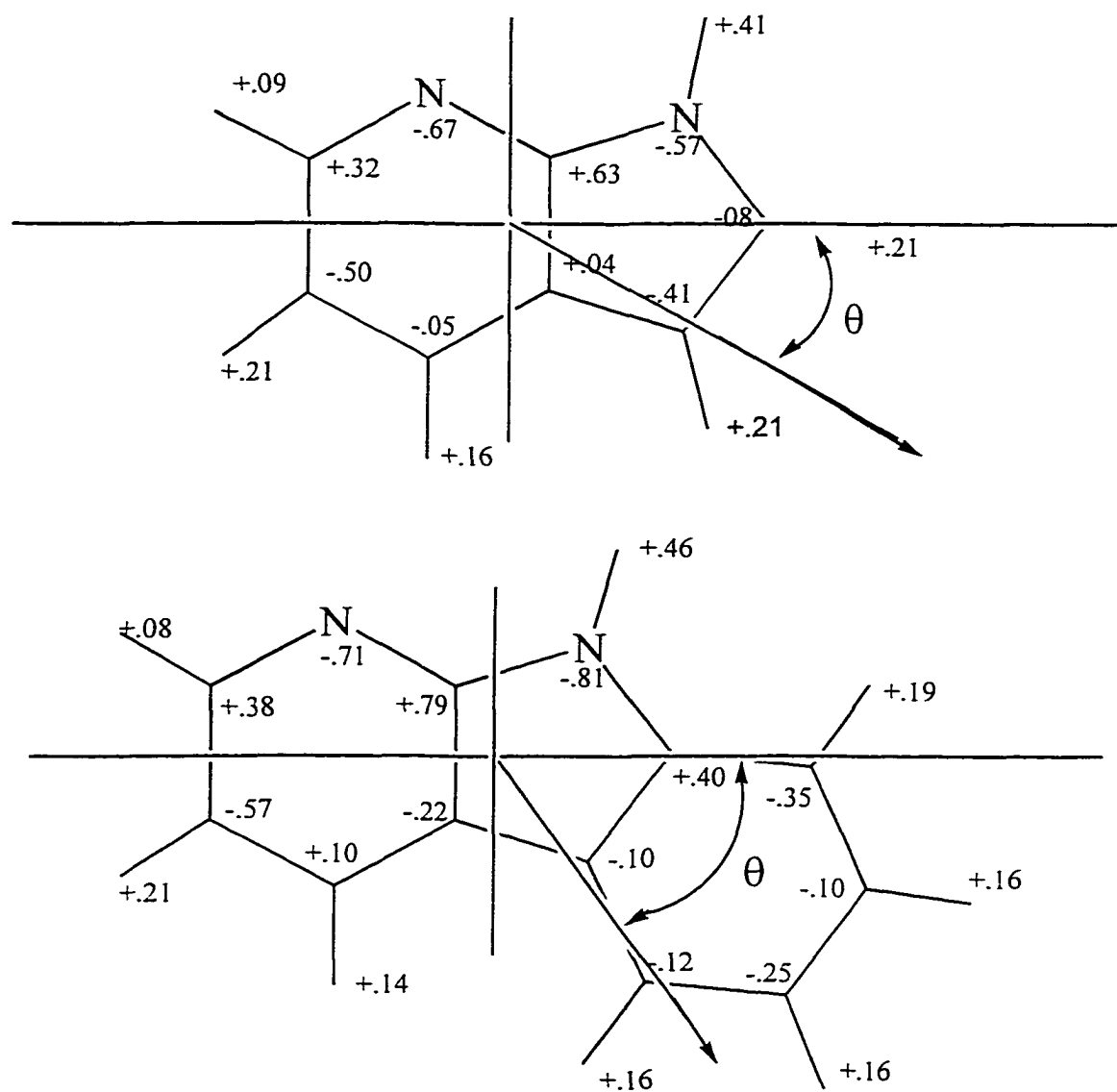


Figure 2.2. Charges used in modeling the solutes 7-AI and 1-AC. These charges are from ESP fits to the HF 6-31G* ab initio wave functions of the solutes (for geometries optimized using the MNDO semiempirical method).

trust that the ESP-fit charges calculated at the 6-31G* provide good representations of electrical interactions between the ground states of these solutes and other molecules. However, it is not possible to calculate excited-state properties of such large molecules using either *ab initio* or semi-empirical methods with comparable accuracy. Thus, we rely on the ground state charges and assume that, at least at the solute “active sites” for reaction and hydrogen bonding, they do not differ much between the ground and excited states. Some evidence in support of this assumption is provided by the semi-empirical calculations shown in Table 2.1B. Here we compare some electrical characteristics of the solutes in different electronic states derived from AM1-CI calculations [35]. As can be seen from this table, there is very little difference between the charges that should determine solute- solvent hydrogen bonding in the ground and lowest-lying excited states of either solute.

2.2.2.3. Solvent Models. Two different solvent representations based on the OPLS models of Jorgensen [37-39] were employed here. Parameters are listed in Table 2.2. Both representations use the standard bond lengths and bond angles of the OPLS set, which are described in Ref. 38. These parameters are kept fixed during the simulations, but torsional motion is included using the torsional potentials also taken from the OPLS parameterization [38]. The difference between the two types of solvent representation involves only the charges on the H and O atoms of the hydroxyl group and the C atom to which it is attached (“C_O” in Table 2). The first set comprises what we will term the “*ab initio*” solvents, so-called because charges were obtained from ESP fits to the charge

Table 2.2. Parameters of the Solvent Models^a

Solvent	atom/group	q (au)	σ (Å)	ϵ (kcal/mol)
"Ab Initio Solvents"				
methanol	- O	-0.674	3.070	0.170
	- H	+0.424	0.0	0.0
	- CH ₃	+0.250	3.775	0.207
ethanol	- O	-0.710	3.070	0.170
	- H	+0.417	0.0	0.0
	- CH ₂	+0.338	3.905	0.118
	- CH ₃	-0.045	3.775	0.207
1-propanol	- O	-0.717	3.07	0.170
	- H	+0.421	0.0	0.0
	- CH ₂	+0.311	3.905	0.118
	- CH ₂	+0.077	3.905	0.118
	- CH ₃	-0.092	3.775	0.207
2-propanol	- O	-0.756	3.070	0.170
	- H	+0.430	0.0	0.0
	- CH	+0.665	3.850	0.080
	- CH ₃	-0.170	3.910	0.160
<i>tert</i> -butyl-alcohol	- O	-0.770	3.07	3.170
	- H	+0.428	0.0	0.0
	- C _o	+0.856	3.80	0.05
	- CH ₃	-0.171	3.96	0.145
	- O	-0.611	3.07	0.170
trifluoroethanol	- H	+0.427	0.0	0.0
	- CH ₂	+0.230	3.905	0.118
	- C(F) ₃	+0.570	3.80	0.1094
	- F	-0.205	3.50	0.061
	- O	-0.667	3.07	0.170
ethylene glycol	- H	+0.423	0.0	0.0
	- CH ₂	+0.244	3.905	0.118
	- O	-0.791	3.1506	0.1521
water	- H	+0.395	0.0	0.0
	- O	-0.684	3.0	0.17
	- H	+0.455	0.0	0.0
	- C	+0.908	3.75	0.105
	- CH ₃	-0.042	3.91	0.16
acetic acid	= O	-0.637	2.96	0.21
	- C ₆ H ₁₂	+0.000	5.65	0.590
	- C ₆ H ₁₂	+0.000	5.65	0.590
OPLS Solvents				
alcohols	- O	-0.700	3.070	0.170
	- H	+0.435	0.0	0.0
	- C _o	+0.265	3.775	0.207
TIP3P water	- O	-0.834	3.1506	0.1521
	- H	+0.417	0.0	0.0
SPC water	- O	-0.820	3.1656	0.1554
	- H	+0.410	0.0	0.0

^a Other than the charge parameters for the ab initio solvents, which were obtained from ESP fits to the 6-31G* wave functions, all but the F atom parameters are from the OPLS set described in refs 37-39. Parameters for the CF₃ group were adapted from ref 40.

distribution generated from geometry-optimized 6-31G* calculations. The second set of solvents are the true OPLS models, in which these charges were optimized for liquid state properties by Jorgensen and coworkers [38,39]. The latter solvents maintain the same charges for the three atoms mentioned above in all alcohols. In reality, over the set of alcohols examined here one observes significant variations in the ESP-fit / *ab initio* charges at these sites. Since such variations might be significant in determining the reactive fractions of interest, we chose the *ab initio* solvents as our primary working models despite their slightly poorer performance in reproducing properties of the pure liquid solvents. (See the Appendix for details.)

2.3. Results and Discussion

2.3.1. *General Behavior: Isolated Complexes versus Bulk Solvents.*

One of the clearest indications that solvation structure is a primary determinant of reaction rates in 7-AI and 1-AC / alcohol systems is the contrast between the rates observed in bulk alcohol solvents and dilute solution. In the latter case, when only isolated 1:1 complexes are formed, reaction occurs hundreds to thousands of times faster than in bulk alcohol solvents. We therefore begin with a comparison of the differences in the solvation structures simulated under these two conditions. We consider 1:1 and 1:2 complexes of 7-AI with methanol and other hydrogen bonding partners in dilute solution. To mimic a non-associating background solvent of the sort employed in experiment, we

use a single-site Lennard-Jones model of “cyclohexane” (Table 2.2). Representative results are shown in Fig. 2.3.

In Fig. 2.3 and later figures we display the solvation structure in a given system using 2-dimensional plots of the relative frequency of occurrence of a pair of distances, R_{NH} and R_{HO} . These two distances specify the hydrogen bonding between the solvent and the two “active sites” for reaction, the pyridyl N: atom and the transferring H atom, as indicated in Fig. 2.3. When only a single methanol molecule is present in the simulation (“7-AI:MeOH”), the configurations observed are predominantly structures in which both distances R_{NH} and R_{HO} are approximately 2 Å. These distances imply that most of the time the lone alcohol molecule is simultaneously hydrogen bonded to both active sites of the solute, as illustrated in Scheme 2. This structure is presumably what is required for reaction and, in keeping with past nomenclature, we label it as “cyclic”. Note that the distribution of the 7-AI:MeOH complex shows it to be reasonably “loose”, with a substantial fraction of the population occurring with R_{NH} distances that are larger than nominal hydrogen bonding distances (~ 2.5 Å). Thus, whereas the H_U-O_V hydrogen bond is intact nearly all of the time, the N_U-H_V hydrogen bond is frequently broken in the cyclic complex. (Here and in what follows the subscripts “U” and “V” denote atoms of the solute and solvent, respectively.) This situation in the methanol 1:1 complex should be contrasted with that of the 1:1 7-AI:acetic acid complex, also shown in Fig. 2.3. In this complex, short hydrogen bonding distances to the acid H(-O) and O(=C) atoms are found essentially 100% of the time.

When more than a single alcohol molecule is present there is a marked change in the type of solvation observed. As illustrated by the 7-AI:(MeOH)₂ data in Fig. 2.3, two peaks rather than one appear in the population distribution. These peaks occur with one of the distance parameters being ~ 2 Å (hydrogen bonded), and the other being distinctly greater than 2 Å, spanning a range from about 2.5 to 4 Å. This change reflects the loss of cyclic complexes and the dominance of the second type of structure shown in Scheme 2. This class of configurations, which we designate as “8-membered ring” structures is one in which two solvent molecules are singly hydrogen bonded to the solute, and also hydrogen bonded to one another. It has been speculated that this type of arrangement may facilitate tautomerization via a 3-proton shuttling mechanism in systems such as 7-hydroxyquinoline, in which the active sites are too widely separated to be bridged by a single solvent molecule [42]. However, the results presented below suggest that such a 3-proton shuttling mechanism does not play a significant role in the 7-AI or 1-AC reactions. Note that the peaks in the distribution of the 2:1 complex are much narrower than in the 1:1 case, which reflects the more rigid hydrogen-bonding present in this case.

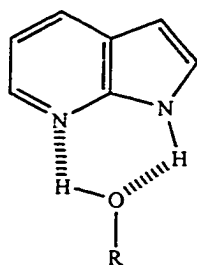
The situation in bulk methanol appears outwardly similar to that existing in the 1:2 complex. The addition of many more possible hydrogen bonding partners results in even fewer occurrences of “cyclic” solvation. However, careful inspection of Fig. 2.3 also reveals that the long R_{NH} and R_{HO} distances are in fact larger than in the 1:2 complex. The peaks are also broader. These differences reflect the fact that the predominant mode of solvation in bulk methanol does not involve the 8-membered ring

SCHEME 2

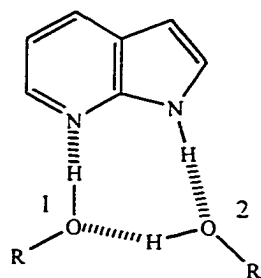
Hydrogen Bonding Structures

Reactive Configuration

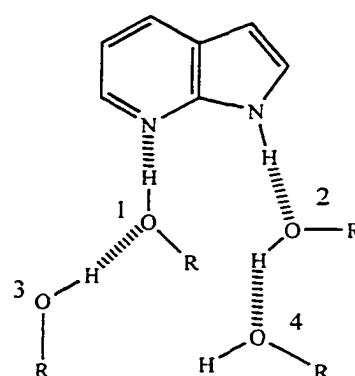
"Cyclic"

Unreactive Configurations

"8-membered ring"



"Neighbor Bonded"



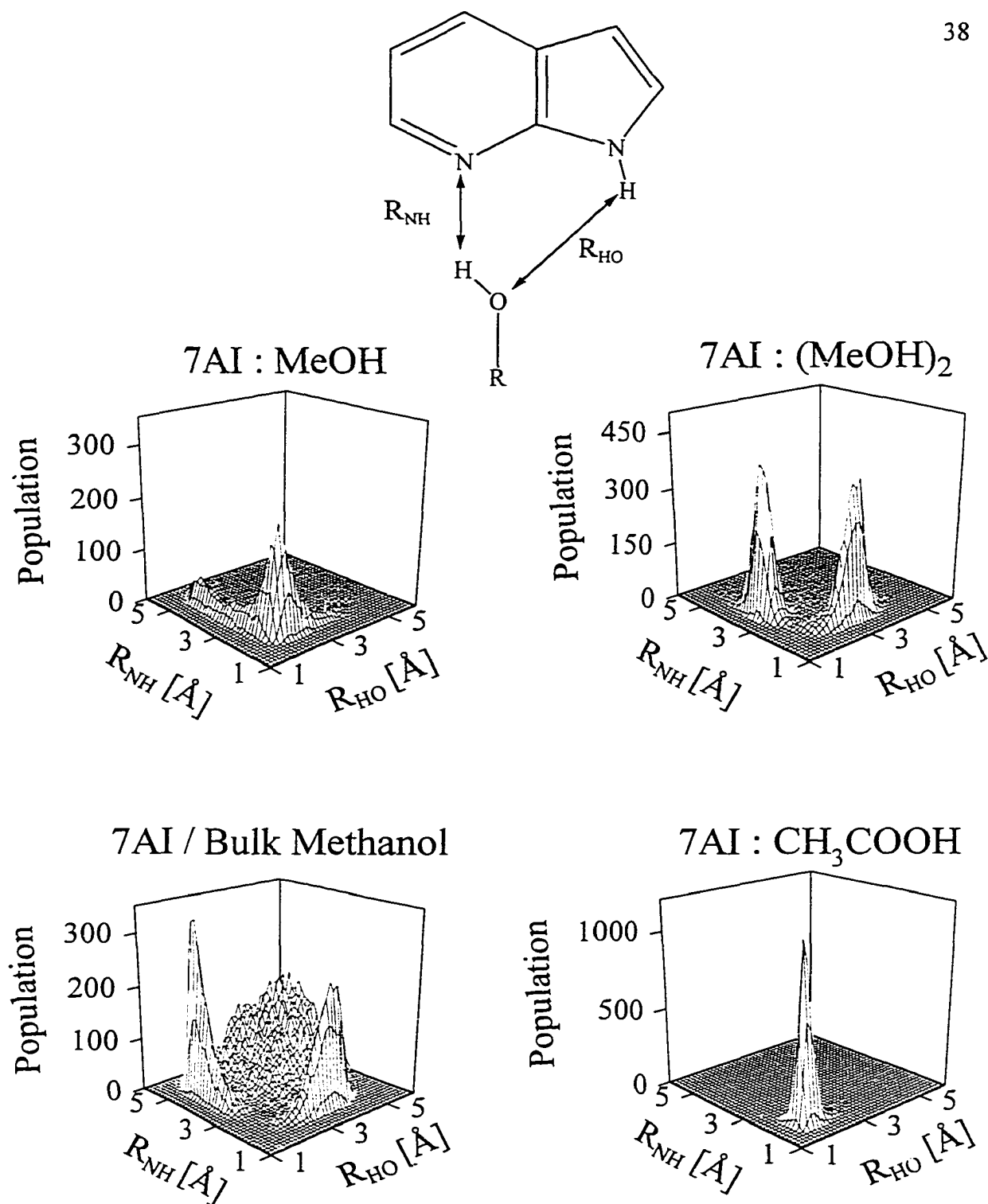


Figure 2.3. Hydrogen-bonding distance distribution (see text) observed in simulations of 7-AI in cyclohexane containing either one or two molecules of methanol, one molecule of acetic acid, or bulk methanol solvent. In the case of acetic acid, the R_{HO} distance plotted is the distance from the carbonyl oxygen of the acetic acid to the H(N) atom of 7-AI.

structure but rather “neighbor-bonded” structures of the sort illustrated in Scheme 2. In bulk solution the two alcohol molecules hydrogen bonded to the solute mainly form hydrogen bonds to other neighboring solvent molecules rather than to one another. (As will be discussed later, in methanol one only observes the 8-membered ring structure to occur ~7% of the time.)

These examples, taken from simulations of methanol with 7-AI, are typical of the behavior observed with 7-AI or 1-AC in other alcohol solvents. The general conclusions one draws from such simulations are in keeping with what has been postulated on the basis of experimental results. When 7-AI or 1-AC can form 1:1 complexes with alcohols or other appropriate hydrogen bonding partners it usually forms cyclically hydrogen bonded structures which facilitate rapid reaction. But formation of “correct” cyclic structures is severely inhibited in bulk alcohol solvents. In bulk alcohols, or indeed whenever more than a single alcohol molecule is available there is a strong preference for two different solvent molecules to hydrogen bond to the solute, a situation which appears to prohibit proton transfer.

The reason why cyclic forms are disfavored in bulk alcohols is simply a matter of the poor hydrogen bonds afforded by the cyclic structure. Figure 2.4 serves to illustrate this point. Here we have plotted distributions of the molecular pair interaction energies corresponding to the systems in Fig. 2.3. The average interaction energy between 7-AI and methanol in the isolated 1:1 complex, where the cyclic structure predominates, is -27.5 kJ/mol. Dividing this value by the number of hydrogen bonds in the structure

yields ~14 kJ/mol per hydrogen bond -- a relatively small value indicative of weak hydrogen bonding [43]. In the 7-AI:(MeOH)₂ complex, where the 8-membered ring structure predominates, the three solute-solvent and solvent-solvent interactions amount to ~25 kJ/mol per hydrogen bond, a much more respectable number. A similar value is also found in the “neighbor bonded” structure characteristic of bulk methanol solvation, ~24 kJ/mol per hydrogen bond. Thus, as soon as more than a single alcohol molecule is available for hydrogen bonding with the solute it is energetically advantageous to break up the cyclic structure in favor of these other, non-cyclic structures. As will be discussed later, the free energy penalty paid for reaching the cyclic form is essentially just this energy cost of trading strong for weak hydrogen bonds.

Hydrogen bonds are relatively weak in cyclic 7-AI alcohol complexes mainly as a result of the poor geometric fit that a single O-H bond from an alcohol molecule makes with the 7-AI “active site”. This fact is evident when one compares the energetics and geometries of the 1:1 acetic acid and alcohol complexes. Energy minimized structures of these complexes derived from the simulation potentials are shown in Fig. 2.5. (*Ab initio* calculations of these complexes yield similar structures [4,44,45].) With acetic acid and geometrically comparable molecules such as amides [4] the 1:1 complex is “tighter” (as shown by the distributions in Fig. 2.3) and the average hydrogen bonding energy is much larger, ~28 kJ/mol. This is primarily because the complexing agent’s geometry allows for more nearly linear hydrogen bonds to both solute sites.

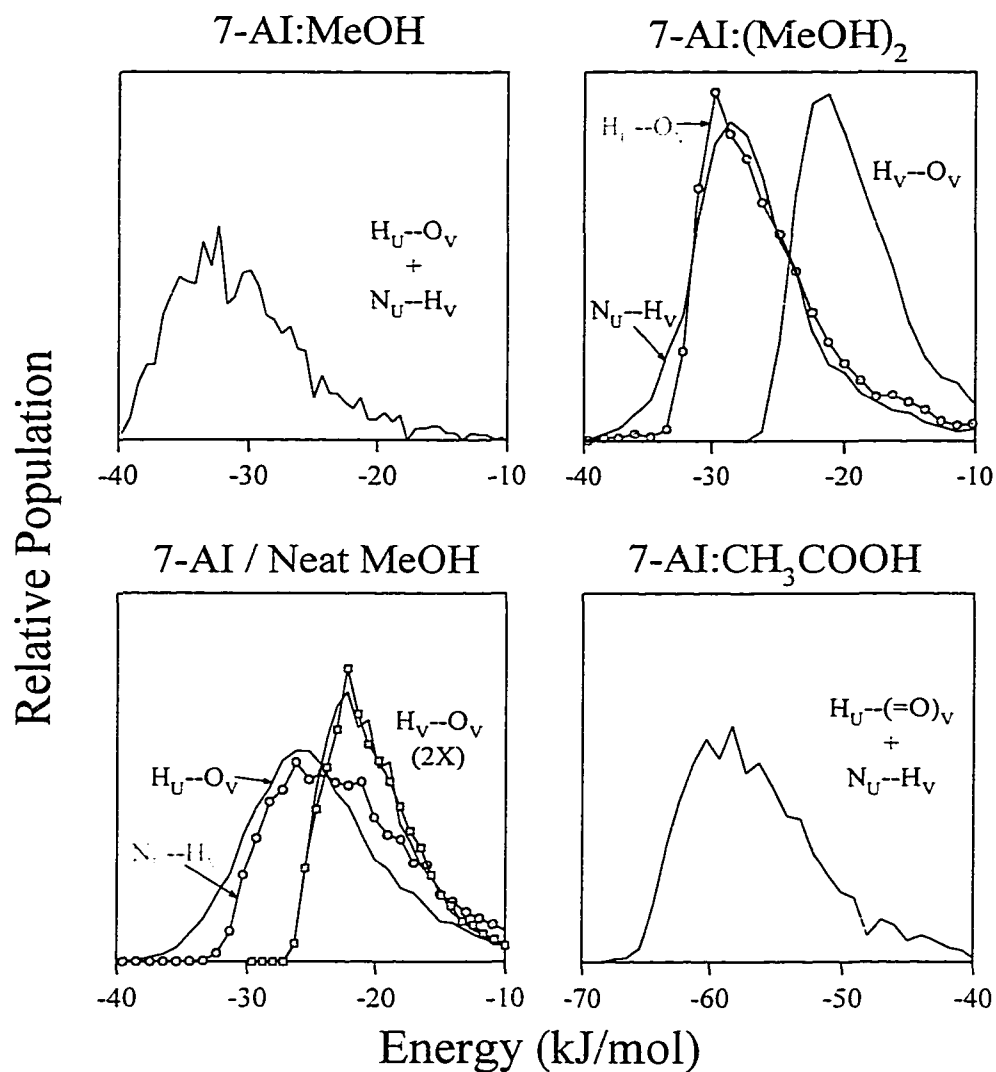


Figure 2.4. Pair energy distributions observed in the same systems as in Figure 2.3. These energies are the total interaction energies between pairs of molecules in the solvation structures shown in Scheme 2. Indicated on each panel are the particular hydrogen-bonding interactions involved in each pair interaction, with N_U and H_U denoting the solute active sites and H_V and O_V solvent sites. In the case of the 1:1 complexes, the single molecular pair interaction incorporates two hydrogen-bonding interactions, while the 1:2 complex and bulk solvent there are three and four pairs involved, respectively (see Scheme 2).

The two solutes 7-AI and 1-AC should be nearly identical in this regard (see Part F) and variation of the identity of the alcohol also makes little difference to this observation. It is useful to recognize, however, that a single alcohol molecule can provide strong cyclic bonding in some situations. A recently reported case is the solute “DPC” illustrated in Fig. 2.6. In this case, the additional separation of the active sites leads to a good geometric fit and strong cyclic hydrogen bonding. As shown in the top panel of Fig. 2.6, the population distribution of DPC in bulk methanol is such that there is essentially always an alcohol molecule cyclically bonded to one of the two active sites. In contrast to the 7-AI and 1-AC reactions, this solute was observed to undergo unresolvably rapid ($\tau_{\text{rxn}} < 30$ ps) tautomerization in methanol at room temperature [46].

2.3.2. Possible Dynamical Solvent Effects on the Reaction Rate.

The interpretation of the 7-AI and 1-AC reactions described in Section 2.1 assumes that the solvent’s influence is primarily a static rather than a dynamic effect. That is, differences in the reaction rates observed in different solvents are viewed as resulting from variations in the equilibrium free energy change between reactive and non- reactive forms, and not the dynamics of inter-conversion between these forms. In order to verify this assumption we have performed molecular dynamics simulations in two bulk solvents, methanol and water.

To assess the importance of dynamical solvent effects, we employ the “stable-

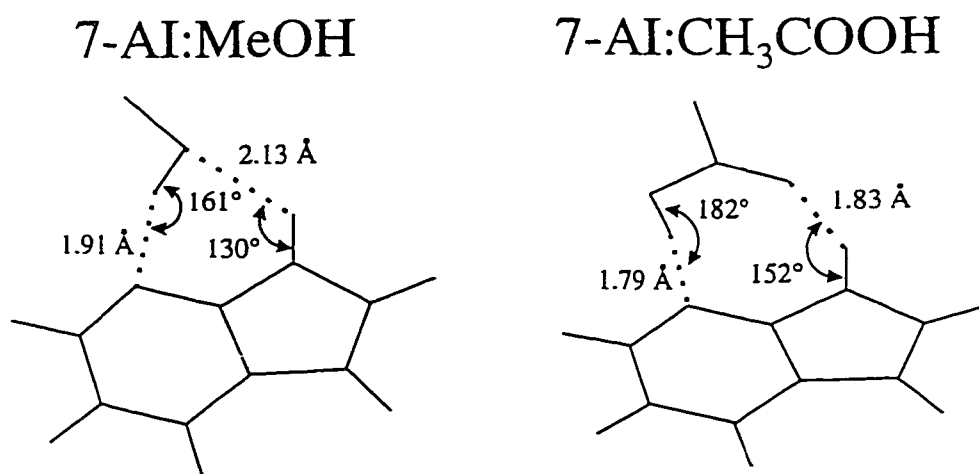


Figure 2.5. Structures of the energy-minimized (gas-phase) 7-AI-methanol and 7-AI-acetic acid complexes. These structures were derived with the classical potential energy functions used in the simulation.

Dipyrido[2,3-*a*:3',2'-*i*]carbazole (DPC) ⁴⁴

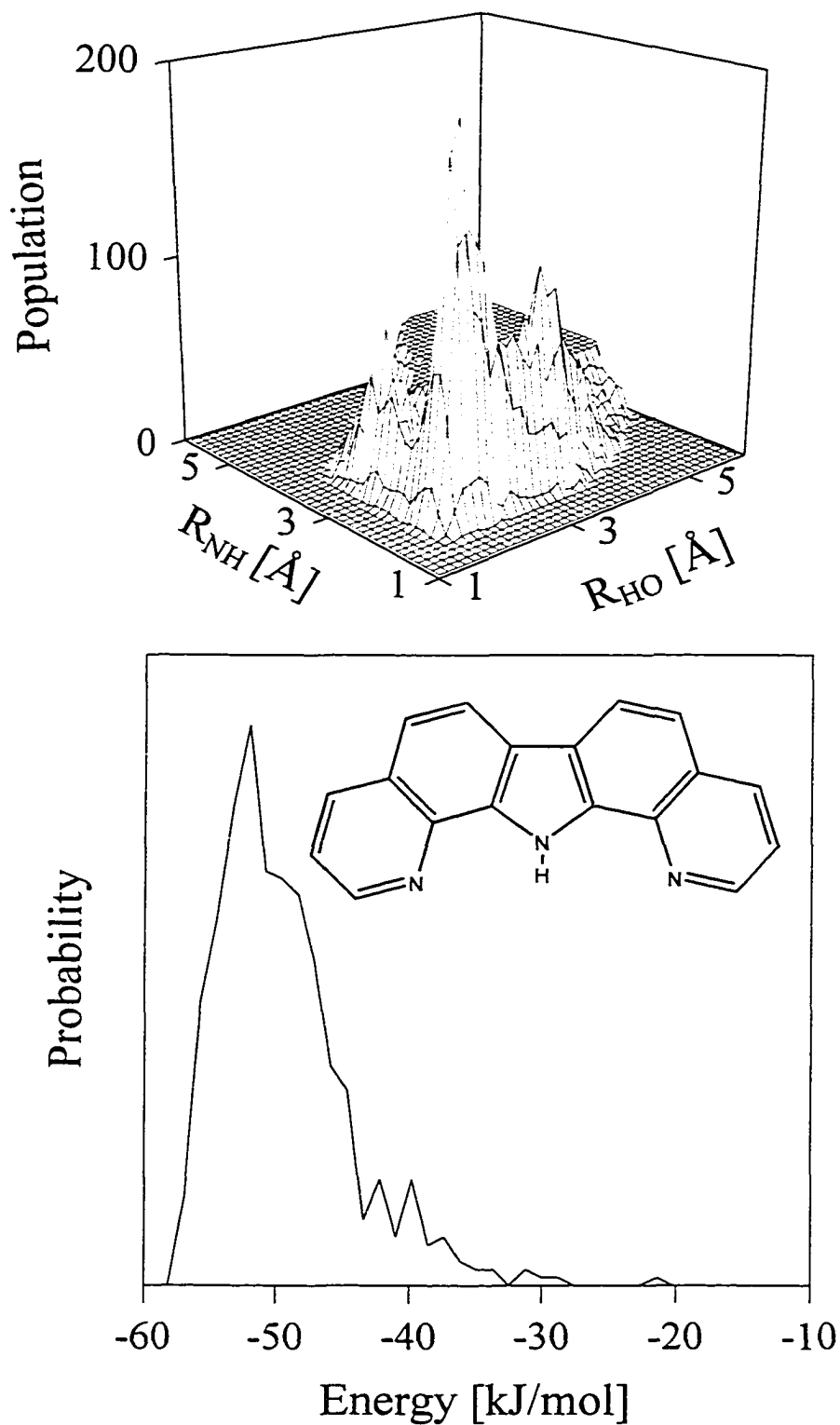


Figure 2.6. Hydrogen-bonding distance and pair energy distribution simulated for the DPC solute in methanol.

states picture” (“SSP”) of Hynes and coworkers [47]. Within the SSP formalism the net rate constant k_{net} observed for an irreversible activated process is given by:

$$k_{net}^{-1} = k_i^{-1} + k_D^{-1} \quad (2.6)$$

where k_i is the rate constant associated with the barrier crossing when internal equilibrium is maintained within the reactant region and k_D is the rate constant associated with producing this reactant equilibrium. In the present context k_i represents the reaction rate (k_{obs}) of Eq. 2.1, which implicitly assumes that solvent dynamics are rapid enough that f^\ddagger represents the equilibrium fraction of reactive species. The constant k_D then represents the rate at which the hydrogen bonding rearrangements inter-convert between the reactive and non-reactive forms. From Eq. 2.6 one sees that for $k_D \gg k_i$ the solvent dynamics becomes irrelevant and $k_{net} = k_i$, as has been assumed in writing Eq. 2.1. Thus, the equilibrium assumption can be tested by comparing k_D with $k_i = k_{PT} f^\ddagger$. According to the SSP, k_D is given by [48]

$$k_D^{-1} = \frac{1}{f^\ddagger} \int_0^\infty dt \{P(\ddagger, \ddagger; t) - f^\ddagger\} \quad (2.7)$$

where $P(\ddagger, \ddagger; t)$ is the conditional probability that if the system is in the reactive configuration (“ \ddagger ”) at time zero it will also be found there at some later time t . Since $f^\ddagger \ll 1$ (see below), given the form of Eqs. 2.7 and 2.1, the comparison to be made here reduces to comparing the “survival time” of the reactive configuration,

$$\tau_{\ddagger} = \int_0^{\infty} dt P(\ddagger, \ddagger; t) \quad (2.8)$$

with the intrinsic proton transfer rate τ_{PT} once the reactive geometry is achieved.

Figure 2.7 shows the survival probabilities $P(\ddagger, \ddagger, t)$ determined for 7-AI in bulk methanol and water solvents. (How we define a reactive geometry is discussed in detail in the following section; here we employ the criterion $R_{NH}=R_{HO}=2.69$ Å.) The plots in Fig. 2.7 were generated from equilibrium molecular dynamics simulations simply by waiting for the system to adopt a reactive geometry and then following its fate forward and backward in time from there. Although the data are somewhat noisy (only 19 occurrences of reactive geometries were observed in methanol and 22 in water) they suffice to show that the survival times for this definition of reactive geometry are in the sub-picosecond range. As will be discussed in the following section, the estimated value of τ_{PT} is predicted to be at least 10-fold larger for this same definition of reactive geometry. Other definitions also yield comparable results. In all cases the cyclic geometry is sufficiently unstable in bulk methanol and water that it not only occurs infrequently but when it does occur it persists for only a very short time [49]. Thus, the assumption that it is a static solvation property (f^{\ddagger}) and not the time dependence of solvation that determines the reaction rates appears justified.

In addition to these survival times, it is also of interest to briefly consider other measures of the dynamics of the solute-solvent hydrogen bonding structure in these

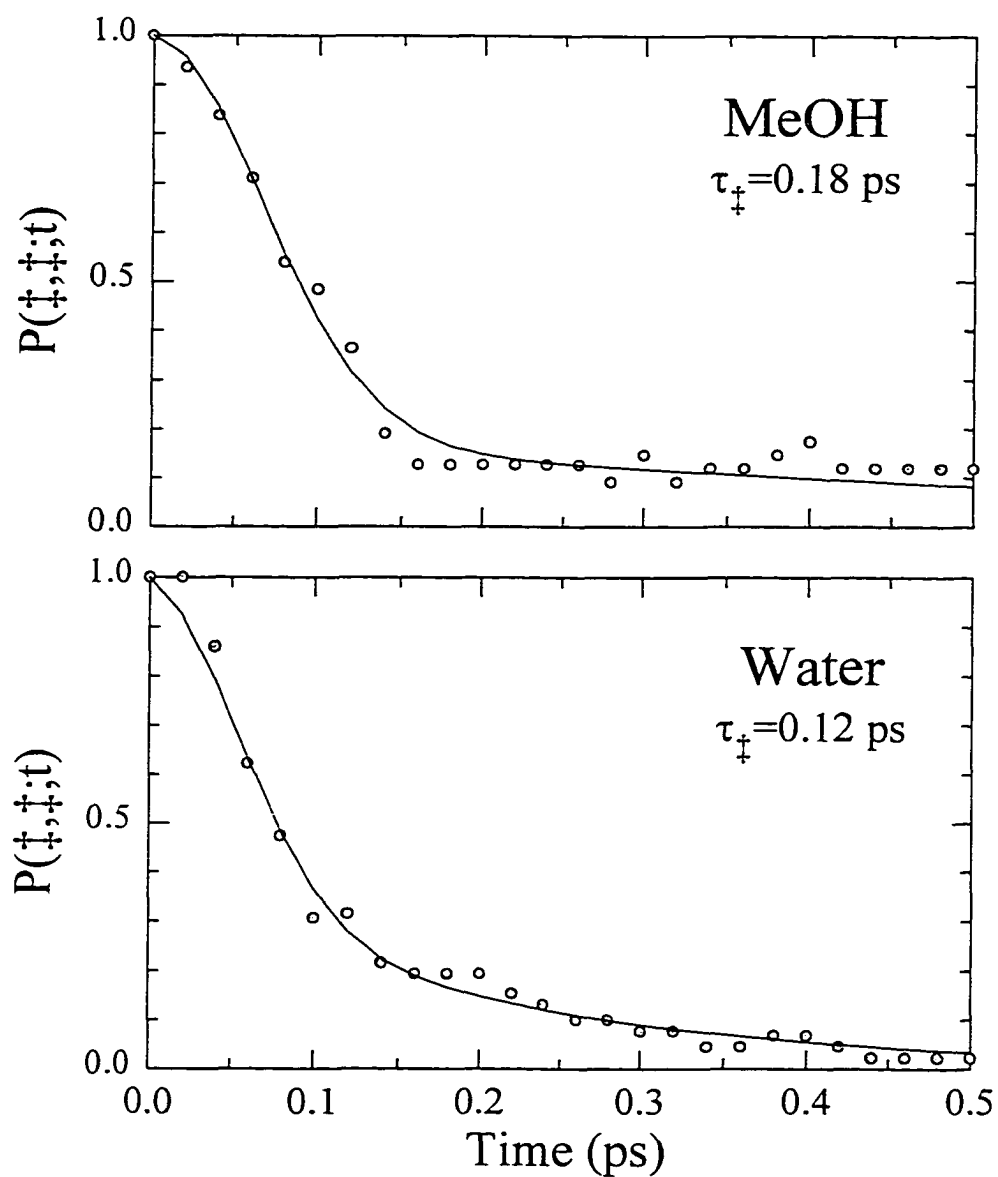


Figure 2.7. Time-dependent survival probabilities of cyclic structures ($R_{\text{NH}}, R_{\text{HO}} < 2.69$ Å) observed in methanol and water. The values of τ_{\ddagger} are the integrals under these functions.

systems. We do so mainly in light of conjectures about “blocked” solvation states of 7-AI in alcohol and water solvents. To explain the distinctive spectral features of 7-AI in water, other workers have proposed that while some 7-AI molecules can undergo rapid reaction, a large fraction exist in solvation environments that preclude reaction for times of a nanosecond or more [15,16,18]. Several features of the present simulations make such long-lived solvation states seem unlikely. For example, we find that solvent molecules bound to 7-AI have roughly the same diffusional characteristics as bulk solvent molecules. (Experimentally, water and methanol have approximately the same self-diffusion constant at room temperature, $2.3\text{-}2.4 \times 10^{-5} \text{ cm}^2 \text{ s}^{-1}$ [50]) A molecule of methanol or water hydrogen bonded to either “active site” of 7-AI is observed to diffuse out of the first solvation shell (i.e. move a distance of $\sim 3 \text{ \AA}$) in a time of 3-5 ps, just as would be expected from these bulk diffusion constants. The lifetime of a solute-solvent hydrogen bonded pair observed here is comparable to the lifetimes of solvent-solvent hydrogen bonds in the neat liquids [51].

As another measure of the time scale for structural relaxation we also examined how long a particular group of solvent molecules maintained “contact” with the solute. By defining a spherical region of radius R surrounding the “active-site” for reaction (choosing the origin midway between the N_U and H_U atoms) we monitored the exchange dynamics of molecules within this region via the correlation function:

$$C_N(t) \equiv \frac{\left\langle \sum_i \theta[R - r_i(t)] \cdot \theta[R - r_i(0)] \right\rangle}{\left\langle \sum_i \theta[R - r_i(t)] \right\rangle} \quad (2.9)$$

In this expression θ represents the Heaviside step function and r_i denotes the position of the oxygen atom of solvent molecule i . This correlation function reports on the fraction of the molecules that were originally solvating the active site still remaining in this region after an elapsed time t . Figure 2.8 shows such $C_N(t)$ functions for 7-AI in methanol and water. For R values encompassing a reasonable number of solvent molecules (5-20), the decay of this function is relatively insensitive to the particular choice of R . (As illustrated in the top panel of Fig. 2.8, one finds nearly identical $C_N(t)$ functions for two choices of R (5.0 and 6.0 Å) which contain an average of 5 and 9 solvent molecules.) As noted on the figure, the correlation times of these correlation functions involving ~10 solvent molecules are 9 and 3 ps in methanol and water, respectively. By times of order 100 ps there is little probability of finding even a single one of the original ten solvent molecules still solvating the active site of the 7-AI solute. We also note that there is nothing exceptionally slow about water compared to alcohols like methanol. To the contrary, the reorganization dynamics in water are considerably faster than the dynamics in methanol, and presumably also those in larger alcohols. Thus, if the simulations performed here are at all realistic, it is difficult to envision how “blocked” solvation states could persist for times of order a nanosecond in the 7-AI/water system.

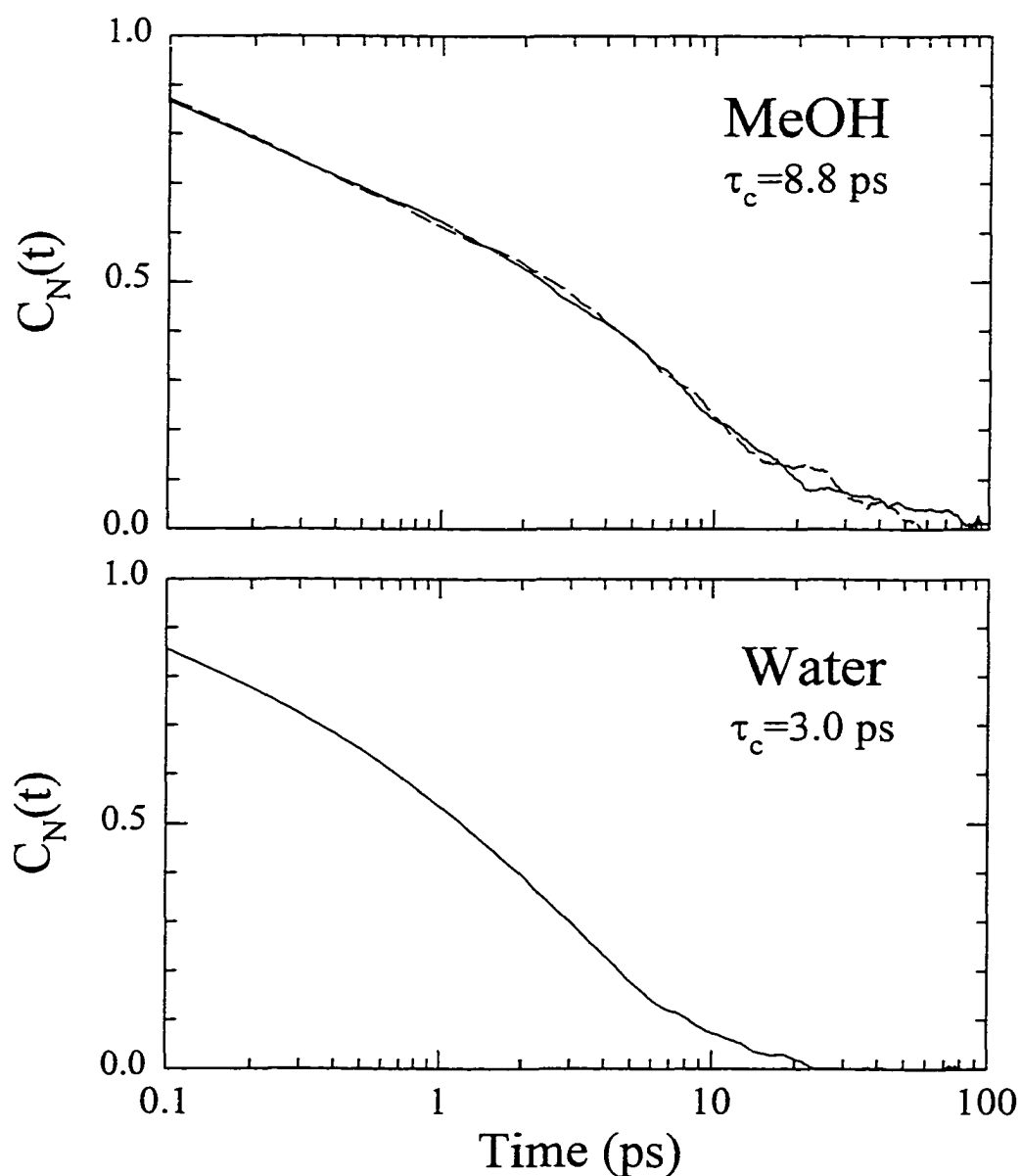


Figure 2.8. Structural time correlation functions (eq.2.3.4) in methanol and water. In the methanol case two curves are shown, corresponding to calculations involving spherical regions surrounding the solute active site with radii $R = 5$ (solid) and 6 (dashed) Å. These two regions enclose an average of five and nine solvent molecules, respectively. In the water case the radii was 5 Å and the region contained an average of ~ 10 solvent molecules. The values of τ_c noted are the integrals under these functions.

2.3.3. *Quantitative Estimation of Reactive Fractions and Reaction Rates.*

Given that the dynamics of the solvation process exert only a minor influence over the rates of these reactions, we now focus exclusively on quantitative estimates of the reactive fraction f^\ddagger , or equivalently, the free energy change ΔG^\ddagger . Doing so requires that we choose a definition of which solvent configurations constitute reactive forms. Although there has been some study of the ground-state reaction path in 1:1 complexes of 7-AI with water and methanol [45], the choice is not clear cut. After considering several possible geometric and energetic criteria [52] we settled on the simplest choice, which is based on the two hydrogen bonding distances R_{NH} and R_{HO} already discussed. Specifically, we measure the fractional populations $f(R^\ddagger)$ contained within regions of (R_{NH}, R_{HO}) space defined $(R_{NH} \leq R^\ddagger, R_{OH} \leq R^\ddagger)$, for three different values of R^\ddagger : 2.19, 2.44 and 2.69 Å. The smallest value, $R^\ddagger = 2.19$ Å, corresponds approximately to the distances observed in the minimum energy structures of gas phase complexes between 7-AI and water or methanol as determined from either *ab initio* calculations [44,45] or from classical calculations using the simulation potentials (Fig. 2.5). The largest distance, 2.69 Å, is approximately equal to the position of the first minimum in the $N_{U'}-H_V$ and $H_{U'}-O_V$ radial distribution functions, and 2.44 Å is simply an intermediate value.

The fractions so obtained for the systems discussed in Part 1 are listed in Table 2.3A. These quantitative estimates of the reactive fractions amplify the observations

made earlier. Depending on the distance criterion chosen, in 1:1 7-AI:methanol complexes, somewhere between 9-40% of the systems are prepared for reaction at any given time. (Reaction in the remaining fraction of the system would also be expected to be rapid since there is little to prohibit the non-cyclic to cyclic inter-conversion in this case.) In 1:1 acetic acid complexes, the much stronger hydrogen bonding present renders $f^{\ddagger} \sim 100\%$ for all three reaction criteria. Compared to these two cases, the fractions estimated for the 1:2 methanol complex are much smaller, $<1\%$ for all three choices of R^{\ddagger} . These observations are in qualitative accord with experimental observations. However, there are as yet no experimental data available that can be quantitatively compared to these dilute solution results.

More direct comparison is available in the case of the bulk alcohols. In neat methanol, and in many other alcohols as we will show shortly, the reactive fractions calculated are in reasonable quantitative agreement with experimental data. Even for the largest value of R^{\ddagger} examined here the fraction of reactive molecules is quite small, less than 2% in the 7-AI / bulk methanol system. Such a small fraction is consistent with the observation of no noticeable ($<5\%$) prompt reaction in either 7-AI/methanol, 1-AC/methanol, or other bulk alcohol solutions [12,13,21]. The fractions observed are also consistent with the kinetic model described by Eq. 2.1. Using the reactive fractions listed in Table 2.3 and the experimentally observed rate of the 7-AI reaction in bulk methanol,

Table 2.3: 7-Azaindole-Methanol Results

A. Isolated Complexes and Bulk Methanol^a

system	$f^{\ddagger}(2.19 \text{ \AA})$ (10 ⁻³)	$f^{\ddagger}(2.44 \text{ \AA})$ (10 ⁻³)	$f^{\ddagger}(2.69 \text{ \AA})$ (10 ⁻³)
7AI-(MeOH) ₁	89 ± 11	278 ± 14	412 ± 13
7AI-(MeOH) ₂	9 ± 3	40 ± 10	92 ± 16
7AI-MeOH	2.5 ± 0.4	9.0 ± 1.3	20 ± 2
7AI-CH ₃ COOH	923 ± 20	980 ± 15	995 ± 5

B. Solute Charge Variations^b

(q _N , q _H)	$f^{\ddagger}(2.19 \text{ \AA})$ (10 ⁻³)	$f^{\ddagger}(2.44 \text{ \AA})$ (10 ⁻³)	$f^{\ddagger}(2.69 \text{ \AA})$ (10 ⁻³)
“low q” (-0.57, +0.31)	3.1 ± 0.5	15 ± 2	32 ± 3
“normal” (-0.67, +0.41)	2.5 ± 0.4	9.0 ± 1.3	20 ± 2
“high q” (-0.77, +0.51)	0.39 ± 0.13	1.8 ± 0.3	7.8 ± 0.4

C. Solvent Charge Variations^c

(q _O)	$f^{\ddagger}(2.19 \text{ \AA})$ (10 ⁻³)	$f^{\ddagger}(2.44 \text{ \AA})$ (10 ⁻³)	$f^{\ddagger}(2.69 \text{ \AA})$ (10 ⁻³)
“low q” (-0.600)	3.5 ± 0.7	17 ± 3	35 ± 5
“normal” (-0.674)	2.5 ± 0.4	9.0 ± 1.3	20 ± 2
“high q” (-0.800)	1.2 ± 1.2	3 ± 2	10 ± 4

^a Reactive fractions $f^{\ddagger}(R^{\ddagger})$ are the fractional populations contained within regions ($R_{\text{NH}} \leq R^{\ddagger}$, $R_{\text{HO}} \leq R^{\ddagger}$), where R_{NH} and R_{HO} are the solute-solvent hydrogen-bonding distances defined in Figure 2.3. Uncertainties listed are \pm standard deviation of the mean of 10 subsets of the overall simulation. ^b Changes on the 7-Azaindole “active sites” (the pyrrolic N atom and the H-(N) atom) varied is indicated. The solvent is “normal” (ab initio) bulk methanol. ^c Charges on the methanol solvent varied from their “normal” (Gaussian) values by moving the charge from the O atom from the CH₃ united atom which is attached.

$\tau_{obs} = k_{obs}^{-1} = 124 \pm 30$ ps, an estimate of the time constant of the proton transfer event can be estimated as:

$$\tau_{PT} = k_{PT}^{-1} = f^{\ddagger} \tau_{obs} \quad (2.10)$$

From such a calculation we obtain proton transfer times ranging from 0.31 ps ($R^{\ddagger}=2.19$ Å) to 2.5 ps ($R^{\ddagger}=2.69$ Å). Based on the reaction time measured in the 7-AI dimer (~ 1 ps [2,3]) and the time estimated for the 1-AC:acetic acid complex (0.7 ± 0.2 ps [4]), this range of times nicely brackets the value anticipated for a 1:1 7-AI:MeOH complex. (Given the steep dependence of tunneling probability on distance, the best criterion to choose is probably $R^{\ddagger}=2.19$ Å, which would predict a value of 0.31 ± 0.09 ps for the proton transfer event.) Thus, while our incomplete knowledge of the geometry required for reaction and lack of more experimental data on isolated complexes precludes a very precise comparison between experiment and simulation, these results are encouraging. It appears that the hydrogen bonding equilibria simulated here are at least semi-quantitatively consistent with Eq. 2.1 and the description on which it is based. We will show shortly (Part 4) that the same can also be said for the other solvents examined here.

Before discussing values of f^{\ddagger} simulated in different solvents, it is useful to first consider the extent to which these values are sensitive to the uncertainties in charge representation discussed in Sec. 2. Toward this end we have carried out two sets of simulations of 7-AI in bulk methanol in which the most important charges in the solute

and solvent have been systematically varied. The results of such simulations are displayed in Fig. 2.9 and Table 2.3.

Consider first the effects of varying the charges on the solute “active sites” (top of Fig. 2.9 and Table 2.3B). Figure 2.9 shows that the solute-solvent hydrogen-bonding distribution changes markedly with such charge variations. One might intuitively expect that increasing these solute charges and thus its hydrogen bonding to the solvent would lead to enhanced formation of cyclic structures. However, just the opposite occurs. The sharpening of the features in Fig. 2.9 with increasing solute charge leads to a reduction in the occurrence of reactive configurations -- the values of f^* (Table 2.3) decrease by factors of between 3-6 (depending on R^*) for a $0.1e$ increase in charge over the normal values. The reason for this trend is that increasing the strength of the hydrogen bonding between the solute and solvent increases the energy penalty that one must pay to make the poorer hydrogen bonds characteristic of the cyclic structure relative to the hydrogen bonds available in the non-cyclic and non-reactive neighbor-bonded structures (Scheme 2).

The variations found when the solvent charges are modified are illustrated in the bottom panel of Fig. 2.9 and listed in Table 2.3C. As Fig. 2.9 shows, increasing the magnitude of the charge on the solvent O site has the expected effect of increasing the extent of H_U-O_V hydrogen bonding. In spite of the fact that the charge on the solvent H atom is not changed, there is a parallel decrease in the amount of N_U-H_V hydrogen bonding. This change reflects the decreasing availability of solvent H atoms for solute-

solvent hydrogen bonding as they are increasingly tied up in solvent-solvent hydrogen bonds. Table 2.3C shows that these two opposite trends lead to a net decrease in the fraction of solute molecules cyclically hydrogen bonded, i.e. to a decrease in the predicted reactivity.

These two sets of simulations provide some calibration of the effects of possible inaccuracies in our potential functions. The semi-empirical calculations in Table 2.1 indicate that electronic excitation of 7-AI or 1-AC probably does not lead to more than a $\pm 0.05e$ change in N_U and H_U atoms involved in hydrogen bonding. The data in Table 2.3 imply that if the solute charges were incorrect by this amount, the values of f^\ddagger calculated would be in error by a factor of ~ 1.6 . In the case of the solvent, this same error in charge would lead to a factor of ~ 1.4 error in f^\ddagger . Thus, we conclude that the uncertainties in our predictions of the reactive fractions resulting from uncertainties anticipated in the charge representations used here are comparable to the those incurred by our imprecise knowledge of how to define a reactive geometry. While these uncertainties warn against placing too much emphasis on small differences in f^\ddagger calculated for different alcohols, they do not cloud the basic picture. In particular, it is worth noting that even the largest plausible variations of solute and solvent charge examined here still indicate that only a small fraction ($< 2\%$ for most definitions of R^\ddagger) of 7-AI molecules in bulk methanol are in a reactive configuration at any given time. The basic idea of “incorrect” hydrogen bonding being a viable explanation for the slow reaction times observed in bulk alcohols is therefore not in doubt.

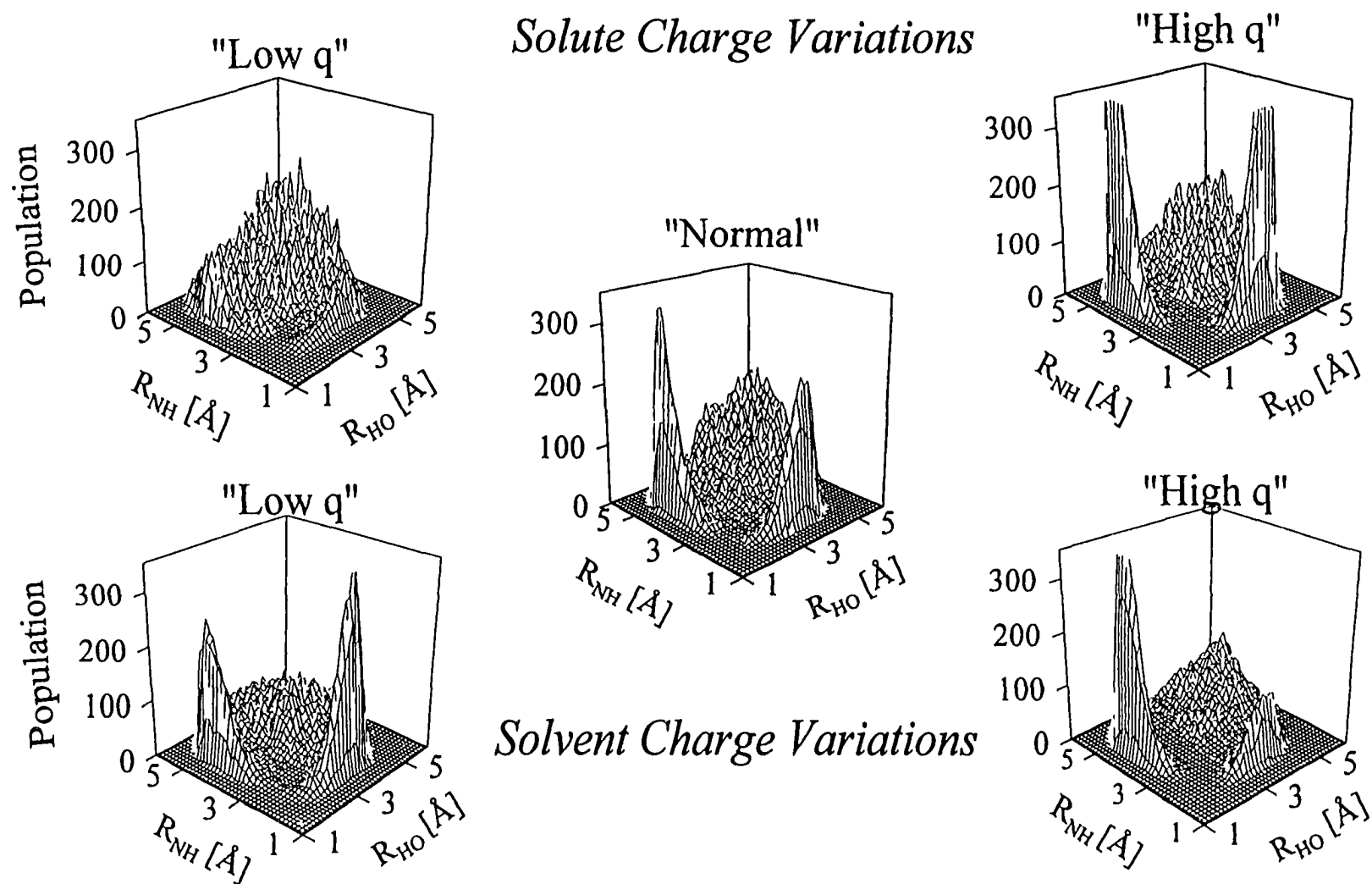


Figure 2.9. Illustration of the effect of varying the solute charges on the hydrogen-bonding distance distributions of 7-AI in methanol solution. The meaning of "high" and "low" charge is discussed in the text and defined in Table 2.3.

2.3.4. Solvation Structure and the Solvent Dependence of the Reactive Fractions.

We now consider the solvation structures and reactive fractions in a number of different solvents in order to examine whether the differences in simulated values of f^\ddagger can account for the variations in reaction rates observed experimentally. As discussed in Sec. 2, we have examined two sets of solvent models, the “*ab initio*” charge model solvents, whose charges were determined from *ab initio* calculations, and the more standard “OPLS” models of Jorgensen and coworkers [37-39]. We expect the *ab initio* solvents to be more realistic for the present problem and consider this set to be our primary set. The OPLS models are employed to help assess the sensitivity of the conclusions to choice of solvent representation.

The solvents examined here include the first three normal alcohols methanol through 1-propanol, the fluorinated alcohol 2,2,2-trifluoroethanol (“TFE”), the two non-primary alcohols 2-propanol and *t*-butanol (2,2-dimethyl-2-propanol), and the two dihydroxy solvents ethylene glycol (1,2-ethanediol) and water. Table 2.4 summarizes the main features of the solvent-solvent hydrogen bonding in the neat solvents. V_{pair} is the interaction energy between a pair of hydrogen bonded solvent molecules, and R_{pk} , $FWHM$, and N_C are the positions, widths, and coordination numbers associated with the first peaks in the intermolecular O_V-H_V and O_V-O_V radial distribution functions. From these data one observes that the basic hydrogen bonding characteristics of all of the

mono-alcohols, with the exception of TFE, are remarkably similar. The $O_V\cdots O_V$ coordination numbers are all $2.00 \pm .05$, a value which indicates that each solvent molecule acts as both a hydrogen bond donor and acceptor virtually 100% of the time. Among this set one finds that the non-primary alcohols *t*-butanol and especially 2-propanol are more strongly hydrogen bonded (largest V_{pair} and smallest R_{pk} and $FWHM$ values) by virtue of their larger oxygen charges (Table 2.2). In the case of 2-propanol, this feature is probably exaggerated by the *ab initio* model compared to the real solvent, based on the fact that the enthalpy of vaporization calculated for this model is too large by 18% (Table 2.7). 2,2,2-Trifluoroethanol stands out among the mono-alcohols as being significantly more weakly hydrogen bonded, with coordination numbers that reflect the presence of a substantial fraction of broken hydrogen bonds. (This feature may be exaggerated in our TFE model, as discussed in the Appendix.) Finally, ethylene glycol and water differ from the mono-hydroxy solvents in that, especially in water, each solvent molecule is simultaneously hydrogen bonded to more than two other solvent molecules (i.e. $N_C(O_V\cdots O_V)$ is significantly larger than 2).

We now move to the features of the solvation of 7-AI in these different solvents that should be of importance for determining its reactivity. Relevant data are provided in Fig. 2.10 and Table 2.5. Figure 2.10 contains 2-dimensional distributions of the R_{NH} , and R_{HO} distances of the sort already considered in methanol. The most obvious feature to note from Fig. 2.10 is that all of these solvents exhibit a 2-peaked distribution comparable to the bulk methanol case. With the exception of TFE, all of these

Table 2.4. Solvent-Solvent Hydrogen-Bonding Characteristics

solvent	$-V_{\text{pair}}^a$ (kJ/mol)	O-H RDF ^b			O-O RDF ^b		
		R_{pk} (Å)	fwhm (Å)	N_c	R_{pk} (Å)	fwhm (Å)	N_c
methanol	22.5	1.83	0.37	0.97	2.75	0.37	2.02
ethanol	23.4	1.83	0.37	0.95	2.76	0.37	2.01
1-propanol	24.9	1.82	0.36	0.93	2.75	0.35	1.95
2,2,2-trifluoroethanol	19.9	1.95	0.46	0.69	2.82	0.45	1.66
2-propanol	29.7	1.78	0.32	0.97	2.70	0.31	2.00
<i>tert</i> -butyl alcohol	27.9	1.82	0.34	0.93	2.74	0.34	1.94
ethylene glycol	22.9	1.86	0.47	0.82	2.80	0.57	2.54
water	16.0	1.88	0.48	1.80	2.83	0.55	4.50

^a V_{pair} is the most probable interaction energy between pairs of hydrogen-bonded molecules. ^b R_{pk} , fwhm, and N_c are the position, full width at half-maximum, and number of molecules (coordination number) corresponding to the first peak in the respective radial distribution functions. The coordination number is integrated to the first minimum after R_{pk} .

Table 2.5 Structural Characteristics of Solvation in Various Solvents^a

Solvent ^a	N _U —H _V Bonding ^b							H _U —O _V Bonding ^b							Structure ^c	
	1D rdfs			2D distributions				1D rdfs			2D distributions					
	<i>R</i> _{pk} (Å)	<i>N</i> _C	- <i>V</i> _{UV} kJ/mol	< <i>R</i> ₁ > (Å)	δ <i>R</i> ₁ (Å)	< <i>R</i> ₂ > (Å)	δ <i>R</i> ₂ (Å)	<i>R</i> _{pk} (Å)	<i>N</i> _C	- <i>V</i> _{UV} kJ/mol	< <i>R</i> ₁ > (Å)	δ <i>R</i> ₁ (Å)	< <i>R</i> ₂ > (Å)	δ <i>R</i> ₂ (Å)		
															% 8	% nn
7-Azaindole																
methanol	1.93	0.88	26.2	2.06	0.21	3.80	0.51	1.83	1.00	24.9	1.98	0.23	4.57	0.57	7	91
ethanol	1.94	0.71	24.9	2.03	0.21	3.82	0.47	1.81	1.00	29.4	1.90	0.20	4.22	0.64	16	79
1-propanol	1.95	0.75	28.4	2.09	0.21	3.76	0.54	1.81	0.98	30.0	1.92	0.20	4.49	0.59	18	71
TFE	2.04	1.09	19.0	2.16	0.21	3.44	0.71	1.89	0.91	33.2	2.08	0.25	4.06	0.94	22	64
2-propanol	1.89	0.90	30.4	2.05	0.21	3.62	0.49	1.81	0.89	26.9	1.97	0.27	4.23	0.69	3	92
<i>tert</i> -butyl alcohol	1.91	1.08	36.4	2.02	0.19	3.48	0.51	1.80	0.95	27.5	1.92	0.21	3.86	0.61	32	51
ethylene glycol	1.98	0.66	19.4	2.13	0.22	3.66	0.66	1.81	1.24	23.4	1.97	0.24	4.17	0.63	14	72
water	1.96	1.28	18.1	2.15	0.23	3.84	0.54	1.83	0.99	23.4	2.02	0.25	4.19	0.56	1	98
1-Azacarbazole																
methanol	1.91	0.98	27.1	2.07	0.21	3.98	0.52	1.82	1.03	27.4	1.93	0.20	4.48	0.61	9	88
water	1.97	1.08	18.7	2.15	0.23	3.75	0.54	1.80	1.02	24.3	1.98	0.24	4.20	0.56	3	97

^a TFE denotes 2,2,2-trifluoroethanol. ^b *R*_{pk} and *N*_c are the peak position and coordination number associated with the first peak in the one-dimensional radial distribution functions ("rdfs") of the two solute-solvent H-bonding coordinates N_U—H_V and H_U—O_V. Coordination numbers were determined from the integral under this first peak out to the minimum in the rdf. *V*_{UV} is the most probable interaction energy between the solute and the solvent molecule hydrogen-bonded to the particular solute active site. The four columns under the heading "2D distributions" characterize the average positions (<*R*>) and widths (standard deviations, δ*R*) of the peaks observed in the two-dimensional distributions depicted in Figure 2.10. The superscripts "1" and "2" label values in primary and secondary dimensions of these plots. ^c "%8" and "%nn" refer to the relative frequency of the noncyclic configurations sampled that are hydrogen-bonded in a manner characteristic of "eight-membered" and "nearest-neighbor bonded" structures, as schematically shown in Scheme 2.

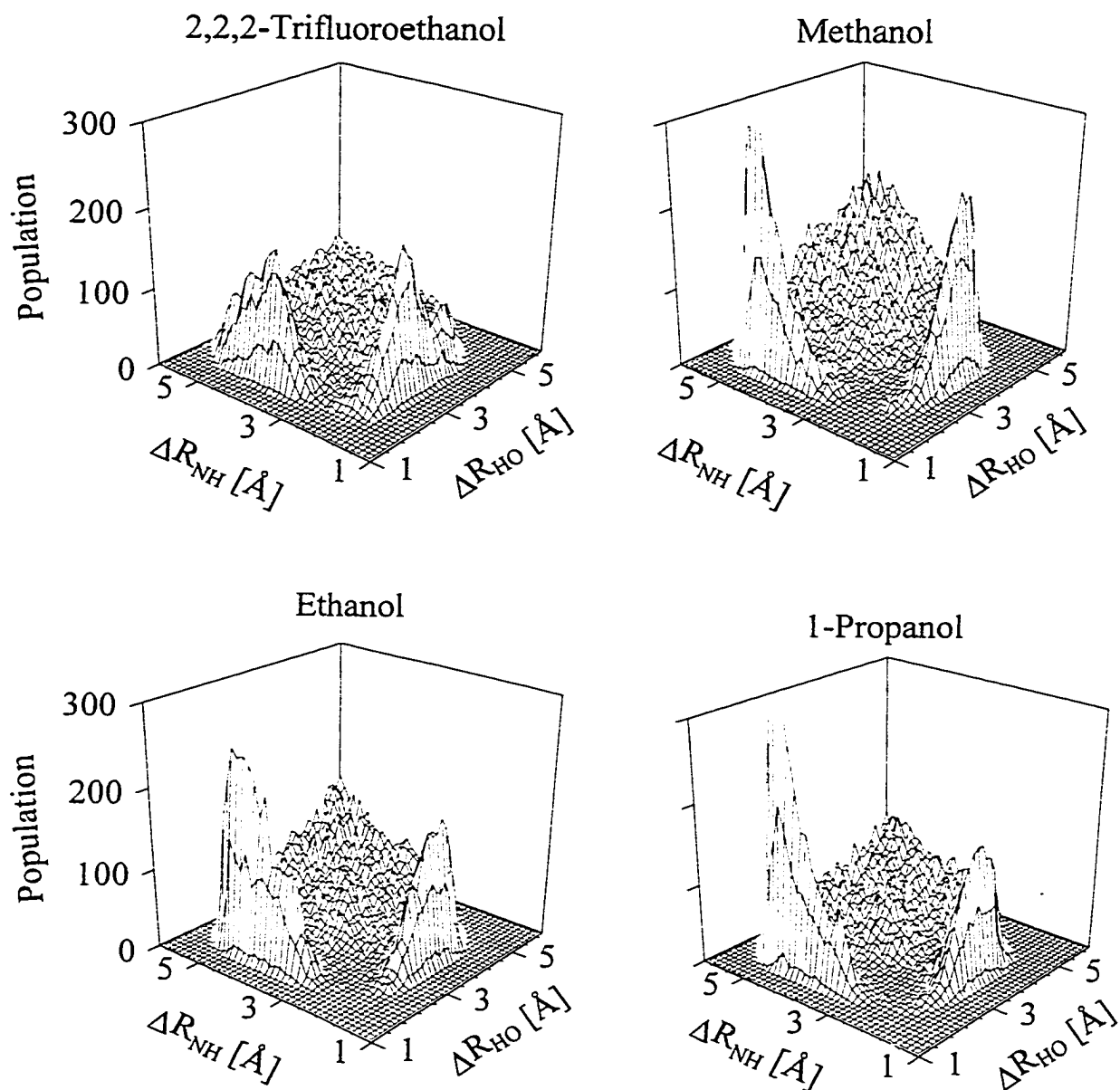


Figure 2.10.a. Hydrogen-bonding distance distributions for 7-AI in four of the solvents studied: 2,2,2-trifluoroethanol, Methanol, Ethanol and 1-Propanol.

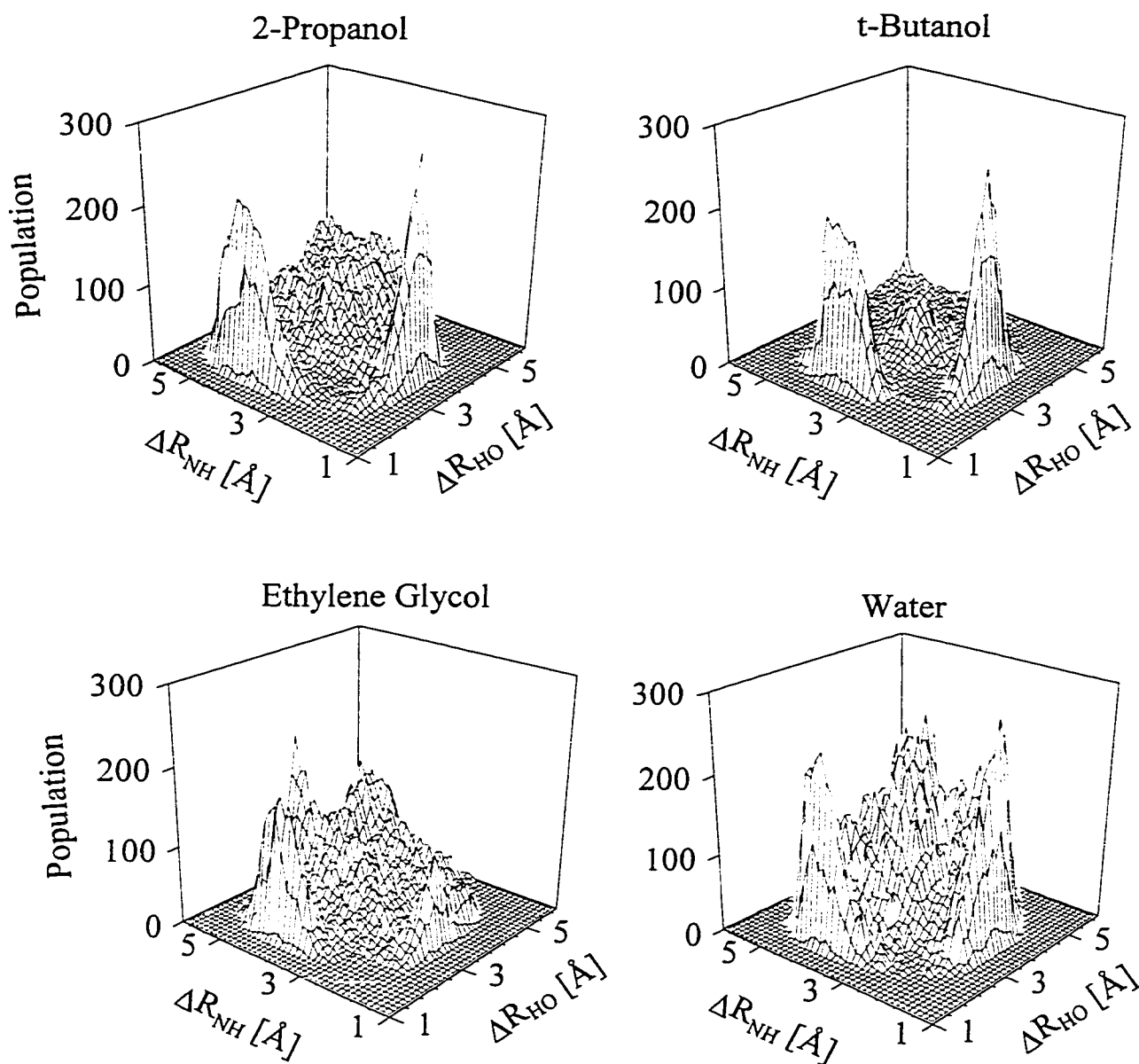


Figure 2.10.b. Hydrogen-bonding distance distributions for 7-AI in four of the solvents studied: 2-Propanol, *tert*-Butanol, Ethylene Glycol, and Water.

distributions show very little population (<1%) in structures that we deem reactive. But, before discussing the calculated fractions, we first consider in more detail how the solute-solvent bonding structure varies with solvent. We do so using the results in Table 2.5, which summarizes characteristics of the distributions of N_U-H_V and H_U-O_V distances observed. In the first two columns under each of these headings some features of the 1-dimensional radial distribution functions of these two H-bonding distances are listed. The interaction energies (“ V_{UV} ”) are pair energies between the solute and the particular solvent molecule which is closest to the solute site of interest. These values are indicative of the strength of the hydrogen bonds made to each of the solute active sites. The next four columns characterize the average positions ($\langle R \rangle$) and widths (standard deviations, δR) of the peaks observed in the 2-dimensional distributions depicted in Fig. 2.10.

The data in Table 2.5 indicate that the solute-solvent bonding is fairly similar in most of these solvents. It is also comparable to the hydrogen bonding that takes place within the solvents themselves. The coordination numbers show that in nearly all cases the N_U and H_U solute sites form hydrogen bonds to (distinct) solvent molecules more than 75% and 95% of the time, respectively. Some differences among the various solvents can also be discerned. For example, while the energies at the two solute sites are usually comparable (and close to V_{pair}), hydrogen bonds to the N_U site can be either stronger or weaker than those at the H_U site. In TFE the difference is most marked. Here the bonding to the N_U site is relatively weak, as are hydrogen bonds in the neat liquid,

whereas the H_U site bonding is uncommonly strong, due to the reduced charge on the hydroxyl oxygen atom (Table 2.2) [54]. A final aspect of the solvation structure that shows significant variations among the different solvents involves the relative disposition of the two solvent molecules that are hydrogen bonded to the solute. This aspect is represented in the last two columns of Table 2.5, where we list the frequency of occurrence of the 8-membered ring (“%8”) and nearest neighbor (“%nn”) structures defined in Scheme 2. The preference for forming 8-membered ring structures versus neighbor-bonded structures generally decreases as the density of available OH bonds in the solvent increases. Thus, the %8 values increase in the order water < methanol < ethanol < 1-propanol < t-butanol. A notable exception in this series is 2-propanol, which forms fewer 8-membered rings than would be expected on this basis. In this solvent (and not others) solvent-solvent bonds are stronger than solvent-solute hydrogen bonds so that nearest neighbor bonding is strongly preferred for energetic reasons.

Having characterized the basic structural features of the active-site hydrogen bonding we now turn to the reactive fractions f^* determined in the different solvents. These results are summarized in Table 2.6 and Fig. 2.11. In Table 2.6 we list reactive fractions for the definitions of reactive geometry discussed previously: $R^{\ddagger} = 2.19, 2.44$, and 2.69 \AA . Also listed for the $R^{\ddagger} = 2.19 \text{ \AA}$ case are the values of τ_{PT} and ΔG^{\ddagger} they imply. (Recall that we expect that the smallest value of R^{\ddagger} should represent the most realistic choice.) Consistent with the distributions displayed in Fig. 2.10, the reactive fractions calculated using this most restrictive definition are all quite small -- less than

Table 2.6. Summary of Reactive Fractions.

solvent	$R^\ddagger = 2.19 \text{ \AA}$			$R^\ddagger = 2.44 \text{ \AA}$	$R^\ddagger = 2.69 \text{ \AA}$
	$f(R^\ddagger) (10^{-3})$	$\tau_{PT} \text{ (ps)}$	$\Delta G^\ddagger \text{ (kJ/mol)}$	$f(R^\ddagger) (10^{-3})$	$f(R^\ddagger) (10^{-3})$
7-Azaindole-Ab Initio Solvent Models					
methanol	2.5 ± 0.4	0.3	15.0	9.0 ± 1.3	20 ± 2
ethanol	1.3 ± 0.2	0.2	16.6	4.7 ± 0.5	13.5 ± 1.7
1-propanol	1.2 ± 0.4	0.2	16.8	4.3 ± 1.0	12.5 ± 1.2
TFE	16 ± 2	0.5	10.3	68 ± 7	146 ± 11
2-propanol	5 ± 3	2	13	16 ± 8	31 ± 12
<i>tert</i> -butyl alcohol	7 ± 3	2	12	19 ± 5	48 ± 4
ethylene glycol	0.8 ± 0.4	0.3	18	12 ± 4	41 ± 11
water	0.66 ± 0.08	0.5	18.3	5.2 ± 0.4	19.4 ± 0.9
7-Azaindole-Other Solvent Models					
methanol (OPLS)	2.3 ± 0.5	0.3	15.0	7.1 ± 1.1	15 ± 1.2
ethanol (OPLS)	1.5 ± 0.4	0.2	16.1	7.5 ± 1.1	24 ± 2
1-propanol (OPLS)	0.8 ± 0.2	0.2	17.6	3.2 ± 0.6	10 ± 2
2-propanol (OPLS)	2.6 ± 1.2	0.6	15	5.5 ± 1.5	18 ± 7
<i>tert</i> -butyl alcohol (OPLS)	4 ± 2	1.3	14	17 ± 2	65 ± 13
water (SPC)	1.0 ± 0.3	0.8	17	5.5 ± 1.2	23 ± 3
water (TIP4P)	2.0 ± 1.0	1.6	15	8 ± 4	30 ± 11
1-Azacarbazole-Ab Initio Solvent Models					
methanol	2.3 ± 0.7	1.2	15	8 ± 2	18 ± 4
water	0.8 ± 0.3	2	18	5 ± 2	23 ± 4

^a Reactive fractions $f(R^\ddagger)$ are the fractional populations contained within ($R_{NH} \leq R^\ddagger$, $R_{HO} \leq R^\ddagger$), where R_{NH} and R_{HO} are the solute-solvent hydrogen-bonding distances defined in Figure 2.3. τ_{PT} is the proton-transfer rate that would be required for a given $f(R^\ddagger)$ in order to obtain the experimentally observed reaction rate (k_{obs} values from refs 13 and 21) according to eq 2.1. Uncertainties in the values of $f(R^\ddagger)$ listed here are ± 1 standard deviation of the mean of 10 subsets of the overall simulation.

2% in all cases. In the normal alcohol series there is a systematic decrease in the reactive fraction (for all R^\ddagger) in the order methanol>ethanol>1-propanol. This trend parallels the experimentally observed trend in reaction rates [12,13]. TFE has by far the largest population of reactive species, $f^\ddagger \sim 1.6\%$, which is consistent the experimental observation of very rapid reaction in this solvent [13]. Alternatively, the reactive fractions determined in ethylene glycol and water are smaller than those in the normal alcohols, which is again consistent with the slower reaction observed in these two solvents [13,14].

In addition to these qualitative trends, the reactive fractions calculated for 7-AI in these six solvents are in semi-quantitative agreement with the idea that the rates are being simply proportional to f^\ddagger . This point is illustrated in Fig. 2.11 where observed reaction rates are plotted as a function of $f(R^\ddagger=2.19\text{\AA})$. With the exception of water, all of the data in these six solvents can be fit to Eq. 2.1 using a value of $k_{PT}=3.3\text{ ps}^{-1}$ (or $\tau_{PT} = 300\text{ fs}$). In light of what is known about the 7-AI reaction in isolated catalytic complexes, such a rate constant seems quite reasonable [4]. In the case of water, the calculated fraction is roughly two-fold larger than expected based on this correlation. If the reactive fractions are assumed correct, these results would imply a roughly two-fold slower proton transfer ($\tau_{PT} \sim 0.6\text{ ps}$) in water [55] compared to the primary alcohols. Isotope effect data [15,21] indicate that there may in fact be some quantitative differences in the proton transfer step (k_{PT}) in water compared to alcohol solvents, so this computed difference in reactive fractions could in fact be correct. However, given the variations in f^\ddagger provided by different

water models, it is unwise to attach much significance to the deviation. With respect to all of the aforementioned solvents, including water, it is best to conclude that the simulation results are consistent with the main solvent dependence of these reactions deriving from the equilibrium fractions f^* , as proposed on the basis of experimental results [21].

However, Fig. 2.11 also clearly shows that two of the solvents studied here, the two non-primary alcohols 2-propanol and *t*-butanol do not fit neatly into this picture. The reactive fractions in these two solvents are significantly larger than the fractions in methanol, whereas the observed reaction rates are actually much smaller. There is about a factor of 5 discrepancy between the calculated fractions and what would be expected based on the results in the other solvents. This “deviant” behavior can be interpreted in a number of ways. One interpretation would be to conclude that the focus on f^* alone is incorrect. Differences in k_{PT} between primary and secondary/tertiary alcohols could just as well give rise to the different reaction rates in these systems. Or, contrary to the test cases studied in Sec. IIIB, the *dynamics* of solvation could be important in these particular solvents. While these possibilities cannot be ruled out entirely, given the extensive experimental data implicating an equilibrium solvent property like f^* as being the sole solvent effect [21], it seems unlikely that this underlying idea is incorrect. A more likely interpretation is that the equilibrium fractions of these solvents are not accurately portrayed by the present simulations, probably as a result of inaccuracies in the intermolecular potential functions used for these solvents. Some perspective on this possibility can be gleaned from the results on OPLS solvents also provided in Table 2.6

and Fig. 2.11. We note that the different charges in the OPLS and *ab initio* models produce roughly 2-fold differences in the values of f^\ddagger predicted in the case of 2-propanol and *t*-butanol, but much smaller differences in the case of the normal alcohols. These differences reflect only the choice of charge representation. It may also be that our use of united-atom representations of CH₂ and CH₃ groups does not do justice to the steric interactions in these solvents, which would be expected to be significantly different from those in primary alcohols. A final possibility is that both the basic idea and the simulation models are basically sound but that our use of the criterion $R_{NH}=R_{OH}=2.19 \text{ \AA}$ to define reactive configurations is too crude. We note that there are some differences between the distributions of H-bonding angles in the cyclic forms of primary and these secondary / tertiary alcohols that perhaps are important. Recent high-resolution jet studies indicate that 7-Al:H₂O complexes may be cyclic in the sense defined here but nevertheless non-reactive due to angular displacements that are difficult to overcome at the low temperatures achieved in supersonic expansion [56]. However, until more is known about the real geometric constraints involved, it does not seem fruitful to try to adopt more complicated criteria in order to better correlate all of the solvents.

With these considerations in mind, we conclude that the results presented in Table 2.5 and Fig. 2.11 generally support the notion that the variation in the reaction rates of 7- Al in bulk alcohols and water are due mainly to variations the equilibrium populations

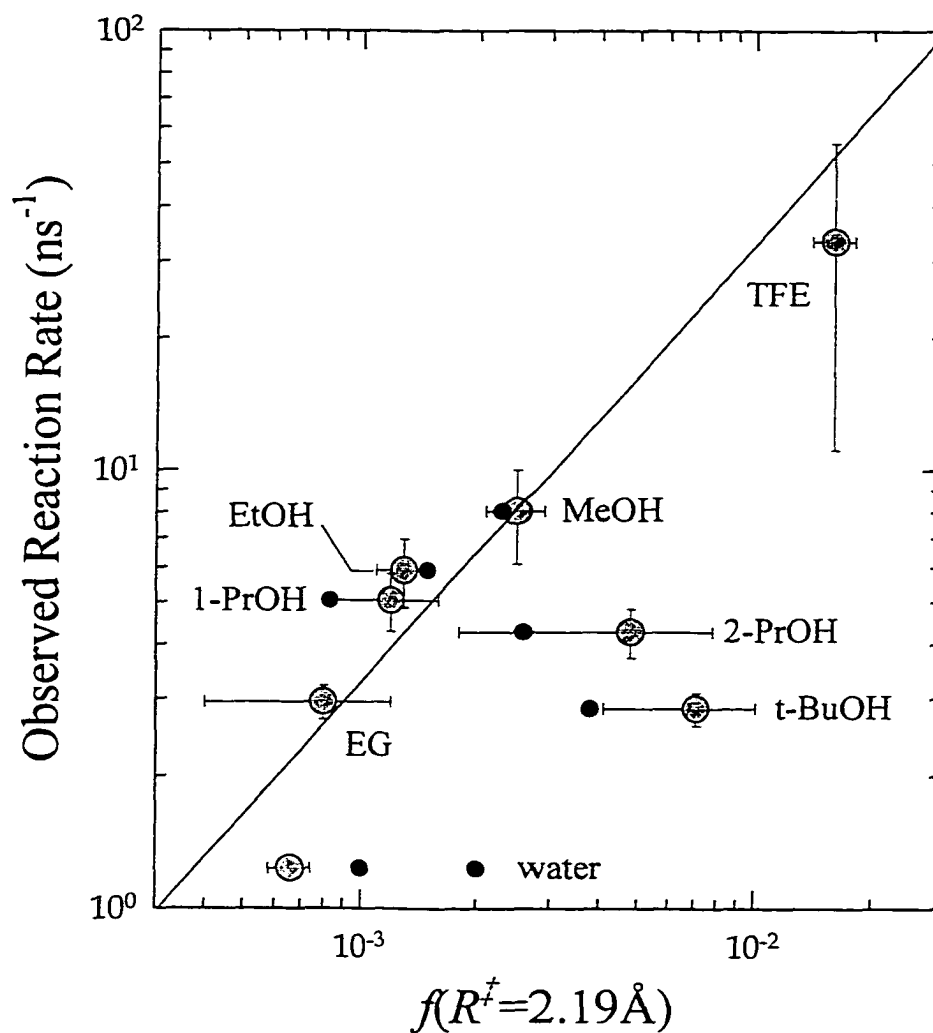


Figure 2.11. Comparison of simulated reactive fractions and observed reaction rates of 7-AI in bulk alcohol solvents. The larger symbols are results obtained using the ab initio solvent set, and the smaller symbols are those obtained with OPLS models. The line shown is the best fit of the ab initio data (in a linear format) excluding 2-propanol and *tert*-butyl alcohol. It represents the proportionality $k_{\text{obs}} = (3.3 \text{ ps}^{-1}) f^{\ddagger}$.

of reactive forms, as described by Eq. 2.1. Indeed, given the simplicity of the modeling performed here, the fact that all of the experimental results can be rationalized using the simulated fractions and values of k_{PT} (or τ_{PT} in Table 2.5) that are all near the expected value of ~ 0.5 ps should probably be viewed as a strong support of the basic picture discussed in the Introduction.

It is therefore interesting to consider what differences in solvation are responsible for the different reactive fractions and thus reaction rates in these various solvents. We have not discerned any clear links between the relatively subtle variations in solvent structure observed in the different alcohol solvents and differences in their reactive fractions. Nevertheless, there is a clear connection between f^\ddagger and the energetics of solvation. At least in the mono-hydroxy alcohols, the origin of the solvent dependence of f^\ddagger , or equivalently of ΔG^\ddagger , can be simply explained on the basis of the pair bonding energies of the reactive and non-reactive forms. Making the assumption that every alcohol molecule has strong interactions with exactly two other alcohol molecules (invalid in the cases of water and ethylene glycol), an accounting of the energy cost of adopting a reactive geometry in a bulk alcohol solvent can be made according to the approximate relation:

$$\Delta E_{cyc} \cong \{V(cyc) + 2V(vv)\} - \{V(U,1) + V(U,2) + V(1,3) + V(1,4)\} \quad (2.11)$$

In this expression we consider the energetics of the two key solvent molecules labeled “1” and “2” in Scheme 2, which we assume make a total of four hydrogen bonds to other

molecules. The $V(x)$ are average interaction energies of various solute - solvent and solvent-solvent pairs x , averaged over distributions of the sort illustrated in Fig. 2.4. The energy of an non-reactive neighbor-bonded or 8-membered ring structure is given by the second term in brackets in Eq. 2.11. $V(U,1)$ in this latter term refers to the interaction energy between the solute (“ U ”) and solvent molecule 1 , defined as the particular solvent molecule having the minimum N_U-H_V distance, and $V(1,3)$ is the interaction energy between this solvent molecule and whichever other solvent molecule (“ 3 ”) has the smallest O_V-H_V distance. $V(U,2)$ and $V(2,4)$ are defined analogously. (In 8-membered ring structures, labels “ 3 ” and “ 4 ” refer to the same solvent molecule, whose interactions are included twice in the accounting procedure.) The energy of the cyclic structure is estimated as the average interaction energy simulated for an isolated 1:1 complex in cyclohexane, $V(cyc)$, plus the energy of two solvent-solvent bonds that solvent #2 makes once freed from the solute. The latter energy is from the average bulk pair energy $V(vv)$.

A comparison of these cyclic energy estimates ΔE_{cyc} to the actual free energies ΔG^\ddagger is provided in Figure 2.12. Although the above accounting scheme only considers four pair interactions, the values of ΔE_{cyc} are nearly within uncertainties of the values of ΔG^\ddagger in the mono-alcohol solvents. The only exception is *t*-butanol, for which ΔE_{cyc} is nearly 10 kJ/mol greater than ΔG^\ddagger . From this remarkable agreement we conclude that, in all but one of these solvents, the primary determinant of the reactive fraction is simply the

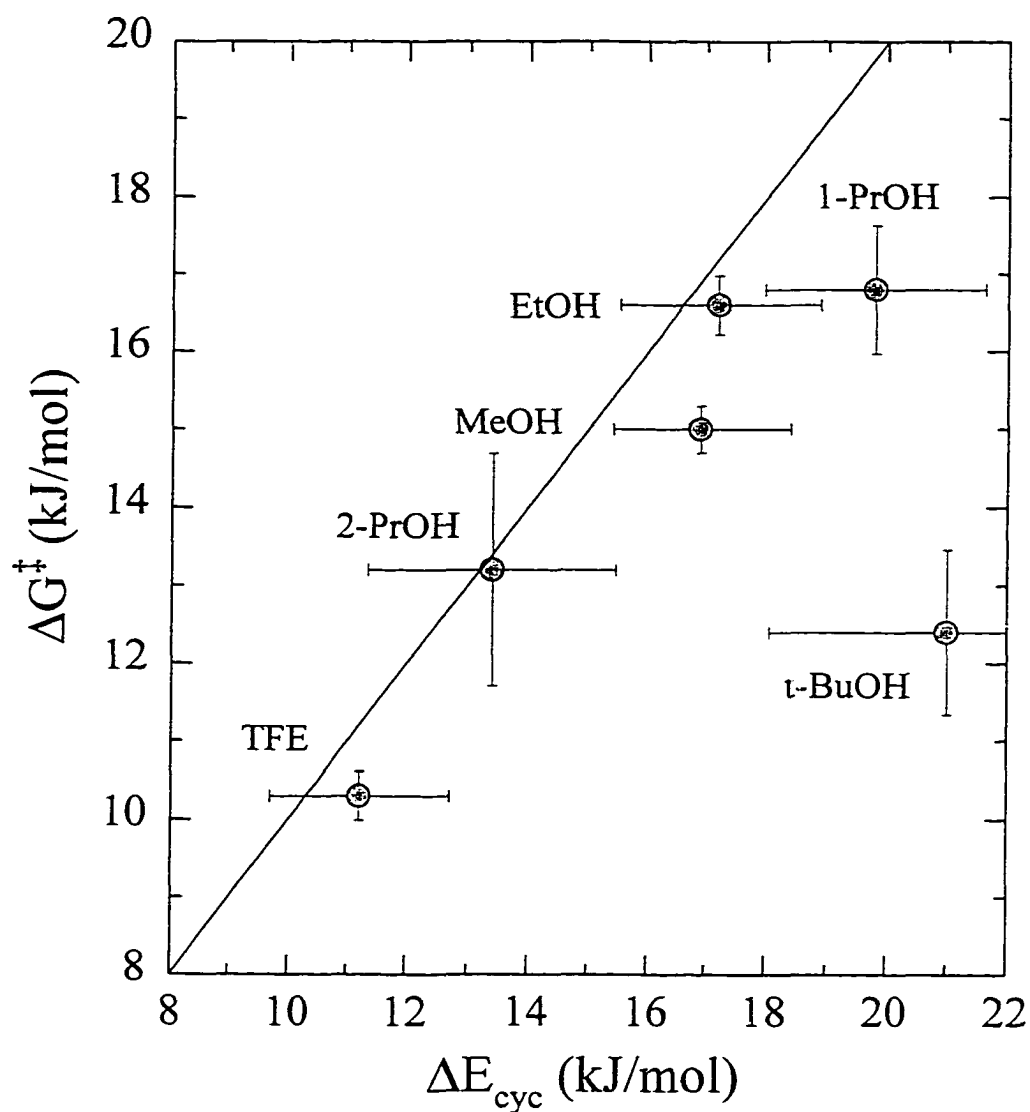


Figure 2.12. Comparison of the approximate energy (ΔE_{cyc} , eq. 2.11) with the free energy (ΔG^\ddagger , eq. 2.1) required to form cyclic structures. The line shown is the line of equal value.

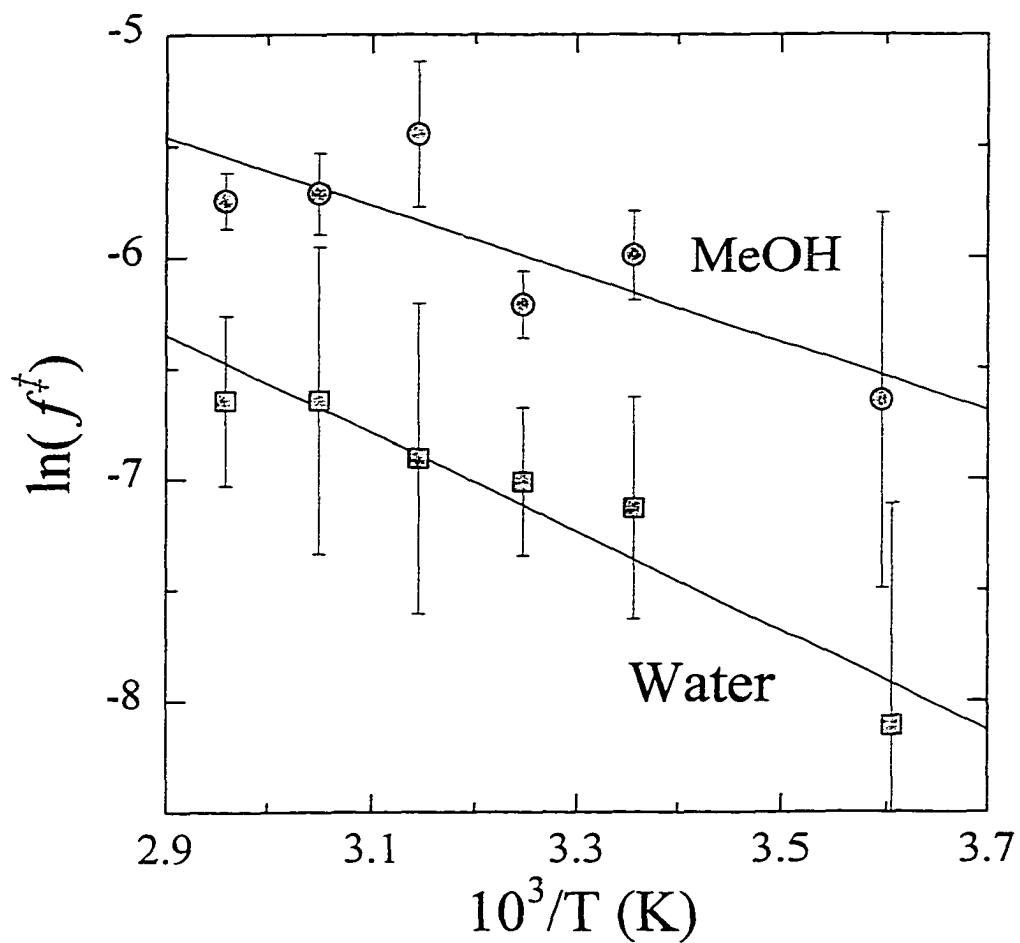


Figure 2.13. Arrhenius plots of the temperature dependence of the reactive fractions of 7-AI in methanol and water.

differential strength of the hydrogen bonds that can be formed in cyclic versus non-cyclic structures. With the exception of *t*-butanol, entropic considerations must therefore play a minor role in determining f^\ddagger in these mono-alcohols. (Water is also an exception, as is discussed in the next section.)

2.3.5. *Temperature and Solute Dependence.*

Two final aspects of the simulated behavior lend further support to the notion that the reactive fractions are primarily responsible for the solvent dependence of the reaction rates in these systems. The first involves the temperature dependence of f^\ddagger . Experimentally, the rates of the 7-AI and 1-AC reactions are observed to exhibit activation energies of ~ 10 -15 kJ/mol in a variety of alcohol solvents [21]. Within the context of Eq. 2.1, this activation energy for reaction is interpreted as being the enthalpy change in forming the reactive form [57]. As a further test of the model we have therefore performed simulations of 7-AI in methanol and water for six temperatures in the range of 275-340 K. The results are displayed as Arrhenius plots in Fig. 2.13. These plots yield values of ΔH^\ddagger of 13 ± 4 and 11 ± 3 kJ/mol for methanol and water, respectively. The activation energies observed experimentally for the 7-AI reaction are 10.4 ± 0.4 kJ/mol [58] in methanol and 8.8 ± 1 kJ/mol [14] in water. Thus, the observed activation energies for reaction in both solvents are within uncertainties of the temperature dependence of the simulated reactive fractions (ΔH^\ddagger), supporting the above interpretation.

It is interesting to compare these values of ΔH^\ddagger with the results calculated in Part 4. In the case of methanol the simulated value of ΔH^\ddagger is consistent both with the estimate of ΔE_{cyc} derived previously (17 ± 2 kJ/mol) and ΔG^\ddagger itself (15.0 ± 0.3 kJ/mol), as anticipated. In water, on the other hand, the activation energy appears to be significantly lower than the value of $\Delta G^\ddagger = 18.3 \pm 0.3$ kJ/mol. (Estimates of ΔE_{cyc} also lead to values significantly lower than ΔG^\ddagger .) These differences could reflect the fact that entropic as well as energetic effects play a role in determining f^\ddagger in water. The entropic contribution appears to be large in this case, accounting for more than a 10-fold reduction in f^\ddagger compared to what would be expected on energetic grounds alone. Since this conclusion rests on the accuracy of our ΔG^\ddagger estimates, which are by no means assured, it is comforting to note that there is also experimental evidence for such a distinction between water and most alcohol solvents. Using the notation of Eq. (2.1), the ratio $k_{obs} / \exp(-E_a / RT)$, where E_a is the experimentally observed activation energy, should be approximately constant if $\Delta G^\ddagger \cong E_a$. For the 7-AI and 1-AC reactions in alcohols this ratio appears to be approximately constant among the normal alcohols, but roughly an order of magnitude larger in water [21], in complete agreement with the simulation results.

The final aspect of these reactions we consider is their solute dependence. As discussed in the Introduction, striking parallels between the solvent dependence of the tautomerization rates of 7-AI and 1-AC have been observed experimentally [20,21]. This

observation has been interpreted within the context of Eq. 2.1 as reflecting the fact that the solvent dependence of f^\ddagger is nearly the same for these two solutes. Given the similarity in their active-site geometries and charges (Table 2.1) such closeness is not surprising. Nevertheless, it is important that the simulations bear out this expectation. As displayed in Table 2.5, the simulated features of the solute-solvent hydrogen bonding differ little between 7-AI and 1-AC. The slightly larger charges on the active sites of 1-AC lead to a small enhancement of the hydrogen bonding to both sites relative to 7-AI, as indicated by the decrease in R_{pk} and increase in N_C and V_{UV} . These modest changes do not, however, significantly alter the reactive fractions calculated, as indicated by comparison provided in Table 2.6. Thus, with respect to both the solute and temperature dependence of the reactive fractions, the present simulations appear to corroborate the picture of the solvent involvement constructed to explain the experimental data.

2.4. Summary and Conclusions

In this work we have used classical Monte Carlo and molecular dynamics computer simulations to explore the role played by hydroxylic solvents in the excited state tautomerization of 7-azaindole and 1-azacarbazole. We have examined the solvation structure in a variety of 7-AI and 1-AC / alcohol and water systems with a view towards testing the mechanism of solvent catalysis proposed on the basis of experimental work [21]. This mechanism postulates that the slow tautomerization observed in bulk

alcohol solvents results from the scarcity of reactant molecules properly solvated for reaction. “Proper” solvation is assumed to involve a cyclically hydrogen bonded complex with single alcohol solvent molecule bridging the sites of proton transfer. The mechanism further supposes (Eq. 2.1) that the rates observed in different bulk solvents are proportional to the equilibrium fraction of molecules in the reactive geometry, with the proportionality constant being the rate of the actual proton transfer step (k_{PT}), which is assumed to be rapid (<5 ps) and solvent independent.

The simulations performed here generally support this proposed mechanism. In all of the bulk solvents examined, which included six alkyl alcohols, ethylene glycol, and water, the fraction of solute molecules in “reactive” solvation states (f^*) was observed to be small, typically less than 1%. Molecular dynamics simulations in methanol and water showed these reactive fractions, and not solvent dynamical effects, should control the reaction rates, as is assumed in Eq. 2.1. In most of the solvents studied a good correlation was found between the simulated reactive fractions and the rates experimentally measured for the 7-AI reaction (Fig. 2.11). This correlation implies a value of $k_{PT} \sim (0.3 \text{ ps})^{-1}$ for the rate of proton transfer step in properly solvated 7-AI / alcohol complexes, a value consistent with what is known about reaction rates in dilute solution. Most of the results reported here involved simulations of the 7-AI reaction. However, several simulations of the 1-AC solute indicate that the reactive fractions in the 1-AC system should be very close to those in 7-AI. This finding is consistent with the remarkable parallelism observed in the solvent dependence of the two reactions. Finally, we also

simulated the temperature dependence of the reactive fractions of 7-AI in two solvents, methanol and water. The agreement between the enthalpy changes associated with formation of reactive solvation states and the activation energies observed experimentally in these two solvents lends further support to the validity of the proposed mechanism.

Two of the eight solvents studied here, the two non-primary alcohols 2-propanol and *t*-butanol, were observed to deviate significantly from the correlation established by the other solvents. The values of the reactive fractions calculated in these two solvents are roughly five-fold larger than expected based on the experimentally observed reaction rates. Of the possible reasons considered for these deviations, it seems most likely that inaccuracies in the intermolecular potential models used here are primarily to blame. Some tests of the sensitivity of the simulated behavior to variations in the potential parameters were performed in the present work, and from these it can be concluded that an accuracy of no better than a factor of two should be expected for the values of the reactive fractions calculated here. While relative variations among similar solvents should be better reproduced, it seems reasonable to suspect that possibly subtle differences between solvation in primary and secondary alcohols might not be captured by the simple potential functions employed. We are currently performing simulations of the solvatochromic behavior of solutes sensitive to hydrogen bonding in order to explore just what level of realism is to be expected from different potential models of alcohol solvents [59].

In spite of these difficulties, the present simulations provide considerable evidence that the mechanism of solvent involvement inferred from experimental evidence is basically correct. What further insight do the simulations offer regarding the nature of solvation / reaction in these systems? One observation is that in most respects solvation of 7-AI and 1-AC is not qualitatively different in water compared to alcohol solvents. Dynamical studies show that reorganization of the solvation structure in water occurs on a 10-100 ps time scale, making the idea that long-lived solvation states block reaction in water for times in the nanosecond range appear untenable. In water and in alcohol solvents, the *dynamics* of solvation appear to be irrelevant to the reaction. The slower reaction times observed in water compared to alcohol solvents merely reflect the smaller fraction of reactive (cyclically bonded) forms present. The reason for the small proportion of reactive solvation states in water and in hydroxylic solvents in general is geometrical in nature. The hydrogen bonding sites in 7-AI and 1-AC are positioned such that a single water or alcohol molecule simultaneously bound to both sites can only make relatively weak, highly non-linear hydrogen bonds to the solute (Fig. 2.5). In bulk solvents, 8-membered ring or neighbor-bonded structures (Scheme 2) prevail over cyclically bonded forms simply because stronger hydrogen bonds can be formed when two different solvent molecules bind to the solute “active sites”. In most of the solvents studied here the free energy change to reach the reactive geometry can be accurately accounted for simply in terms of the energy penalty associated with exchanging two strong hydrogen bonds made in the non-reactive structures for the two weaker bonds made in the cyclic form. Entropic effects are therefore of little importance in the reactive

equilibrium in most alcohol solvents. It is interesting to note that water is qualitatively different in this regard. In water, the reactive fraction is significantly smaller than is accounted for by this energy effect alone, such that there must also be a sizable entropy penalty to adopting the reactive geometry in water.

We can summarize the findings of the present work by stating that the reaction rates of 7-AI and 1-AC in hydroxylic solvents can be understood in terms of geometric hydrogen bonding requirements between the solute and solvent molecules. Such geometric control over the reaction is of course rather specific to these particular solutes and solvents, as discussed in Sec. IIIA (Figs. 2.5 and 2.6.). It is therefore of interest to examine these same reactions in other solvent types (such as amides [60]) as well as other reactions, for example DPC [46] (Fig.2.6) and 7-hydroxyquinoline [42], in alcohol solvents in order to form a more complete picture of the role of solvation structure and dynamics in solvent-catalyzed proton transfer processes. Work along these lines is currently in progress in our group.

2.5. Appendix

To check the reasonableness of the “*ab initio*” potential models used here we have compared the solvent-solvent radial distribution functions, densities, and enthalpies of vaporization of the pure liquids to results obtained with the OPLS models [38,39] and to experiment. Some characteristics of the radial distribution functions and pair interaction

energies of the *ab initio* models are provided in Table 2.4 of the main text. Comparisons to OPLS results (available for all solvents except for TFE and ethylene glycol) for these and other structural / energetic properties the neat solvents showed the *ab initio* models to be quite similar to the OPLS models in almost all cases. Table 2.7 summarizes the comparison of the densities and enthalpies of vaporization (ΔH_{vap}) obtained with the *ab initio* and OPLS models to the experimental values. These data show that in cases of overlap, the *ab initio* properties deviate more from the experimental values than their OPLS counterparts. The average absolute error in the simulated densities is 4% for the *ab initio* parameterization and 2.5% for the OPLS parameterization. In the case of ΔH_{vap} the errors are 7% (*ab initio*) versus 1.5% (OPLS). The better agreement for the OPLS set is to be expected since the parameters of these models were optimized in order to reproduce these specific experimental quantities. (For consistency to the other representations we have used a 3-site model for water, whereas the properties reported here are for the preferred 4-site (TIP4P [39]) version.) Nevertheless, in nearly all cases the agreement between the calculated and experimental values appears to be acceptable. The *ab initio* models of 2-propanol and ethylene glycol are too strongly bound by some 15-20% whereas water is too weakly bound by 16%. These departures from experiment should probably be expected to give rise to some quantitative inaccuracies in the results obtained here but to still be qualitatively reliable. However, this may not be true in one solvent, TFE. There is no OPLS model of this solvent we have therefore adopted Lennard-Jones parameters for the CF_3 group from another source [40]. These

parameters, combined with our *ab initio* charges lead to a system with a much lower density (>20% lower!) than is observed experimentally. ΔH_{vap} is also smaller than in experiment by some 11%. Given the large deviation in density it seems prudent to view the results obtained with this solvent model with some caution. We are currently looking for a better potential model with which to represent this particular solvent.

Table 2.7. Thermodynamic Properties of the Neat Solvents^a

Solvent	density (g cm ⁻³)			H _{vap} (kJ/mol) ^b		
	expt	ab initio	OPLS	expt	ab initio	OPLS
methanol	0.786	0.758 (-4)	0.759(-3)	37.4	35.8(-4)	37.9(+1)
ethanol	0.785	0.811(+3)	0.748(-5)	42.3	42.7(+1)	41.8(-1)
1-propanol	0.800	0.835(+4)	0.788(-1)	47.3	46.2(-2)	47.4(+0)
TFE	1.374	1.088(-21)		43.4	38.7(-11)	
2-propanol	0.781	0.722(-1)	0.799(-0)	45.5	53.8(+18)	47.0(+3)
tert-butyl alcohol	0.781	0.755(-3)	0.773(-1)	46.8	46.1(-2)	46.4(-1)
ethylene glycol	1.110	1.075(-3)		67.8	78.7(+16)	
water ^c	0.997	0.912(-9)	0.999(+0)	44.0	36.9(-16)	44.6(+1)

^a All values correspond to 298.15 K and 1 atm pressure. Values in parentheses are the percentage errors in the simulated values. OPLS and experimental values taken from the compilations in refs 38 and 39. ^b Enthalpies of vaporization were calculated from the total interaction energies observed in the simulation using an experimental correction for gas nonideality as discussed in ref 38. ^c The OPLS values listed for water are for the preferred TIP4P model.³⁹

2.6. Notes and References

1. Ingham, K. C. and El-Bayoumi, M. A. *J. Am. Chem. Soc.* **1974**, *96*, 1674.
2. Share, P., Pereira, M., Sarisky, M., Repinec, S. and Hochstrasser, R. M. *J. Luminesc.* **1991**, *48 and 49*, 204.
3. Takeuchi, S. and Tahara, T. *Chem. Phys. Lett.* **1997**, *277*, 340.
4. Reynolds, L. E. and Maroncelli, M. *J. Phys. Chem.* **1998**.
5. Douhal, A., Kim, S. K. and Zewail, A. H. *Nature* **1995**, *378*, 260.
6. Fuke, K., Tsukamoto, K., Misaizu, F. and Kaya, K. *J. Chem. Phys.* **1991**, *95*, 4074.
7. Chang, C.-P., Hwang, W.-C., Meng-Shin, K., Chou, P.-T. and Clements, J. H. *J. Phys. Chem.* **1994**, *98*, 8801.
8. Chou, P.-T., Wei, C.-Y., Chang, C.-P. and Chiu, C.-H. *J. Am. Chem. Soc.* **1995**, *117*, 7257.
9. Avouris, P., Yang, L. L. and El-Bayoumi, M. A. *Photochem. Photobiol.* **1976**, *24*, 211.
10. Herbich, J., Sepiol, J. and Waluk, J. *J. Mol. Spectrosc.* **1984**, *114*, 329.
11. McMorow, D. and Aartsma, T. J. *Chem. Phys. Lett.* **1986**, *125*, 581.
12. Konijnenberg, J., Huizer, A. H. and Varma, C. A. G. O. *J. Chem. Soc., Faraday Trans. II* **1988**, *84*, 1163.
13. Moog, R. S. and Maroncelli, M. *J. Phys. Chem.* **1991**, *95*, 10359.
14. Chapman, C. F. and Maroncelli, M. *J. Phys. Chem.* **1992**, *96*, 8430.

15. Smirnov, A. V., English, D. S., Rich, R. L., Lane, J., Teyton, L., Schwabacher, A. W., Luo, S., Thornburg, R. W. and Petrich, J. W. *J. Phys. Chem. B* **1997**, *101*, 2758; Chen, Y., Rich, R. L., Gai, F. and Petrich, J. W. *J. Chem. Phys.* **1993**, *97*, 1770. 2106; Gai F., Chen Y. and Petrich, J. W. *J. Am. Chem. Soc.* **1992**, *114*, 8343.
16. Chen, Y., Gai, F. and Petrich, J. *Chem. Phys. Lett.* **1994**, *222*, 329.
17. Chen, Y., Gai, F. and Petrich, J. W. *J. Am. Chem. Soc.* **1993**, *115*, 10158.
18. Chou, P.-T., Martinez, M. L., Cooper, W. C., McMorro, D., Collins, S. T. and Kasha, M. *J. Phys. Chem.* **1992**, *96*, 5203.
19. Waluk, J., Kamorowski, S. J. and Herbich, J. *J. Phys. Chem.* **1986**, *90*, 3868.
20. Boryschuk, S. J., *The Excited-State Double Proton Transfer Reaction of 1-Azacarbazole in Alcohols*, MS thesis (Penn State University, 1993); see also Chapman, C. F. *Time-Resolved Fluorescence Studies of Solvation Dynamics and Chemical Reaction*, Ph.D. Thesis (Penn State University, 1992).
21. Reynolds, L. E., Boryschuk, S. J., Chapman, C. F. and Maroncelli, M. "The Excited-State Tautomerization of 1-Azacarbazole and 7-Azaindole in Hydroxylic Solvents: A Revised View of the Solvent's Role," to be submitted to *J. Phys. Chem.* **1998**.
22. In Ref. 16 Petrich and coworkers suggested that the differences in reaction rates of 7-AI in different alcohols may be due to differences in the acidity of different alcohols affecting the actual proton transfer step. In our view, the fact that the

isotope effect does not vary substantially over a range of alcohol solvents makes this interpretation seem unlikely.

23. Note that our notation differs somewhat from that conventionally used in TST in that the ΔG^\ddagger here is a true equilibrium constant -- i.e. we have not extracted the reaction coordinate motion from ΔG^\ddagger and thus there is no $(k_B T/h)$ factor here.
24. One exception to this statement is the short note published during the earliest stages of the present work: Chapman, C. F., Marrone, T. J., Moog, R. S. and Maroncelli, M., in *Ultrafast Phenomena VIII* (eds Martin, J.-L., Migus, A., Mourou, G. A. and Zewail, A. H.) 624 (Springer-Verlag, Berlin, 1993).
25. Jorgensen, W. L., BOSS Version 3.5; Yale University: New Haven CN., 1994.
26. Under these conditions tertiary-butanol is actually a solid (m.p. 25.5 °C), however, no behavior signaling an incipient phase transition was observed in this case.
27. See for example, *Computer Simulation of Liquids* (Allen, M. P. and Tildesley, D. J.) (Oxford, Oxford, 1987).
28. This $w(R_{NH}, R_{HO})$ function, which is somewhat unusual, was arrived at by trial and error. The more commonly used harmonic constraint potentials were not as useful for our purposes.
29. Kumar, P. V. and Maroncelli, M. *J. Chem. Phys.* **1995**, *103*, 3038.
30. The semi-empirical calculations performed with the program AMPAC version 5.0 SemiChem: 7128 Summitt, Shawnee KS 66216 (1995).

31. Pranata, J., Wierschke, S. G. and Jorgensen, W. L. *J. Am. Chem. Soc.* **1991**, *113*, 2810.
32. *Ab initio* calculations were performed with the Gaussian94 program: Gaussian 94, Revision B.1, M. J. Frisch, G. W. Trucks, H. B. Schlegel, P. M. W. Gill, B. G. Johnson, M. A. Robb, J. R. Cheeseman, T. Keith, G. A. Petersson, J. A. Montgomery, K. Raghavachari, M. A. Al-Laham, V. G. Zakrzewski, J. V. Ortiz, J. B. Foresman, J. Cioslowski, B. B. Stefanov, A. Nanayakkara, M. Challacombe, C. Y. Peng, P. Y. Ayala, W. Chen, M. W. Wong, J. L. Andres, E. S. Replogle, R. Gomperts, R. L. Martin, D. J. Fox, J. S. Binkley, D. J. Defrees, J. Baker, J. P. Stewart, M. Head-Gordon, C. Gonzalez, and J. A. Pople, Gaussian, Inc., Pittsburgh PA, 1995. Charges fit according to the Merz-Singh-Kollman scheme, U.C. Singh and P.A. Kollman, *J. Comp. Chem.* **1984**, *5*, 129. B.H. Besler, K.M. Merz and P.A. Kollman, *J. Comp. Chem.* **1990**, *11*, 431.
33. See the examples and discussion in: Reynolds, L., Gardecki, J. A., Frankland, S. J. V., Hornig, M. L. and Maroncelli, M. *J. Phys. Chem.* **1996**, *100*, 10337.
34. We have used MC simulations to compute the association constants for 1:1 complexes between these solutes and a number of complexing partners for which there is dilute solution data available. We find reasonably good agreement using the same solute-solvent potentials employed here. [S. Mente, R. S. Moog, and M. Maroncelli, manuscript in preparation].
35. These values are from geometry-optimized AM1/CI calculations performed with the AMPAC program [30] using key word "CI=12" specifying use of an CI

calculation of 100 microstates formed from selected excitations among the 12 molecular orbitals bracketing the HOMO-LUMO gap.

36. L. E. Reynolds and M. Maroncelli, unpublished results on 1-AC acid-base equilibria.
37. Jorgensen, W. L., Madura, J. D. and Swenson, C. J. *J. Am. Chem. Soc.* **1984**, *106*, 6638.
38. Jorgensen, W. L. *J. Phys. Chem.* **1986**, *90*, 1276.
39. Jorgensen, W. L., Chandrasekhar, J., Madura, J. D., Impey, R. W. and Klein, M. L. *J. Chem. Phys.* **1983**, *79*, 926.
40. Gough, C. A., DeBolt, S. E., and Kollman, P. A. *J. Comput. Chem.* **1992**, *13*, 963.
41. Fuke, K., Yoshiuchi, H. and Kaya, K. *J. Phys. Chem.* **1984**, *88*, 5840; Fuke, K., Yabe, T., Chiba, N., Kohida, T. and Kaya, K. *J. Phys. Chem.* **1986**, *90*, 2309.
42. See, for example, Nakagawa, T., Kohtani, S. and Itoh, M. *J. Am. Chem. Soc.* **1995**, *117*, 7952, and references therein.
43. *An Introduction to Hydrogen Bonding* (Jeffrey, G. A.) (Oxford University Press, New York, 1997).
44. Chou, P.-T., Wei, C.-Y., Chang, C.-P. and Meng-Shin, K. *J. Phys. Chem.* **1995**, *99*, 11994.
45. Gordon, M. S. *J. Phys. Chem.* **1996**, *100*, 3974.
46. Herbich, J., Dobkowski, J., Thummel, R. P., Hegde, V. and Waluk, J. *J. Phys. Chem. A* **1997**, *101*, 5839.

47. Northrup, S. H. and Hynes, J. T. *J. Chem. Phys.* **1980**, *73*, 2700; Hynes, J. T., in *The Theory of Chemical Reactions* (eds Baer, M. and Csizmadia, I. G.) 171 (CRC Press, Boca Raton, 1985); Northrup, S. H. and Hynes, J. T. *J. Chem. Phys.* **1978**, *69*, 5246.
48. Northrup, S. H. and Hynes, J. T. *J. Chem. Phys.* **1980**, *73*, 2700, Appendix C.
49. This need not be the case. One might have imagined the cyclic form to be a local minimum in the solvation free energy surface, in which case the reactive geometry once formed would persist for some time. However, in none of the systems studied have we found evidence of the cyclic geometry being at a local minimum in free energy.
50. Pratt, K. C. and Wakeham, W. A. *Trans. Faraday Soc.* **1977**, *II/73*, 997. Self-Diffusion in Water and Monohydric Alcohols
51. Matsumoto, M. and Gubbins, K. E. *J. Chem. Phys.* **1990**, *93*, 1981.
52. Different criteria have been used by other researchers to define hydrogen bonding in pure liquid systems. These have included the use of molecular pair interaction energies or more elaborate geometric criteria. In our case, the use of interaction energies is not possible because we are attempting to differentiate the higher-energy end of many possible hydrogen-bonded configurations, rather than just distinguishing between hydrogen bonded and non-hydrogen bonded structures. Geometrically, we have considered using, in addition to the two distance parameters, an extra dimension, the angle denoted " χ " (formed by connecting the solute hydrogen active site with the solvent oxygen and the first carbon), which

would pick out configurations in which less nuclear rearrangement would be needed if the actual proton shuttling were to occur. However, even using the non-Boltzmann sampling scheme, it was too difficult to obtain accurate results for f^* using this criterion.

53. This manner of charge variation was motivated by *ab initio* calculations which show that in different alkyl alcohols the H atom charge is nearly constant while the O-atom charge and the group to which it is attached account for most of the variations observed.
54. This feature of the TFE model is disturbing since empirically TFE is found to be a much stronger hydrogen bond donor than methanol. See for example, Abraham, M. H. *Chem. Soc. Rev.* **1993**, 22, 73; Marcus, Y. *J. Sol. Chem.* **1991**, 20, 929.
55. We note that these comparisons for water assume the overall reaction time of 830 ps reported by Chapman and Maroncelli [14]. However, there are two time constants observed in the 7AI/water system, this slow time and a much faster time of ~100 ps and there is some disagreement in the literature as to which of these two times to associate with the reaction [14,15]. If instead of this 830 ps we use the time of 70 ps favored by Petrich and coworkers [15] (ignoring the fact that in their model only a small fraction of molecules are envisioned to react) we would compute a time constant of $\tau_{PT} \sim 50$ fs.
56. Nakajima, A., Hirano, M., Hasumi, R., Kaya, K., Watanabe, H., Carter, C. C., Williamson, J. M., and Miller, T. L. *J. Phys. Chem. A* **1997**, 101, 392.

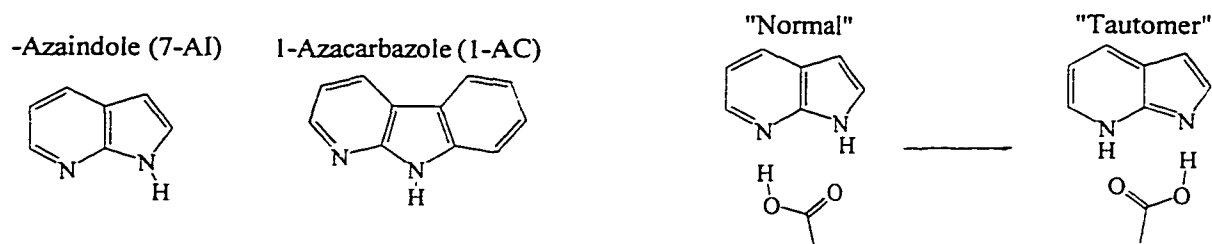
57. This identification assumes that k_{pT} is activationless, which is implied by the experimental observation that the isotope effect is temperature independent [21].
58. Based on the data in Ref. 20 over the temperature range 203-323 K. Uncertainties listed here are ± 2 standard deviations.
59. Mente, S. and Maroncelli, M., work in progress.
60. Reynolds, L. E. and Maroncelli, M., to be published.

Chapter 3

EVALUATION OF CLASSICAL POTENTIAL FUNCTIONS FOR HYDROGEN BONDING IN 7-AZAINDOLE AND 1-AZACARBAZOLE COMPLEXES

3.1. Introduction

The previous chapter reported a series of calculations aimed at elucidating how structural and energetic characteristics of the hydrogen bonding between 7-AI or 1-AC and hydroxylic solvents dictate the proton transfer rates observed in bulk alcohol solvents. One of the more important considerations in those studies was the choice of potential functions, which were simple classical atom-centered Lennard-Jones plus Coulomb terms of the sort commonly used in this type of simulation. However, rather than adopting one of the many force fields currently in the literature, we found it more appropriate to employ a mixed representation in which standard Lennard-Jones parameters are combined with charges determined from electrostatic potential fits to *ab initio* wavefunctions [1], as has been advocated by Kollman & coworkers [2]. In Section 2.7, some of the pure solvent properties of these models were examined and it was shown that they are not significantly less accurate than the OPLS potentials [3] which had been specifically parameterized to reproduce bulk alcohol properties.



Scheme 1

In the present chapter, we discuss how well these potential functions represent the interactions between 7-AI and 1-AC and isolated hydrogen bonding partners using two different comparisons. The first test makes use of energies of interaction computed for 1:1 solute-solvent complexes via *ab initio* calculations. We compare the results of the classical potential calculations to these presumably more accurate *ab initio* calculations as substitutes for experimental data on gas phase complexes. The second test compares solution-phase free energies calculated with the classical potentials to available experimental data on 7-AI and 1-AC complexes measured in dilute alkane solution. From these two comparisons we find that, in addition to yielding reasonable representations of bulk solvent properties, these simple classical potentials also quantitatively reproduce both the *ab initio* and experimental results on the energetics of association.

3.2. Computational Procedure

For all simulations, molecules were represented as rigid collections of interaction sites which interact via pairwise site-site terms of the form:

$$v_{ij} = 4\varepsilon_{ij} \left[\left(\frac{\sigma_{ij}}{r_{ij}} \right)^{12} - \left(\frac{\sigma_{ij}}{r_{ij}} \right)^6 \right] + \frac{q_i q_j}{r_{ij}} \quad (3-1)$$

Lennard-Jones parameters were standard values taken from the OPLS parameterizations of alcohols [3] and nucleic acids [4]. Parameters between unlike atoms were determined from the like-atom parameters using the (OPLS) mixing rules $\sigma_{ij}=(\sigma_i\sigma_j)^{1/2}$ and $\varepsilon_{ij}=(\varepsilon_i\varepsilon_j)^{1/2}$. All atoms of the solutes (7-AI and 1-AC) were treated as individual interaction sites. However, the CH_n groups on the complexing partners were represented as united atoms [5]. Similarly, molecules of cyclohexane, used as an inert supporting solvent in the dilute solution studies, were represented as single Lennard-Jones sites. The charges used in the modeling were obtained from electrostatic potential fits of *ab initio* wavefunctions of the various molecules, as discussed below. A complete listing of the parameters and geometries of most of the species employed in these simulations has been detailed in Chapter 2 and will not be repeated here.

Structures and energies of the gas-phase binary complexes generated by these classical potentials were computed using a Monte Carlo search algorithm which efficiently explores the entire potential energy surface. This algorithm samples a large collection of random initial orientations and generates a collection of minimum-energy structures via a temperature-ramped MC walk as described in detail in Ref. 6.

To calculate solution-phase association constants, Monte Carlo simulations were performed using the “BOSS” molecular simulation program developed by Jorgensen [7]. Free energies of association ΔG_{assoc} were determined using the relations:

$$\Delta G_{assoc} = -k_B T \ln K_{assoc} \quad (3-2)$$

and

$$K_{assoc} = 4\pi \int_0^\infty r^2 e^{-w(r)/k_B T} dr \quad (3-3)$$

In these expressions $w(r)$ is the potential of mean force calculated as a function of the “reaction coordinate” r taken as the hydrogen bond distance between the N: of the 7-AI or 1-AC and the H-bond donating site on the complexing partner (labeled N_U---H_V in Fig. 3.1). Simulations were performed using a single pair of complexing partners surrounded by a bath of 104 model cyclohexane solvent molecules. Constant temperature and pressure (298 K, 1 atm) and the usual cubic periodic boundary conditions were employed. The potential of mean force was determined by moving r from contact to roughly 9 Å [8] in a sequence of equilibrium simulations using statistical perturbation theory [9] and double-wide sampling [10]. Each simulation consisted of an equilibration period of 6×10^5 configurations after which the ensemble was averaged for an additional 10^6 configurations.

All *ab-initio* calculations were performed using the Gaussian 94 program [11] at the HF/6-31G* level. The individual solute and solvent molecules were geometry

optimized, and atom-centered point charges were fit to the molecular electrostatic potential using the Merz-Kollman-Singh method [1]. For determining the energies of formation of isolated complexes, initial pair geometries were taken from the classical MC minimizations. The structure of the complexes were then optimized by allowing all atoms to relax to a stationary point in the *ab initio* calculation. The energy of formation was then computed simply as the difference between the energy of the pair and their individually optimized energies:

$$\Delta E_0 = E_{\text{complex}} - E_{\text{solute}} - E_{\text{solvent}} \quad (3-4)$$

3.3. Results and Discussion

Energy minimized structures of gas-phase complexes of 7-AI and 1-AC with various hydrogen bonding partners were obtained using both the classical potential functions and *ab initio* calculations. The Monte Carlo search algorithm [6] provided a convenient way to explore the local minima of the potential energy surfaces. In all cases two main sorts of complexes were observed: π -complexes, in which the smaller partner is hydrogen bonded to one of the aromatic rings of the 7-AI or 1-AC molecule, and cyclic, doubly hydrogen bonded complexes of the sort illustrated in Fig. 3.1 [13]. In all cases studied here the cyclic structures were found to be the most stable, typically by 20-35

kJ/mol. Since the latter structures are of most relevance for the proton-transfer problem, we focus attention only on these cyclic forms.

Table 3.1 lists the two hydrogen bonding distances and angles (Fig. 3.1) calculated for gas-phase cyclic complexes from the classical potential functions. One feature which is immediately noticeable is the geometric distinction between the complexes that 7-AI and 1-AC form with water and alcohol molecules as compared to the other partners. The hydrogen bonding angles θ_1 and especially θ_2 are significantly non-linear in these alcohol and water complexes whereas the hydrogen bonds made in most other complexes are within 10° of linearity. Similarly, the hydrogen bonding distances are longer in the alcohol and water complexes, especially the $R(H_U \cdots X_V)$ distance. Both of these features underlie the energetic differences between these complexes to be discussed shortly.

Also listed in Table 3.1 are the hydrogen bonding distances determined from *ab initio* calculations. Assuming the *ab initio* results to be the more reliable, the comparison in Table 3.1 reveals that hydrogen bonding distances are generally underestimated by the classical calculations, typically by ~ 0.2 Å. This deviation from the *ab initio* results has been noted previously by Pranata, Wiershke and Jorgensen [4]. In their attempt to model nucleotide base pairs using similar classical potential functions, these authors also found uniformly shorter hydrogen bond distances compared to *ab initio* methods. They pointed

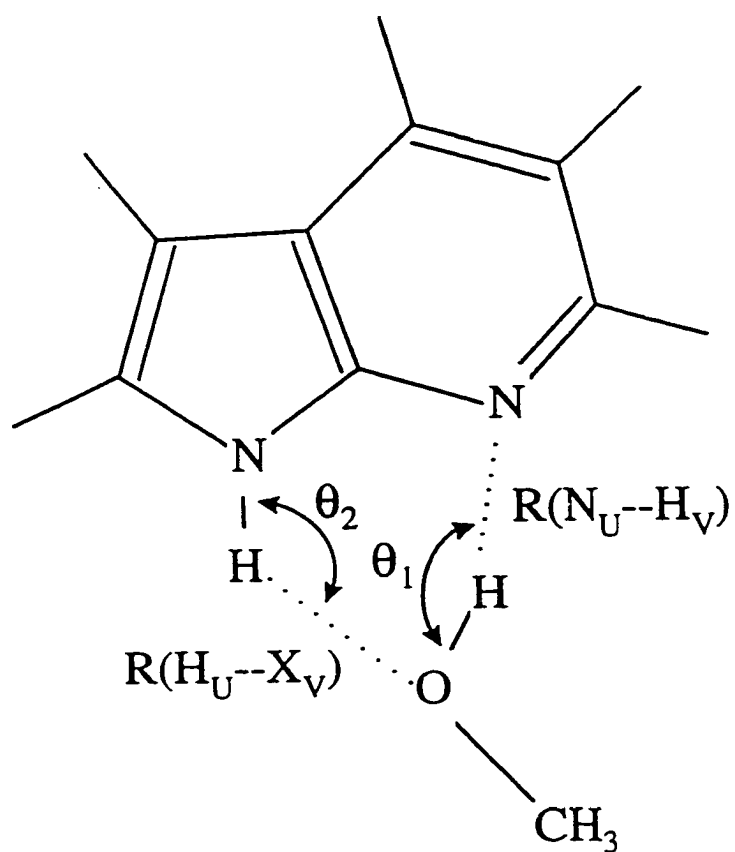


Figure 3.1. Structure of the energy-minimized (gas phase) 7-Al:ethanol complex.

Table 3.1. Summary of calculation results

Systems	Gas-phase interaction energies, -E (kJ/mol)				Gas-Phase normal structures						Solution-phase energies		
	normal		tautomer		R(Nu-Hv) (Å)		R(Hu-Xv) (Å)		θ_1 (°)	θ_2 (°)	- ΔG_{assoc} (kJ/mol)		-(ΔE) (kJ/mol)
	MC	ab initio	MC	ab initio	MC	ab initio	MC	ab initio			MC	observed	
1-Azacarbazole:													
water	37.04		48.28		2.03		2.07		162	134	8.0 ± 0.10		29.7 ± 0.4
MeOH	40.24	36.57	51.69	50.67 ^c	1.95	2.14	2.12	2.12	161	130	9.7 ± 0.04		35.2 ± 0.4
1-BuOH	43.70		55.75		1.97		2.05		160	133	14.4 ± 0.03	8.4 ± 1.2 ^d	40.0 ± 0.9
AcOH	66.75	58.37	83.67	76.11	1.81	1.92	1.80	2.02	172	154	24.71 ± 0.03	22.8 ± 0.5 ^d	64.8 ± 0.2
1-AC	66.91		98.88		1.87		1.83		178	176	23.07 ± 0.16	16.2 ± 0.3 ^e	59.8 ± 0.5
δ-VL	64.96				1.99		1.83		178	176	17.08 ± 0.12	19.8 ± 0.4 ^f	58.5 ± 0.4
formamide	63.83	51.30	73.82	75.56	1.95	2.16	1.73	1.98	179	169			
NMF	59.02	51.30	66.11	70.79	1.91	2.18	1.72	1.97	179	168			
7-Azaindole:													
water	37.00	34.7 ^b	47.05		2.01	2.14 ^b	2.10	2.12 ^b	163	133	7.2 ± 0.11		29.4 ± 0.5
methanol	40.10	38.5 ^b	50.04		1.95	2.12 ^b	2.13	2.12 ^b	162	130	8.4 ± 0.10	11.0 ± 0.4 ^b	33.2 ± 0.5
AcOH	65.77	59.4 ^b	80.56	81.1 ^b	1.90	1.91 ^b	1.79	2.01 ^b	168	154	23.49 ± 0.03	24.3 ± 0.7 ^b	63.2 ± 0.3
7-AI	63.45	47.2 ^b	93.18	90.3 ^b	1.84	2.12 ^b	1.88	2.12 ^b	179	170	19.37 ± 0.09	19.1 ± 0.6 ^b	54.8 ± 0.4
δ-VL	63.0				1.94		1.72		175	167	21.8 ± 0.11	19.2 ± 0.5 ^g	57.5 ± 0.16

^a The complexing partner abbreviations are: MeOH = methanol; 1-BuOH = 1-butanol; AcOH = acetic acid; 1-AC = 1-azacarbazole; δ-VL = δ-valerolactam; NMF = *n*-methylformamide; and 7-AI = 7-azaindole.

^b Ref. [19].

^c This structure did not formally converge to a stationary point.

^d Ref. [25].

^e Ref. [26].

^f L. Reynolds, experimental estimate from spectrophotometric titration.

^g Ref. [27].

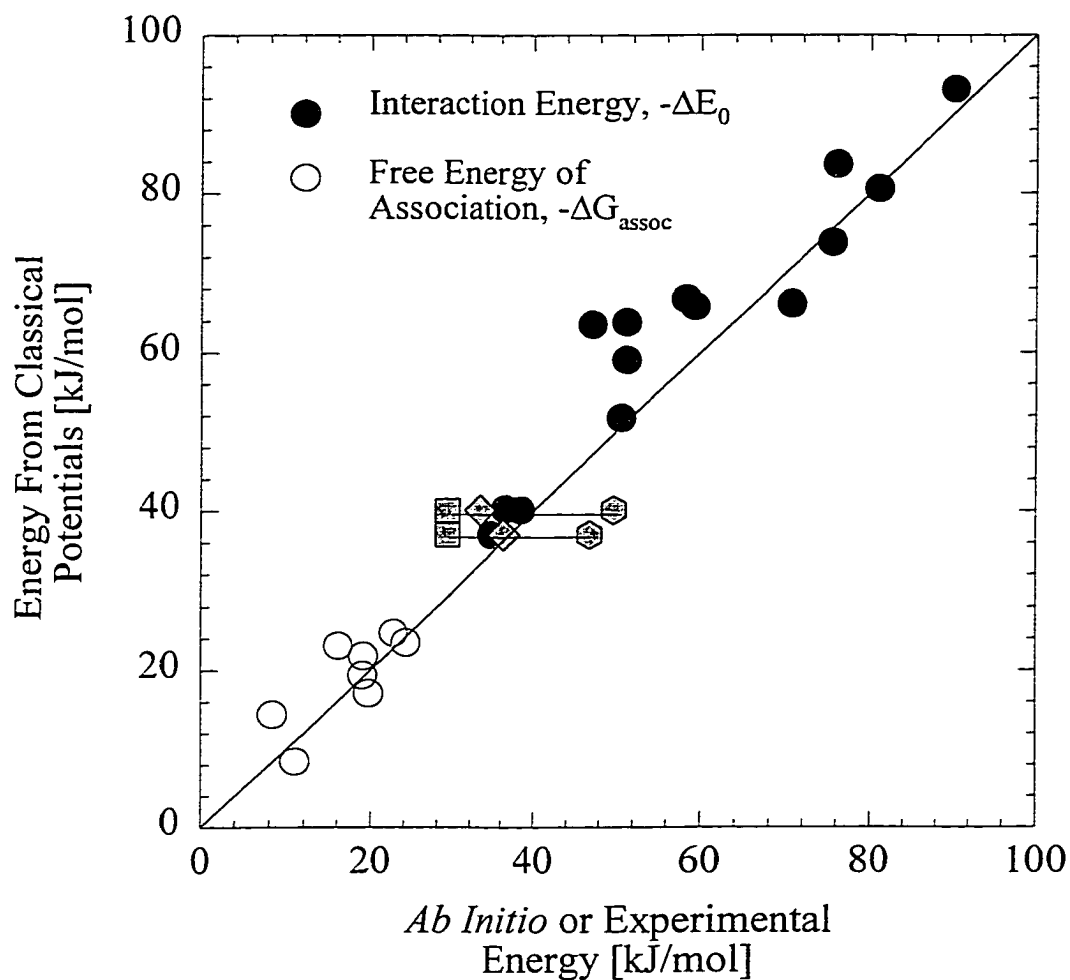


Figure 3.2. Comparison of simulated energies with observed free energies of association (open circles) and ab initio determined interaction energies (closed symbols). Black circles indicate calculations using the 6-31G* basis set. Grey symbols indicate values Ref. [18] for the SCF/DZP (diamonds), SCF/aug-cc-DZP (squares) and MP2/aug-cc-DZP (hexagons) basis sets. The line shown is the line of equal value.

out that such deviations reflect the choice of nitrogen-atom Lennard-Jones parameters, which yield short hydrogen-bonding distances in gas-phase complexes if parameterized to yield accurate liquid phase densities for amide solvents [20]. In spite of this geometric error, the energetic results obtained with these potentials are quite satisfactory.

Energies of the gas phase complexes computed using both the classical and *ab initio* methods are listed in Table 3.1 and plotted in Fig. 3.2 (solid symbols). In addition to complexes formed from the “normal” forms of 7-AI and 1-AC in Fig. 3.2, we have also plotted energies calculated for complexes involving the tautomers of 7-AI and 1-AC (see Scheme 1) [21]. Generally good agreement is found between the *ab initio* energies and those calculated using the classical potential functions. The average absolute deviation for the set of 13 complexes studied is 5.6 kJ/mol (9.8 %). However, a systematic deviation between the two calculations is apparent, with the classical energies being an average of 5.3 kJ/mol higher than the *ab initio* energies. This stabilization of the classical energies relative to the *ab initio* ones is a result of the choice of charges employed in the classical potential functions. Our practice is to use the Lennard-Jones parameters of the OPLS potential set [7] with ESP-fit charges. In the aforementioned studies of hydrogen bonding in DNA base pairs, Jorgensen and coworkers [4] employed these same Lennard-Jones parameters but chose to adjust the charges on various atoms in order to derive a charge set which best matched *ab initio* energies of the sort examined here. The resulting charges found in that work tend to be slightly smaller than those obtained from the ESP fit alone. For example, the average charges on the N atoms in our

7-AI and 1-AC solutes are ~ 0.17 au more negative and the H(-N) atoms ~ 0.06 au more positive than the comparable atoms on their nucleotide bases. A similar charge exaggeration is seen for formamide, N-methylformamide and, to a lesser extent, acetic acid. The energy stabilization observed in our calculations results directly from this slight charge enhancement of our models compared to the OPLS models. While better agreement with the *ab initio* results on these gas-phase complexes could be anticipated if the OPLS charges were used, for the purposes of our work [Ref. 5] accurate charges were deemed more important. The comparisons provided in Fig. 3.2 demonstrate that this choice does provide a good representation of the gas-phase energetics.

It should be recognized that the energies of association (electronic interaction energies) calculated here with *ab initio* methods do not necessarily reflect the exact values. For example, the results reported in Ref. 18 indicate that the choice of basis set alone can change the predicted complexation energies by as much as 20 kJ/mol [22]. This point is illustrated in Fig. 3.2, where we show the range of values (grey symbols) calculated for 7AI-methanol and 7AI-water complexes using *ab initio* methods [18,19]. Furthermore, corrections for the effects of electron correlation and basis set superposition error have not been applied here [12]. In the absence of experimental data with which to judge the quality of these *ab initio* energies, it is therefore best to view these *ab initio* calculations, as being approximate tests of the classical potential functions accurate to only ~ 8 -12 kJ/mol.

Experimental data on solution-phase complexes can be used to judge the accuracy of the classical potential functions in a more absolute sense. A number of workers have measured complexation constants of 7-AI and 1-AC with different hydrogen-bonding agents in alkane solvents near room temperature [19, 23-27]. Results for eight complexes in dilute alkane solution are listed in the form of free energies of association ΔG_{assoc} in Table 3.1. These values are compared to free energies simulated using the classical potential functions in Table 3.1 and Fig. 3.2 (open symbols). We note that in all cases the complexes formed in solution are structurally similar to the gas phase (0 K) complexes. There is a close correlation between the average interaction energies of the complexing partners in solution at 298 K ($\langle \Delta E \rangle$ in Table 3.1) and the gas-phase interaction energies (ΔE_0) for these complexes ($\langle \Delta E \rangle \cong 0.9 \Delta E_0$). Especially for the most strongly bound complexes, the complex geometry remains relatively well defined in room-temperature solution. For this reason the potentials of mean force calculated here are smooth and yield fairly accurate values of ΔG_{assoc} .

Figure 3.2 demonstrates that the solution free energies calculated using the classical potentials are also in good agreement with experimental values. The average absolute deviation of the 8 data points reported here is 3.0 kJ/mol (19 %). It should be mentioned that the poorest agreement comes from data on the association between 7-AI and 1-AC and alcohol partners. For these weakly associating partners experimental determination of the association constants is difficult due to the prevalence of multimeric

complexes [19], thus their larger error estimates. Ignoring these 2 values in calculating the average absolute deviations gives 2.5 kJ/mol (9.4 %) for the remaining 6 values.

Before concluding, two additional features of the comparisons made here may be noted. First, the solution-phase free energies are reasonably well correlated ($r^2=0.90$) to the minimum energies found from gas phase calculations ($\Delta G_{\text{assoc}} \cong 0.31 \Delta E_0$, Fig. 3.3). The systematically lower free energies correspond to a loss of entropy upon complex formation which is approximately what one would expect for an association process between two rigid molecules in the gas phase ($\sim 100 \text{ JK}^{-1}\text{mol}^{-1}$) [28]. As discussed in some detail in Ref. 5, it appears that the association between 7-AI and 1-AC and the sort of partners examined here is dictated largely by the energetics of the pair of hydrogen bonds that can be formed between the two molecules in the complex. These hydrogen bond energetics are controlled mainly by the geometry of the 7-AI / 1-AC “active site”. As already mentioned, the alcohols and water form a relatively poor fit to these solutes. The requirement that a single O-H bond in these ROH species simultaneously bond to both solute sites results in highly non-linear and elongated hydrogen bonds, which are therefore relatively weak. The added flexibility and/or perfect fit afforded by the remaining partners (which all bridge the solute (N-)H and N: sites using a 3-bond bridge) make the latter complexes much more stable.

Second, the energies and free energies of complex formation computed for 7-AI and 1-AC are nearly identical. A comparison of all of the various classically derived

energies plotted in Fig. 3.4 shows that $E_{7AI} = 0.96 \times E_{1-AC}$ with a correlation coefficient of 0.997. This near identity of the interactions of these two solutes with different hydrogen bonding partners underlies the striking similarities observed in their tautomerization kinetics [29-32].

3.4. Summary and Conclusions

We have examined the performance of simple classical potential functions for representing the hydrogen bonding between 7-AI and 1-AC and various complexing partners. The potential functions employed here and in our previous study [5] consist of standard atom-centered Lennard-Jones plus Coulomb representations of intermolecular interactions. The Lennard-Jones parameters are from the OPLS set [3,4,7] and charges are derived from ESP fits to *ab initio* wavefunctions of the monomers. As such, these potentials are reasonably easy to generate for virtually any typical organic molecule of moderate size. We find that for reproducing the energetics of complexation of 7-AI and 1-AC with a range of partners, such simple potential functions work fairly well. On average the deviations between these calculations based on classical potentials and available experimental data are on the order of ± 3.8 kJ/mol or ± 13 %. This level of agreement implies that such potentials should provide sufficient accuracy for many applications, such as the investigation of the solvation / hydrogen bonding effects on reaction kinetics undertaken in Chapter 2.

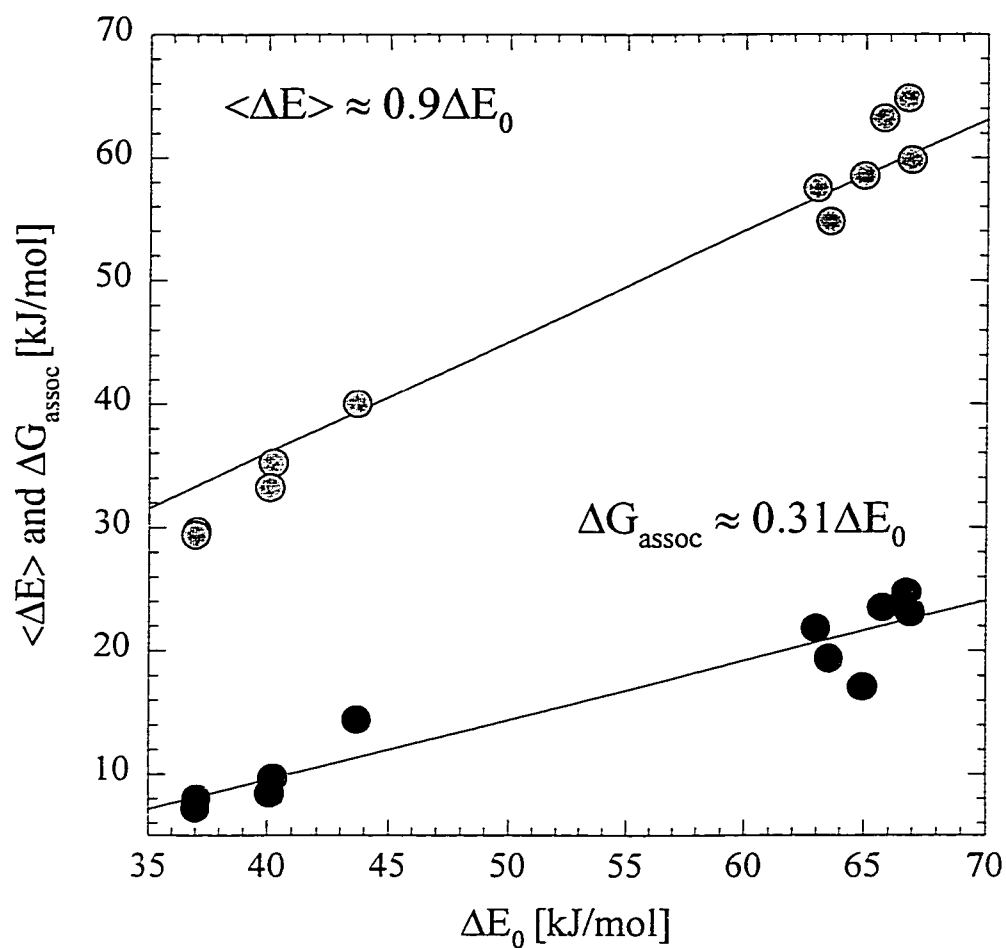


Figure 3.3. Comparison between the average interaction energies of the complexing partners in solution at 298 K (grey symbols) and the solution free energies (black symbols) with the gas-phase interaction energies (grey symbols).

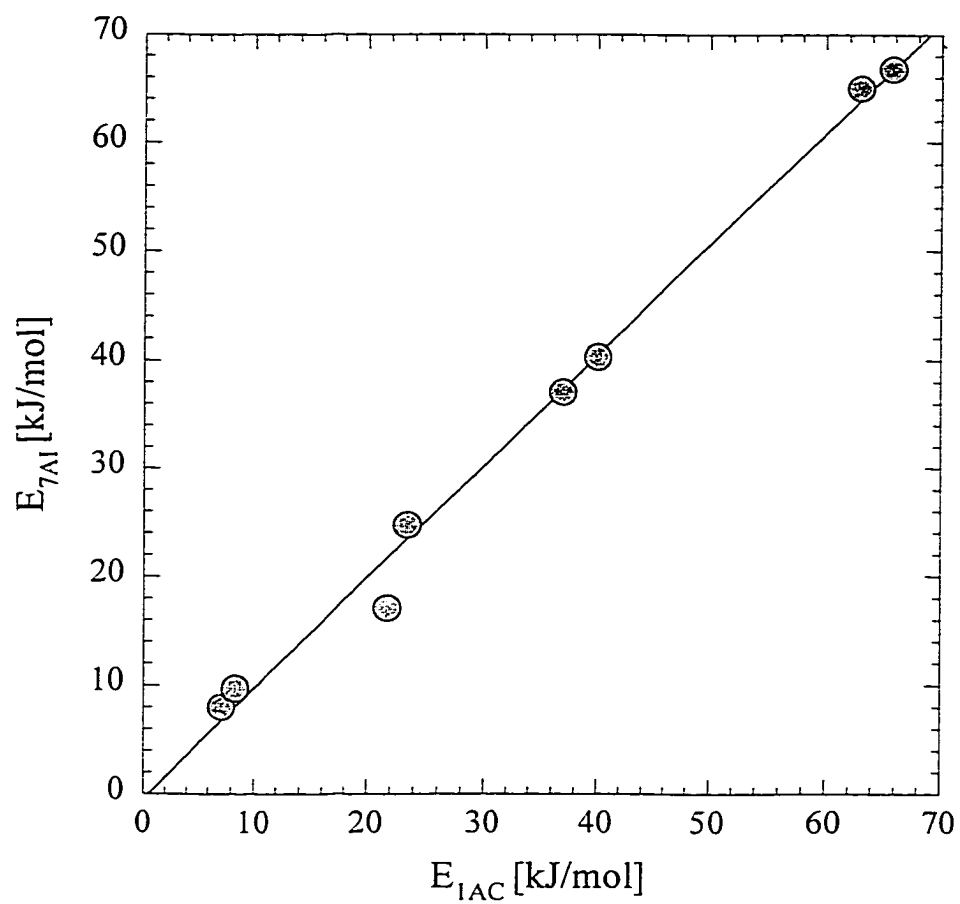


Figure 3.4. Comparison of all classically derived energies and free energies of complex formation for 7-AI and 1-AC.

3.5. References and Notes

1. B.H. Besler, K.M. Merz and P.A. Kollman, *J. Comp. Chem.* **1990**, *11* 431.
2. L. Kuyper, D. Ashton, K.M. Merz, and P.A. Kollman, *J. Phys. Chem.* **1991**, *95*, 6661.
3. W.L. Jorgensen, *J. Phys. Chem.* **1986**, *90*, 1276.
4. J. Pranata, S.G. Wierschke, and W.L. Jorgensen, *J. Am. Chem. Soc.* **1991**, *113*, 2810.
5. S. Mente, and M. Maroncelli, *J. Phys. Chem. A.* **1998**, *102*, 3860.
6. S.J.V. Frankland, Ph.D. Thesis, Penn State University (1997).
7. W.L. Jorgensen, BOSS Version 3.5; Yale University: New Haven CN (1994).
8. The simulations were performed until only small random variations were observed in the potentials of mean force. Generally, this occurred at distances from 8-12 Å.
9. R.L. Zwanzig, *J. Chem. Phys.* **1954**, *22*, 1420.
10. W.L. Jorgensen, and C. Ravimohan, *J. Chem. Phys.* **1985**, *83*, 3050.
11. *Ab initio* calculations were performed with the Gaussian94 program: Gaussian 94, Revision B.1, M. J. Frisch, G. W. Trucks, H. B. Schlegel, P. M. W. Gill, B.

- G. Johnson, M. A. Robb, J. R. Cheeseman, T. Keith, G. A. Petersson, J. A. Montgomery, K. Raghavachari, M. A. Al-Laham, V. G. Zakrzewski, J. V. Ortiz, J. B. Foresman, J. Cioslowski, B. B. Stefanov, A. Nanayakkara, M. Challacombe, C. Y. Peng, P. Y. Ayala, W. Chen, M. W. Wong, J. L. Andres, E. S. Replogle, R. Gomperts, R. L. Martin, D. J. Fox, J. S. Binkley, D. J. Defrees, J. Baker, J. P. Stewart, M. Head-Gordon, C. Gonzalez, and J. A. Pople, Gaussian, Inc., Pittsburgh PA (1995).
12. For a general discussion on the determination of interaction energies using *ab initio* methods, see: S. Scheiner, *Hydrogen Bonding: A Theoretical Perspective*. (New York, Oxford University Press, 1997).
 13. Molecular beam experiments have also shed light on the structure of these complexes. The 7-AI dimer and 1-AC dimer are reported to form reactive, cyclically hydrogen-bonded structures as well as nonreactive conformations [14]. 7-AI:(H₂O)₁ complexes are planar, cyclically hydrogen-bonded structures [15,16]. For discussions on other complexes with protic complexing agents, see [17]. In Ref. [17] Kim and Bernstein have argued that π complexes are the lowest in energy. However, recent *ab initio* calculations also report the cyclically hydrogen-bonded structures as most stable [18,19].
 14. K. Fuke and K. Kaya, *J. Phys. Chem.* **1989**, 93, 614.
 15. A. Nakajima, M. Hirano, R. Hasumi, K. Kaya, H. Watanabe, C. C. Carter, J. M. Williamson, and T. A. Miller, *J. Phys. Chem. A* **1997**, 101, 392.

16. Y. Huang, S. Arnold, and M. Sulkes, *J. Phys. Chem.* **1996**, *100*, 4734.
17. S.K. Kim and E.R. Bernstein, *J. Phys. Chem.* **1990**, *94*, 3531.
18. M.S. Gordon, *J. Phys. Chem.* **1996**, *100*, 3974.
19. P.T. Chou, C. Wei, C. Chang, and K. Meng-Shin, *J. Phys. Chem.* **1995**, *99*, 11994.
20. W.L. Jorgensen, and C.J. Swenson, *J. Am. Chem. Soc.* **1985**, *107*, 1489.
21. In the case of 7-AI and 1-AC dimers and in the amide and lactams the tautomer calculations involved tautomeric forms of both partners involved in the complex.
22. In Ref. 18 Gordon determined that using higher level calculations (MP2/aug-cc-DZP) enhanced the complexation energies of the 7-AI:Water (46.82 kJ/mol) and 7-AI:MeOH (49.74) well beyond those found using the 6-31G* basis set.
23. J. Sepiol and U.P. Wild, *Chem. Phys. Lett.* **1982**, *93*, 204.
24. C. Chang, H. Wen-Chi, K. Meng-Shin, P.T. Chou, and J.H. Clements, *J. Phys. Chem.* **1994**, *98*, 8801.
25. R. S. Moog, personal communication, March 1998.
26. C. Chang, N. Shabestary, and M.A. El-Bayoumi, *Chem. Phys. Lett.* **1980**, *75*, 107.
27. P.T. Chou, C. Wei, C. Chang, and C. Chiu, *J. Am. Chem. Soc.* **1995**, *117*, 7259.
28. The entropy of association for two rigid gas-phase molecules may be calculated using the translational and rotational partition functions with knowledge of the principal moments of inertia of both the separated species and the complex: D.

McQuarie, Statistical Thermodynamics. (New York, Harper and Row Publishers, 1973).

29. R.S. Moog, and M. Maroncelli. *J. Phys. Chem.* **1991**, *95*, 10359.
30. C.F. Chapman, and M. Maroncelli. *J. Phys. Chem.* **1992**, *96*, 8430.
31. S.J. Boryschuk, M.S. Thesis, Penn State University (1993).
32. L. Reynolds, S.J. Boryschuk, C.F. Chapman, M. Maroncelli, manuscript in preparation.

Chapter 4

MONTE CARLO SIMULATIONS OF SOLVATOCHROMISM AND THE $E_T(30)$ SOLVENT POLARITY SCALE

4.1. Introduction

The experimentally observed proton-transfer rates of 7-azaindole and 1-azacarbazole in monoalcoholic solvents have been found to vary logarithmically with empirical solvent polarity parameters and other measures of hydrogen bonding strength [1-3]. An especially good correlation has been observed with the $E_T(30)$ scale of solvent polarity for a wide range of mono-hydroxy solvents (Figure 4.1) [2, 3]. This correlation is generally thought to reflect the importance of hydrogen bonding between the solvent catalyst and the solute, although the exact molecular mechanisms that determine how the reaction rate depends upon hydrogen bonding are unclear. Moreover, the contribution to the overall solvatochromic behavior of betaine-30, the molecule used to define the $E_T(30)$ scale, that may be attributed to hydrogen bonding is not well defined due to the fact that other, non-hydrogen bonding interactions contribute significantly to the shift. This chapter will present results from Monte Carlo computer simulations which examine, from a molecular level, the solvent dependent $\pi \rightarrow \pi^*$ electronic transition band of Reichardt's betaine-30 molecule (see Figure 4.2).

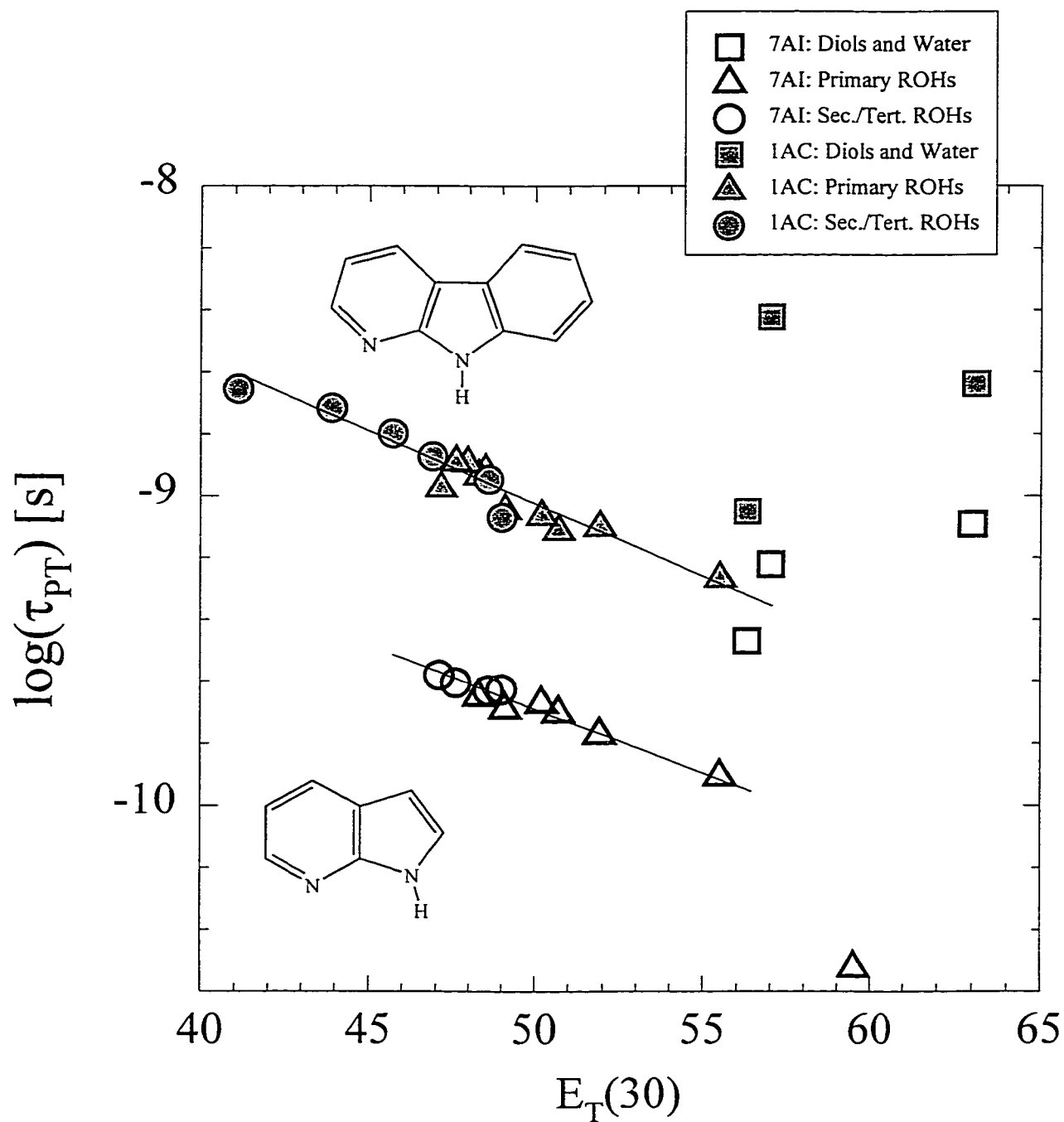


Figure 4.1. Tautomerization times versus polarity.

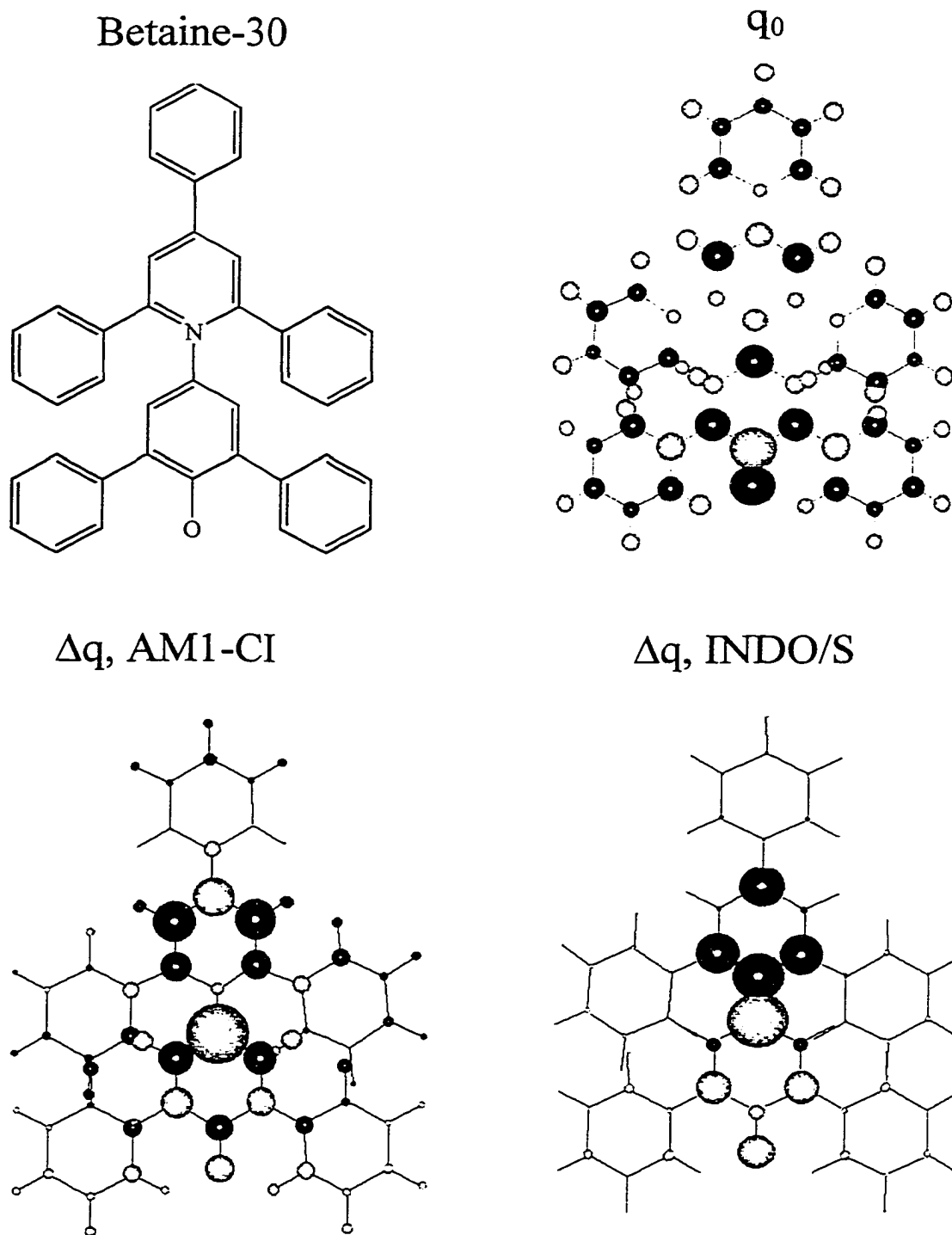


Figure 4.2. Molecular Structure of betaine-30 and the ground and difference (S_1-S_0) charge distributions. The volume of the spheres representing the charge distributions is proportional to the magnitude of the charge. Open circles denote positive charge and filled circles negative charge.

Historically, spectroscopic methods have long been utilized to study solute-solvent interactions. The term “solvatochromism” refers to the solvent influence on the position, intensity and shape of UV absorption and emission spectra. The magnitude of a particular solvatochromic effect depends ultimately on the solute-solvent interactions in the equilibrium ground state and the Frank-Condon excited state. These interactions, in turn, depend on the chemical structure and physical properties of the solute and the solvent molecules.

To better quantify the solute-solvent interactions, chemists have tried to explain various interactions in terms of solvent “polarity.” Polarity is a fairly generic term, best defined as the solvents capacity to solvate a species, and may be more rigorously described as a sum total of all possible intermolecular interactions [4]. These include purely electrostatic forces arising from coulombic interactions between charged species and dipolar molecules (ion/ion, ion/dipole, dipole/dipole), polarization forces that arise from dipole-induced dipole interactions, as well as specific forces such as hydrogen-bonding between pairs of donor-acceptor species.

Prior to the advent of spectroscopically based solvent polarity scales, investigations of intermolecular interactions focused on the solvent’s dielectric response function, $\epsilon(\omega)$ [5]. The values of this function represent the reduction of the attractive force between two oppositely charged plates when a bulk fluid is introduced between them. In this way the function is a measure of the collective properties of the bulk fluid (or material). On this scale all molecular detail has been lost, and the dielectric constant describes a homogeneous, isotropic medium, or continuum of matter. Still, molecular

effects are present in an average sense, and different intermolecular contributions have been discerned using the frequency dependence of the response of these bulk volumes. For instance, abrupt drops in the response occur at frequencies that can be identified with typical frequencies of molecular and atomic motions. For molecules with permanent dipole moments the change in orientation of the molecule contributes to a majority of the dielectric response. As the field changes direction the molecules reorient so as to align these permanent moments with the field direction. Interactions with neighboring molecules tend to hamper this motion, and as a result, a finite amount of time is required before the molecules may be properly reoriented. For obvious reasons, this component is called the orientational response. Two additional components may also be identified. The first is the contribution from vibrational motions within the molecule as they also attempt to accommodate the oscillating field. This component is always small and generally ignored. The remaining component is the electronic response, ϵ_∞ , and is thought to follow the changing field instantaneously. Just as the slow response measures the interactions between permanent moments of the molecules in the fluid, the electronic response measures the interacting molecular polarizabilities.

Since the electronic excitation of the solute is a similar event to the imposition of an electric field, the solvent may be expected to respond in a similar manner to both cases. From this hypothesis have sprung a number of predictive theories that attempt to correlate various spectroscopic events to dielectric parameters characteristic of the bulk fluid [6]. These so-called “continuum” theories have been used to describe a variety of molecular processes. However, due to the neglect of more specific interactions and

molecular shapes, these theories are somewhat limited in their applicability to many chemical problems. Of particular relevance is the neglect of specific interactions, such as hydrogen bonding, in continuum models.

In an attempt to better quantify solvent polarity, Reichardt used the negatively-solvatochromic betaine probe, "betaine-30" (Figure 4.2), to construct the $E_T(30)$ solvent polarity scale [4]. The wavelength maximum of the $S_0 \rightarrow S_1$ $\pi-\pi^*$ absorption of betaine-30 shifts substantially with solvent polarity due to the fact that the ground state of the molecule possesses a much larger dipole moment than the first excited state. This change affects both the direction (the shifts are negatively solvatochromic) and the solvent dependence of the shifts as a result of the solvent mediated stabilization of the ground state relative to the first excited state. The sensitivity to solvent "polarity" can be thought of as arising from the following characteristics of the betaine-30 molecule: (a) the aforementioned large change in dipole moment, which registers dipole/dipole and dipole/induced dipole interactions; (b) The large polarizability (42 π electron system) and likely polarizability change on excitation which registers dispersion interactions; (c) The phenolate oxygen atom gives the molecule a highly basic (hydrogen-bond acceptor, or electron pair donor) center. This last point is generally credited with the variation of the absorption band over a given range of alcoholic solvents.

Although empirical relationships between polarity scales, such as the $E_T(30)$ scale and other phenomena such as reaction rates, have been helpful in understanding specific and general cases of solvation, confusion may arise regarding which specific interactions are responsible for observed correlations. In the case of the solvent-mediated excited-

state proton transfer that occurs in 7-azaindole (7-AI) and 1-azacarbazole (1-AC), the correlation between the tautomerization rate and the $E_T(30)$ solvent polarity scale may be indicative of a variety of intermolecular phenomena. First, the local hydrogen-bonding energetics measured by $E_T(30)$ may affect the time scales of local solvent-solute reorganization (k_l , see Figure 2.1). Simulation results presented in Chapter 2 indicate that this is not the case; the dynamics of the hydrogen bonding in bulk water and methanol are much too rapid to reflect the observed rate. From this observation we concluded that the correlation with $E_T(30)$ instead reflects the nature of the distribution of solvent configurations surrounding the solute. Furthermore, in Chapter 2 we assumed for simplicity that k_{PT} (the rate of the actual proton-shuttling event) was constant for all solvents. Of course this need not be the case. It is likely that the rate of the actual proton-shuttling step, which we have never explicitly measured in bulk polar-protic solvents, probably also influences the value of the observed rate. Any correlation k_{PT} may have with $E_T(30)$ would also manifest itself in the observed rate. In fact, it seems likely that k_{PT} should reflect a solvent's acidity/hydrogen bonding donating ability to some unknown degree.

Considering the points outlined above, it is remarkable that the tautomerization rates of 7-AI and 1-AC are as well correlated with a single empirical parameter as they are. Figure 2.11 seems to suggest that the correlation between K_{eq} and k_{obs} fails for a few of the solvents studied. Do the different chemical phenomena (k_{PT} , k_l and K_{eq}) combine in an unlikely manner as to have the observed tautomerization rate, k_{obs} , correlate linearly with $E_T(30)$, or do the solvent models fail to accurately reproduce solvent "polarity" as

defined by $E_T(30)$? More generally, how do different intermolecular interactions contribute to the overall shifts, and how well are they represented by the classical models?

Both experimental and theoretical studies of the betaine molecule have shed some light onto the microscopic details that relate the measured polarity values to solute-solvent interactions. Catalan, Perez, Elguero and Meutermans studied solvatochromic probes that are structurally similar to Reichardt's betaine molecule, and used t-butyl groups to block the hydrogen bond acceptor site [7]. They observed that steric hindrance greatly diminishes the solvent sensitivity of the absorption band shift. This evidence suggests that these probes are primarily measuring hydrogen bond donating ability, and that more generic polarity/polarizability interactions have no substantial effect on the observed solvent-induced shifts. In a theoretical study, De Alencastro, Da Motta Neto and Zerner calculated the absorption spectrum for three gas-phase betaine-solvent (1:4) hydrogen bonded complexes (betaine-(chloroform)₄, betaine-(methanol)₄, and betaine-(water)₄) using the INDO/S Hamiltonian. They were able to achieve excellent agreement with experimental solution phase shifts [8], which also indicates that the betaine-30 molecule is a good measure of hydrogen bonding strength.

The intent of the study reported in this chapter is twofold. The first goal is to use classical Monte Carlo computer simulations to determine the intermolecular structure and interactions responsible for the observed solvatochromic shift in betaine-30. Here, particular attention will be focused on determining what fraction of the shift may be considered to be due to specific hydrogen-bonding interactions with a few solvent

molecules. Second we are interested in determining how well the classical potential models used in studies of proton transfer can reproduce the solvent dependent frequency shifts and reorganization energies for the $\pi \rightarrow \pi^*$ electronic transition of betaine-30.

4.2. Methods

In like fashion to the previous chapter, two sets of simulations were undertaken. The first series of simulations are of “isolated” molecular complexes of the sort described in Chapter 3 as well as in reference [9]. The second set of simulations use the BOSS molecular simulation program [10] to examine the spectroscopic properties of the solutes in bulk liquids. All simulation parameters (cutoffs, etc...) have been discussed in previous chapters, and only differences in the computational procedures will be addressed here.

4.2.1. Calculation of Electronic Shifts in Isolated Complexes and Bulk Solvents.

In simulations involving the betaine molecule, the energies of a vertical transition from state 1 to state 2 is termed ΔE ,

$$\Delta E = \langle H_1 - H_0 \rangle_0 \quad (4.1)$$

The subscript “0” outside the brackets indicates that the average is taken in the ground state, and Hamiltonians, H_0 and H_1 , are of the “Lennard-Jones + Coulomb” form

previously described in Chapters 2 and 3 (equations 2.4 and 3.1). Neglecting any changes that may occur in the solute's polarizability and size upon excitation, H_0 and H_1 differ only in the solute partial charges, and the solvent induced shifts of the spectrum reflect only the energetics associated with the differences in charge distribution.

In the isolated-molecule calculations, three models of electronic excitation will be compared. The first two models involve charge difference calculations using the AM1 and INDO/S semi-empirical. The final model is much simpler; it merely consists of a shift of 0.311 e from the oxygen to the nitrogen. This method is designed to approximate the shifts based on a general electron transfer. For the "isolated molecule" Monte Carlo simulations no averaging of the sort implied by the brackets in equation 4.1 was performed. Rather, shifts of the two lowest energy conformations will be reported.

In the simulations involving bulk solvent systems, the electrostatic potentials at 17 solute sites along the central portion of the betaine frame are output every 1000 configurations, over a simulation of 10 million configurations. Similarly to the "isolated molecule" simulations, the shifts are calculated by changing the charge distributions and recalculating the energies for these selected configurations.

Reorganization energies are calculated directly from the line width of the resulting spectrum of ΔE values assuming a Gaussian line shape of the form:

$$P_{1\leftarrow 0}(\Delta E) = (2\pi\sigma^2)^{-1/2} \exp\left[-(\Delta E - \Delta\bar{E})^2 / 2\sigma^2\right] \quad (4.2)$$

using the equation [11]:

$$\lambda = \frac{\sigma^2}{2k_B T} \quad (4.3)$$

where σ is the width of the line, ΔE is the mean energy for a vertical transition from state 0 to state 1, and λ is the reorganization energy.

4.2.3. Potential Functions and Simulation Methods.

In these simulations both the geometric structure of the solute as well as its electrostatic characteristics are required. In the preliminary work involving the isolated molecule Monte Carlo algorithm, a solute geometry is used in which the central torsion angle has been fixed to keep the π -electron system in the planar arrangement. This geometry does not represent the lowest energy conformation, and in the simulations involving “bulk” fluids, this feature was corrected. In all bulk-fluid simulations, the geometry of the molecule used was that determined using the semi-empirical AM1 Hamiltonian and specifying the keyword, “CI=14” to include selected excitations among the 14 molecular orbitals bracketing the HOMO-LUMO gap. All AM1 calculations were performed with the AMPAC program [12]. Once a representation of the equilibrium ground-state geometry had been determined, the ground state charges were obtained from electrostatic potential fits of the wave functions generated at the HF/6-31G* level using the Gaussian-94 program [13]. Excited state charge distributions were determined using two semi-empirical hamiltonians: AM1 and INDO/S [14]. In addition to the electrostatic

Table 4.1. Solute Properties and Potential Parameters

A. Lennard-Jones Parameters^a

atom type	σ (Å)	ϵ (kcal/mol)
C	3.55	0.07
N	3.25	0.17
H(-C)	2.42	0.03
O(-C)	2.96	0.21

^a Parameters Ref. 9.

B. Electrical Properties Calculated for the Ground and First Excited States of Betaine.

state	calculation	E^a (kJ/mol)	μ (D)	q_O^b (au)	q_N^b (au)	q_{p1}^b (au)	q_{p2}^b (au)	q_{p3}^b (au)	q_{p4}^b (au)	q_{p5}^b (au)	q_{p6}^b (au)	q_{p7}^b (au)
S ₀	6-31G*	(0)	16.44	-0.66	0.24	0.39	-0.19	0.07	0.08	0.08	0.12	0.12
S ₀	AM1/CI	(0)	9.09	-0.34	0.12	0.17	-0.02	0.03	0.00	0.00	0.08	0.08
S ₁	AM1/CI	119	1.89	-0.27	0.14	-0.17	0.28	0.02	0.03	0.03	0.04	0.04
S ₀	INDO/S	(0)	17.85	-0.71	-0.12	0.27	0.26	0.05	-0.02	-0.03	0.10	0.09
S ₁	INDO/S	161 (113)	4.46	-0.61	-0.33	-0.41	0.75	0.04	0.01	0.01	0.11	0.10

^a Values in parantheses are experimental gas-phase values from Ref. 5. ^b Charges listed for AM1/CI and INDO/S calculations are Mulliken charges whereas for the 6-31G* calculations they are ESP-fit charges.

characteristics found using these basis sets, the oscillator strengths were also determined as a function of the dihedral angle torsion about χ and are reported.

All Lennard-Jones potential parameters for the betaine-30 molecule are summarized in Table 4.1. The solute is represented using a rigid all-atom model. Each atomic site of the solute interacts with solvent molecules via a Lennard-Jones (LJ) plus Coulomb interaction potential of the usual form (equation 2.4 and 3.1). The charges were obtained as described above, and the Lennard-Jones parameters of the solute atoms were obtained from the OPLS parameter set [10]. Details of the solvent models have been given in Chapter 2.

4.3. Results and Discussion

4.3.1. Quantum Chemical Calculations of the Betaine Molecule.

The calculated shifts reported here are a direct function of the change in the betaine-30 charge distribution. With that in mind, an examination of the charge differences predicted by the semi-empirical methods is presented first. The geometry for all calculations was obtained by performing a geometry optimization with the AM1 Hamiltonian. From this initial geometry, charge distributions were calculated for the ground state and first excited state of betaine-30 using the AM1 and INDO/S Hamiltonians, as well as for the ground state using the 6-31G* basis set. These charge distributions are presented in Tables 4.1 and 4.2, and are shown in Figure 4.2.

Table 4.2. Charge Distributions [au] along the backbone structure of betaine-30.

no.	element	S_0 6-31G*	(S ₁ -S ₀) Difference Charge Distributions		
			"Simple"	AM1-CI=14	INDO/S
1	carbon	0.0099	0.0000	-0.0812	-0.1538
2	carbon	-0.1396	0.0000	-0.1518	-0.0018
3	carbon	0.0032	0.0000	0.1385	-0.1527
4	carbon	-0.1396	0.0000	-0.1523	-0.0016
5	carbon	0.0100	0.0000	-0.0832	-0.1555
6	nitrogen	0.2349	-0.3110	0.0095	-0.1831
7	hydrogen	0.1590	0.0000	-0.0136	0.0000
8	hydrogen	0.1590	0.0000	-0.0140	0.0000
9	carbon	-0.0802	0.0000	0.3222	0.3099
10	carbon	-0.1918	0.0000	-0.1050	-0.0506
11	carbon	-0.2324	0.0000	0.0796	0.1163
12	carbon	0.5736	0.0000	-0.0637	0.0349
13	carbon	-0.2322	0.0000	0.0817	0.1167
14	carbon	-0.1919	0.0000	-0.1044	0.0069
15	hydrogen	0.1772	0.0000	0.0347	0.0000
16	hydrogen	0.1773	0.0000	0.0347	0.0000
17	oxygen	-0.6100	0.3110	0.0683	0.1144

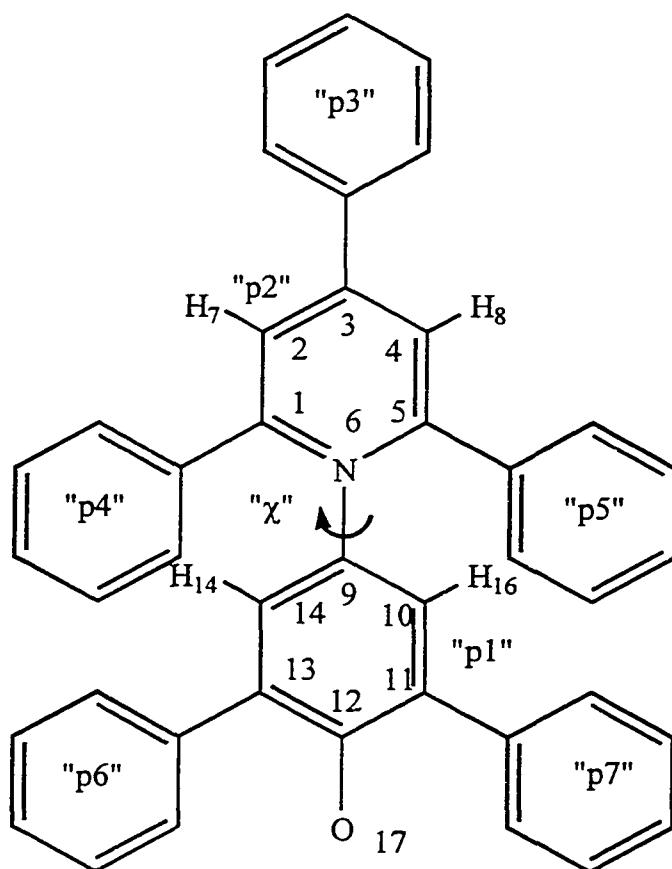


Figure 4.3. Definition of atom numbering scheme and nomenclature. In the text "pN" refers to *phenyl ring with the Nitrogen atom*.

Both of the semi-empirical calculations used give a significant decrease in dipole moment upon going from the ground to the first excited state. This general trend is consistent with experiment, where the dipole moment change has been estimated to be approximately 8.6 D in dioxane [15]. Theoretically, this change is found to occur primarily from electron transfer from the “p1” phenyl ring to the “p2”/nitrogen ring (see Figure 4.3 for nomenclature). The AM1-CI calculation predicts a movement of about 0.35 e from “p1” to “p2”. Most of the charge lost from the “p1” ring is from the 9-carbon. Surprising, very little charge transfer is predicted to occur from the oxygen site. The INDO/S calculations show a similar trend, although the charge migration is more pronounced. These calculations predict a net transfer of roughly 0.7 e from the “p1” phenyl ring. Like the AM1-CI calculations, the most significant change in charge is from the 9-carbon site (although there is also significant, ~ 0.1 e, change from the oxygen site and the 11, and 14 carbon sites). The INDO/S calculation shows that a substantial fraction of the electron transfer is to the nitrogen site, while in the AM1-CI calculation, the electron transfer is primarily to the 2 and 4 carbon sites. The overall greater charge transfer character predicted by the INDO/S calculation is again reflected in the fairly large change in dipole moment of 13.4 Debye. The corresponding AM1-CI calculation predicts a more modest change of only 7.2 Debye. Also worth noting is the similarity of the ground-state dipole moments as predicted by the semi-empirical INDO/S method and the *ab initio* method using the 6-31G* basis set. Based on these results, namely the greater electron transfer character, the INDO/S charge distributions appear to be the most

realistic with respect to reproducing the experimentally observed excited state characteristics.

To further clarify the role of the INDO/S predicted gas-phase spectroscopic properties, the effect of rotation along the 1-6-9-10 dihedral angle have been investigated and summarized. The calculated molecular properties as a function of dihedral rotation are summarized in Table 4.3. The molecule has a minimum energy at 47.8 degrees. As the dihedral changes from 0° to 180°, the oscillator strength decreases presumably due to less overlap between the two relevant π -systems, and the transition energy decreases as shown in Figure 4.4. In addition, less electron transfer is observed as the orbital overlap decreases. Although a fairly wide range of dihedral angles can be thought of as existing in room temperature liquids, the minimum energy geometry occurs when $\chi = 47.8$ degrees. Therefore, this geometry should provide the largest contribution to the absorption maximum which are the basis of the $E_T(30)$ scale, and has been adopted as the rigid solute geometry to be used later in the betaine:bulk solvent simulations.

The simulations in the following section attempt to reproduce experimental shifts by recalculating the solute-solvent energies using the excited-state charge distributions. Since significant charge shifts are observed only within the “p1” and “p2” fragments, just this 17 atom backbone (“p1” + “p2” + oxygen site) is considered in the next section when charge shifts will be recalculated based on the electrostatic potentials at these atom sites.

Table 4.3. Summary of INDO/S calculations.

χ [deg.]	Energy ^a [kJ/mol]	μ_{S0} [D]	μ_{S1} [D]	Transition Dipole	Δq "p1"	Δq "p2"	Δq oxy.	Oscillator Strength
0.00	62.10	16.99	4.16	-12.31	0.41	-0.52	0.09	1.13
10.00	46.75	16.69	4.90	-11.93	0.39	-0.50	0.08	1.02
20.00	25.50	16.75	4.99	-11.41	0.40	-0.51	0.08	0.89
30.00	13.63	17.10	5.28	9.62	0.44	-0.59	0.09	0.61
40.00	4.05	17.85	4.43	9.06	0.49	-0.67	0.10	0.50
50.00	2.18	18.78	3.89	7.09	0.56	-0.73	0.11	0.27
60.00	16.65	20.01	2.55	-5.68	0.63	-0.76	0.13	0.15
70.00	23.80	21.28	1.04	-1.48	0.69	-0.83	0.15	0.01
80.00	23.80	21.28	1.04	-1.48	0.69	-0.83	0.15	0.01
90.00	21.33	21.45	0.61	0.38	0.70	-0.85	0.15	0.00

^a Energies are referenced to the minimum, $\chi = 47.8^\circ$.

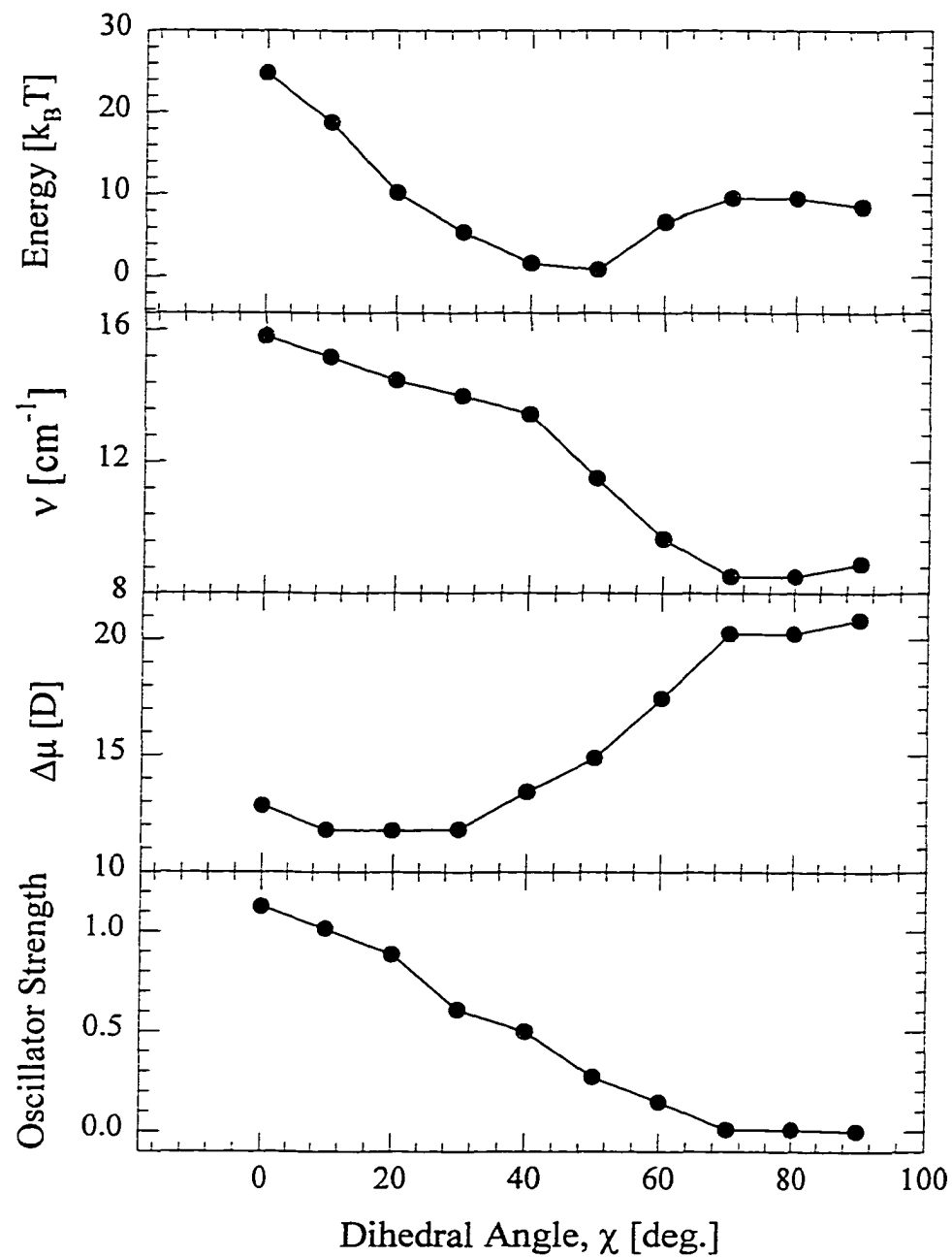


Figure. 4.4. INDO/S calculated properties of Reichardt's Betaine-30.

4.3.2. *Betaine Energetics in Isolated Complexes.*

The initial attempts at modeling betaine-alcohol complexes are simple simulations of the sort described in Chapter 3. The primary motivation behind these elementary calculations is to determine if any trend exists between single molecule complexation energies with solvent type, and to determine the magnitude of the total shift that may be attributed to a single hydrogen-bonded partner. The energy-minimized structures are for the hydrogen-bonded 1:1 betaine-alcohol complexes that are determined from the Monte Carlo search algorithm, and the shifts are calculated using equation 4.1, in which the excited state energies are calculated in three different manners as described in the Methods section.

Figure 4.5 shows an example of the two lowest energy conformations found using the search algorithm. The hydrogen-bonded complexes are, for all solvents studied, the lowest energy conformation. However, using the two types of semi-empirically determined excited-state charge distributions, the π -complexes yield the larger shifts. Only for the generic charge-transfer model do the hydrogen-bonded complexes give significantly greater shifts. For most solvents the relative percentage of the overall shift (as defined by the $E_T(30)$ scale) due to the hydrogen bonding solvents is about 5-11 % using the INDO/S model, 4-7 % using the AM1 model and 9-20 % using the “local” model. The π -complexes contribute a slightly greater percentage (~10-15 %) using the INDO/S and AM1 models, and give a relatively small percentage (about 2-3 %) using the “simple” model for all solvents studied. Obviously, the relatively small shift of charge

away from the oxygen site in the semi-empirical modeling leads to significantly less shift in the hydrogen-bonded complexes.

Zerner, De Alencastro and Da Motto Neto performed a more in-depth calculation of betaine complexes with water and methanol and found, that 1:4 complexes (two solvents hydrogen bonded to the oxygen site, and two centered near the nitrogen site) were sufficient to reproduce experimental solution phase shifts [8]. Clearly, as in Zerner's work, a greater number of solvents must be complexed to reproduce the full shift. To this end we have attempted a set bulk solution simulations of the betaine probe in these alcohols.

4.3.3. Bulk Solvation of Betaine-30.

Using the semi-empirical calculations as a guide for determining excited state distributions, this section examines the predicted shifts for two possible charge variations. Ensembles were sampled using the ground state (S_0) charge distributions of betaine-30 generated from the 6-31G* calculations (reported in Table 4.2). The Δq values for the 17-atom backbone are given in Table 4.2. The calculated reorganization energies and shifts determined using the INDO/S Δq values are reported in Table 4.6 and Table 4.7 respectively, and the simulated shifts are plotted vs. the observed shifts in Fig. 4.5. Using the INDO/S representation as a model for electronic excitation, good agreement is found between the experimental and simulated spectral shifts. Considering the fact that the Δq values were derived directly from the INDO/S wavefunction without any scaling, the agreement with experiment is particularly pleasing. Before discussing the shifts in detail,

Table 4.4. Summary of isolated complex energetics and shifts.

Solvent	Complexation Energy [kcal/mol]		$\Delta E (S_1-S_0)$ [kcal/mol]				
			INDO/S		AM1		"simple" ^b
	π -complex ^a	h-bonded	π -complex ^a	h-bonded	π -complex ^a	h-bonded	h-bonded
<i>"ab initio"</i> models							
Methanol	10.8	13.3	6.4	3.8	6.0	1.9	7.0
Ethanol	11.8	14.1	6.7	3.7	6.1	1.9	7.0
1-Propanol	12.8	15.3	6.2	4.0	6.5	2.8	7.4
2-Propanol	12.3	14.7	6.4	3.9	5.3	1.7	7.4
t-Butanol	13.5	16.9	6.6	4.4	6.4	2.9	8.2
TFE	10.8	17.0	4.8	3.9	5.3	3.1	7.6
Water	8.3	13.3	6.2	5.7	5.7	3.1	6.0
OPLS models							
Methanol	9.1	13.6	6.6	3.8	6.1	1.9	7.2
Ethanol	9.1	14.6	6.8	3.9	6.2	1.6	7.4
1-Propanol	12.9	14.8	6.1	3.9	6.4	2.7	7.3
2-Propanol	10.5	15.3	6.8	4.0	5.7	1.6	7.4
t-Butanol	13.6	15.0	7.3	3.6	5.6	1.5	7.0
Water	8.5	14.5	6.2	3.6	6.0	2.9	6.7

^a π -complexes represent the lowest energy, non-hydrogen bonded complexes sampled.

^b "simple" refers to the model in which the excitation is modeled as a shift of charge (0.311 au) from the oxygen site to the nitrogen site of betaine-30.

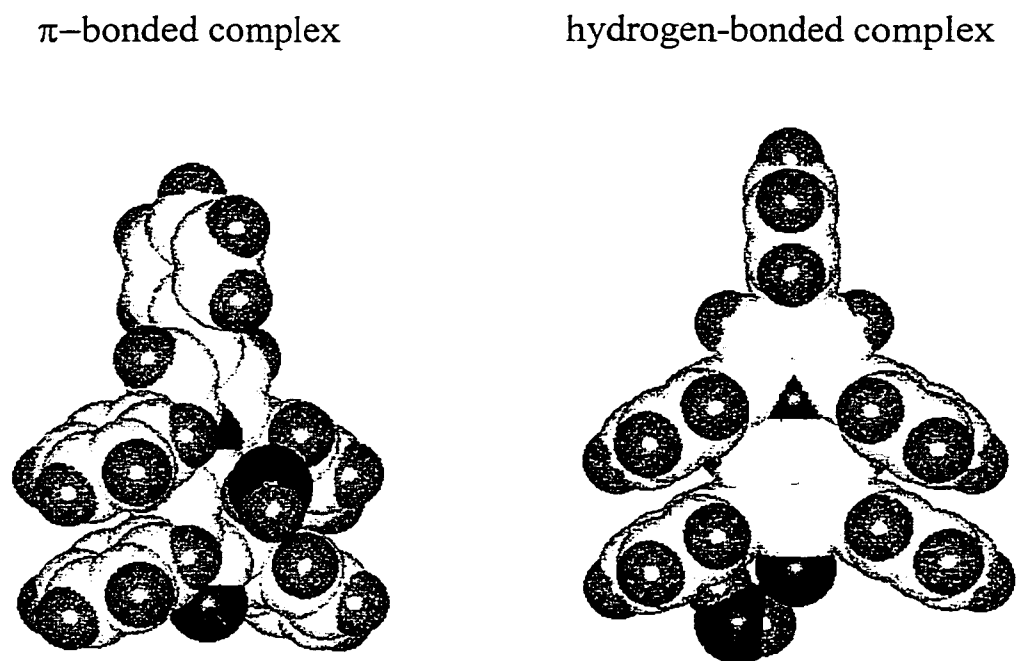


Figure 4.5. Space filling representations of two conformational structures of betaine-30:water complexes. The geometries depicted are created from the Monte Carlo energy-minimized structures.

the energetic and structural characteristics of the solute-solvent hydrogen-bonded interactions will be examined.

4.3.3.1. Solvation Structure and Energetics.

We now consider the solvation structures and energetics to better characterize the hydrogen bonding abilities of a number of different solvents. In Table 4.5 V_{pair} is the interaction energy between a pair of hydrogen-bonded solute-solvent molecules, and N_C is the coordination number associated with the first peaks in the intermolecular O_U-O_V radial distribution functions. We consider both values to be indicative of the strength of the hydrogen bonds made to the oxygen site of the betaine-30 molecule.

The data in Table 4.5 indicates that the solute-solvent bonding is fairly similar in most of these solvents. For instance, the coordination numbers show that, in nearly all cases, the solute oxygen site is hydrogen-bonded to an average of more than one solvent molecule. All of the water models studied show that up to three solvents may simultaneously form hydrogen bonds to the oxygen site of betaine-30. The pair interaction energies are generally very strong for “non-ionic” hydrogen bonded interactions [16], and are considerably stronger than what was observed for the solute-solvent interactions studied previously in aza-aromatic systems, as well as for the solvent-solvent pair interaction energies observed in the pure fluids [17]. In TFE, which is distinguished experimentally as having the ability to form particularly strong hydrogen bonds, the hydrogen bond strength, as measured by V_{pair} , is substantially enhanced compared to the other mono-alcoholic solvents. In the case of water, it is worth noting that in none of the models studied here are the pair interaction energies

Table. 4.5. Summary of energetic and structural features betaine-30 simulations in bulk solvents.

Solvent	N_{CRD}	V_{Pair}	$N_{\text{CRD}} \times V_{\text{Pair}}$	$-V_{\text{UV}}$ [kcal/mol]
“ab initio” solvent models				
Methanol	1.4	-9.9	-19.10	103
Ethanol	1.7	-8.4	-12.35	95
1-Propanol	1.2	-10.9	-11.55	113
2-Propanol	1.4	-13.2	-13.5	106
t-Butanol	1.7	-12.7	-22.1	89
TFE	1.5	-12.5	-18.8	93
Ethylene Glycol	1.0	-9.3	-36.3	134
Water	2.0	-7.4	-16.5	116
OPLS solvent models				
Water (TIP3P)	2.2	-7.8	-17.16	125
Water (TIP4P)	2.1	-8.2	-17.22	128
CHCl_3				89
ACN				126
Methanol	1.5	-9.9	-14.85	105
Ethanol	1.4	-9.9	-16.81	97
1-Propanol	1.8	-11.2	-17.42	100
2-Propanol	1.4	-10.5	-15.51	99
t-Butanol	0.8	-11.8	-10.07	81

particularly strong. The high solvent polarity reported by the $E_T(30)$ scale does not measure the energetic strength of the hydrogen bonding interaction, at least in terms of single solute-solvent hydrogen-bond. Rather, the only unusual characteristic of this solvent, in terms of local bonding, appears to simply be the ability to make more hydrogen bonds relative to its alcoholic cousins.

4.3.3.2. *Reorganization Energies.*

One aspect of the solvatochromic behavior of the betaine-30 probe that has come under recent experimental scrutiny is the reorganization energy that accompanies the $S_0 \leftrightarrow S_1$ transition [18-21]. This quantity is a measure of the change in solvation energies of the S_0 and S_1 electronic states due to the repolarization of the nuclear degrees of freedom of the solvent. It is of general interest due to its relation to the solute-solvent coupling in electron-transfer systems [22].

Estimates of the reorganization energies have been derived from the widths of the shift distributions according to equations 4.2 and 4.3. They are presented in Table 4.6 along with experimental values [20, 23], and values from continuum dielectric calculations as well as other estimates found in literature [19, 24]. The values calculated from simulation range from over 6000 cm^{-1} to just below 1000 cm^{-1} , depending on the solvent. As expected, acetonitrile and water have the largest reorganization energies. In acetonitrile, the value obtained is close to that derived from resonance-Raman line shapes [23]. In contrast, the calculated reorganization energy in methanol is roughly two-thirds lower in magnitude compared to the experimentally determined values [20]. Most

theoretical estimates are substantially lower, although only one solvent (acetonitrile) has been studied extensively in all but the reaction field estimates. In nearly all of the alcohols studied, the calculated reorganization energies appear to decrease with increasing solvent size. *n*-Propanol is an obvious exception to this trend. Here, the widths are enhanced. This may be due to either the insufficient sampling present as a result of the increased longitudinal dielectric relaxation in longer chain primary alcohols, or perhaps the presence of two distinct hydrogen bonded species. *iso*-Propanol is also unusual, in that the distribution of the shift is bimodal. In this case, it seems more likely due to the variation in shift due to the presence of two types of hydrogen bonded complexes in solution, although it is puzzling that no such phenomenon is observed in the other alcohols.

A final consideration regarding the simulated widths of the electronic absorption band is the use of non-polarizable solvent models. While the solvent shifts in absorption and emission lines depend on both α_∞ and α_0 (the electronic and nuclear polarizabilities, respectively), the widths of these lines depend solely on α_0 . Bader and Berne explain this phenomena by describing a system in which the total polarizability of the solvent is given by α_{tot} [11]. In the imagined limit that the total polarizability of the solvent is due to only electronic polarizability ($\alpha_\infty/\alpha_{\text{tot}} = 1$), the absorption line shape would be remain a δ -function, but would be shifted from the gas phase. That is, the redistribution of the solvent electrons to accommodate a change in solute charge is instantaneous. As a result,

Table. 4.6. Summary of estimated betaine-30 reorganization energies.

Solvent	λ , Simulated [cm^{-1}]		Cavity Diel. [cm^{-1}]	λ , Experiment [cm^{-1}]		λ , Molecular Theory [cm^{-1}]	
	<i>ab initio</i>	OPLS		McHale ^a	Barbara ^b	Raineri ^c	Matyushov ^d
Methanol	4100	5100	1385	5835	-	2557	
Ethanol	4200	3200	1298				
1-Propanol	6000	5000	1237				
2-Propanol	2200	3400	1233				
t-Butanol	900	1400	1084				
TFE	2000	-	1383				
Ethylene Glycol	3100	-	1304				
Water	5400	6600	1469			2724	
Chloroform	-	1000	568			636	
Acetonitrile	-	5900	1380	6040	2221	936	

^a Estimate based on Resonance Raman Spectroscopy data. "Model 2" as reported in Ref. 18 and 20.

^b Experimental estimate reported in Ref. 19.

^c Theoretical HXA model reported in Ref. 22.

^d Theoretical estimate reported in Ref. 24.

the solvent relaxation does not manifest itself in the line shape. Supposing one could slowly add a component due to the nuclear degrees of freedom of the solvent to the overall polarizability in such a way as to keep the total polarizability constant, the result would be to shift and broaden the center of the absorption. The simulations presented here utilize intermolecular interaction terms which are parameterized in such a manner that the total polarizability is due to only nuclear relaxation of the solvent, $\alpha_0/\alpha_{\text{tot}} = 1$. In this limit, the widths may be expected to be slightly overestimated by roughly 5-10 % [11].

4.3.3.3. *Solvent Dependence of the Simulated Shifts.*

We now consider the solvent-dependent shift calculated from the Monte Carlo simulations in more detail to dissect the contributions to the “polarity” measured by betaine-30. The solvents examined here include the first three normal alcohols (methanol through 1-propanol), the fluorinated alcohol 2,2,2-trifluoroethanol (“TFE”), the two nonprimary alcohols (2-propanol and tert-butyl alcohol), two dihydroxy solvents (ethylene glycol and water), and some aprotic solvents (acetonitrile, chloroform and carbon tetrachloride). Again, all shifts, both observed and simulated, are summarized in Table 4.7.

The general experimental trend is well reproduced by the simulated models. Thus, calculated shifts decrease in order water > ethylene glycol > methanol > ethanol > 1-propanol > tert-butyl alcohol. The 2-propanol model derived from *ab initio* methods has a substantially larger shift when compared to 1-propanol, placing it outside the

observed trend. This is also found in the OPLS solvent ordering, although to a substantially lesser degree.

One aspect of the simulations which is of particular interest to us is the measurement of the fraction of the total shift which may be attributed to the solvent molecules hydrogen-bonded to the oxygen site of betaine-30. Based on the position of the first minimum of the radial distribution functions, a solvent is considered hydrogen bonded if the O_U-H_V (solute oxygen site-solvent hydroxy hydrogen site) distance is measured to be less than 2.65 Å. The shift induced by the hydrogen bonded solvents can easily be separated from the total shift, giving separate “local” (hydrogen bonded) and “non-local” (everything else) components.

The relative contribution due to hydrogen-bonded solvents is also dependent upon solvent size, although the magnitude of the shift due to these closest solvents is fairly constant for all solvents (~ 6-7 kcal/mol). That is, for a large solvent (i.e.: *tert*-butyl alcohol), the shift due to the one or two hydrogen-bonded solvents is 6.8 kcal/mol, and the average total shift is slightly more than twice that value, about 13.5 kcal/mol. In water, the closest two or three solvents contribute roughly the same amount to the shift as did the hydrogen-bonded *tert*-butyl alcohol. However, in the case of water, this only amounts to about 20 % of the total shift. From this, it seems that the greater dipole density in water is the primary source of polarity as measured by the $E_T(30)$ probe.

Experimental results suggest this may not be the case. A plot of measured $E_T(30)$ values versus reaction field (Figure 4.7) suggests that this interpretation may be inaccurate. In this comparison, polar-protic solvents appear to give enhanced shifts

compared to the trend established by the aprotic solvents (the small black dots). Presumably, this extra shift is due to hydrogen bonding contributions, and from this relation such contributions are expected to account for roughly 15-60 % of the total shift, depending on the particular solvent. The striking difference between this analysis and the simulated results is the differing trends with respect to solvent size that is apparent from inspection of Table 4.7. Water, for instance, has a much larger shift than what one would expect based on the trend in aprotic solvents. This feature is not well represented with the simulated models. It may be the case that the lack of explicit polarization in the modeling causes the enhancement due to hydrogen bonding to be under represented. That is, very polar protic solvents, such as water and ethylene glycol, may more efficiently stabilize charge on the oxygen site when the betaine-30 molecule is in its ground state. If this is the case, then upon excitation, the hydrogen bonded solvents would have a much more enhanced contribution to the overall shifts.

Also apparent in this plot is the enhanced hydrogen bonding which appears to be present in the solvent 2,2,2-trifluoroethanol (TFE). This feature is not well reproduced by the simulated model. In fact, of all the solvent models studied in the simulations, TFE model performs the poorest in terms of reproducing the experimentally determined shifts. In this case, the simulated shifts are in error by a factor of two. Considering the amount of shift due to hydrogen bonds formed at the oxygen site by this solvent, it seems as though the increased hydrogen bond strength of the solvent is not being accounted for. For instance, the simulated value of hydrogen-bonded component of the shift for TFE is about the same as that calculated for methanol. However, based on the experimental

trend, the component of the shift due to hydrogen-bonded interactions is expected to be considerably greater. It is also insightful to consider non-local effects of these two solvents. Both methanol and TFE have very similar dielectric constants. From this, it follows that both solvents should have roughly similar contributions from non-hydrogen bonded components of the shift. However, the simulated portion of shift due to non-hydrogen bonding interactions is substantially less in TFE when compared to methanol. Further, since the refractive index of neat TFE is somewhat low relative to most alcohols, it is unlikely that “missing” electronic polarization plays a significant role in determining the total shift. More likely, the current TFE model probably fails to accurately reproduce both enhanced hydrogen bonding strength as well as adequate orientational polarizability.

As a final note, some comment should be made regarding the differences in the various calculated values between the two types of solvent models used. Focusing first on the monoalcoholic solvents, the OPLS set seems to match the experimentally determined trend with solvent polarity, although the simulated shift values are uniformly smaller by approximately 11 %. The *ab initio* solvent are less well correlated. In particular, the 2-propanol and t-butanol models give significantly enhanced shifts compared to their OPLS counterparts.

This result may be explained by taking a closer look at the fundamental difference between the two sets of solvent models. Comparing the charge distributions presented in Table 2.2, it is clear that of the monoalcohols the two non-primary alcohols (2-propanol and t-butanol) have the most significant deviations in charge distribution compared to the

Table 4.7. Summary of betaine-30 simulated shifts in bulk solvents.

Solvent	E _T (30) ^a	Total Shifts [kcal/mol]				Contribution From H-bonded Solvents					
						Simulated (INDO/S)		Simulated ("Simple")		Experiment	
		Observed ^b	AM1	INDO/S	"Simple"	Shift [kcal/mol]	%	Shift [kcal/mol]	%	Shift [kcal/mol]	%
"ab initio" solvent models											
Methanol	55.4	24.7	9.2 ± 0.2	20.1 ± 0.7	19.5 ± 1.2	5.8	29	10.2	46	11.8	45
Ethanol	51.9	21.2	9.0 ± 0.5	19.0 ± 1.1	18.2 ± 0.9					8.52	40
1-Propanol	50.7	20.0	7.9 ± 0.3	17.1 ± 1.0	16.7 ± 1.0	5.0	29	7.1	42	7.88	37
2-Propanol	48.6	17.9	8.7 ± 0.6	19.6 ± 1.2	20.3 ± 1.2	7.1	36	10.0	50	5.64	32
t-Butanol	43.9	13.2	6.1 ± 0.2	14.7 ± 0.3	16.7 ± 0.4	6.7	47	10.4	63	1.90	14
TFE	59.5	28.8	6.5 ± 0.1	13.9 ± 0.3	16.0 ± 0.5	5.7	41	9.3	58	9.93	34
Ethylene Glycol	56	25.3	10.8 ± 0.3	21.9 ± 0.6						12.85	51
Water	63.1	32.4	11.2 ± 0.2	24.6 ± 0.5	23.3 ± 0.3	6.3	26	9.1	39	18.14	56
OPLS solvent models											
Water (TIP3P)	63.1	32.4	12.0 ± 0.5	26.5 ± 0.7	25.1 ± 0.4					18.14	56
Water (TIP4P)	63.1	32.4	12.3 ± 0.5	27.9 ± 0.9	26.9 ± 0.8					18.14	56
CHCl ₃	39.1	8.4	3.6 ± 0.3	7.7 ± 0.4						2.50	30
ACN	45.6	14.9	9.1 ± 0.2	19.7 ± 0.3	16.0 ± 0.2					1.50	-
Methanol	55.4	24.7	9.5 ± 0.4	21.1 ± 0.9	20.6 ± 1.0					11.8	45
Ethanol	51.9	21.2	8.2 ± 0.3	18.5 ± 0.7	19.0 ± 0.8					8.52	40
1-Propanol	50.7	20.0	7.3 ± 0.5	16.0 ± 1.2	16.9 ± 1.3					7.88	37
2-Propanol	48.6	17.9	7.2 ± 0.4	15.6 ± 0.8	15.2 ± 0.9	5.2	33	7.1	47	5.64	32
t-Butanol	43.9	13.2	5.5 ± 0.2	11.4 ± 0.2	11.4 ± 0.2	3.3	29	5.9	52	1.90	14

^a Values for $E_T(30)$ from Ref. [4].

^b "Observed" refers to experimental absorption shifts relative to tetramethylsilane (30.7 kcal/mol).

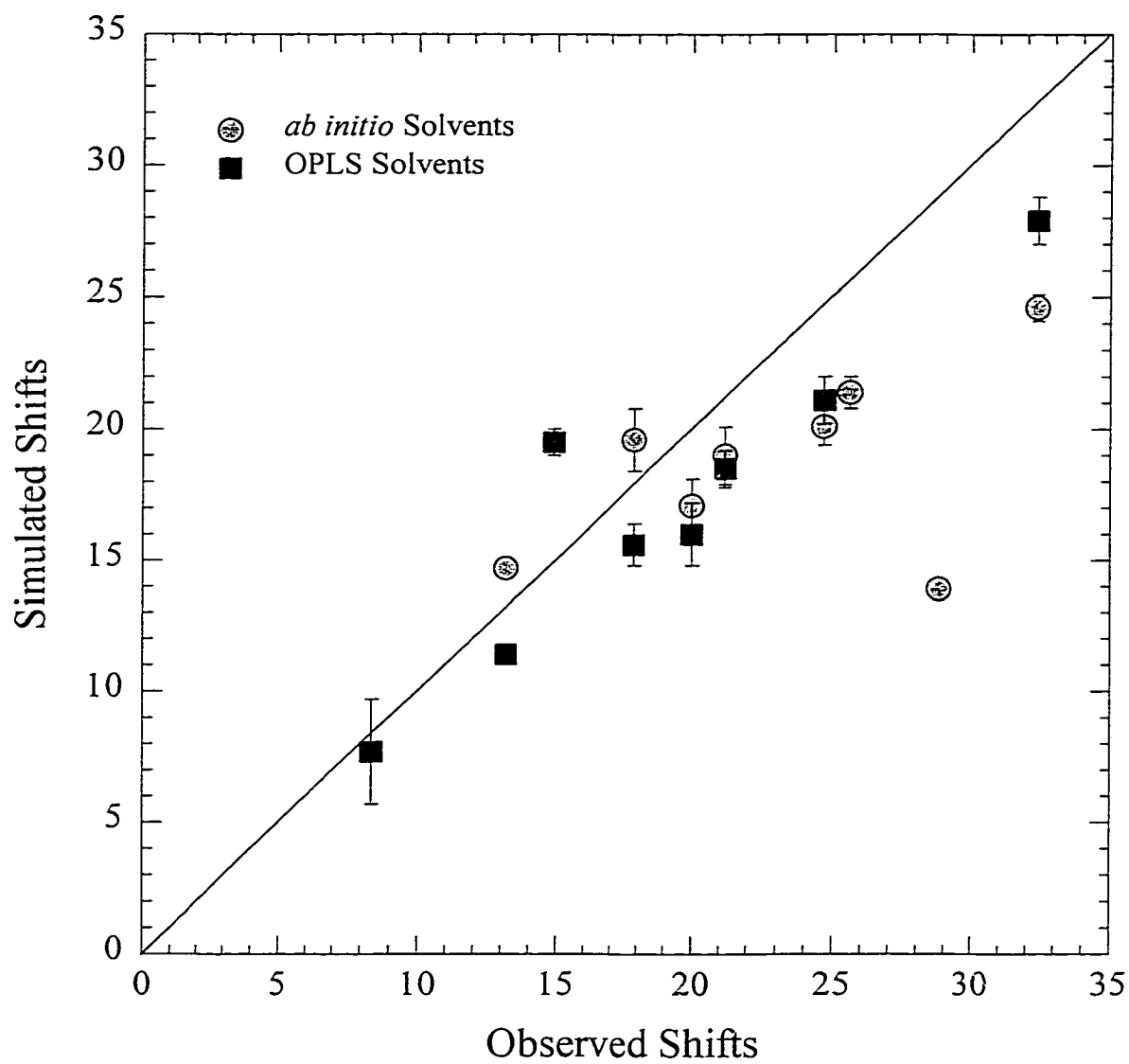


Figure 4.6. Plot of simulated versus experimental values for the $E_T(30)$ parameter.

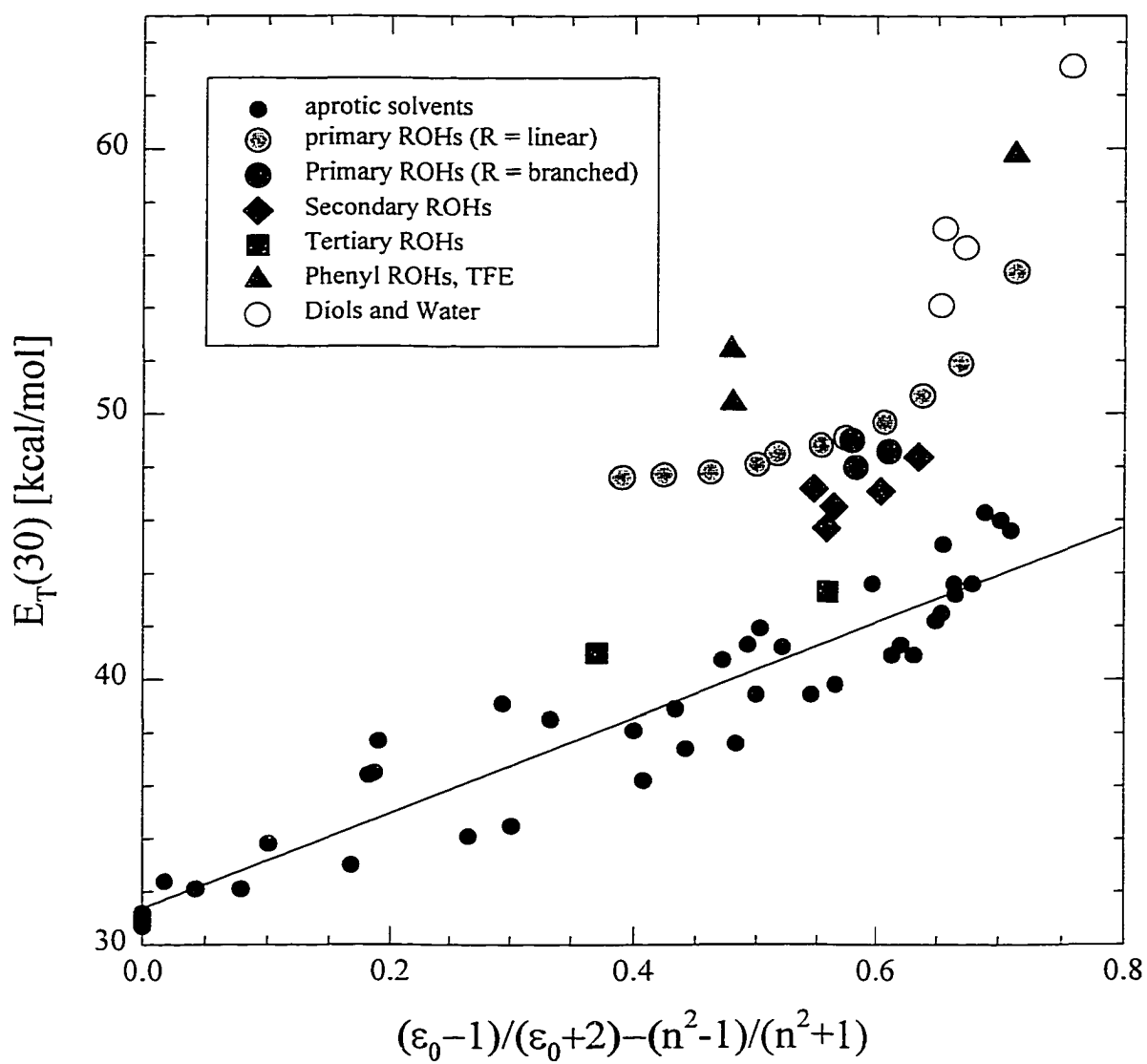


Figure 4.7. $E_T(30)$ solvent polarity versus Reaction Field factor.

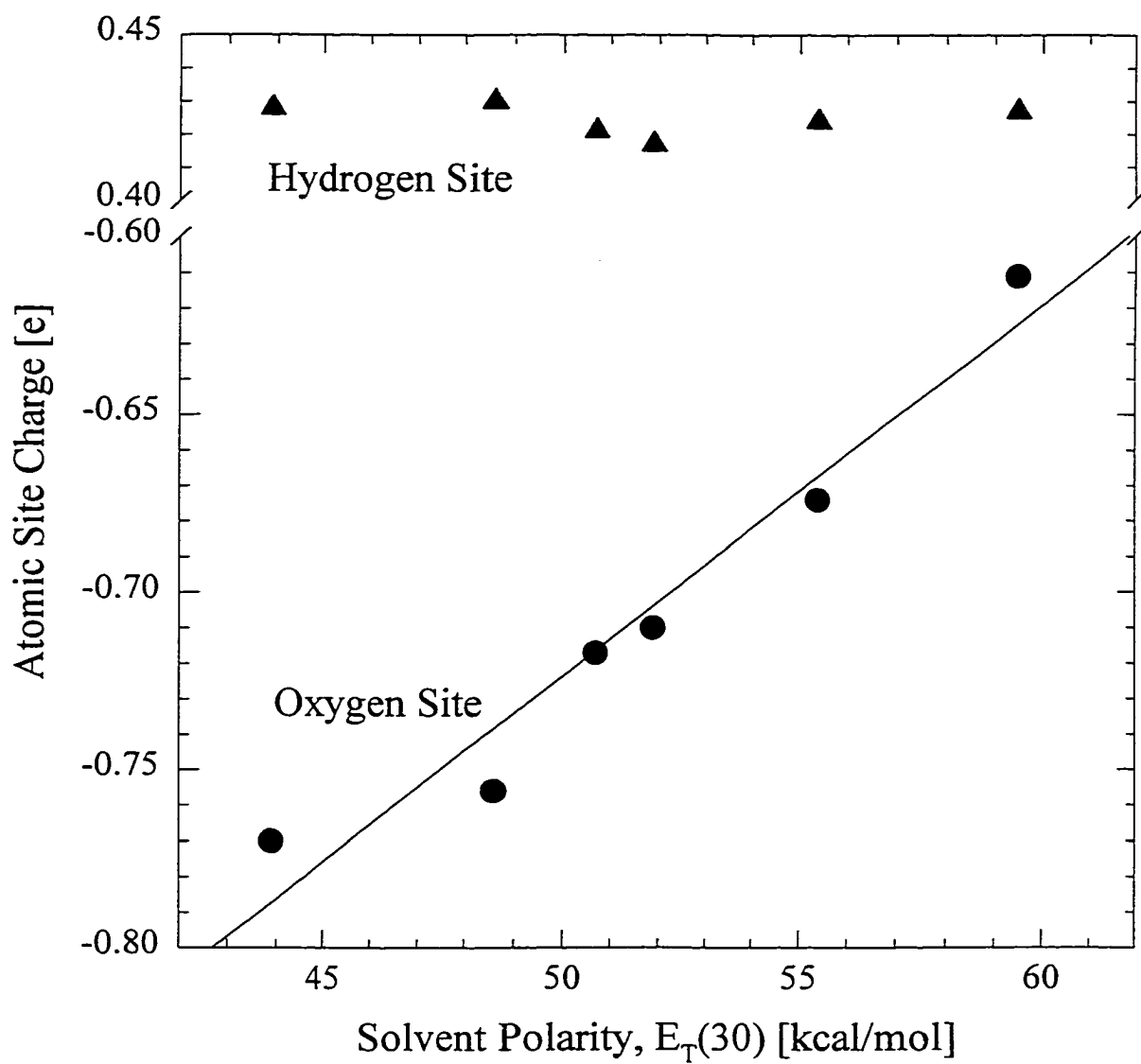


Figure 4.8. Solvent variation in ESP-MK fit atomic-site charges.

OPLS solvents. In particular, the oxygen atomic site has a larger amount of negative charge in these two solvent models. Do these distributions reflect *real* differences in the solvent's charge density? Is there any need to deviate from the OPLS set when modeling alcohols? The original idea of using charges derived from electrostatic potential fits to the 6-31G* wavefunction arose from the desire to simulate TFE. This solvent is not included in the OPLS set and is expected to have a charge distribution that is significantly altered due to the presence of the tri-fluoro groups. Indeed, atomic site fits of the electrostatic potential, determined from quantum chemical calculations, do produce a lower amount of electrical charge on the oxygen site due to the electron withdrawing fluoro groups. This was thought to be a significant finding, especially when considering that TFE is the most polar of the monoalcohols. Do the larger, less-polar alcohols have more charge centered at the oxygen site? The correlation between the charge distribution and solvent polarity is presented in Figure 4.8. The quantum chemically determined charges at the solvent oxygen site certainly seem to correlate to the solvent polarity. Since these atomic site charges are of great importance for determining the strength of intermolecular interactions for many systems, the "*ab initio*" derived models have been used extensively throughout this thesis. Most likely, the magnitude of this charge variation and lack of further parameterization results in slightly poorer pure liquid properties (see appendix 2.1), and possibly the apparent deviation in the shifts displayed in Figure 4.6.

4.4. Summary and Conclusions

In this chapter I have sought to clarify the nature of the hydrogen bonding contribution to solvent “polarity” using quantum chemical techniques and Monte Carlo computer simulations. The systems under scrutiny involved the betaine-30 dye molecule, used to construct the “ $E_T(30)$ ” solvent polarity scale. This scale has been used to measure polarity for literally hundreds of solvents, thus giving practicing chemist a quantitative measure of the ability of pure solvent systems to “solvate” polar species. Since this scale has been used previously in the construction of free-energy relationship with the tautomerization rates of proton-transfer reactions, it is important from our perspective to better understand the various molecular contributions to the observed spectroscopic shifts from which the scale is based. Further, these simulations hope to calibrate the level of realism that may be expected from different potential models of polar-protic solvents.

The simulations performed here seem to reproduce the solvent polarity scale over an impressive range of polar-protic solvents. In all of the normal mono alcohols examined, which include five alkyl alcohols, the simulated shifts match the qualitative trend observed in experiment. The simulated results also suggested that about 20-50 % percent of the total shift can be ascribed to specific interactions between the solute and the solvent molecules forming hydrogen bonds to the oxygen atom of betaine-30. Although it is not possible to directly perform a similar separation in experimental systems, the analysis shown in Figure 4.7 suggests that this general percentage range is

correct. Also, the simulations tend to suggest that the percent of the total shift, due to hydrogen bonded solvents, is greater in the larger solvents (t-butanol, 2-propanol,...), and generally smaller for the smaller solvents; a result which is opposite of what the experimental breakdown appears to be. Reorganization energies also appear to fall within the same range as what is predicted from molecular theories, although the results appear slightly enhanced for the more polar solvents. Experimental values of the reorganization energy are limited, and few direct comparisons are possible.

4.5. References and Notes

1. Y. Chen, F.G., J. W. Petrich. *Chem. Phys. Lett.* **1994**, *222*, 329-334.
2. Moog, R.S. and M. Maroncelli. *J. Phys. Chem.* **1991**, *95*, 10359.
3. Chapman, C.F. and M. Maroncelli. *J. Phys. Chem.* **1992**, *96*, 8430-8441.
4. Reichardt, C. *Chemical Reviews.* **1994**, *94*, 2319-2358.
5. Bottcher, C.J.F. and P. Bordewijk, *Theory of electric polarization*. Vol. 2. 1978, Amsterdam.
6. Tomasi, J. and M. Persico. *Chem. Rev.* **1994**, *94*, 2027-2094.
7. Catalan, J., *et al.* *J. Phys. Chem.* **1992**, *96*, 3615-3621.
8. Alencastro, R.B.d., J.D.D.M. Neto, and M.C. Zerner. *Int. J. Quantum Chem. Symp.* **1994**, *28*, 361-377.
9. Mente, S., *et al.* *Chem. Phys. Lett.* **1998**, *293*, 515-522.
10. Jorgensen, W.L., . 1994, Yale University: New Haven, CT.
11. Bader, J.S. and B.J. Berne. *J. Chem. Phys.* **1996**, *104*, 1293-1308.
12. . 1995, SemiChem: Shawnee, KS.
13. Frisch, M.J., *et al.*, . 1994, Gaussian Inc.: Pittsburg, PA.
14. Thompson, M.A., . 1992.
15. Liptay, W.Z. *Naturforsch., Part A.* **1965**, *20a*, 1441-1471.

16. Jeffrey, G.A., *An introduction to hydrogen bonding*. paper back ed. Topics in Physical Chemistry, ed. D.G. Truhlar. 1997, New York, Oxford: Oxford Press. 303.
17. Mente, S. and M. Maroncelli. *J. Phys. Chem. A*. **1998**, *102*, 3860-3876.
18. Kjaer, A.M. and J. Ulstrup. *J. Am. Chem. Soc.* **1987**, *109*, 1934-1942.
19. Matyushov, D.V., R. Schmid, and B.M. Ladanyi. *J. Phys. Chem. B*. **1997**, *101*, 1035-1050.
20. McHale, J.L. and Y. Zong. *J. Chem. Phys.* **1997**, *107*, 2920-2929.
21. Walker, G.C., *et al.* *J. Phys. Chem.* **1992**, *96*, 3728-3736.
22. Marcus, R.A. and N. Sutin. *Biochim. Biophys. Acta*. **1985**, *811*, 265.
23. McHale, J.L. and Y. Zong. *J. Chem. Phys.* **1997**, *106*, 4963-4972.
24. Perng, B.C., *et al.* *J. Chem. Phys.* **1996**, *104*, 7177-7204.

Chapter 5

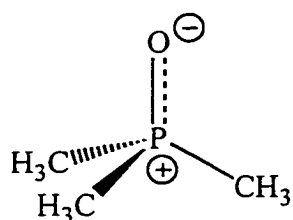
MONTE CARLO SIMULATIONS OF SOLVENT EFFECTS ON THE P-O STRETCHING BAND OF TRIETHYLPHOSPHINE OXIDE IN ALCOHOLS AND WATER

5.1. Introduction

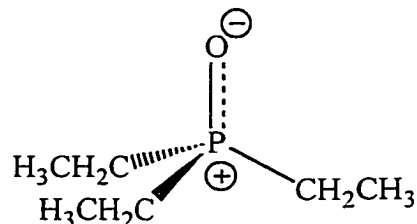
This chapter examines the solvent-induced spectral shifts of the P-O stretching bands of phosphine oxide probe compounds in polar-protic solvents in an attempt to help understand the hydrogen bond donating abilities of solvents. In the previous chapter we examined electronic spectra of Reichardt's betaine-30 dye with this same purpose. The betaine-30 molecule is generally considered a proximate measure of the hydrogen bond donating ability of protic solvents [1], although its large size, dipole moment and polarizability are troublesome attributes with respect to molecular simulations. As an alternative, the calculated vibrational spectra of phosphine oxide probe compounds will be presented. The frequency shifts of the P-O stretching band of trimethylphosphine oxide (TMPO) and triethylphosphine oxide (TEPO) in alcohols varies in a manner that appears to be directly related to either the strength of the hydrogen bonding interaction, or the number of solvates coordinated to the hydrogen bonding acceptor site, or both [2-5]. Using these probes, we hope to offer a connection between "polarity" and hydrogen bonding. In addition, the ability of the classical potential models to reproduce bulk polarity will be further discussed.

Scheme 5.1

Trimethylphosphine oxide



Triethylphosphine oxide



These compounds are attractive systems from a simulation standpoint compared to betaine-30. Both TMPO and TEPO contain a similar basic (hydrogen bond accepting) site to that of the oxygen site in betaine-30. As a result, these molecules are expected to register hydrogen bonding in a way comparable to $E_T(30)$. However, unlike betaine-30, both TMPO and TEPO have the advantages of being substantially smaller and possess considerably smaller dipole moment. This last point is important, in that the shifts due to the tremendous dipole moment change observed in the betaine-30 molecule are expected to possess a significant long-range component. Although different vibrational energy states have different electrostatic characteristics, the solvent induced effects reflected in the vibrational absorption spectrum are certainly expected to be substantially less when compared to those felt by the differing electronic states of the betaine-30 molecule. Thus, the vibrational shift can be thought of as a much more “local” probe of solvent polarity. Consequently, the long-range electrostatic interactions, though present, should not have as serious of an effect on the solvent-induced spectroscopic shifts. Also, like electronic spectroscopy, vibrational spectroscopy has a considerable experimental history, with respect to the study of solvent effects, to facilitate the present inquiry.

Solvation effects on vibrational frequencies reflect a balance between repulsive and cohesive intermolecular interactions [6]. In hydrogen bonding systems at normal liquid temperatures and pressures, the interactions between the hydrogen-bond donor and hydrogen-bond acceptor pair will broaden the potential energy well of both species due to the dominating cohesive interactions. As a result, the vibrational spectrum will always shift to lower frequencies. The magnitude of the shifts, of course, depend on how much the potential energy wells broaden, which reflects the strength of the hydrogen bond donor-acceptor interactions.

Although vibrational spectroscopy provides a useful tool for studying intermolecular interactions, the use of phosphine oxide probe compounds has its origins in NMR spectroscopy. The initial attempts to measure solvent electrophilicity (Lewis acid-strength), made by Mayer, Gutmann and Geiger, utilized the ^{31}P -NMR shifts of triethylphosphine oxide (TEPO)[7]. This particular probe possesses a few attractive qualities from an experimental point of view: (1) the ^{31}P nucleus is easily accessible for NMR measurements, and is removed from the actual interaction site (the oxygen) which, supposedly, eliminates ill-definable contributions to the chemical shift values; (2) TEPO is a strong base, and possesses partial double bond character along the P-O bond, which insures that the phosphorous resonance will be sensitive to environmental changes; (3) the solute-solvent interactions are, for the most part, limited to the oxygen site, and coordination to the phosphorous is blocked by ethyl groups; (4) TEPO is soluble in a wide variety of solvents, and (5) is chemically stable. Using this compound, Mayer and

coworkers derived the “acceptor number” scale as a measure of solvent electrophilicity [7].

The capacity of empirical solvent polarity scales, such as the $E_T(30)$ solvent polarity scale, to register hydrogen-bond donating ability is well documented. However, as a consequence of a scale’s ability to measure overall polarity, it fails to separate and indicate specific solvent interactions. Figure 5.1 demonstrates the correlation between ^{31}P -NMR shifts of TEPO and the $E_T(30)$ solvent polarity scale. Generally, the correlation is good ($R^2 \sim 0.9$): a sensible result considering both probes share a common hydrogen-bond accepting group. However, this correlation does reveal that some solvents may exhibit significant positive deviations. Most notably, acetic acid and chloroform seem to possess enhanced “electrophilic” character compared to what would otherwise be expected based on this correlation. Both of these solvents have unusually low dielectric constants compared to other solvents on this scale which possess similar electrophilic character. Consequently, they do not cause as large of a shift in the electronic spectrum of betaine-30, which clearly has a substantial dielectric component. A similar phenomenon may be seen when looking at polar-aprotic solvents (shown as the black circles in Figure 5.1). Here, the solvents tend to have lower NMR shifts compared to what one would expect based on their polarity, due to the lack of hydrogen-bond donating ability of these solvents.

Roughly a decade later Symons revisited the study of solvent electrophilicity, performing IR-spectroscopy of the TEPO solute [2-4]. Symons studied the shifts of the P-O vibration band, ν_{PO} , and found a near-perfect correlation between this observable the

^{31}P NMR shifts tabulated by Mayer (figure 5.2) [7]. Symons argued that the shifts may be viewed as reflecting the strength of the solute-solvent interactions and that these interaction strengths in protic solvents are a function of the number of solvents coordinated to the phosphine oxide species [2]. Further, he demonstrates how quantitative fractions of solvent coordination can be obtained by integrating the area under the peaks corresponding to a given solvation complex [2].

Mayer and coworkers also revisited this system, and like Symons, turned to IR-spectroscopy to further elucidate the meaning of the “acceptor numbers.” [5, 8] In these studies, Mayer discussed solvation of this probe and loftily presented a “unified description of solvent effects on chemical reactions and physical processes in aprotic and protic solvents.” [5] He also asserted that the relationship between the observed shifts and the solvent reflects the strength of the solute-solvent complexes and is free from non-specific contributions [5, 8]. If true, this probe provides an important compliment to the betaine probe, in which the shifts reflect both specific and non-specific intermolecular interactions.

This final chapter presents both computer simulations and experimental FTIR spectroscopy to examine the solvent-induced frequency shifts in the P-O vibration of two probe compounds: trimethylphosphine oxide (TMPO) and triethylphosphine oxide (TEPO). The vibrational spectrum of these compounds in a polar-protic solvent is distinctly bimodal, where it has been suggested that each peak corresponds to a differently coordinated solute-solvent complex [2]. Through examination of these peak values and average vibrational shifts, a connection may be established between the

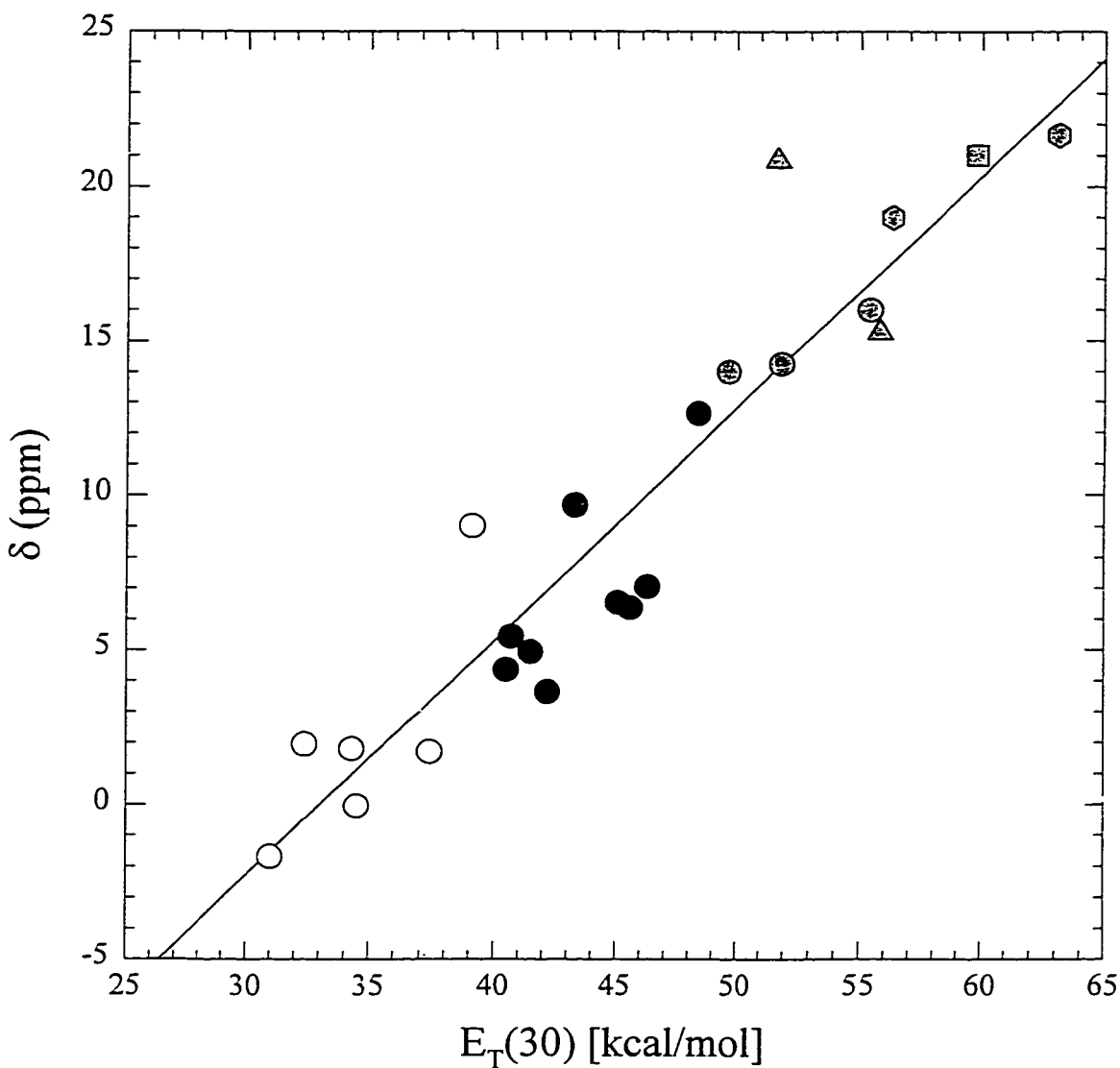


Figure 5.1. Correlation between the $E_T(30)$ solvent polarity parameter and the ^{31}P -NMR shifts of TEPO.

Key: Open Circles = aprotic solvents with $\epsilon < 10$.
 Closed Circles = aprotic solvents with $\epsilon > 10$.
 Diamonds = monoalcohols (Dark Grey = non-primary)
 Triangle = formamide and acetic acid
 Square = 2,2,2-trifluoroethanol
 Hexagon = water and ethylene glycol

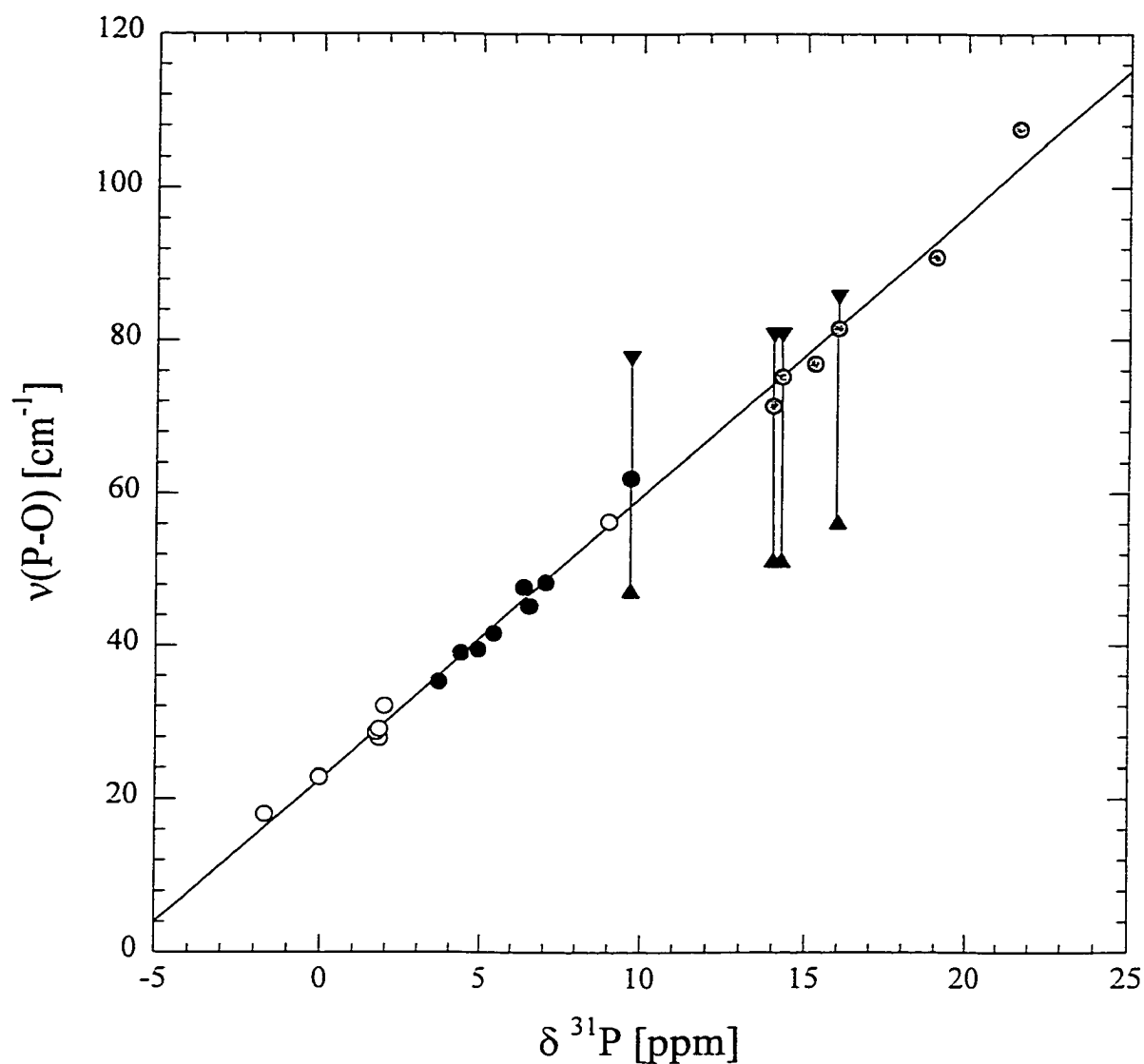


Figure 5.2. Correlation between the $\nu(\text{P-O})$ frequency shift (from vapor) and the ^{31}P -NMR shifts of TEPO.

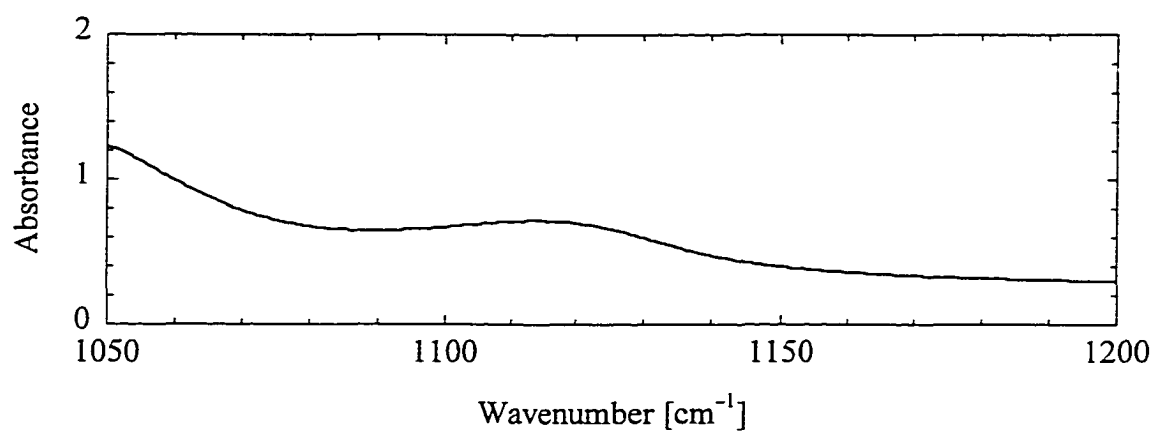
Key: Open Circles = aprotic solvents with $\epsilon < 10$.
 Closed Circles = aprotic solvents with $\epsilon > 10$.
 Grey Circles = monoalcohols (Dark Grey = non-primary)
 Triangles designate the peak frequencies, the circles designate the weighted average.

empirical values for solvent polarity and hydrogen-bond donating ability. Further, simulations will be used in an attempt to predict vibrational shifts using a perturbative expansion technique. The applicability of this method will be analyzed, and the results will be discussed in order to assess the modeling techniques and the hydrogen-bonding character of the potential functions used.

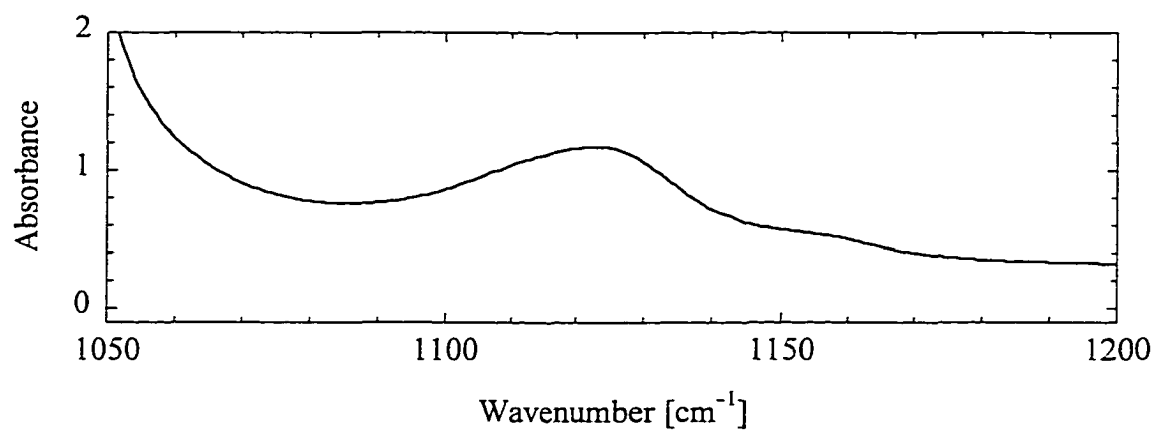
5.2. Experimental

FTIR-spectra were recorded with a Matson Galaxy Series 3000 spectrophotometer with 1 cm^{-1} resolution. Solution spectra were recorded at 0.5 mol/L concentrations by means of demountable cells with CaF_2 windows and 25 μm pathlength. Unless otherwise stated, the spectra shown have had the pure liquid spectrum subtracted. The reported peak positions and widths have been generated from fits to gaussian functions using Jandel's PeakFit program. Example unsubtracted and pure solvent spectra are shown in Figure 5.3. The C-O stretch from the alcohol solvents absorbs in the same region as the P-O stretch of the phosphine oxide compounds, making the subtraction process necessary.

Sample preparation did not include any particular efforts to keep the TEPO dry, despite the hygroscopic nature of this compound. All TMPO samples were prepared in a dry box. Sample concentrations were generally in the range of 0.1 – 0.5 mol/l, unless specifically stated. For a comprehensive study of the concentration dependence of the observed spectral properties, see Ref. [5].



B. TEPO + Methanol



C. Subtracted Spectrum

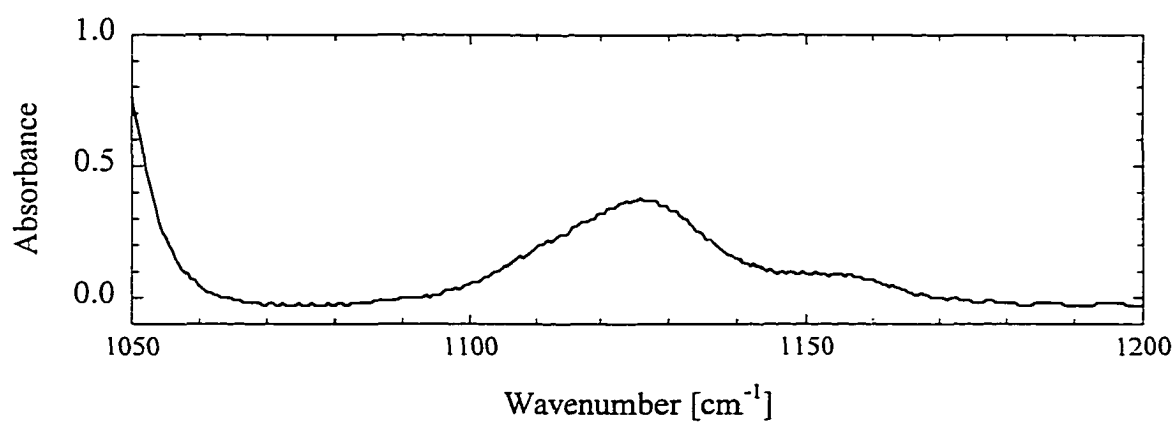


Figure 5.3. Example of spectral subtraction: TEPO in bulk methanol.

5.3. Theoretical Background

5.3.1. Modeling Ω

For the calculation of the solvent induced vibrational frequency shifts, we employ the method originally developed by Oxtoby [9]. He described the instantaneous shift Ω by expanding about $Q=0$;

$$\hbar\Omega \cong [Q_{11} - Q_{00}] \left(\frac{\partial V}{\partial Q} \right)_{Q=0} + \frac{1}{2!} [(Q^2)_{11} - (Q^2)_{00}] \left(\frac{\partial^2 V}{\partial Q^2} \right)_{Q=0} + \dots \quad (5.1)$$

where Q_{ii} and Q_{ii}^2 are expectation values of Q and Q^2 in vibrational state i . If the unperturbed vibrational hamiltonian is assumed to be of the form

$$\hat{H}_0 = \frac{1}{2\mu} \hat{P}_Q^2 + \frac{\mu\omega_0}{2} \hat{Q}^2 + \frac{1}{6} f \hat{Q}^3 \quad (5.2)$$

then these expectation values can be written in terms of the harmonic frequency ω_0 , the reduced mass μ , and the cubic anharmonicity f of the vibrational mode:

$$Q_{11} - Q_{00} = -\frac{\hbar f}{2\mu^{3/2}\omega_0^3}, \quad (Q^2)_{11} - (Q^2)_{00} = \frac{\hbar}{\omega_0} \quad (5.3)$$

The quantities ω_0 , μ and f are characteristics of the isolated solute, which may be determined via *ab initio* calculations.

The first assumption required to determine the solvent induced vibrational shifts from equation 5.1 is that the only relevant change in solute-solvent interactions between a

solute in its $v=0$ and $v=1$ states results from the effective expansion of the molecule along Q when the solute is vibrationally excited. Further, it must be assumed that the shift can be directly related to the solvent-induced forces on the vibrator in its ground vibrational state, as denoted in equation 5.1. Lastly, we make the added assumption that the first and second derivative terms may be approximated, by direct calculation from the simulation.

In order to represent the 1st and 2nd derivatives of the potential with respect to the normal coordinate, we first express the typical atom-atom simulation potential as:

$$V = V_{LJ} + V_{Coul} = \sum_i \sum_\alpha \{v_{LJ}(\bar{s}_\alpha, \bar{r}_i, p_\alpha) + v_{Coul}(\bar{s}_\alpha, \bar{r}_i, q_\alpha, q_i)\} \quad (5.4)$$

where the vector quantities $s_\alpha(Q)$ represents the coordinates of solute atom α , r_i represents the coordinates of solvent atom i , $p_\alpha(Q)$ represents the Lennard-Jones parameters of the pair, $q_\alpha(Q)$ and q_i are the solute and solvent atom charges. Using this notation, the Lennard-Jones, v_{LJ} , and coulombic parts of the overall potential from the previous chapters may be rewritten in the form:

$$v_{LJ}(\bar{s}_\alpha, \bar{r}_i, p_\alpha) = 4\varepsilon_\alpha(p_\alpha) \left\{ \left(\frac{\sigma_\alpha(p_\alpha)}{|\bar{s}_\alpha - \bar{r}_i|} \right)^{12} - \left(\frac{\sigma_\alpha(p_\alpha)}{|\bar{s}_\alpha - \bar{r}_i|} \right)^6 \right\} \quad (5.5)$$

$$v_{Coul}(\bar{s}_\alpha, \bar{r}_i, q_\alpha, q_i) = \frac{q_\alpha q_i}{|\bar{s}_\alpha - \bar{r}_i|} \quad (5.6)$$

Supposing that vibration causes not only alteration of the solute atom positions, but also the interaction parameters of the solute represented by ϵ_α and q_α , then:

$$\frac{\partial V_{LJ}}{\partial Q} = \sum_i \sum_\alpha \left\{ \left(\frac{\partial v_{LJ}}{\partial \bar{s}_\alpha} \right)_{\bar{r}, p} \cdot \left(\frac{\partial \bar{s}_\alpha}{\partial Q} \right) + \left(\frac{\partial v_{LJ}}{\partial p_\alpha} \right)_{\bar{r}, \bar{s}} \cdot \left(\frac{\partial p_\alpha}{\partial Q} \right) \right\} \quad (5.7a)$$

$$\frac{\partial V_{Coul}}{\partial Q} = \sum_i \sum_\alpha \left\{ \left(\frac{\partial v_{Coul}}{\partial \bar{s}_\alpha} \right)_{\bar{r}, q} \cdot \left(\frac{\partial \bar{s}_\alpha}{\partial Q} \right) + \left(\frac{\partial v_{Coul}}{\partial q_\alpha} \right)_{\bar{r}, \bar{s}} \cdot \left(\frac{\partial q_\alpha}{\partial Q} \right) \right\} \quad (5.7b)$$

Here, the first terms in the summations refer to the changes in potential which occur as the molecule vibrates along the normal coordinate due to the spatial displacements of the atomic sites. This represents the limit in which atomic charges and polarizabilities remain constant as a function of the molecular vibrations, and is termed the “0th-order” model. In reality, significant redistribution of electron density also occurs upon vibration which can be viewed as changing the values of the atomic site parameters (q , ϵ , and σ). Such effects are described by the second terms in equation 5.7. To calculate the 1st and 2nd derivatives of the potential in a simulation we proceed numerically. Defining:

$$V_0 \equiv V(Q = 0) \quad (5.8)$$

$$V_\pm \equiv V(\pm \delta Q)$$

we can use the simple numerical differences

$$\left(\frac{\partial V}{\partial Q} \right)_{Q=0} \equiv \frac{V_+ - V_-}{2\delta Q} \quad (5.9)$$

$$\left(\frac{\partial^2 V}{\partial Q^2}\right)_{Q=0} \cong \frac{V_+ + V_- - 2V_0}{(\delta Q)^2} \quad (5.10)$$

The first two terms of equations 5.7a and 5.7b may be evaluated by simply recalculating the potential energy at small displacements δQ of the solute atomic positions along Q . This is the 0th-order calculation of the shifts. Here it is assumed that the solute polarizability and charge distribution are not significantly altered during the vibration. A more complete calculation of the solvent induced shifts must account for these two important variations. For a simulation of a rigid solute, these considerations must be approximated. To this end we assume that the parameters vary in the simple linear manner:

$$\begin{aligned} \varepsilon_{ai}(\pm\delta Q) &= \varepsilon_{ai}(0)\{1 \pm f_\varepsilon \delta Q\} \\ \sigma_{ai}(\pm\delta Q) &= \sigma_{ai}(0) \end{aligned} \quad (5.11)$$

$$q_{ai}(\pm\delta Q) = q_{ai}(0)\{1 \pm f_q \delta Q\}$$

With these choices the individual atom-atom terms become

$$v_{LJ}[\bar{s}_\alpha(\pm\delta Q), \bar{r}_i, p_\alpha(\pm\delta Q)] = v_{LJ}[\bar{s}_\alpha(\pm\delta Q), \bar{r}_i, p_\alpha(0)]\{1 \pm f_\varepsilon \delta Q\} \quad (5.12)$$

$$v_{Coul}[\bar{s}_\alpha(\pm\delta Q), \bar{r}_i, q_\alpha(\pm\delta Q)] = v_{Coul}[\bar{s}_\alpha(\pm\delta Q), \bar{r}_i, q_\alpha(0)]\{1 \pm f_q \delta Q\}$$

and the numerical derivatives may be calculated using the parameters for $Q=0$:

$$\left(\frac{\partial V_{LJ}}{\partial Q}\right)_{Q=0} \cong \frac{V_{LJ}[\bar{S}(+)] - V_{LJ}[\bar{S}(-)] + f_\varepsilon \delta Q \{V_{LJ}[\bar{S}(+)] + V_{LJ}[\bar{S}(-)]\}}{2\delta Q} \quad (5.13)$$

$$\left(\frac{\partial V_{Coul}}{\partial Q}\right)_{Q=0} \cong \frac{V_{Coul}[\bar{S}(+)] - V_{Coul}[\bar{S}(-)] + f_q \delta Q \{V_{Coul}[\bar{S}(+)] + V_{Coul}[\bar{S}(-)]\}}{2\delta Q} \quad (5.14)$$

$$\left(\frac{\partial^2 V_{LJ}}{\partial Q^2}\right)_{Q=0} \cong \frac{V_{LJ}[\bar{S}(+)] + V_{LJ}[\bar{S}(-)] - 2V_{LJ}[\bar{S}(0)]}{(\delta Q)^2} \quad (5.15)$$

$$\left(\frac{\partial^2 V_{Coul}}{\partial Q^2}\right)_{Q=0} \cong \frac{V_{Coul}[\bar{S}(+)] + V_{Coul}[\bar{S}(-)] - 2V_{Coul}[\bar{S}(0)]}{(\delta Q)^2} \quad (5.16)$$

In terms of running the simulations, only the potential energies calculated for the normal mode displacements need be output during a simulation run. An attempt to include the parametric changes for solute charge and polarizability may be made after the fact. The change in the electrostatic charge distribution of the solute as a function of the vibration may be determined from *ab initio* calculations. The change in solute polarizability must be determined empirically to achieve agreement with experiment. The fitting of this term, f_ϵ , and its physical significance will be reported in the results and discussion section.

5.3.2. Potential Functions and Simulation Method.

The structure and charge distribution for the TMPO molecule was calculated at the 6-31G** level using the Gaussian 94 quantum chemical software package [10]. The

charge distributions were determined from fits to the electrostatic potentials using the MKS method [11]. All potential parameters for the TMPO molecules are summarized in Table 5.1. The solute is represented using a rigid all atom model. To simplify the evaluation of the shifts, which are based on the normal mode vibration, no dihedral variation was allowed for the H-C-P-O torsions. Each atomic site of the solute interacts with solvent molecules via a Lennard-Jones plus Coulomb interaction potential of the form specified in previous chapters (equations 2.4 and 3.1). Lennard-Jones parameters of the solute were obtained from the OPLS parameter set [12]. Details of the solvent models have been outlined in previous chapter.

The frequencies, reduced masses, and normal modes were calculated using Gaussian 94 [10] for the optimized geometry. The anharmonicity constant of the P-O vibration was determined by moving the solute atomic coordinates along the relevant normal mode of vibration and performing a series of single point calculations which was also at the HF/6-31G** level. The resulting plot of energy versus normal mode displacement was fit to a cubic function of the form:

$$U_{vib} = \frac{1}{2}k\hat{Q}^2 + \frac{1}{6}f\hat{Q}^3 \quad (5.17)$$

Where k is the force constant of the vibration, q is the normal mode coordinate, q_{eq} is the equilibrium position, and f is the anharmonicity constant.

The Cartesian displacements corresponding to the P-O “stretch” are shown in Figure 5.4. There are significant displacements of atoms other than the oxygen and

Table 5.1. Solute Potential Parameters^a

atom type	σ (Å)	ϵ (kcal/mol)	q (au)
O	2.96	0.210	-0.7836
P	3.74	0.200	1.2033
C	3.50	0.066	-0.6100
H	2.50	0.030	0.1567

^a Parameters from in Ref 12.

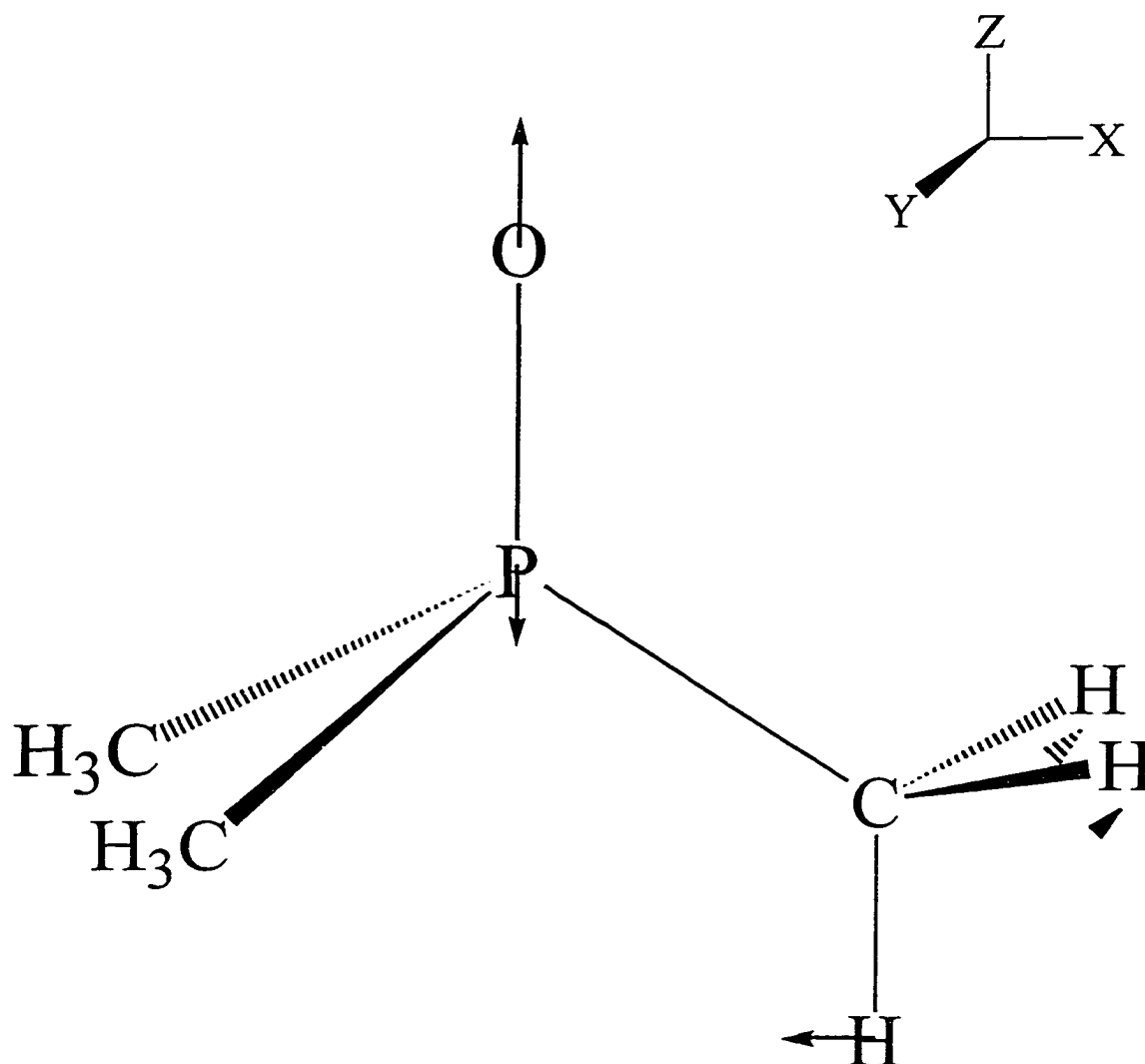


Figure 5.4. Nuclear displacements corresponding to the normal mode associated with the “ $\nu(\text{P-O})$ ” spectral line computed at the HF/6-31F** level. The displacements are presented as XYZ coordinates.

phosphorous. In the simulation, all of the atom sites are moved to calculate difference potential quantities, V_+ and V_- .

5.4. Results and Discussion

5.4.1. Vibrational Spectroscopy of the P-O Stretching Mode of TEPO and TMPO.

The IR spectra of TEPO in various solvents are presented in Figure 5.5. The spectra of TEPO in various alcohols all display either a distinctly observable second band or a substantial shoulder. The appearance of more than one band has been attributed to the presence of more than one type of solute-solvent hydrogen bonded complex existing in these solutions. The peak positions and relative weighting, when available, agree well with previously published values [2, 5].

A tabulation of the spectral characteristics for all solvents is given in Table 5.2. The spectra have been decomposed into their gaussian components using the Jandel Peakfit data fitting software. From these decompositions the points of maximum intensity and the full widths at half-max values have been determined. The P-O vibrational spectra observed in alcohols show the presence of two well-separated bands. Based on binary solvent data, both Symons et al [2-4]. and Mayer [5], have attributed the lower energy band to that of the di-hydrogen-bonded complex, and the second peak to the mono-hydrogen-bonded complex. All alcohols with the exceptions of methanol and t-butanol, have a low-energy band shifted $\sim 80 \text{ cm}^{-1}$, and a higher energy band shifted $\sim 50 \text{ cm}^{-1}$. Based on the integrated areas under these two components, the percentage of di-

complexed and mono-complexed species is estimated at ~70 % and ~30 % respectively. Methanol has considerably more of the di-complexed species (~87%), while t-butanol has substantially less of the di-complexed species (~58%).

In water the P-O vibrational frequencies show the largest shifts: 108 cm^{-1} for the primary band. The shoulder “peaks” are also considerably shifted, although the magnitudes of these shifts are about 20 cm^{-1} .

Ethylene glycol, like water, has a single peak and a higher energy shoulder, as opposed to a distinct second-higher energy- band. The peak position of single band is shifted $\sim 90\text{ cm}^{-1}$: a value that is between the tri-hydrated water band and the di-complexed methanol band. The binary solvent data presented by Symons demonstrates that peaks *attributed to a given chelate complex* shift as a function of the relative concentration of the two components [2], suggesting that assignment of the band to either the tri-complexed or di-complexed form cannot be determined exclusively by the shift of the band. That is, if the 90 cm^{-1} shift is due to a di-hydrogen bonded complex, then it is shifted to lower frequencies relative to methanol, due to the different solvent environment. Mayer and coworkers assigned the 90 cm^{-1} shift in ethylene glycol to a di-complexed species that have somewhat stronger “acceptor” properties compared to the monoalcohols [5].

The spectra of TMPO in carbon tetrachloride and acetonitrile show only a single peak. Although these bands have an extended high-energy shoulder, there is no indication of a second peak. The P-O “stretching” frequencies ($\nu(\text{P-O})$) in the spectra of TMPO are all qualitatively similar to the analogous spectra of TEPO in the same solvent.

Figure 5.5 shows the agreement between these two data sets. The P-O stretch of TMPO appears to have a similar solvent dependence as the same stretch in TEPO. The only difference being that the TMPO values are uniformly lower in energy by approximately 24 cm^{-1} .

The peak positions, bandwidths, and percentages (based on integrated intensities) are summarized in table 5.2.a. and 5.2.b. Table 5.2.a presents the spectral characteristics generated by using two gaussian functions to fit the observed spectra, while the results presented in table 5.2.b are from fits using three gaussian functions. Since it is proposed that each gaussian function obtained from the spectral deconvolution represents a distinct coordination environment, this choice is crucial in understanding the hydrogen bond strengths of the solvents. The fits using three gaussian functions do not yield a better statistical fit in any of the solvents studied. Nevertheless, based on the simulated results reported in the next section, the possibility of using a third gaussian function is considered.

Regardless of the number of gaussian functions used to fit the spectra, the average shift values may be calculated for the set of solvents and may be interpreted as an apparent measure of hydrogen bonding strength of those solvents. These values are presented in table 5.2, and shown plotted versus the $E_T(30)$ in figure 5.7. Considering only the series of mono-alcohols, the correlation with $E_T(30)$ is rather poor, although there does appear to be a general trend with solvent polarity. In particular, it is difficult to distinguish between the alcohols of intermediate polarity (ethanol, 1-propanol, 1-butanol, 2-propanol, and 2-butanol) using the phosphine oxide spectra. That is, they all

seem to have similar hydrogen-bond strength, as measured by TEPO. Although the band is shifted less in bulk t-butanol, this solvent also appears to overestimate hydrogen bond strength compared to what one might predict based on the $E_T(30)$ scale.

Acetonitrile and chloroform are also poorly correlated with $E_T(30)$. Chloroform forms a much stronger hydrogen bond than expected, while acetonitrile shifts the P-O vibrational band only a meager 37 cm^{-1} . The fact that these two solvents are as poorly correlated as they are with “polarity” suggests that TEPO is, in fact, a good probe of hydrogen bond strength. That is, acetonitrile, which is a polar-*aprotic* solvent, has a smaller shift than the less-polar *protic* solvents due to its inability to form hydrogen bonds. Chloroform, on the other hand, induces a much larger shift due to its ability to donate a hydrogen bond.

Ethylene glycol and water appear well correlated with $E_T(30)$. Although whether or not this enhanced shift is due to the strength of the hydrogen bonds formed, or the number of hydrogen bonds formed is not clear. Symons has suggested that water is capable of donating three hydrogen bonds to TEPO [2], compared to only two for the alcohols. In support of this, he presented spectral series of acetonitrile/water mixtures, as well as binary mixtures of alcohol/aprotic mixtures which demonstrated the appearance of distinct peaks as a function of mole-fraction of protic solvent [2].

To further test this hypothesis, a spectral titration of TMPO in the binary acetonitrile/water system is presented in figure 5.6. This series of spectra agree well with a similar study performed by Symons for the TEPO probe. In both cases, four distinct

Table 5.2. Comparison of spectral characteristics of TMPO and TEPO in various solvents.

A. Two Gaussian Fits

solvent	1 st Peak			2 nd Peak		
	ν_{\max}	ν_{fwhm}	%	ν_{\max}	ν_{fwhm}	%
TMPO						
Vapor	1228	22.12	70.48	1132	22.45	29.52
Water	1112					
Methanol	1142	24.30	94.44	1170	9.04	5.56
Acetonitrile	1165	15.10	13.85	1182	16.47	86.15
TEPO						
Vapor	1209			1125		
Water	1101.5					
Methanol	1123	28.74	81.62	1153	28.74	18.38
Ethanol	1128	27.14	71.16	1158	27.14	28.84
1-Propanol	1127	28.14	65.40	1158	28.14	34.59
1-Butanol	1128	29.07	67.94	1158	29.07	32.06
2-Butanol	1127	29.98	66.73	1159	29.98	33.27
t-butanol	1131	24.40	48.31	1162	24.40	51.69
Ethylene Glycol	1119	21.42	57.83	1140	35.67	42.17

Average peak separation: $\Delta\nu_{12} = 30.86 \text{ cm}^{-1}$

B. Three Gaussian Fits

solvent	1 st Peak			2 nd Peak			3 rd Peak		
	ν_{\max}	ν_{fwhm}	%	ν_{\max}	ν_{fwhm}	%	ν_{\max}	ν_{fwhm}	%
TEPO									
Vapor									
Water									
Methanol	1112	20.4	26.8	1128	20.4	56.1	1154	20.4	17.0
Ethanol	1115	23.6	11.7	1129	23.6	60.6	1158	23.6	27.6
1-Propanol	1108	24.6	17.0	1129	24.6	53.7	1158	24.6	29.6
1-Butanol	1114	25.5	14.5	1130	25.5	55.9	1159	25.5	29.6
2-Butanol	1111	26.0	9.25	1128	26.0	58.2	1158	26.0	32.6
t-butanol	1119	21.9	10.3	1134	21.9	41.2	1162	21.9	48.6

Average peak separation: $\Delta\nu_{12} = 28.50 \text{ cm}^{-1}$

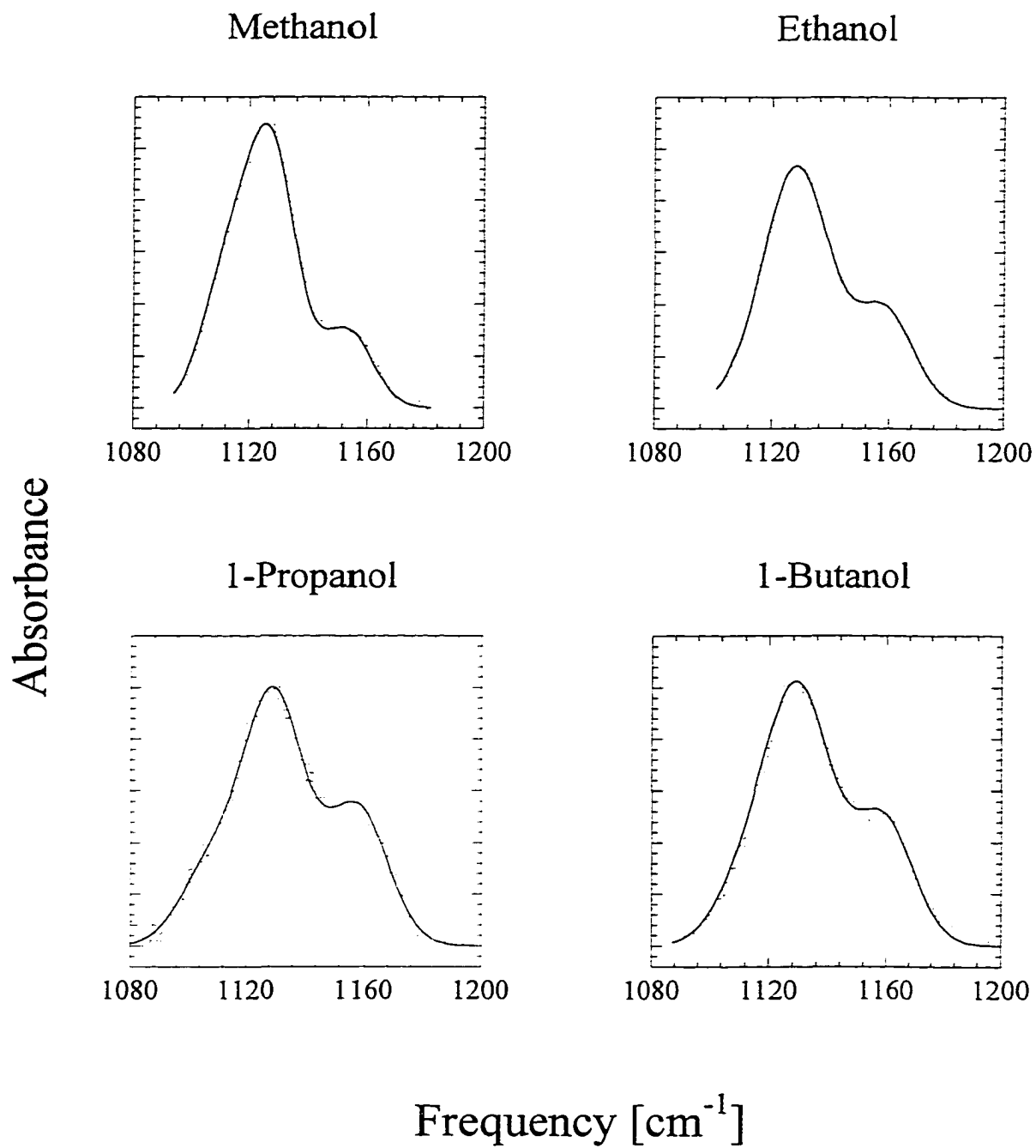


Figure 5.5.a. Infrared Spectra of TEPO in bulk methanol, ethanol, 1-propanol, and 1-butanol.

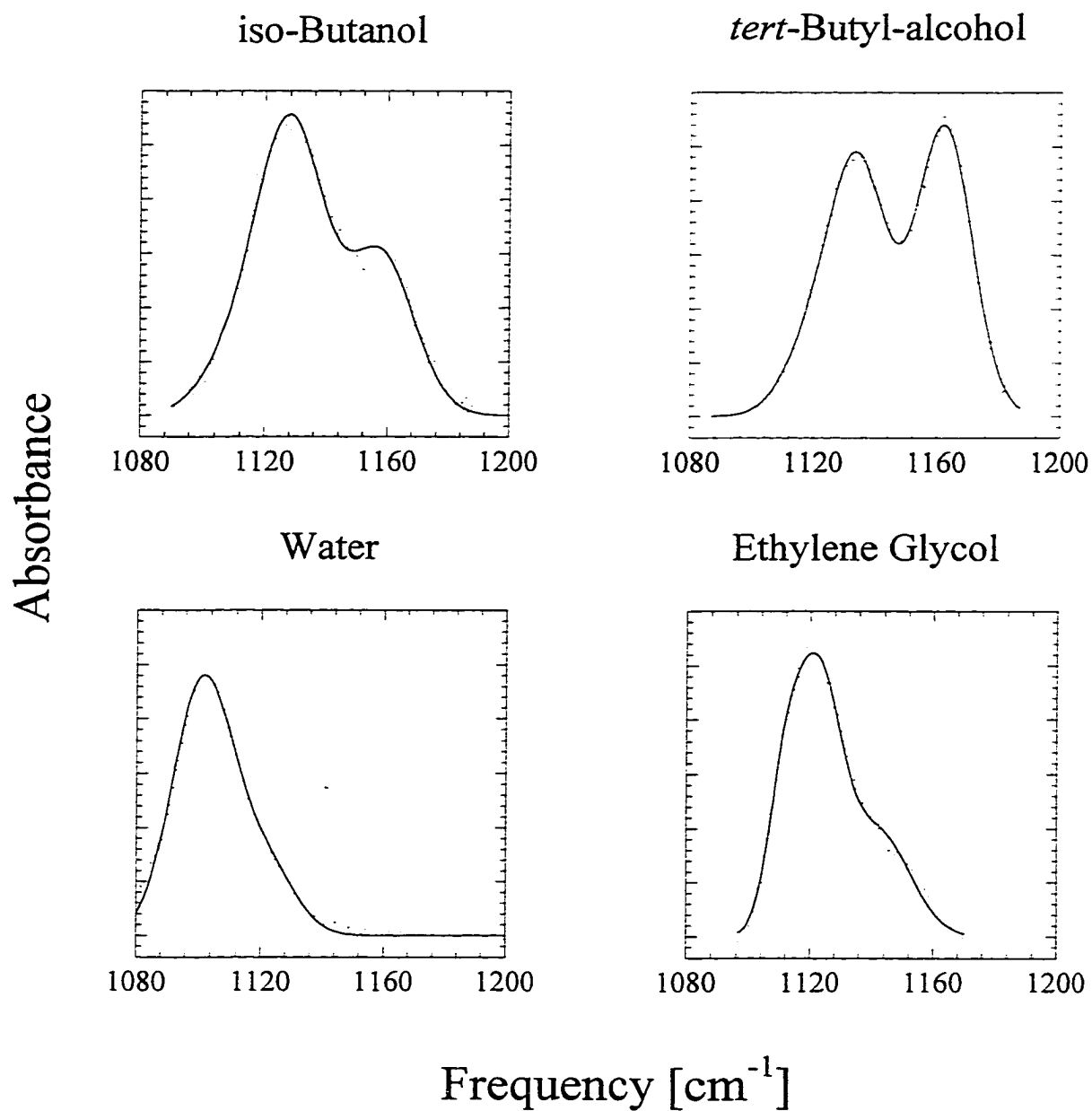


Figure 5.5.b. Infrared spectra of TEPO in bulk iso-butanol, tert-butanol, ethylene glycol, and water.

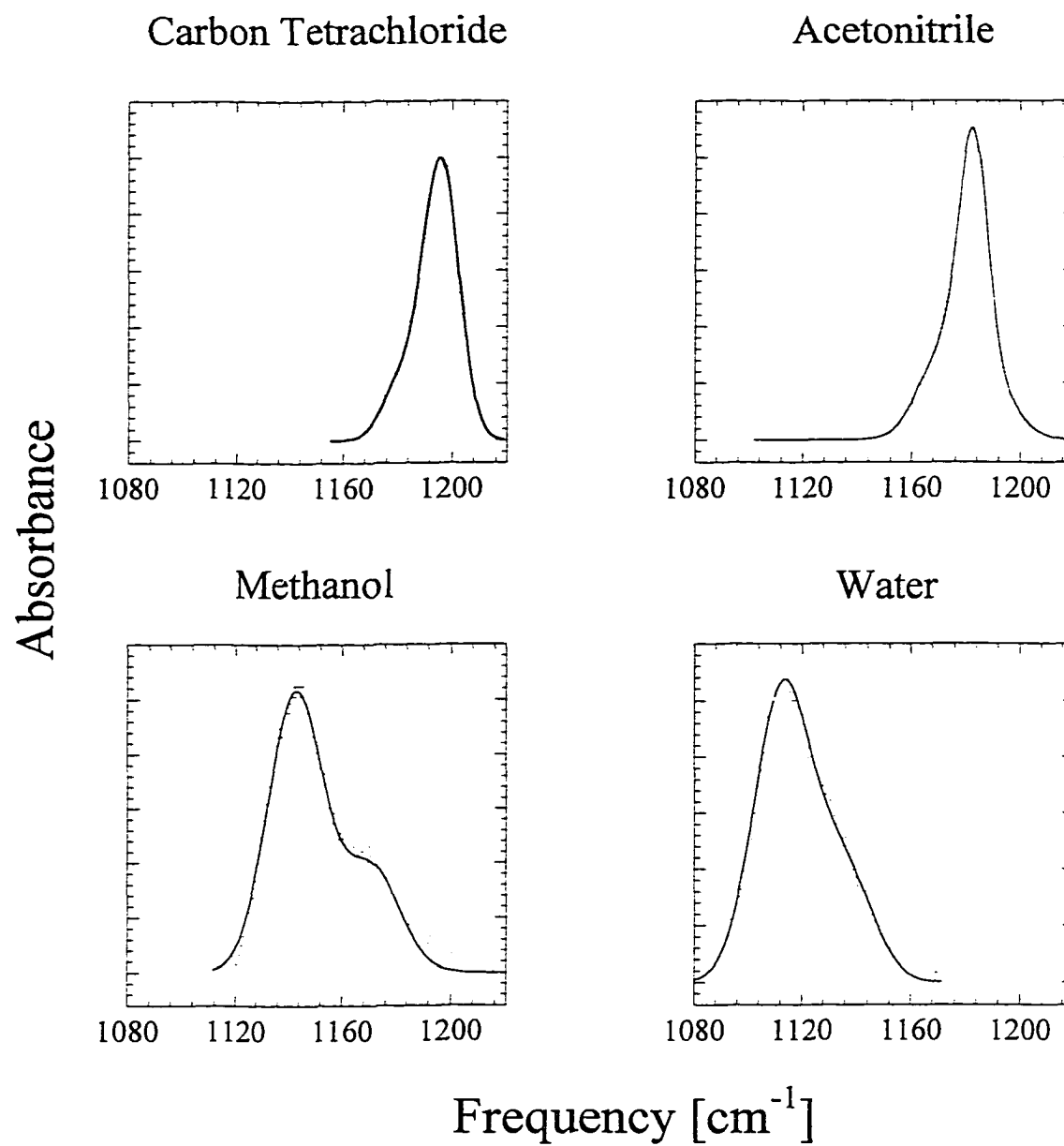


Figure 5.5.c. Infrared spectra of TMPO in bulk carbon tetrachloride, acetonitrile, methanol and water.

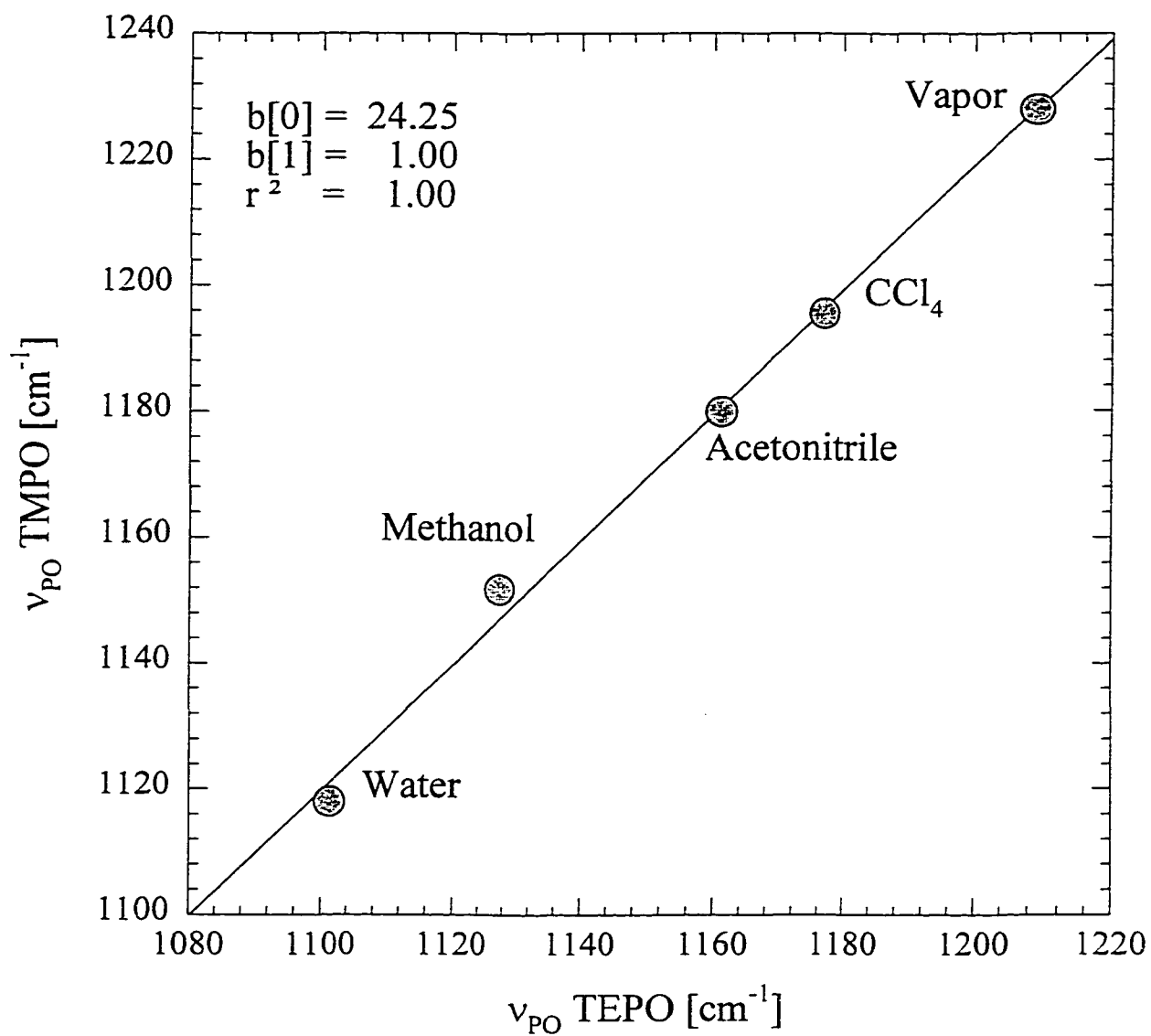


Figure 5.6. Comparison of Phosphine Oxide Vibrational Shifts
 ν_{PO}

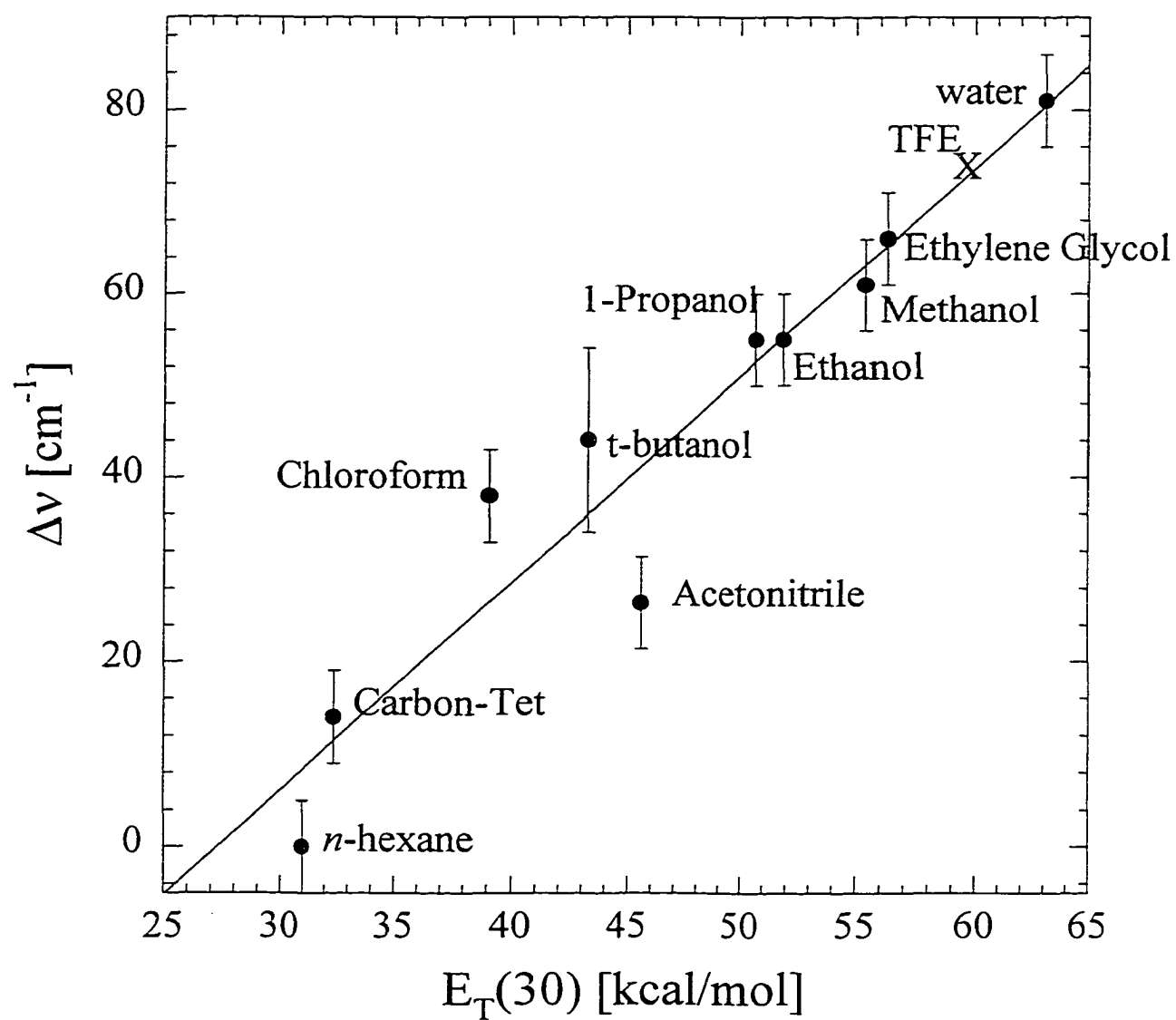


Figure. 5.7. Correlation between TEPO frequency shifts and $E_T(30)$.

Table 5.3. Summary of TMPO-binary solvent spectra.

χ_{ACN}	non-hydrated		mono-hydrated		di-hydrated		tri-hydrated		FWHM
	ν_{max}	%	ν_{max}	%	ν_{max}	%	ν_{max}	%	
1.00	1182	72.0	-	-	-	-	-	-	16
0.79	-	-	1165	21.3	1144	58.7	1120	20.0	25
0.07	-	-	-	-	1131	33.9	1113	66.1	18
0.00	-	-	-	-	1131	29.9	1112	70.1	21

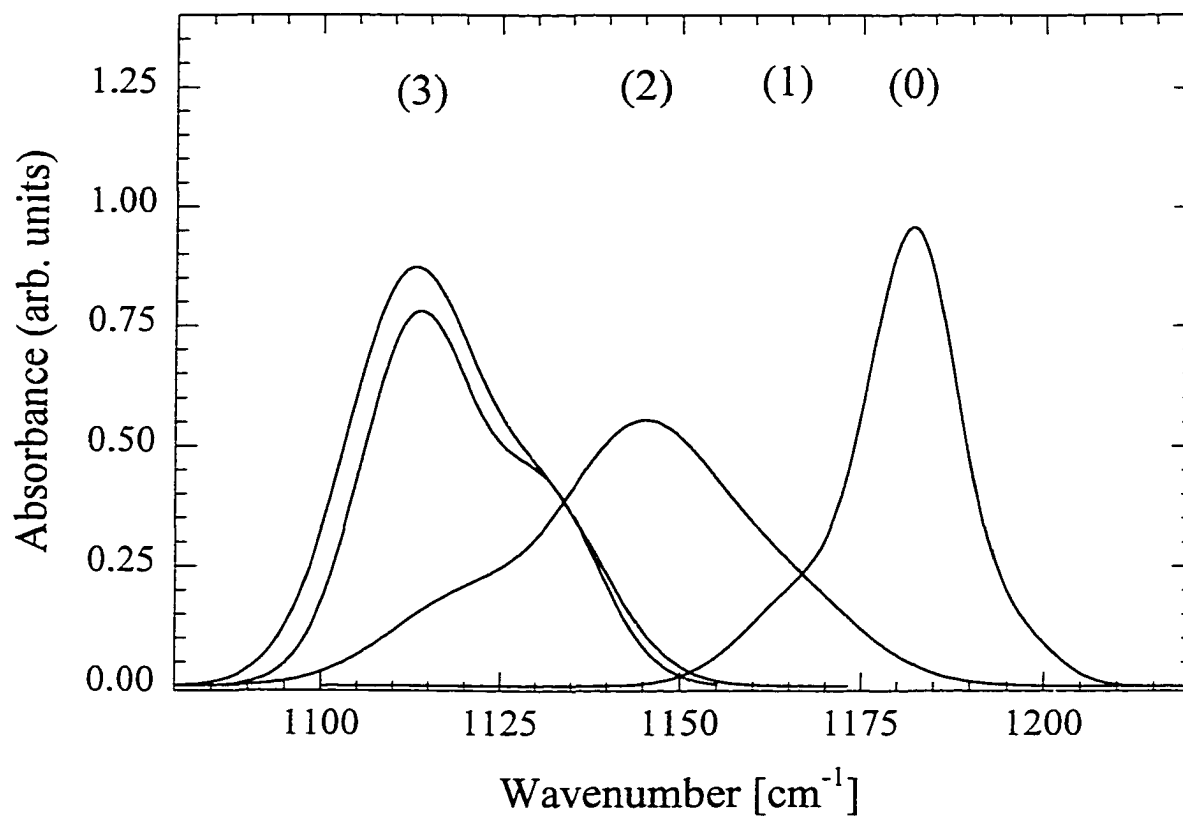


Figure 5.8. Infrared spectra for Mh_3PO in a range of $H_2O + MeCN$ solvents. KEY (in approximate mole fraction of MeCN): 1 = 0.00, 2 = 0.07, 3 = 0.79, 4 = 1.00. The numbers indicating the postulated number of water molecules.

species of R_3PO appear to be involved: tri-hydrate, di-hydrate, mono-hydrate and non-hydrated species. There are clear shifts in these components as the composition changes, especially for band (2), which shifts strongly to higher frequencies as the concentration of acetonitrile increases.

5.4.2. *Computer Simulations of TMPO.*

We now attempt to calculate the solvent-induced spectral shifts of the TMPO solute in a variety of bulk solvents. The primary goal of doing this is to test the assertion that the solvent-induced infrared absorption and ^{31}P -NMR shifts of TMPO (and TEPO) are caused primarily by local interactions between the solute and nearby electrophilic solvents. To our knowledge, no previous simulations of solvent effects on vibrational lineshapes have been reported at the level of detail attempted here. For this an honest evaluation of the methods employed here must also be presented.

In doing so, the results are presented “from the ground – up.” That is, this section will first look at what will be termed the “0th order” calculation of vibrational shifts. This calculation of the shift uses only the spatial displacements of the solute to calculate the derivatives of the potential energy needed for the determination of the shift via equation 5.1. When examining these results, it is important to remember the philosophy at work behind the potential energy functions and parameterization. The atom-site charges and Lennard-Jones parameters are usually chosen in such a manner as to include polarization effects in an average sense. That is, in all *real* chemical systems,

molecules are vibrating, and forming and breaking hydrogen bonds. These and other processes, cause electrons to slosh about, and as a result the intermolecular interactions (polarization, induction, etc...) will change dynamically in time. However, the average effect on the intermolecular interactions is meant to be included in the parameterization. A second attempt will be then presented, in which a slightly more sophisticated model will be employed in the calculation of spectral shifts.

For simplicity, only the TMPO molecule will be used as a solute. The TEPO molecule has a slightly more complicated normal mode vibration, due to the presence of C-C-P-O dihedral angles that are not present in TMPO. Since the experimentally observed vibrational shifts of TEPO and TMPO are nearly perfectly correlated (see figure 5.6) the solvent-dependent shifts are expected to be virtually interchangeable. As with previous chapters, two sets of solvent models have been examined: the “*ab initio*” charge model and the standard “OPLS” models of Jorgensen and co-workers [13]. The first part of this section will examine the solvation structure and energetics of these systems to better characterize their hydrogen bonding abilities.

5.4.2.1. Solvation Structure and Energetics

Table 5.4 summarizes the main structural and energetic features of the solute-solvent interactions. In the first two columns the characteristics of the solute-solvent pair-energy distribution functions are listed. These are also plotted in figures 5.9a and 5.9b. The OPLS set of solvents exhibits a trend of increasing hydrogen bond energies with increasing alcohol size and branching. This trend is not surprising, and reflects the

trend observed for the self-dimerization energies of the pure alcohols. It is worth noting that the all-atom *tert*-butyl alcohol model makes substantially weaker hydrogen bonds with TMPO compared to the united atom model. This feature is unusual considering that the solvent-solvent pair energies have just the opposite ordering (the all-atom model has a substantially larger pair energy and heat of vaporization) [13, 14]. The *ab initio* solvents display similar trend, although the increase in solute-solvent pair energies is enhanced for the two branched alcohols, reflecting the enhanced oxygen-site charges in these models.

The radial distribution functions all possess pronounced first peaks; a quintessential characteristic of hydrogen bonded systems. The coordination numbers, calculated from direct integration of the O-O rdfs, are close to those obtained from integration of the pair distributions. Most alcohols donate an average of two hydrogen bonds to the oxygen of TMPO. Slightly lower coordination numbers were observed in the 2-propanol and *t*-butanol systems using the *ab initio* models. Ethylene glycol forms double chelated complexes with TMPO, in which both ends of a single solvent molecule simultaneously donate hydrogen bonds to the oxygen of TMPO. Consequently the solute-solvent pair energies are very large, roughly double that of the methanol-TMPO systems.

Three different chloroform models were simulated. This solvent is particularly interesting due to the deviation observed between the IR-shift values and its $E_T(30)$ solvent polarity values, as shown in Figure 5.2. The first of the three models to be tested was the four-site model parameterized by Jorgensen, Briggs and Contreras to calculate the relative partition coefficients for an organic solute between chloroform and water

[15]. It is interesting to note that this representation of the solvent produced solute-solvent pair-energy distribution functions that show hydrogen-bond like features, despite the fact that this representation does not explicitly use a hydrogen-site. The other two models employed are five-site models developed separately by Kovacs, Kowalewski and Laaksonen [16], and by Dietz and Heinzinger [17]. These representations give similar values to the OPLS representation, for both the coordination numbers (~ 2 molecules) as well as the pair energy (~ 20 kJ/mol).

The two water models used were the TIP4P models favored by Jorgensen [18], and the *ab initio* derived model used in the previous chapters. Both representations form, on average, between two and three hydrogen bonds with the solute. The hydrogen bond strength, as measured by the solute-solvent pair energy, is on par with those observed methanol for the TIP4P representation, but substantially weaker for the *ab initio* derived model. As observed in the previously presented simulations of the betaine-30 molecule in bulk water and alcohols, the water solvents don't form hydrogen bonds which are particularly stronger than those of the alcohols; rather, water simply forms more hydrogen bonds, on average, compared to the alcohols.

Table 5.4. Summary of energetic and structural features: TMPO simulations in bulk solvents.

solvent	N_C^a	$-V_{\text{pair}}^b$ (kJ/mol)	O-O RDF ^c	
			R_{pk} (Å)	fwhm (Å)
“ab initio” solvent models				
methanol	2.05	39.8	2.65	0.29
ethanol	2.18	39.6	2.67	0.30
1-propanol	1.97	42.6	2.65	0.29
2,2,2-trifluoroethanol	1.87	49.7	2.63	0.28
2-propanol	1.52	45.7	2.63	0.27
tert-butyl alcohol	1.72	48.5	2.65	0.30
ethylene glycol	1.00	76.9		
water	2.40	32.5	2.69	0.34
OPLS solvent models				
methanol	2.06	40.3	2.65	0.28
ethanol	1.82	42.3	2.64	0.28
1-propanol	2.06	42.0	2.65	0.29
2-propanol	2.06	43.4	2.66	0.30
tert-butyl alcohol (UA)	1.88	44.0	2.67	0.31
tert-butyl alcohol (AA)	1.54	39.4	2.69	0.31
water (TIP4P)	2.52	39.3	2.64	0.30
Chloroform (OPLS)	1.94	20.4	3.12	0.67
Chloroform (Kovacs)	2.33	20.8	2.59	0.50
Chloroform (Dietz)	2.30	18.9	2.34	0.53

^a N_C is the coordination number associated with the first peak in the solute-solvent O-O radial distribution functions.

^b V_{pair} is the most probable interaction energy between the solute and solvent hydrogen-bonded to the solute oxygen site.

^c "RDF" refers to radial distribution function between the solute oxygen site and the solvent hydroxylic oxygen.

^d OPLS alcohol potentials are from Ref. [13]. OPLS water potentials are from Ref. [18]. OPLS chloroform potential is from Ref. [15]. The Kurtz and Dietz chloroform models are from Ref. [16] and Ref. [17] respectively.

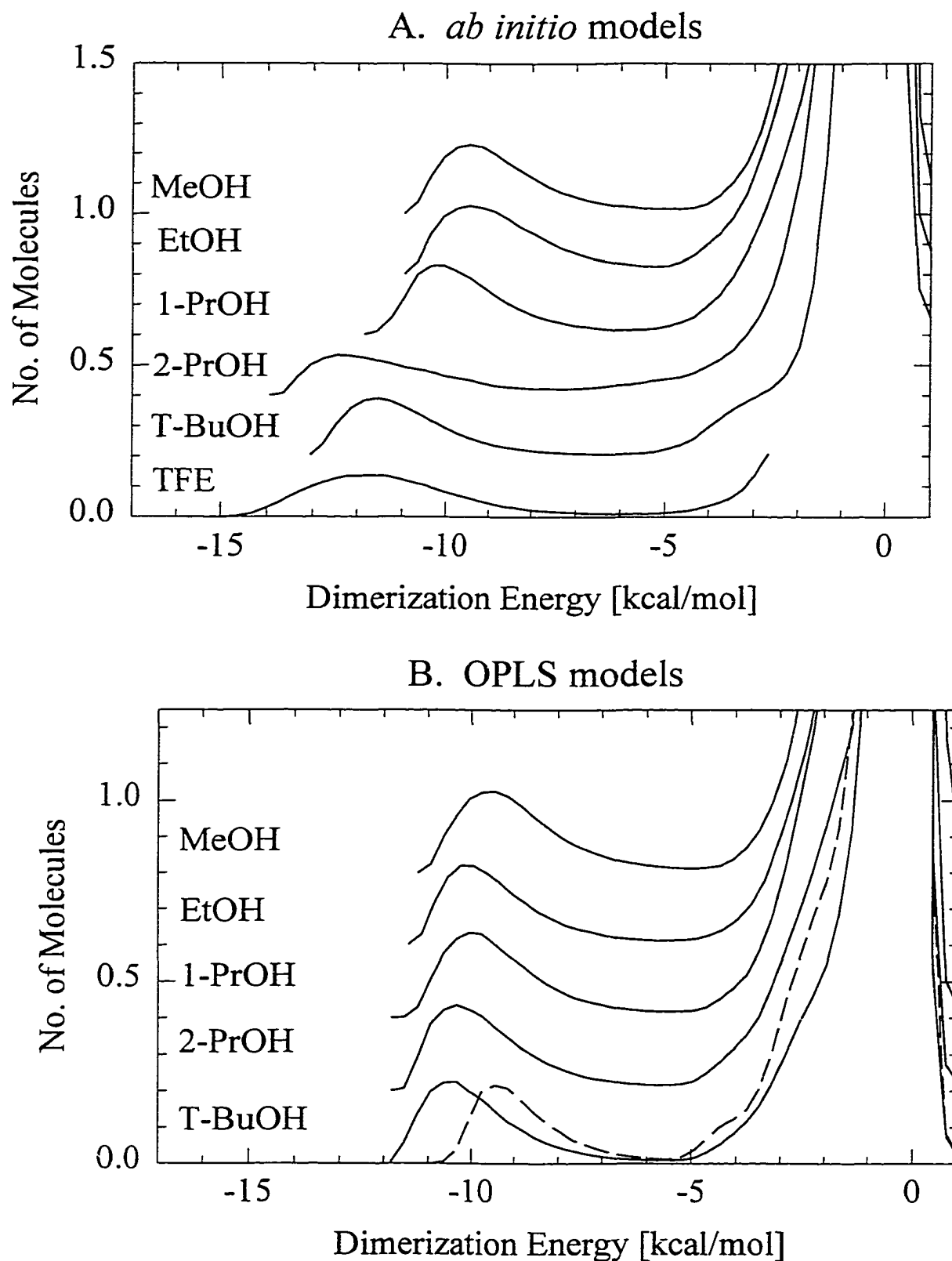
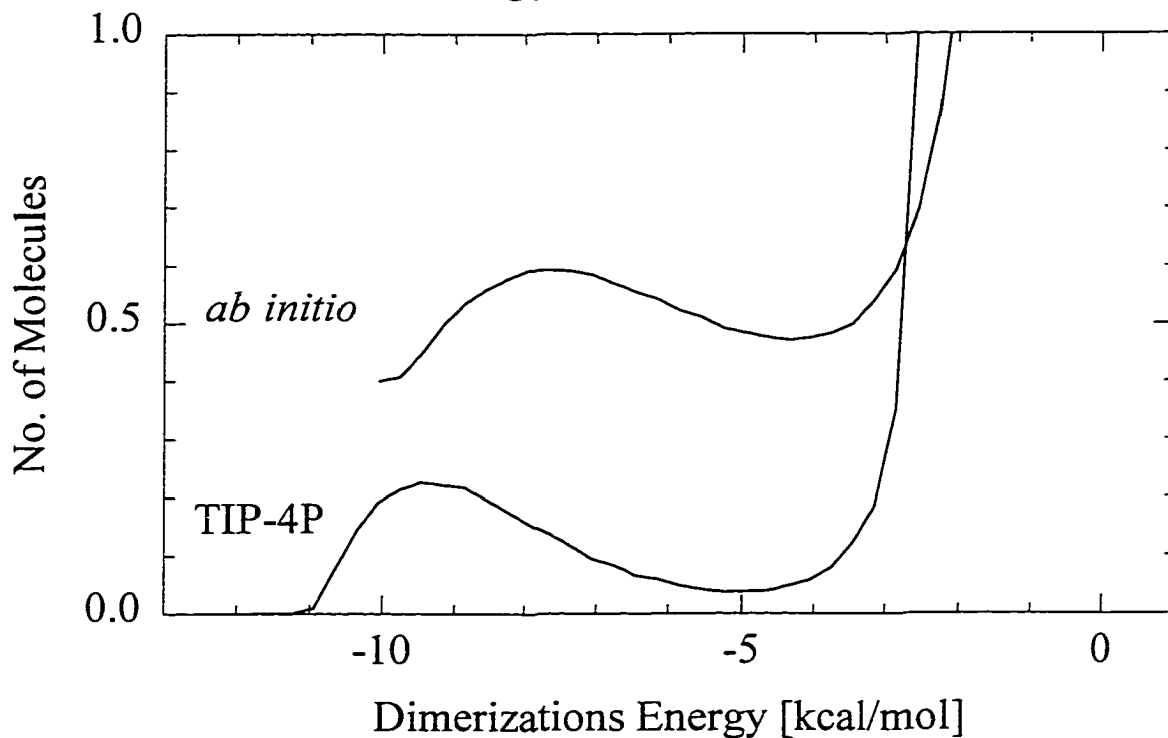


Figure 5.9. Energy Pair Distributions between TMPO and various *ab initio* solvent (A), and OPLS (B) solvent molecules. Units of the ordinate are number of molecules per kcal/mol. Successive curves are offset 0.25 units along the y-axis.



D. Chloroform models

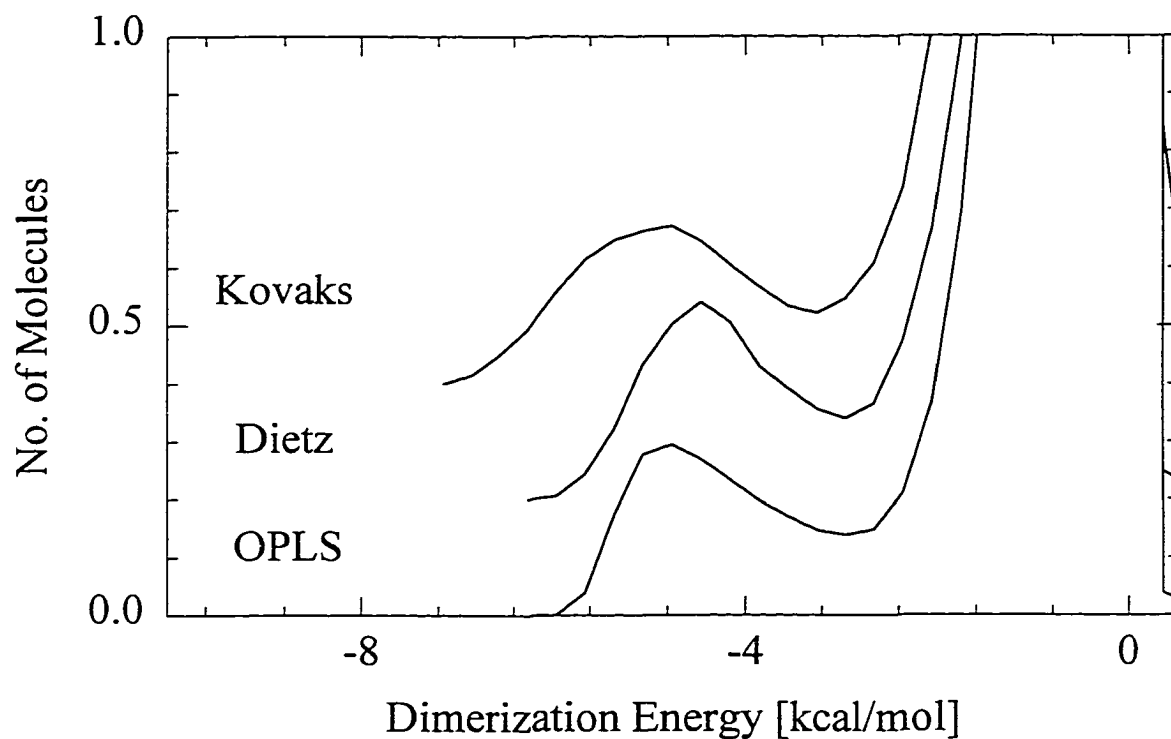


Figure 5.9. Energy Pair Distributions between TMPO and various water solvent (C), and chloroform (D) solvent molecules. Units of the ordinate are number of molecules per kcal/mol. Successive curves are offset by 0.4 and 0.2 units along the y-axis.

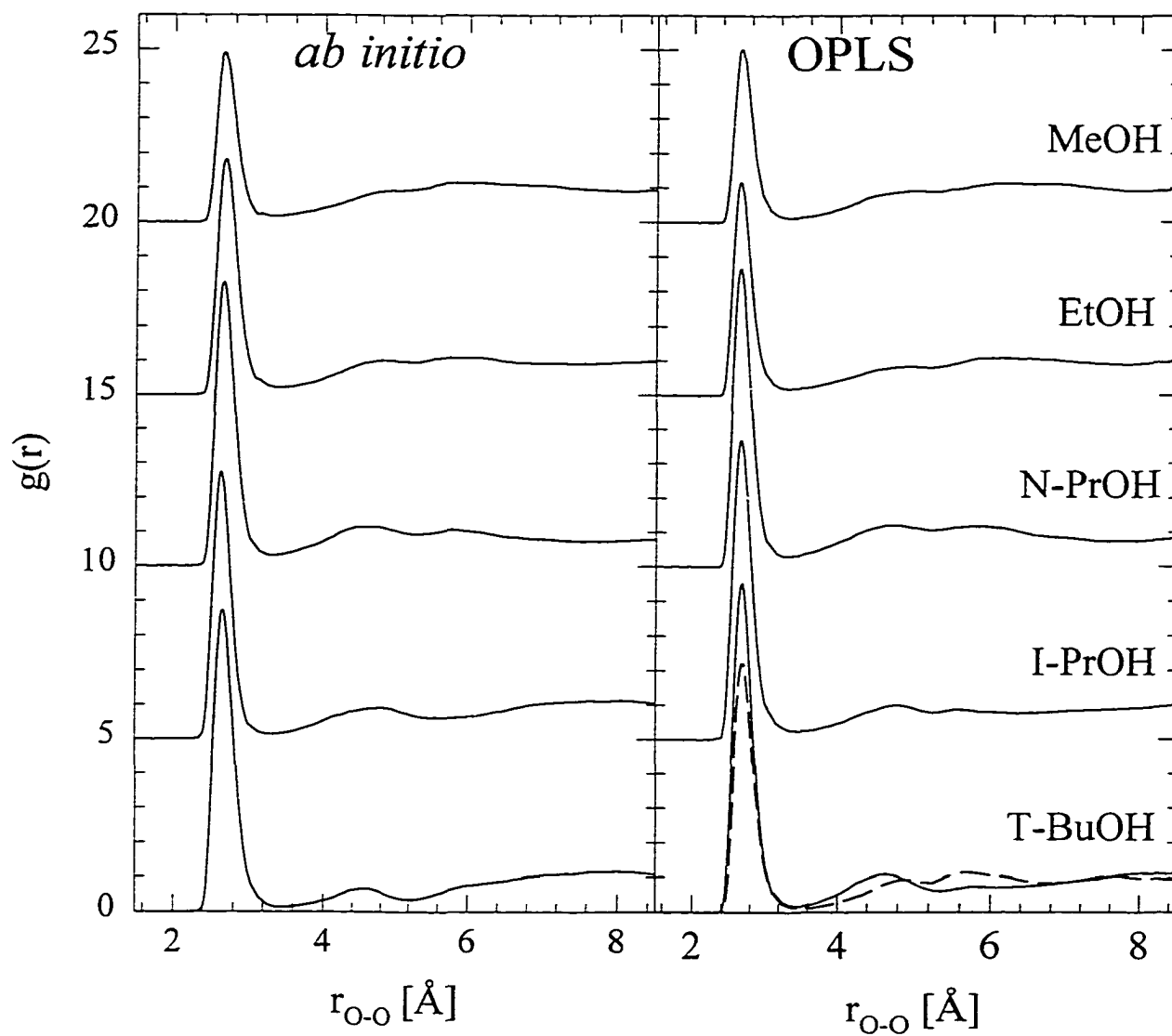


Figure 5.10. Solute-solvent OO radial distribution functions for TMPO-alcohol systems. Successive curves are offset 5.0 units along the y-axis.

5.4.2.2. 0^{th} -Order Vibrational Shifts of TMPO in Bulk Solvent Systems.

The computed 0^{th} -order shifts are presented in table 5.6 and are plotted versus the observed results in figure 5.10. The values have been computed via equation 5.1, with an 18 cm^{-1} correction added to compensate for the experimentally observed difference between the vapor phase value and that of cyclohexane. The actual values presented are meant to be compared with the experimental shifts relative to TEPO vapor ($\sim 1209\text{ cm}^{-1}$). Also, like the experimental values, the simulated values for species exhibiting multiple bands represent a weighted average of components, corresponding to differently coordinated compounds. Subsequently, the reported average values are dependent on the percentage breakdown of the coordinated complexes. A breakdown of the separate components, including band position, width and relative percentage of occurrence, are also presented in table 5.6, along with the average electric field felt at the mid-point of the P-O bond.

Although the general goal of this study is to access the ability of the presented methods to reproduce hydrogen bonding in protic solvents, it is sensible to first examine interactions that are non-electrostatic in nature. That is, electrostatic interactions, arising from the interaction between static charge distributions of the molecules and non-additive inductive interactions are both included in the point-charges of the potential function (equation 3.1). However, other interactions, such as dispersion, and exchange-repulsion interactions are always present, and should contribute an attractive component to the shifts in many systems at room temperatures and pressures. Results from some

representative apolar solvents are presented first, in order to set a baseline of the influence of these non-electrostatic effects.

Looking first at the spectrum (Figure 5.12) and shift of carbon tetrachloride (CCl_4) reveals the lack of a dispersive, or “London” interaction component in this model. That is, when *real* molecules interact, electron-correlation effects lower the interaction energy between atoms. If modeled adequately, this attractive interaction would induce negative (“attractive”) shifts in a given vibrational spectrum. In this case, the solute and solvent models lack any explicit polarizability, and as a result the attractive/dispersive effects are neglected. The previously mentioned 18 cm^{-1} correction to the calculated shifts is designed to compensate this. This correction is based on the shift of the P-O vibration band upon going from vapor phase to cyclohexane (chosen as a generic non-associating solvent). However, carbon tetrachloride is a more polarizable solvent (relative to cyclohexane) and will have enhanced dispersive interactions. Experiments show this feature induces a more attractive shift. Figure 5.12 shows the general lack of attractive shifts resulting from this modeling technique. In fact, the Lennard-Jones component is mostly repulsive. A similar feature is also present in the component breakdown of the acetonitrile spectrum (“MeCN in figure 5.12b). The Lennard-Jones component in this solvent is very repulsive. However, unlike CCl_4 this solvent is very polar and a strong attractive/electrostatic component is also present. The neglect of an attractive Lennard-Jones component is not at all unexpected, and has been observed previously in studies of the C-H stretching Raman bands of cyclohexane- d_{11} in liquid solvents and supercritical CO_2 [19].

In the following section, results from our attempts to account for the changes in bond polarizability which occur upon vibrational excitation will be presented. For now, we assume that the 18 cm^{-1} correction is generally adequate for polar-protic solvents. This assumption is not totally unreasonable, considering that the interactions present in these systems are largely electrostatic in nature.

Figure 5.12c shows the breakdown between the attractive-electrostatic and repulsive components to the total shift for the TMPO:methanol system. This comparison reveals that a general repulsive contribution made by the Lennard-Jones interactions is much more pronounced in the polar-protic solvents ($+ 30\text{--}40\text{ cm}^{-1}$ vs $< 10\text{ cm}^{-1}$ in acetonitrile), and is due entirely to the solvents donating hydrogen bonds to the solute. This, of course, makes sense considering the hydrogen-bond donating solvents are the only molecules close enough to be in the repulsive (r^{-12}) region of the potential function. In contrast, these solvents account for 70 to 80 percent of the attractive coulombic component. Interestingly, due to cancellation of these two components, the remaining 20-30 percent attractive electrostatic contribution arising from non-hydrogen bonded solvents constitutes up to 50 % of the total observed shift.

Another interesting feature revealed by separating the components into attractive and repulsive terms is that the line widths for the total shift are generally about the same as the coulombic components, while the repulsive-Lennard Jones component tends to be slightly more narrow. Compared to the experimentally observed bandwidths, the simulated widths tend to be slightly larger, generally by 10-15 %. Like the previously

studied case of the electronic absorption of betaine-30, this overestimation is probably due to the lack of explicit electronic polarization in classical models being used.

Representative spectra derived from both types of modeling are compared with the experimental spectra in Figure 5.14 for a number of solvents. Focusing first on the 0th-order results, some general conclusions may be made regarding the ability of this model to reproduce the qualitative features of the experimental spectra. First, the peaks of the simulated spectra do not show clearly defined sub-bands as is the case with the experimental spectra. For instance, the separation between bands due to one- and two-coordinated (hydrogen-bonded) complexes is, on average, only 18.6 cm⁻¹ in the simulated spectra compared to the average of 30.86 cm⁻¹ determined from the deconvolution of the experimental spectra. As a result the simulated vibrational spectra do not look particularly bi-modal.

Although difficult to detect visually, the average shifts calculated in this manner show a significant dependence on the relative percentage of differing coordinated species. In fact, due to the strength of the hydrogen bonds being formed, these percentages are slow to average. Despite the generally good agreement with the trend set by the experimentally determined IR-shifts, the slow averaging makes distinguishing between similar solvents difficult. This fact is particularly evident for the OPLS solvents. Here, the percent of singly coordinated complexes is particularly low for both 1- and 2-propanol, compared to the *ab initio* model results and experiment. As a result, these models give average shifts near those of the simulated methanol model: a result that clearly goes against the experimentally observed trend. The *ab initio* solvents tend to

match the experimental trend closely. Although considering the difficulties in averaging, this may merely be good fortune, rather than a definitive endorsement of this solvent model's ability to model hydrogen bonded systems.

For the set of polar-protic solvents studied here, the general trend set by the experimental results is qualitatively reproduced by 0th order simulated shifts, although in general the simulated species fall short of the experimental values. This feature is particularly pronounced for the water models, in which the deviation is greater than 20 cm⁻¹, as well as for the chloroform and TFE models (23 cm⁻¹ and 21 cm⁻¹ deviations, respectively).

A final note regarding the number of solvent molecules hydrogen bonding to the oxygen site of TMPO is the observation of triply coordinated complexes in all polar-protic solvents with the exception of the t-butanol models. As discussed in the presentation of the experimental results, no experimental evidence exists for the presence of tri-coordinated complexes in the TEPO systems. TMPO is a smaller molecule, and work still needs to be done to determine if the ethyl groups are capable of lowering the solvent-assessable surface of the oxygen site. If the presence of tri-coordinated complexes is not verified in experiments involving TMPO, then this finding represents a significant flaw in the ability of these models to accurately reproduce the simple ground-state solvation in these systems.

The overall assessment of the 0th-order calculations of the vibrational shifts is one of partial endorsement. Considering the simplistic manner in which a variety of complex intermolecular interactions are handled, the ability of this method to reproduce the basic

Table 5.5. Tabulation of simulated shifts, calculated using only spatial contributions to the vibrational shift.

Solvent	<v> _{expt.} <v> _{sim.}		Single Coordinated			Double Coordinated			Triple Coordinated			- E _{field} [e/Å ²] × 10 ⁻³
			v _{max}	v _{fwhm}	%	v _{max}	v _{fwhm}	%	v _{max}	v _{fwhm}	%	
"ab initio" models												
Methanol	81.5	75.7 ± 0.4	61	33	2.3	77	44	84.44	87	30	13.23	43.75
Ethanol	75.2	69.5 ± 1.5	58	28	11.9	74	29	79.40	83	34	17.10	40.03
1-Propanol	74	68.2 ± 1.1	54	31	14.2	70	29	51.10	85	30	7.75	38.85
TFE	90.5	67.5 ± 0.7	53	24	18.0	70	26	80.99	76	29	1.16	37.44
2-Propanol	71	67.1 ± 3	58	25	38.5	77	33	62.55	83	34	0.60	38.94
t-Butanol	63	62 ± 4	49	25	38.2	73	22	61.58	-	-	-	32.02
Water	108	81 ± 3										45.43
OPLS models												
MeOH/O	81.5	74.3 ± 1.5	61	27	2.40	74	30	88.17	89	33	8.93	43.75
EtOH/O	75.2	67.7± 3	50	25	21.6	72	29	70.80	88	31	5.31	38.37
1Pr/O	74	73.4 ± 1.9	54	25	8.8	75	29	81.70	90	31	10.73	46.70
2Pr/O	71	73.6 ± 1.9	56	24	7.8	74	27	84.73	94	32	8.92	42.90
Tb ₂ O-UA	63	67 ± 3	48	30	9.6	69	29	90.25	-	-	-	36.45
Tb ₂ O-AA	63	60 ± 3	53		45.9	66		54.03	-	-	-	34.07
Water (TIP4P)	108	85 ± 2										50.89
Acetonitrile	43.3	52.1 ± 0.2										27.90
Chloroform	54.9	33.9 ± 0.7										13.50
Chloroform (K)	54.9	40.8 ± 0.1										18.50
Chloroform (D)	54.9	33.7±0.7										13.90
Carbon Tet.	30.8	15.7 ± 0.7										0.06

Average peak separation: $\Delta v_{12} = 18.60$

$\Delta v_{23} = 13.25$

" All energy values ("shifts") are in units of cm^{-1} .

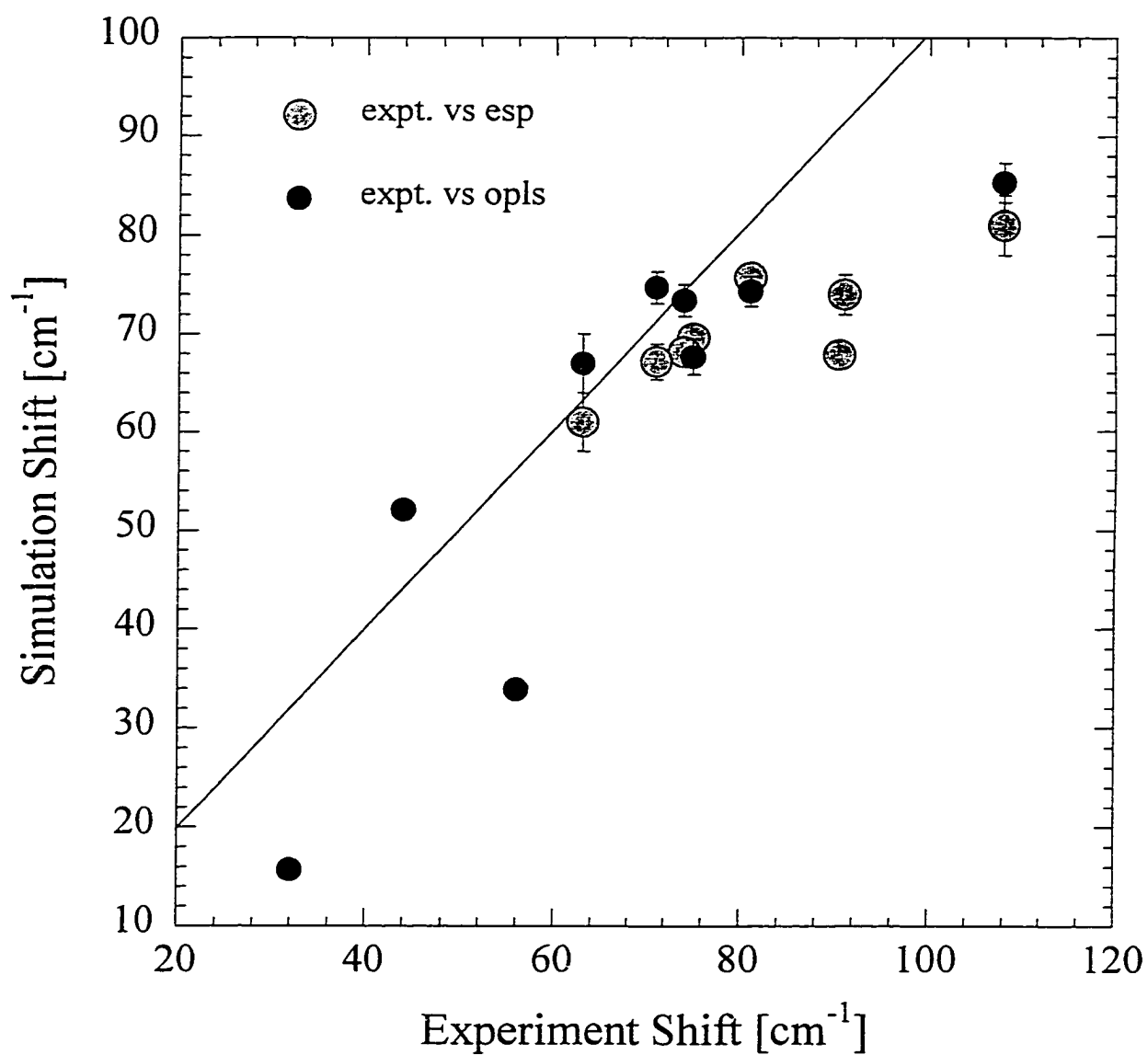
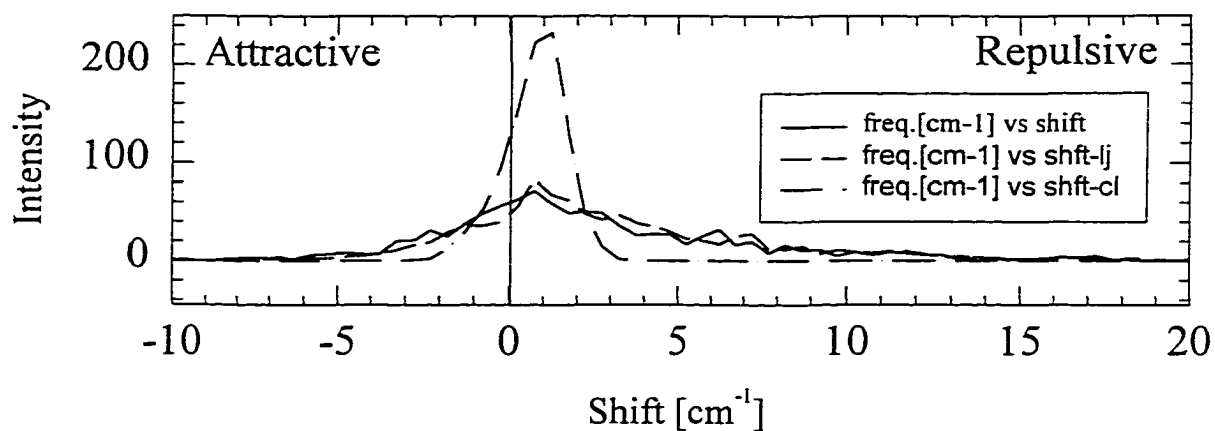
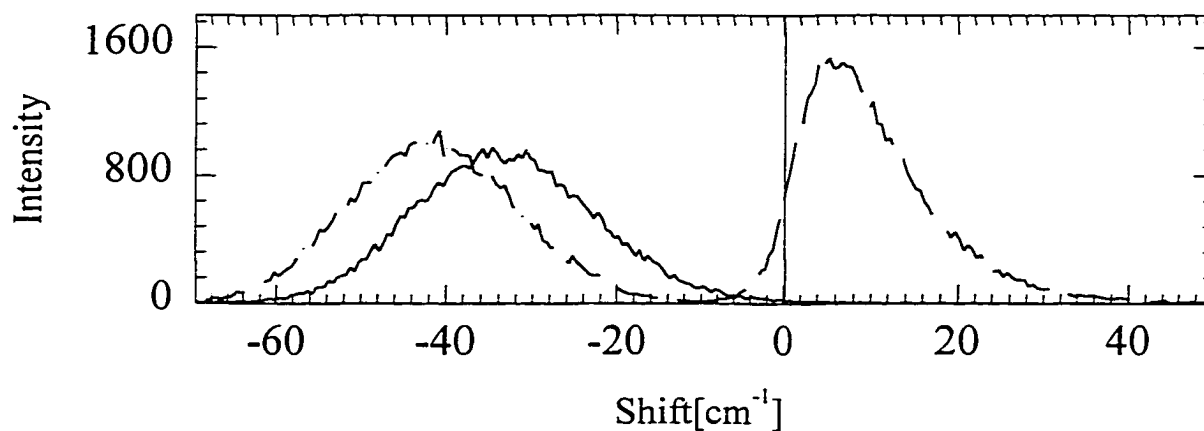


Figure 5.11. Comparison of "0th order" simulated and experimental shifts.

A. TMPO vibrational frequency distribution: CCl_4 

B. TMPO vibrational frequency distribution: MeCN



C. TMPO vibrational frequency distributions: MeOH

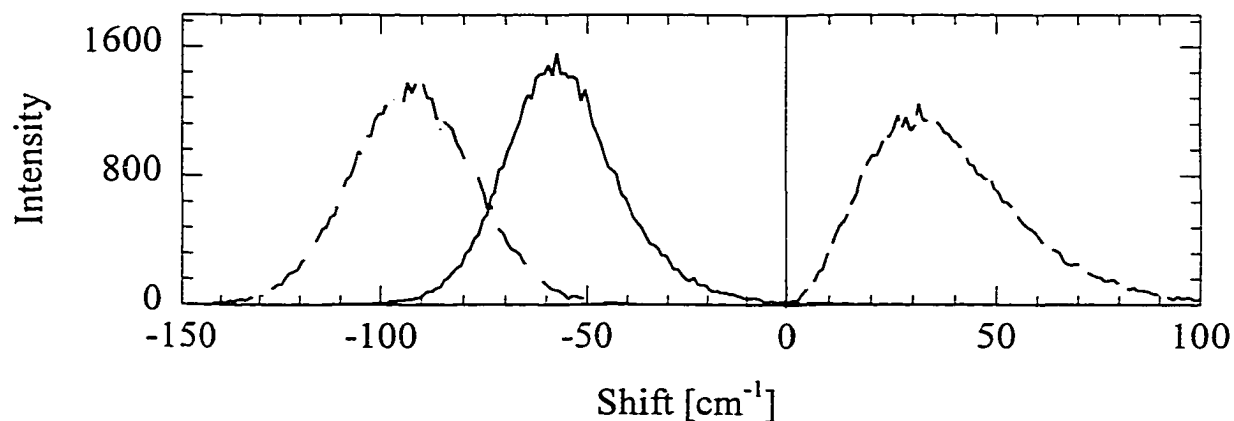


Figure 5.12. TMPO vibrational frequency distribution decompositions. Short-dashed lines indicate the Lennard-Jones contributions to the shifts, dot-dashed lines indicate coulombic contributions to the shifts, and the solid lines indicate the sum of these two components, the total shifts.

experimental trend ($\Delta\nu_{\text{water}} > \Delta\nu_{\text{methanol}} > \Delta\nu_{\text{t-butanol}}$) is satisfying, and represents a significant first step towards our ultimate goal of evaluating hydrogen-bond donating character in polar-protic solvents. Clearly, there is still room for improvement.

5.4.2.3. Model 2. 0th-Order + Polarization.

This method builds on the previously presented results by adding two components to the potential derivatives used to calculate the shifts via equation 5.1. These terms represent the change in electrostatic potential of the solute and the change in polarization of the solute as functions of the vibrational coordinate, Q . These terms are defined via equations 5.7 a and b, and are included in the calculation of the shift via the derivative definitions given in equation 5.13-16. Only values for f_q and f_ϵ need to be determined. These represent the changes in charge and polarization, and are defined by equation 5.11.

f_q accounts for the change in dipole moment which occurs upon vibration, and *isn't* accounted for by the simple, static-charge, dipole change. Figure 5.13a is a plot of dipole moment versus reaction coordinate, calculated from single point *ab initio* calculations at the 6-31G** level. From this plot, it is evident that the dipole moment changes linearly with the vibrational coordinate, with a slope of 7.14 Debye/Å. This slope represents the change in electrostatic potential that should occur when the molecule vibrates. The model employed in the previous section only accounted for 4.92 Debye/Å, as demonstrated by figure 5.13b. This was determined by moving the nuclear positions of TMPO along the reaction coordinate with the fixed point-charges (given in

table 5.1), and calculating the dipole moment at each displacement. The subtraction of these two numbers yields f_q , the change in dipole missing from the 0th-order treatment of the vibration. Changes in the polarizability are not directly calculable from *ab initio* methods. For this reason, f_ϵ is chosen empirically to obtain the best agreement with experimental values.

Again, we begin by looking at the solvation of TMPO in carbon tetrachloride. This solvent may be considered to be inert in terms of electrostatic interactions. As a result, the contribution from the f_q term is very small. Since the empirical parameter, f_ϵ , is designed to account for the enhanced polarization of the vibrationally excited bond the shifts are now compared from the vapor phase value of TMPO. This is done without the correction factor used in the 0th-order modeling, which is no longer needed since the polarization is being directly modeled through f_ϵ . As a result, a moderately large value of f_ϵ is needed to account for the polarization (see table 5.7). Since the excited vibrational state is always more polarizable, the dispersion interactions are larger, and the shift becomes more “attractive”. Because of this, the empirically determined value of f_ϵ for the CCl₄ system should be (and is) a positive value, corresponding to this extra “attractive” shift.

Oddly enough, adding a dispersive component to the acetonitrile shift, in the form of positive f_ϵ values only serves to make the simulated shifts too attractive. It seems that either acetonitrile is not a terribly polarizable solvent (in terms of electronic polarizability), or the dipole orientational component of the model is overestimated. Regardless, both the experimental and simulated results in acetonitrile serve to point out a

key aspect of the TMPO frequencies. The shift in acetonitrile, although small in comparison to that in the protic solvents, is still significantly large, attractive and electrostatic in nature. Since acetonitrile has little, if any hydrogen-bond character, the shifting of the P-O stretching band in this solvent is clearly due to electrostatic effects. These effects are most likely present in all polar solvents.

Polar-protic solvents have substantially different interactions with TMPO than do aprotic solvents, due to the presence of the hydrogen-bonding interactions. One aspect that our model calculations do not compensate for is the changes in the size of the molecule upon vibrational excitation. That is, when a molecule absorbs a photon and becomes vibrationally excited, not only does the vibrating bond become more polarizable, it also becomes larger. To properly model both effects, the simulation parameter, σ , should get slightly larger. Previous studies, which modeled vibrations in a similar manner, did, in fact, employ empirically determined variations in both σ and ϵ to fully compensate for these two effects[19]. Unlike the aprotic systems studied previously, in hydrogen bonded systems, due to the large electrostatic interaction between hydrogen bonded molecules, the dispersive/exchange-repulsion interactions are no longer in the “attractive” regime. Consequently, when the vibrationally excited molecule gets bigger, the effect is to enhance the repulsive interactions between the TMPO molecule and the hydrogen-bonded solvents. Since the added electrostatic contribution (f_q) is known, the value for f_ϵ may be picked empirically, and has been found to be -0.6 for the polar-protic solvents.

It should be pointed out that, for a series of solvents in the same region of the Lennard-Jones potential, the value for f_{ϵ} should be the same. Also, although we are fitting to agree with the experimental shifts, the sign and magnitude of f_{ϵ} vary in a manner that is sensible and intuitive. For instance, negative values do not suggest that the vibrating molecule becomes less polarizable upon excitation. Rather this parameter reflects the region of the Lennard-Jones potential energy function in which the system resides. That is, f_{ϵ} includes both increased polarization and size. When the molecule vibrates in a hydrogen-bonded solvent the repulsive contributions dominate the non-electrostatic term due to the change in size and the proximity of the nearest solvents. In non-associating solvents the closest molecules are further away, and may be thought of as residing in a different area of the Lennard-Jones potential energy function. As a result, the empirically determined values for f_{ϵ} are positive, as they should be to account for the increased polarization.

What qualitative changes occur when these extra terms are included? First, the “extra” electrostatic contribution due to f_q is attractive. That is, the electrostatic solute-solvent interactions may be thought of as coupled to the dipole moment. As demonstrated in figure 5.13, when modeled accurately the dipole moment becomes larger upon vibration, and the electrostatic component of the shift becomes more attractive. The component of the electrostatic contribution due to the nearest solvent molecules is also greater. As a result, the percent of the total shift due to just hydrogen-bonded solvents increases from about 50 % in the 0th-order modeling to 80-95 % in most solvents. The characteristics of the individual line shapes change as well. As f_{ϵ} is made more negative,

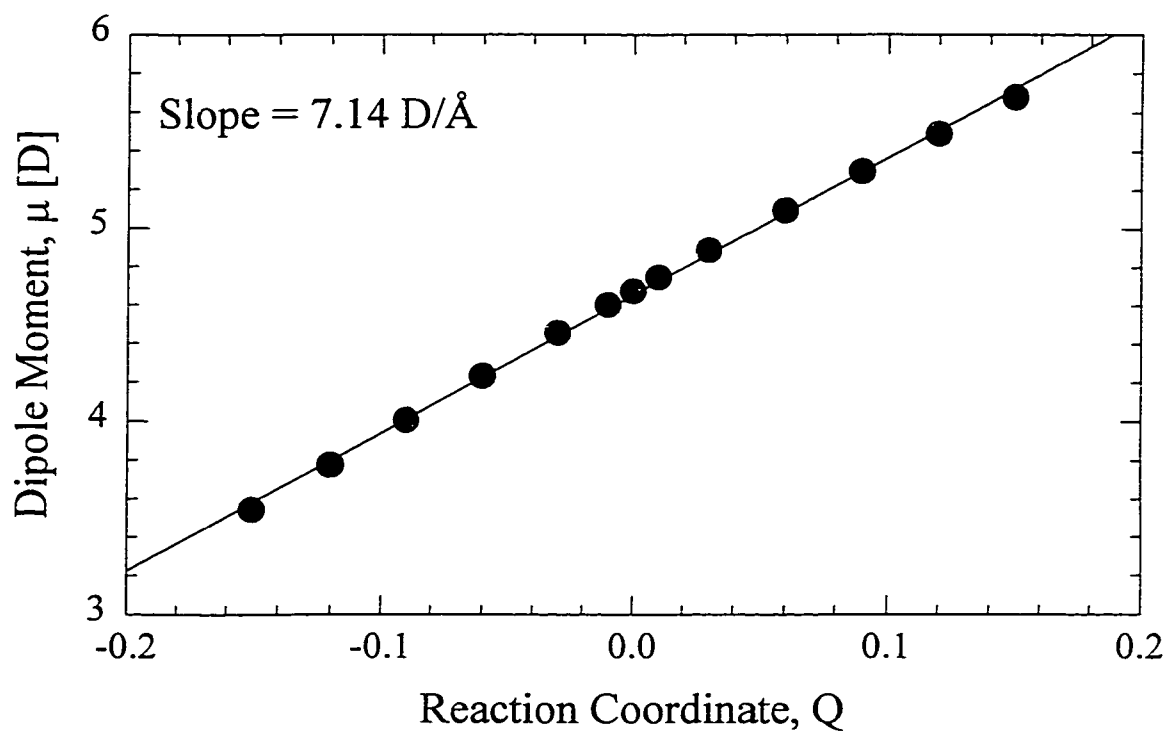


Figure 5.11a. Total dipole moment from ab initio 6-31G** single point calculations along the P-O vibrational coordinate.

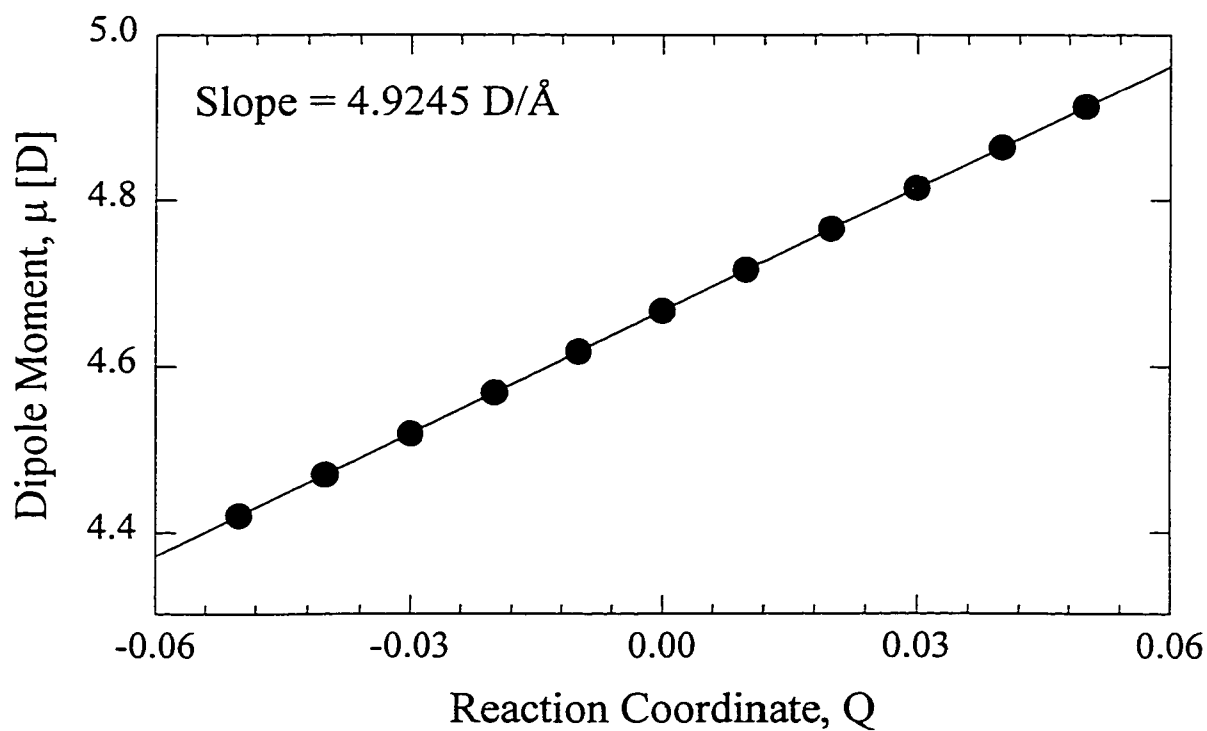


Figure 5.11b. Dipole moment variation along the P-O vibrational coordinate with constant point charges.

Table 5.6. Summary of all calculated and observed average TEPO vibrational frequency shifts.

Solvent	- Average Vibrational Frequency Shifts [cm ⁻¹]			<i>f_ε</i>
	Observed	0 th -Order	Adjusted	
"ab initio" models				
Methanol	81.5	75.7 ± 0.4	90	-0.6
Ethanol	75.2	69.5 ± 1.5	74.7	-0.6
1-Propanol	74	68.2 ± 1.1	76.9	-0.6
TFE	90.5	67.5 ± 0.7	74.9	-0.6
2-Propanol	71	67.1 ± 3	78.99	-0.6
t-Butanol	63	62 ± 4	67.96	-0.6
Water	108	81 ± 3	103.2	-0.6
OPLS models				
MeOH/O	81.5	74.3 ± 1.5		
EtOH/O	75.2	67.7±3		
1Pr/O	74	73.4 ± 1.9		
2Pr/O	71	73.6 ± 1.9		
Tbt/O-UA	63	67 ± 3		
Tbt/O-AA	63	60 ± 3		
Water (TIP4P)	108	85 ± 2		
Acetonitrile	43.3	52.1 ± 0.2		
Chloroform	54.9	33.9 ± 0.7		
Chloroform (K)	54.9	40.8 ± 0.1		
Chloroform (D)	54.9	33.7± 0.7		
Carbon Tet.	30.8	15.7 ± 0.7		

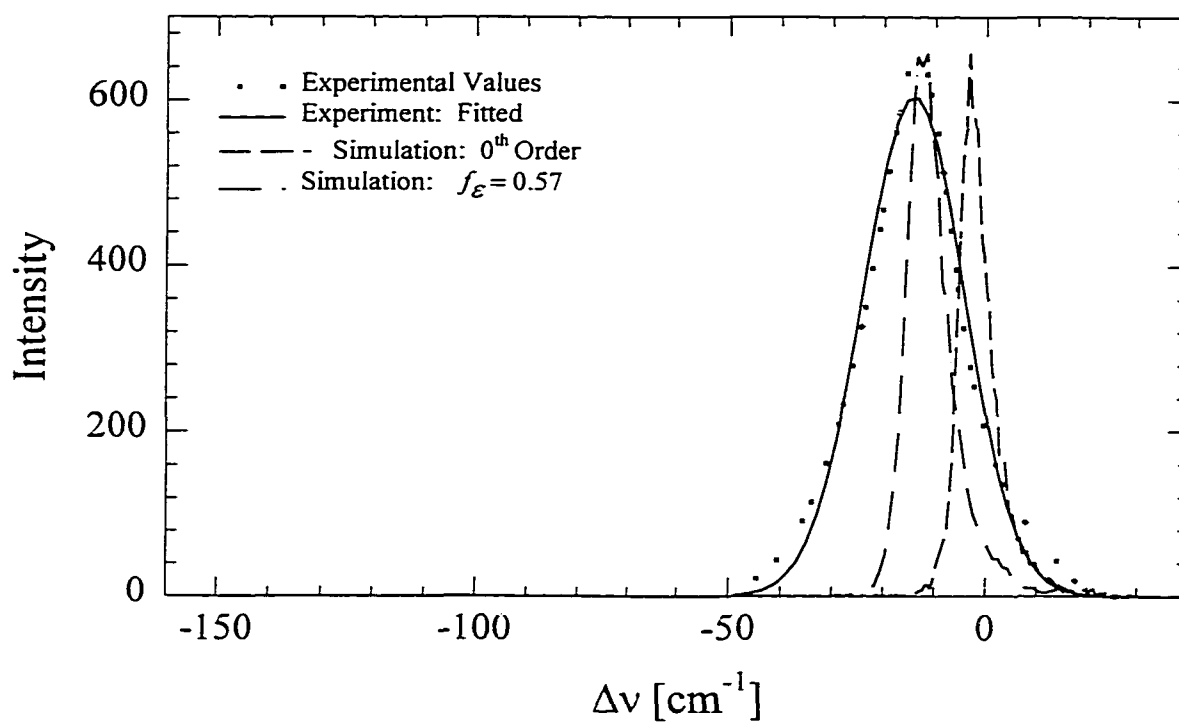


Figure 5.14.a. TMPO vibrational shift distribution: CCl_4
simulation and experiment

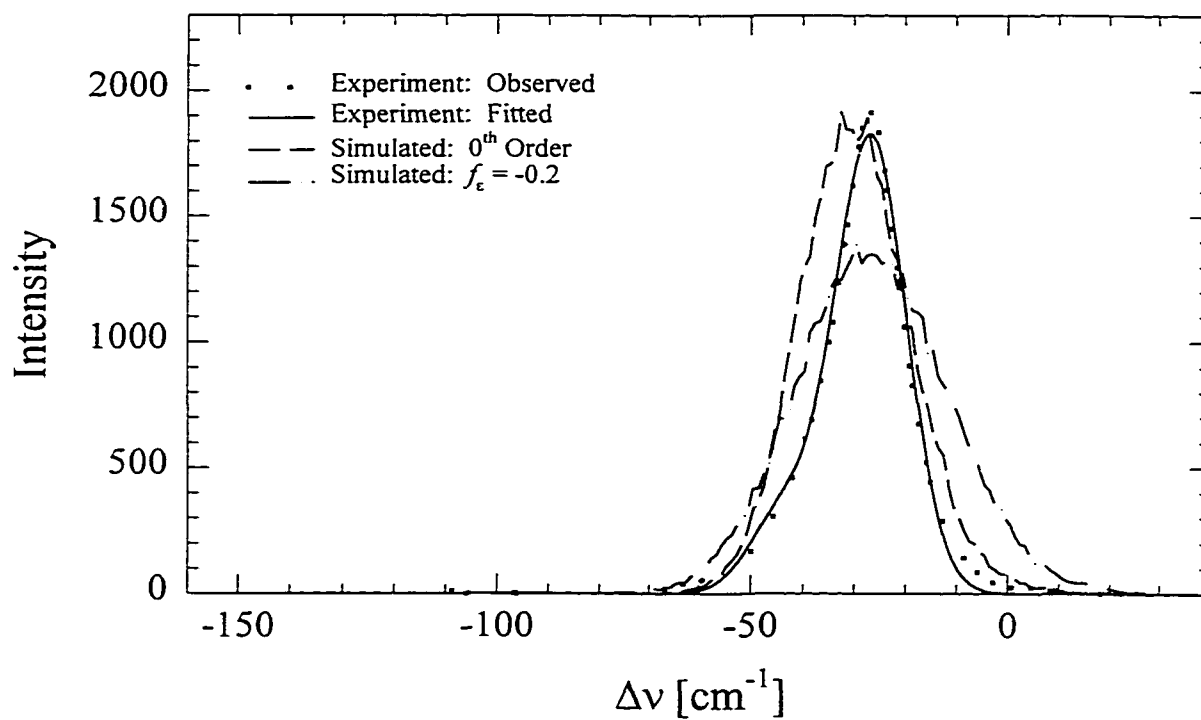


Figure 5.14.b. TMPO vibrational shift distribution: MeCN
simulation and experiment

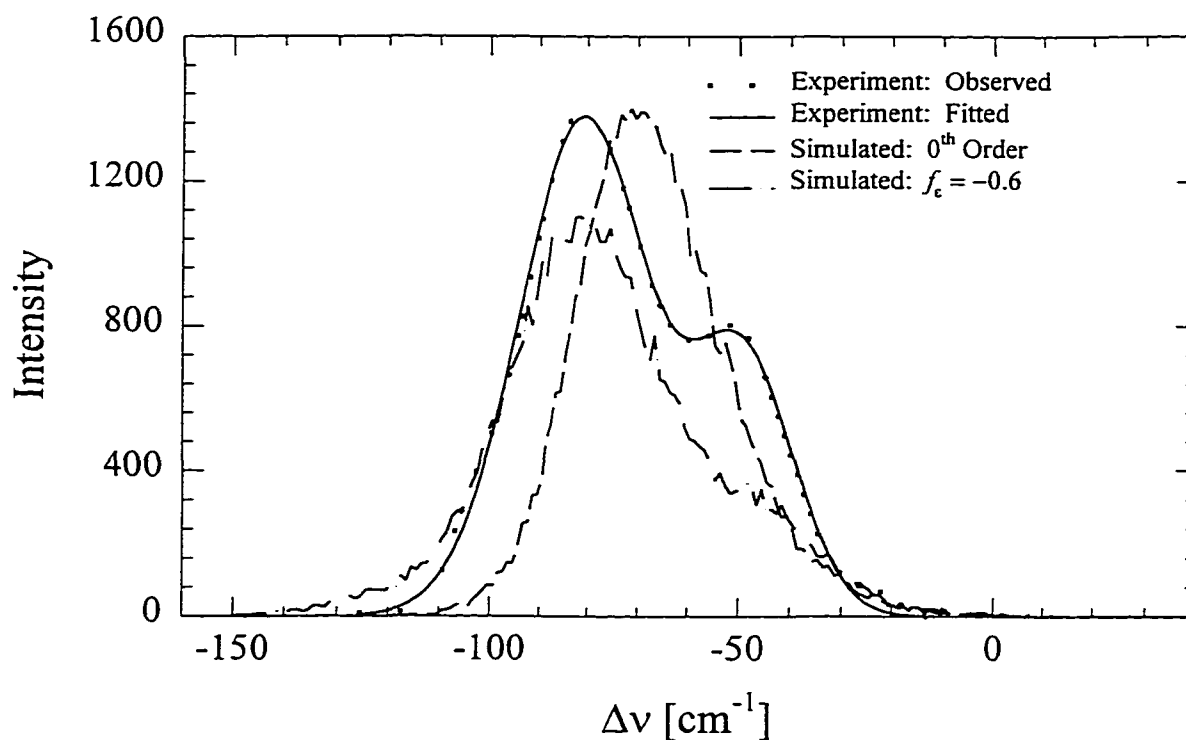


Figure 5.14.c. TMPO vibrational shift distribution: 1-Propanol simulation and experiment

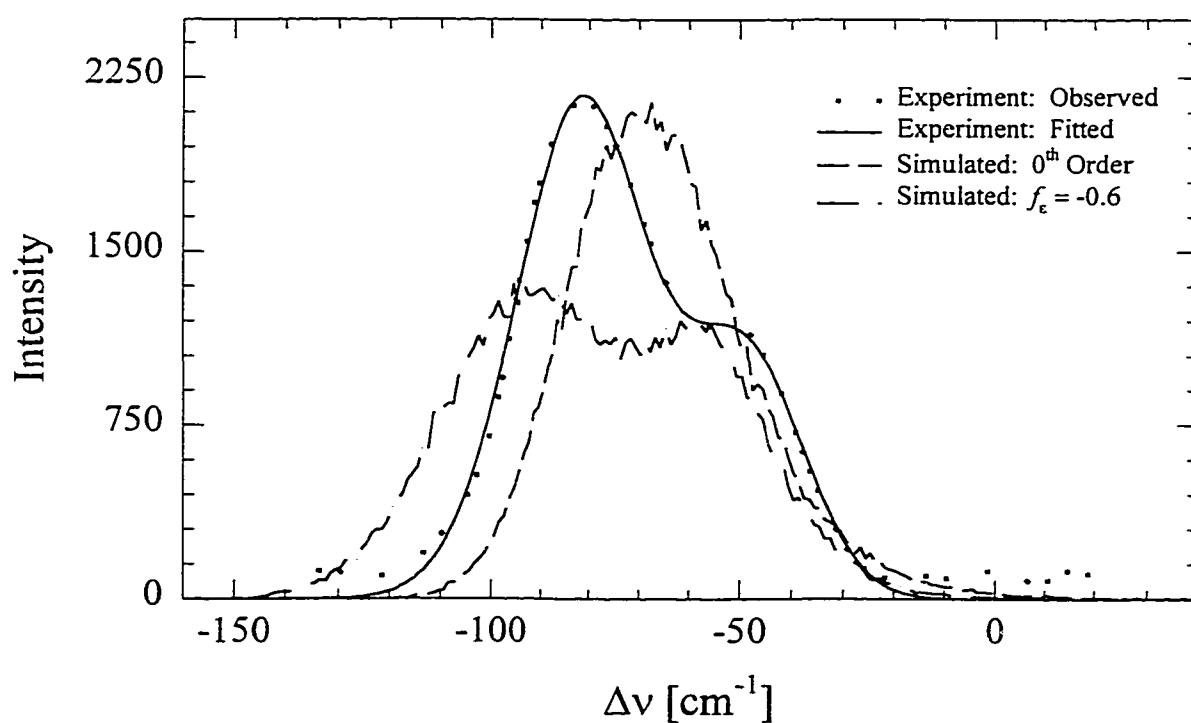


Figure 5.14.d. TMPO vibrational shift distribution: 2-Propanol simulation and experiment

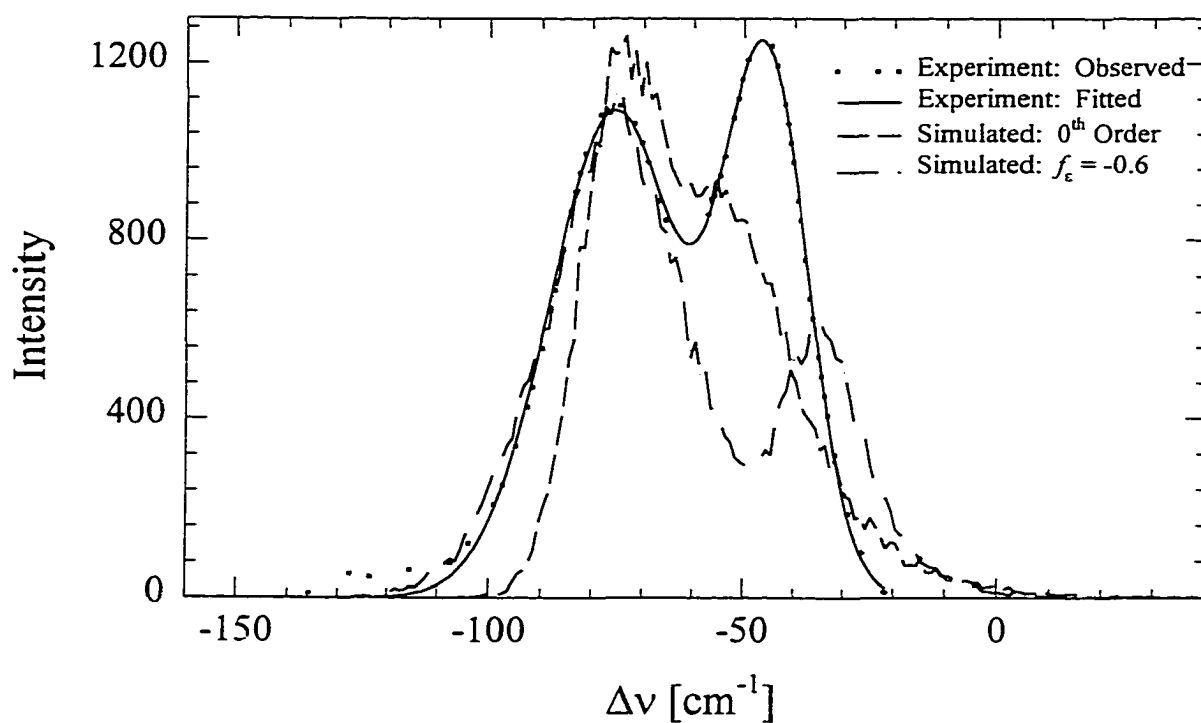


Figure 5.14.e. TMPO vibrational shift distribution: *tert*-butyl alcohol simulation and experiment

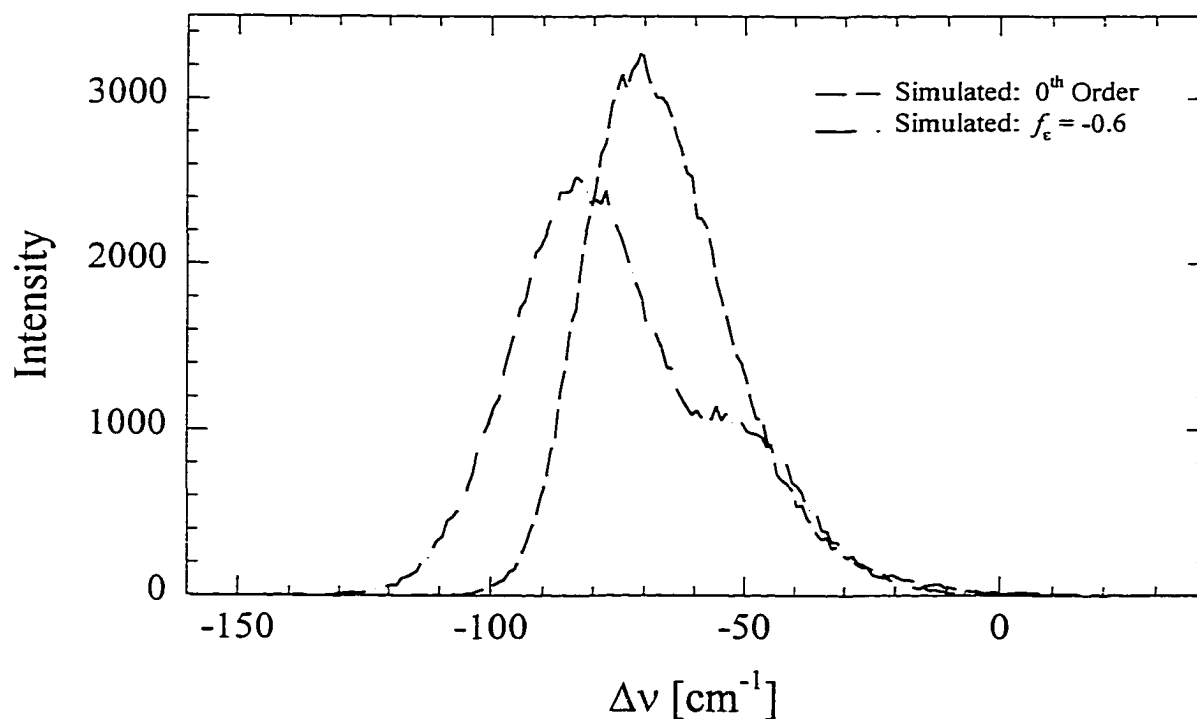


Figure 5.14.f. TMPO vibrational shift distribution: TFE simulation

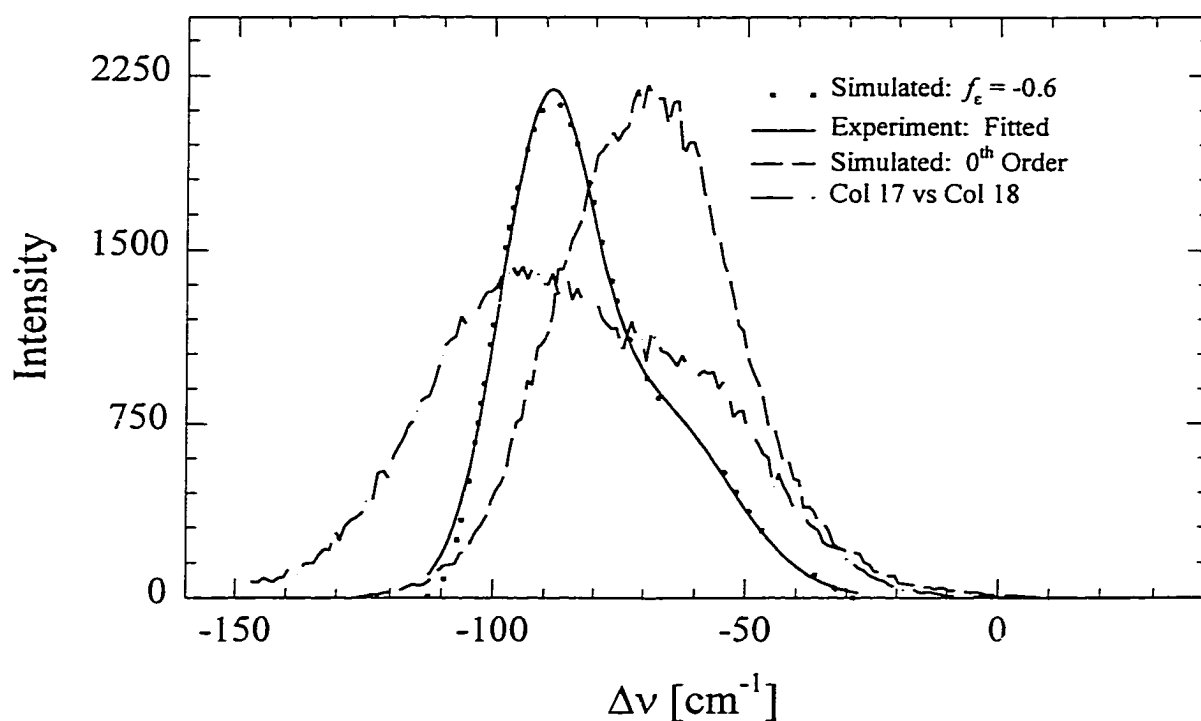


Figure 5.14.g. TMPO vibrational shift distribution: Ethylene Glycol simulation and experiment

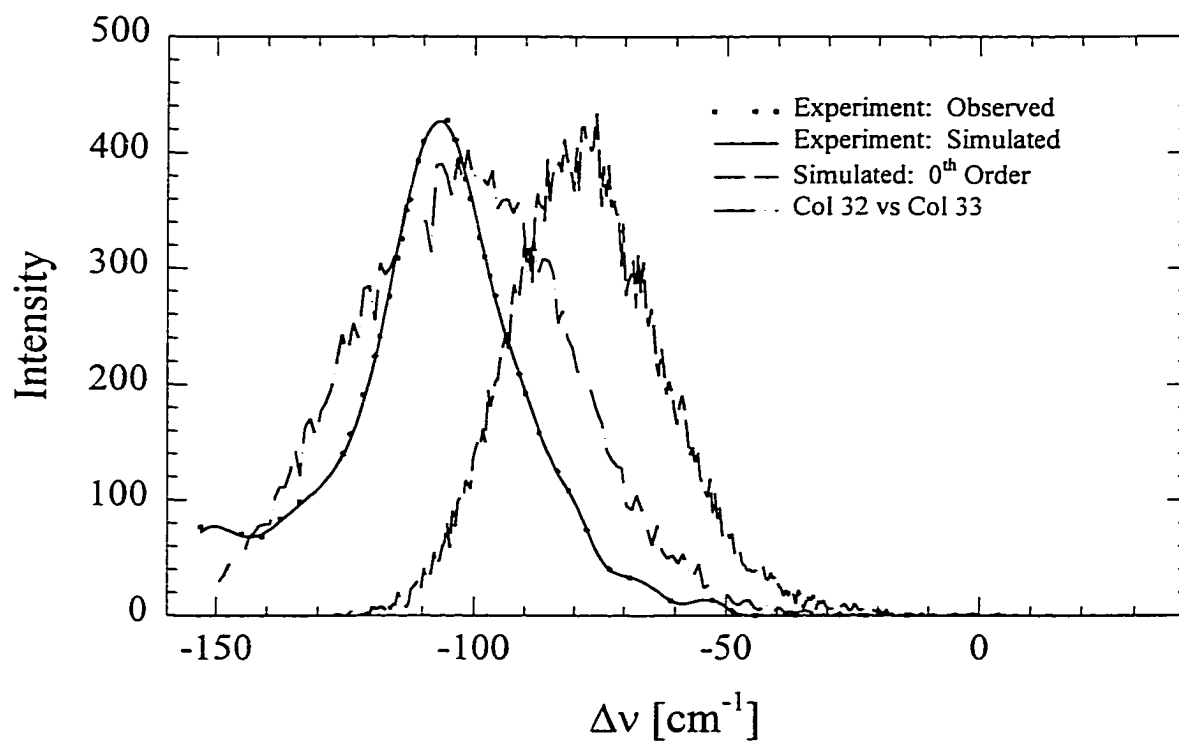


Figure 5.14.h. TMPO vibrational shift distribution: Water simulation and experiment

the lineshapes broaden and the peaks corresponding to different solvent coordination separate more. For the *ab initio* solvents, with f_ϵ set to -0.6 , the average peak separation is $\Delta\nu_{12} \sim 40 \text{ cm}^{-1}$, and the average full-width at half maximum becomes $\sim 36 \text{ cm}^{-1}$. These values are slightly larger compared to experiment, but an improvement upon the 0th-order shifts, in which the bi-modal character of the spectra were not detectable due to the small peak separations.

5.5. Summary and Conclusions

The intent of this chapter was to reproduce the vibrational spectra of a phosphine oxide probe molecule in a series of solvents, with the eventual goal of comparing the hydrogen bonding characteristics of various alcohol solvents. Since both triethylphosphine oxide (TEPO) and trimethylphosphine oxide (TMPO) have been used as measures of solvent electrophilicity [2-5, 7, 8], they represent attractive compliments to solvent polarity scales designed to encompass a broader spectrum of solvent-solute interactions.

The experiments reported here and in other studies demonstrate the sensitivity of the solvent-induced frequency shifts of TEPO and TMPO to their solvent environment. Indeed, for polar-protic solvents, the spectra of the P-O “stretch” clearly shows a bi-modal distribution which may be assigned to the presence of varying types of hydrogen-bonded complexes present in these systems. Further, the excellent correlation between

the shifts of TEPO with TMPO over a range of frequencies validates the comparison of the TMPO simulated shifts to the corresponding experimental shifts of TEPO.

Two sorts of analyses have been used to produce shifts from the simulation results. The simplest model (termed the “0th-order model”) calculated the solvent-induced shifts in the limit that the solute potential parameters do not change upon vibration. In this limit, the bond polarization that occurs upon vibration is not accounted for, and to compensate the shifts are corrected by the difference, $\nu_{\text{cyclohexane}} - \nu_{\text{vapor}} = 18 \text{ cm}^{-1}$.¹ Considering the approximate nature of this model, the calculated shifts agree surprisingly well with the observed shifts, although qualitative features such as band separation (in instances when more than one species is present) and linewidth are not as well reproduced. The second shift model attempted to approximate the change in charge and polarization upon vibration. Although the polarization correction is purely empirical, the sign and magnitude of the correction parameter (f_e) is qualitatively related to the solvent and it’s position along the Lennard-Jones potential curve for the solute-solvent interactions. Further, other qualitative aspects such as band separation and width are in better agreement with experiment.

On a final note, some comment should be made with regard to the use of differing potential parameters throughout the thesis. In Chapter 2, a variation upon the common OPLS set of solvent parameters was adopted in an attempt to better model the hydrogen-bonding characteristics of alcoholic solvents. These models are identical to the OPLS solvents in every way, with the exception of the atomic-site point charges, which have been obtained from ESP fits to the charge distribution generated from geometry-

optimized 6-31G* calculations (thus the moniker, “*ab initio*”). The subsequent comparison of the hydrogen-bond distributions made between the solvent and aza-aromatic solutes revealed differences between these two solvent representations, which ranged from mild (in primary alcohols) to notable (in 2-propanol and t-butanol). Further examination of solvent polarity, reported in Chapter 4, revealed that both representations reproduced the polarity scale, although the unadulterated OPLS models better reproduced the experimental trend. In Chapter 5, a different probe of solute-solvent interactions was employed in which (it was thought) hydrogen-bonding strength of the solvent would be of greater importance. Here, the *ab initio* derived models better reproduced the experimental trend, suggesting that, although the OPLS solvents are perhaps better parameterized to reproduce overall polarity, the *ab initio* models demonstrate a greater proficiency in reproducing hydrogen-bonding interactions.

5.6. References and Notes

1. Reichardt, C. *Chemical Reviews*. **1994**, *94*, 2319-2358.
2. Symons, M.C.R. and G. Eaton. *J. Chem. Soc., Faraday Trans. I*. **1982**, *78*, 3033-3044.
3. Symons, M.C.R. *Chem. Soc. Rev.* **1983**, *12*, 1-34.
4. Symons, M.C.R. *Pure and Appl. Chem.* **1986**, *58*, 1121-1132.
5. Mayer, U., H. Hoffmann, and R. Kellner. *Monatshefte fur Chemie*. **1988**, *119*, 1223-1239.
6. Hutchinson, E.J. and D. Ben-Amotz. *J. Phys. Chem. B*. **1998**, *102*, 3354-3362.
7. Mayer, U., V. Gutmann, and W. Gerger. *Monatshefte fur Chemie*. **1975**, *106*, 1235-1257.
8. Mayer, U., H. Hoffmann, and R. Kellner. *Monatshefte fur Chemie*. **1988**, *119*, 1207-1221.
9. Oxtoby, D.W. *J. Chem. Phys.* **1979**, *70*, 2605-2609.
10. Frisch, M.J., *et al.*, . 1994, Gaussian Inc.: Pittsburg, PA.
11. Singh, U.C. and P.A. Kollman. *J. Comput. Chem.* **1984**, *5*, 129.
12. Jorgensen, W.L., . 1994, Yale University: New Haven, CT.
13. Jorgensen, W.L. *J. Phys. Chem.* **1986**, *90*, 1276-1284.
14. Jorgensen, W.L. *J. Am. Chem. Soc.* **1996**, *118*, 11225-11236.
15. Jorgensen, W.L., J.M. Briggs, and L.M. Contreras. *J. Phys. Chem.* **1990**, *94*, 163.
16. Kovacs, H., J. Kowalewski, and A. Laaksonen. *J. Phys. Chem.* **1990**, *94*, 7378-7385.

17. Dietz, W. and K. Heinzinger. *Ber. Bunsenges. Phys. Chem.* **1984**, *88*, 543-546.
18. Jorgensen, W.L., J. Chandrasekhar, and J.D. Madura. *J. Chem. Phys.* **1983**, *79*, 926-935.
19. Frankland, S.J.V. and M. Maroncelli. *J. Chem. Phys.* **1999**, *110*, 1687-1710.

Chapter 6

SUMMARY

Classical simulations involving a range of different solvent effects in hydrogen-bonded liquid systems have been presented in the foregoing chapters. In Chapter 2 the analysis of the solvent effect upon the proton-transfer rates in bulk polar-protic solvents was examined using classical Monte Carlo and molecular dynamics computer simulations. Chapter 3 provided a comparison between the energetics of dilute solution and isolated complexes hydrogen bonded systems using classical methods versus higher level *ab initio* calculations and experimental results. Finally the solvatochromic properties of polar-protic solvents was examined in Chapters 4 and 5. These included a comparison between the observed and simulated solvent-induced electronic absorption band shifts, which are assumed to measure solvent “polarity”, and a comparison between the solvent-induced vibrational shifts between experimental results and simulated models. Aside from the specific scientific findings that are summarized at the end of each chapter, the results are significant because they demonstrate the ability of classical solvent models to yield semi-quantitative agreement with experiment and important molecular-level insights into a variety of molecular processes. Nevertheless, it is important to realize that a variety of other theoretical methods are available with which one can study reactive chemical systems in solution. This closing chapter offers some perspective as to what

other complimentary computational techniques may offer in terms of additional insights into the modeling of solvent effects in liquid phase reactivity.

At the heart of the simulations performed here are classical “molecular mechanics” force fields. Such force fields are simply a set of equations that describe the potential energy of a system under the Born-Oppenheimer approximation. Generally, these equations are formulated using classical mechanics and electrostatics. The approach of this thesis was to determine the extent in which this description of the intermolecular interactions reproduces hydrogen-bonding energetics and dynamics. The conclusions drawn from Chapter 2 clearly demonstrate that, to a large extent, the solvent effect upon the proton transfer rates may be understood in terms of geometric hydrogen-bonding requirements between the solute and solvent molecules. However, if the treatment of reactive systems (systems involving the breaking and forming of bonds) is desired a more robust quantum chemical treatment is necessary.

A number of researchers have approached proton transfer reactions from a theoretical perspective. Warshel has used an empirical valence bond (EVB) approach to model proton transfer reactions in proteins [1]. Although useful for many applications, this method requires accurate potentials from either experimental or higher-level theoretical methods, and does not include quantal effects explicitly. Hinsen and Roux presented a modified EVB that uses path-integrals to include quantum effects in their study of the intramolecular proton transfer in acetylacetone [2]. As with Warshel’s original work, this method also requires an accurate potential energy surface from which to derive the EVB potentials [3]. Since the tautomerization reactions of 7-AI and 1-AC

both occur on a excited-state potential energy surface, finding an accurate gas-phase reactive surface would be the prohibitive step if one were to attempt such simulations in these systems. To date progress towards the calculation of excited-state potential energy surfaces has focused primarily on CASSCF methods [4, 5]. Although advances have been made in this area, construction of accurate excited-state potential energy surfaces (PES) remains very difficult. Indeed, such basic considerations as to whether or not to include a correction for basis-set superposition error when performing *ab initio* calculations of hydrogen-bonded systems make obtaining an accurate potential energies for the ground-state uncertain at best [6]. Furthermore, it is not entirely clear that solvent effects upon the proton-shuttling PES will be accurately reproduced using the classical representations employed here. That is, if the solvent's influence upon the reaction reflects it's polarity or hydrogen bond donating ability, to what extent may these classical solvent models be expected to reproduce such quantities?

Providing an answer for this question follows logically from the apparent linear free-energy relationship discovered by Chapman and Maroncelli [7], and is the direction that we ultimately decided to pursue. In Ref. 7 these researchers report that the observed tautomerization rates of 7-AI and 1-AC are correlated with the $E_T(30)$ solvent polarity parameter. This relationship suggests a sensible method for determining the extent that these classical models may be expected to reproduce the hydrogen bonding arrangements of interest to the proton-transfer problem. Chapters 4 and 5 of this thesis examine this connection and find that most of the classical potentials due in-fact provide a reasonable representation of both the solvent polarity and the hydrogen-bond donating ability.

Although the results were found to agree well with spectroscopic observables, the approximate nature of the potentials remains, and it is intriguing to reflect upon what improvements may be made to the representation of the solvent models. Force field accuracy may be expected to increase steadily in the coming years as progress in this area continues. Of particular importance to studies of solvation phenomena are the inclusion of explicit polarization functions (to account for the attractive interactions between charges and induced dipoles formed by the presence of charges). A number groups have published classical polarizable force fields [8-11]. These models utilize the formalism developed by Botcher for calculating the polarization energy from a empirically fitted polarizability, α [12].

Solute molecules are generally not treated in this manner due to parameterization difficulties. Rather, polarization is included via a coupled QM/MM technique. Currently a number of these methods exist [13-17]. The effective fragment potentials (EFPs) developed by Gordon et. al. represents one such technique of particular interest due to the simple fact that the calculation of potential energy surface calculations of the proton transfer reaction in 7-azaindole are supposedly under-way using in Gordon's lab [18].

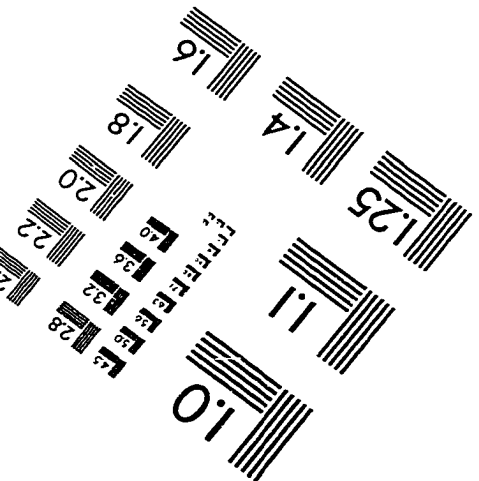
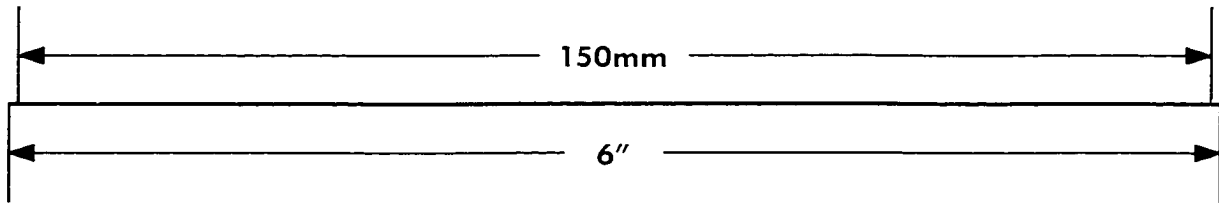
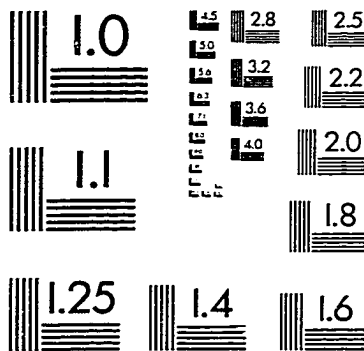
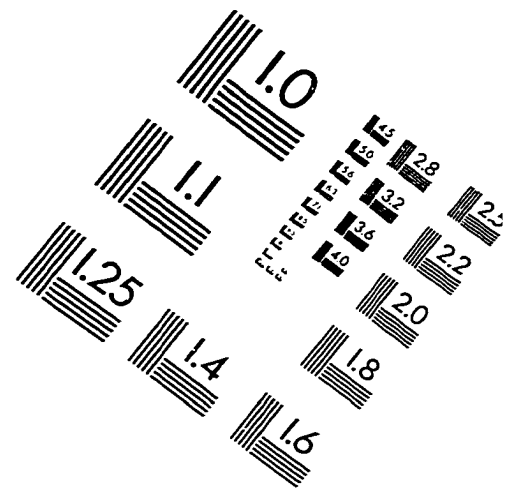
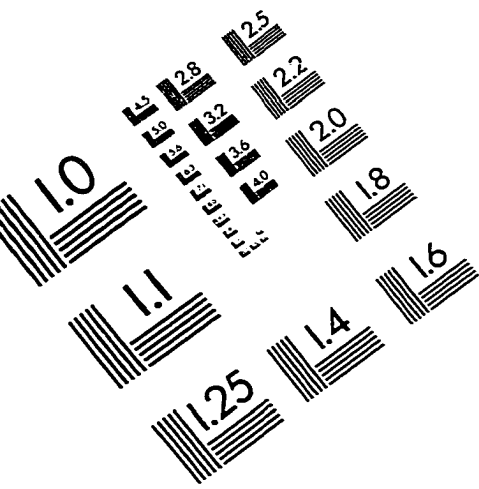
Notes and References

1. Warshel, A. *Biochemistry*. **1981**, *20*, 3167-3177.
2. Hinsen, K. and B. Roux. *J. Chem. Phys.* **1997**, *106*, 3567-3577.
3. Hinsen, K. and B. Roux. *J. Comput. Chem.* **1997**, *18*, 368-380.
4. Olivucci, M., *et al.* *J. Am. Chem. Soc.* **1993**, *115*, 3710.
5. Yamamoto, N., *et al.* *Chem. Phys. Lett.* **1996**, *250*, 373.
6. Scheiner, S., *Hydrogen Bonding: A Theoretical Perspective*. 1997, New York: Oxford University Press.
7. Chapman, C.F. and M. Maroncelli. *J. Phys. Chem.* **1992**, *96*, 8430-8441.
8. Bernardo, D.N., *et al.* *J. Phys. Chem.* **1994**, *98*, 4180-4187.
9. Ahlstrom, P., *et al.* *Mol. Phys.* **1989**, *68*, 563-581.
10. Caldwell, J.W. and P.A. Kollman. *J. Phys. Chem.* **1995**, *99*, 6208-6219.
11. Gao, J., D. Habibollazadeh, and L. Shao. *J. Phys. Chem.* **1995**, *99*, 16460-16467.
12. Bottcher, C.J.F. and P. Bordewijk, *Theory of electric polarization*. Vol. 2. 1978, Amsterdam.
13. Gao, J. *J. Phys. Chem.* **1997**, *101*, 657-663.
14. Field, M.J., P.A. Bash, and M.J. Karplus. *Comput. Chem.* **1990**, *11*, 700.
15. Day, P.N., *et al.* *J. Chem. Phys.* **1996**, *105*, 1968-1986.
16. Thompson, M.A., E.D. Glendening, and D. Feller. *J. Phys. Chem.* **1994**, *98*, 10465-10476.
17. Kaminski, G.A. and W.L. Jorgensen. *J. Phys. Chem. B*. **1998**, *102*, 1787-1796.
18. Chaban, G.M. and M.S. Gordon. *J. Phys. Chem. A*. **1999**, *103*, 185-189.

VITA

Scot Richard Mente was born August 25th 1971 in Mesa Arizona. He graduated from Gilbert High School, Gilbert Arizona in 1989, and received his Bachelor of Science degree in chemistry from Northern Arizona University, Flagstaff Arizona in 1993. He studied physical chemistry in the research group of Dr. Mark Maroncelli, and graduated from Penn State University with a Doctor of Philosophy in 1999. Scot has recently accepted an offer of employment from Pfizer in Groton, CT, to work in the area of drug discovery in their computational chemistry group.

IMAGE EVALUATION TEST TARGET (QA-3)



APPLIED IMAGE, Inc
1653 East Main Street
Rochester, NY 14609 USA
Phone: 716/482-0300
Fax: 716/288-5989

© 1993, Applied Image, Inc., All Rights Reserved

